

UCLA

UCLA Electronic Theses and Dissertations

Title

Large-Scale Neuroimaging Studies Of Psychiatric Disorders: Harnessing The Power Of The ENIGMA Consortium

Permalink

<https://escholarship.org/uc/item/08h6n0dq>

Author

Ching, Christopher

Publication Date

2019

Peer reviewed|Thesis/dissertation

UNIVERSITY OF CALIFORNIA

Los Angeles

Large-Scale Neuroimaging Studies Of Psychiatric Disorders: Harnessing The Power Of
The ENIGMA Consortium

A dissertation submitted in partial satisfaction
of the requirements for the degree Doctor of Philosophy
in Neuroscience

by

Christopher Ching

2019

ABSTRACT OF THE DISSERTATION

Large-Scale Neuroimaging Studies Of Psychiatric Disorders: Harnessing The Power Of The ENIGMA Consortium

by

Christopher Ching

Doctor of Philosophy in Neuroscience

University of California, Los Angeles, 2019

Professor Carrie E. Bearden, Chair

Coordinated, large-scale efforts to study brain disorders are rare, with most neuroimaging studies collecting fewer than 100 study participants. Neuroimaging research is one of many biomedical fields that have suffered from low study power and reproducibility. Genetic variation and psychiatric disorders confer subtle effects on markers of brain structure and function, further complicating the discovery and validation of reproducible neuroimaging biomarkers.

The Enhancing Neuro Imaging Genetics through Meta Analysis Consortium (ENIGMA) has developed harmonized processing and analysis protocols to empower large-scale neuroimaging studies of genetic variation and psychiatric illness. By using standardized methods, prospective meta- and mega-analysis carried out by the ENIGMA consortium improve upon conventional retrospective meta-analyses. ENIGMA working groups include both conventional studies of psychiatric disorders such as the ENIGMA Bipolar Disorder Working

Group, as well as genetics-first approaches like the ENIGMA 22q11.2 deletion working group, which study populations at high risk for psychiatric illness. These ENIGMA studies represent the largest collaborative efforts to study neuroimaging markers in their respective disorders.

The ENIGMA bipolar working group has reported altered cortical and subcortical volumes, which show significant predictive power in discriminating patient populations. The ENIGMA 22q11.2 deletion syndrome working group has reported robust cortical, subcortical and white matter differences between 22q11.2 deletion subjects and healthy controls, differences between common microdeletion subtypes, as well as associations between 22q11.2 deletion-related psychosis and idiopathic schizophrenia. Large-scale, harmonized processing and analysis efforts such as these make cross-diagnostic comparisons possible on an unprecedented scale. Given the known overlap between major psychiatric disorders, such cross-disorder studies may provide robust markers that improve diagnoses, help monitor disease progression, and provide insights into novel therapeutic targets.

This dissertation of Christopher Ching is approved.

Susan Y. Bookheimer

Catherine Ann Sugar

Allan MacKenzie-Graham

Paul Thompson

Carrie E. Bearden, Chair

University of California, Los Angeles

2019

TABLE OF CONTENTS

CHAPTER 1

- 1.1 Modern Brain Mapping (pg. 1)
- 1.2 The Enhancing Neuro Imaging Genetics Through Meta Analysis Consortium (ENIGMA) (pg. 3)
 - 1.2.1 ENIGMA: Studying the effect of genetic variation on brain structure (pg. 4)
 - 1.2.2 ENIGMA methods and disease working groups (pg. 5)
 - 1.2.3 The ENIGMA Model: Advantages and challenges (pg. 7)
 - 1.2.4 Harmonized processing protocols for large samples (pg. 8)
 - 1.2.5 Big Data: Heterogeneity as advantage and disadvantage (pg. 9)
 - 1.2.6 Meta- and Mega-Analysis (pg. 12)
 - 1.2.7 The future of ENIGMA (pg. 13)
 - 1.2.8 ENIGMA Leadership (pg. 16)
- 1.3 Organization of the dissertation (pg. 17)
- 1.4 Chapter 1 references (pg. 21)

CHAPTER 2

- 2.1 Overview (pg. 25)
- 2.2 Tensor-based morphometry (pg. 25)
- 2.3 ENIGMA harmonized protocols for cortical/subcortical quality assurance (pg. 25)
- 2.4. ENIGMA shape analysis pipeline: Development, quality control, and implementation (pg. 26)
 - 2.4.1 Rationale (pg. 26)
 - 2.4.2 Shape analysis protocol (pg. 28)
 - 2.4.3 Tracking disease-specific variation and genetic influence of subcortical structure (pg. 32)
 - 2.4.4 Advantages and limitations (pg. 41)
- 2.5 Chapter 2 references (pg. 46)

CHAPTER 3

- 3.1 Overview (pg. 47)
- 3.2 UCLA 22q11DS cohort subcortical findings (pg. 56)
- 3.3 ENIGMA 22q11DS subcortical volume and shape findings (pg. 74)
- 3.4 Chapter 3 references (pg. 109)

CHAPTER 4

- 4.1 Overview (pg. 111)
- 4.2 Recent findings from the ENIGMA bipolar working group (pg. 114)
 - 4.2.1 Subcortical volumes (pg. 114)
 - 4.2.2 Cortical thickness and surface area (pg. 116)
 - 4.2.3 Machine learning classification using cortical and subcortical measures (pg. 119)
- 4.3 Subcortical shape morphometry: A single site study (pg. 121)

4.4 Subcortical shape morphometry: Results from the ENIGMA bipolar working group (pg. 127)

4.5 Chapter 4 references (pg. 134)

CHAPTER 5

5.1 Future work overview (pg. 136)

5.2 Large-scale cross-disorder studies of psychiatric disorders: Direct comparison of harmonized brain measures (pg. 137)

5.3 Brain age (pg. 142)

5.4 Psychiatric genetics (pg. 143)

5.5 Chapter 5 references (pg. 146)

CHAPTER 6

6.1 Tensor-based morphometry: Scan parameter effects on longitudinal brain change (pg. 148)

6.2 Phantom-based MRI corrections and power to track brain change (pg. 150)

6.3 MRI scan acceleration and power to track brain change (pg. 155)

6.4 Chapter 6 selected works (pg. 167)

CHAPTER 7

7.1 Related works (pg. 168)

7.2 Chapter 7 selected works (pg. 169)

LIST OF FIGURES

Figure 1.2a	(pg. 6)
Figure 1.2b	(pg. 7)
Figure 1.2c	(pg. 8)
Figure 1.2d	(pg. 14)
Figure 2.4a	(pg. 30)
Figure 2.4b	(pg. 32)
Figure 2.4c	(pg. 33)
Figure 2.4d	(pg. 34)
Figure 2.4e	(pg. 36)
Figure 2.4f	(pg. 36)
Figure 2.4g	(pg. 38)
Figure 2.4h	(pg. 39)
Figure 2.4i	(pg. 40)
Figure 3.1a	(pg. 51)
Figure 3.1b	(pg. 52)
Figure 3.1c	(pg. 53)
Figure 3.3a	(pg. 87)
Figure 3.3b	(pg. 89)
Figure 3.3c	(pg. 93)
Figure 3.3d	(pg. 95)
Figure 4.1a	(pg. 113)
Figure 4.1b	(pg. 114)
Figure 4.2a	(pg. 115)
Figure 4.2b	(pg. 117)
Figure 4.2c	(pg. 118)
Figure 4.2d	(pg. 120)
Figure 4.4	(pg. 129)
Figure 5.2a	(pg. 138)
Figure 6.1	(pg. 149)

LIST OF TABLES

- Table 3.3 (pg. 79)
- Table 4.4 (pg. 127)
- Table 5.2 (pg. 138)

ACKNOWLEDGEMENTS

I would like to thank my friends, professors, mentors and colleagues for their advice, support and understanding throughout my graduate studies. Thank you to my primary graduate mentors, Dr. Paul Thompson and Dr. Carrie Bearden. The lessons that I have learned from working with them have helped me become a better researcher and mentor. I offer a special thanks to my family, especially my parents Ward and Melinda, and my brother Andrew Ching for their lifelong support.

Funding Agency Acknowledgements

Projects were also funded by the Alzheimer's Disease Neuroimaging Initiative (ADNI) (NIH Grant U01 AG024904). ADNI is funded by the NIA, NIBIB, and through generous contributions from the following: Abbott, AstraZeneca AB, Bayer Schering Pharma AG, Bristol-Myers Squibb, Eisai Global Clinical Development, Elan Corporation, Genentech, GE Healthcare, GlaxoSmithKline, Innogenetics, Johnson and Johnson, Eli Lilly and Co., Medpace, Inc., Merck and Co., Inc., Novartis AG, Pfizer Inc, F. Hoffman-La Roche, Schering-Plough, Synarc, Inc., as well as nonprofit partners the Alzheimer's Association and Alzheimer's Drug Discovery Foundation, with participation from the U.S. FDA. Private sector contributions to ADNI are facilitated by the Foundation for the National Institutes of Health (www.fnih.org). The grantee organization is the Northern California Institute for Research and Education, and the study is coordinated by the Alzheimer's Disease Cooperative Study at UCSD. ADNI data are disseminated by LONI. This research was also supported by NIMH Grant RO1 MH085953 to Carrie Bearden as well as consortium grant (U54 EB020403) from the NIH Institutes

contributing to the Big Data to Knowledge (BD2K) Initiative, including the NIBIB and NCI. Additional support includes NIH grants P30 AG010129, K01 AG030514, and the Dana Foundation. Algorithm development and image analysis for this study was funded by grants to P.T. from the NIBIB (R01 EB007813, R01 EB008281, R01 EB008432), NICHD (R01 HD050735), and NIA (R01 AG020098), and through the NIH Roadmap for Medical Research, Grants U54-RR021813 (CCB) to Paul Thompson. Christopher Ching was funded, in part, by the UCLA Eugene V. Cota-Robles Fellowship, National Science Foundation Alliance for Graduate Education and the Professoriate Grant, the UCLA Neuroimaging Training Program Fellowship (NIH R90 DA022768 and T90 DA023422), and the UCLA Neurobehavioral Genetics Predoctoral Fellowship (NIH/NIMH 5T32MH073526). The content is solely the responsibility of the authors and does not necessarily represent the official views of the National Institutes of Health.

Co-author Acknowledgements

Chapters 1 through 7 are based on the following studies, I would like to thank all of the co-authors for their contributions.

Adams HH, Hibar DP, Chouraki V, Stein JL, Nyquist PA, Renteria ME, Trompet S, Arias-Vasquez A, Seshadri S, Desrivieres S, Beecham AH, Jahanshad N, Wittfeld K, Van der Lee SJ, Abramovic L, Alhusaini S, Amin N, Andersson M, Arfanakis K, Aribisala BS, Armstrong NJ, Athanasiu L, Axelsson T, Beiser A, Bernard M, Bis JC, Blanken LM, Blanton SH, Bohlken MM, Boks MP, Bralten J, Brickman AM, Carmichael O, Chakravarty MM, Chauhan G, Chen Q, **Ching CR**, Cuellar-Partida G, Braber AD, Doan NT, Ehrlich S, Filippi I, Ge T, Giddaluru S, Goldman AL, Gottesman RF, Greven CU, Grimm O, Griswold ME, Guadalupe T, Hass J, Haukvik UK, Hilal S, Hofer E, Hoehn D, Holmes AJ, Hoogman M, Janowitz D, Jia T, Kasperaviciute D, Kim S, Klein M, Kraemer B, Lee PH, Liao J, Liewald DC, Lopez LM, Luciano M, Macare C, Marquand A, Matarin M, Mather KA, Mattheisen M, Mazoyer B, McKay DR, McWhirter R, Milaneschi Y, Mirza-Schreiber N, Muetzel RL, Maniega SM, Nho K, Nugent AC, Loohuis LM, Oosterlaan J, Pappmeyer M, Pappa I, Pirpamer L, Pudas S, Putz B, Rajan KB, Ramasamy A, Richards JS, Risacher SL, Roiz-Santianez R, Rommelse N, Rose EJ, Royle NA, Rundek T, Samann PG, Satizabal CL, Schmaal L, Schork AJ, Shen L, Shin J, Shumskaya E, Smith AV, Sprooten E, Strike LT, Teumer A, Thomson R, Tordesillas-Gutierrez D, Toro R, Trabzuni D, Vaidya D, Van der Grond J, Van der Meer D, Van Donkelaar MM, Van Eijk KR, Van Erp TG, Van Rooij D, Walton E, Westlye LT, Whelan CD, Windham BG, Winkler AM, Woldehawariat G, Wolf C, Wolfers T, Xu B, Yanek LR, Yang J, Zijdenbos A, Zwiens MP, Agartz I, Aggarwal NT, Almasy L, Ames D, Amouyel P, Andreassen OA, Arepalli S, Assareh AA, Barral S, Bastin ME, Becker DM, Becker JT, Bennett DA, Blangero J, van Bokhoven H, Boomsma DI, Brodaty H, Brouwer RM, Brunner HG, Buckner RL, Buitelaar JK, Bulayeva KB, Cahn W, Calhoun VD, Cannon DM, Cavalleri GL, Chen C, Cheng CY, Cichon S, Cookson MR, Corvin A, Crespo-Facorro B, Curran JE, Czisch M, Dale AM, Davies GE, De Geus EJ, De Jager PL, de Zubicaray GI, Delanty N, Depondt C, DeStefano AL, Dillman A, Djurovic S, Donohoe G, Drevets WC, Duggirala R, Dyer TD, Erk S, Espeseth T, Evans DA, Fedko IO, Fernandez G, Ferrucci L, Fisher SE, Fleischman DA, Ford I, Foroud TM, Fox PT, Francks C, Fukunaga M,

Gibbs JR, Glahn DC, Gollub RL, Goring HH, Grabe HJ, Green RC, Gruber O, Gudnason V, Guelfi S, Hansell NK, Hardy J, Hartman CA, Hashimoto R, Hegenscheid K, Heinz A, Le Hellard S, Hernandez DG, Heslenfeld DJ, Ho BC, Hoekstra PJ, Hoffmann W, Hofman A, Holsboer F, Homuth G, Hosten N, Hottenga JJ, Hulshoff Pol HE, Ikeda M, Ikram MK, Jack CR, Jr., Jenkinson M, Johnson R, Jonsson EG, Jukema JW, Kahn RS, Kanai R, Kloszewska I, Knopman DS, Kochunov P, Kwok JB, Lawrie SM, Lemaitre H, Liu X, Longo DL, Longstreth WT, Jr., Lopez OL, Lovestone S, Martinez O, Martinot JL, Mattay VS, McDonald C, McIntosh AM, McMahon KL, McMahon FJ, Mecocci P, Melle I, Meyer-Lindenberg A, Mohnke S, Montgomery GW, Morris DW, Mosley TH, Muhleisen TW, Muller-Myhsok B, Nalls MA, Nauck M, Nichols TE, Niessen WJ, Nothen MM, Nyberg L, Ohi K, Olvera RL, Ophoff RA, Pandolfo M, Paus T, Pausova Z, Penninx BW, Pike GB, Potkin SG, Psaty BM, Reppermund S, Rietschel M, Roffman JL, Romanczuk-Seiferth N, Rotter JI, Ryten M, Sacco RL, Sachdev PS, Saykin AJ, Schmidt R, Schofield PR, Sigurdsson S, Simmons A, Singleton A, Sisodiya SM, Smith C, Smoller JW, Soininen H, Srikanth V, Steen VM, Stott DJ, Sussmann JE, Thalamuthu A, Tiemeier H, Toga AW, Traynor BJ, Troncoso J, Turner JA, Tzourio C, Uitterlinden AG, Hernandez MC, Van der Brug M, Van der Lugt A, Van der Wee NJ, Van Duijn CM, Van Haren NE, Van TED, Van Tol MJ, Vardarajan BN, Veltman DJ, Vernooij MW, Volzke H, Walter H, Wardlaw JM, Wassink TH, Weale ME, Weinberger DR, Weiner MW, Wen W, Westman E, White T, Wong TY, Wright CB, Zielke HR, Zonderman AB, Deary IJ, DeCarli C, Schmidt H, Martin NG, De Craen AJ, Wright MJ, Launer LJ, Schumann G, Fornage M, Franke B, DeBette S, Medland SE, Ikram MA, Thompson PM. Novel genetic loci underlying human intracranial volume identified through genome-wide association. *Nat Neurosci.* 2016;19(12):1569-82. PMID: 5227112.

Ching CRK, Gutman BA, Hibar DP, Thompson PM, Andreassen OA for The ENIGMA Bipolar Disorder Working Group. Subcortical Shape Morphometry in Bipolar disorder: An ENIGMA Bipolar Disorder Working Group Study. **In preparation**

Ching CRK, Gutman BA, Nir TM, Hua X, Jahanshad N, Harezlak J, Tate DF, Schifitto G, Gongvatana A, Zhong J, Zhu T, Taylor MJ, Campbell TB, Daar ES, Alger JR, Singer E, Cohen RA, Navia B, Thompson OM. High-resolution shape analysis reveals subcortical morphometry

and lymphocyte relationships in HIV+. Organization for Human Brain Mapping (OHBM), Honolulu, Hawaii, 2015.

Ching CRK, Gutman BA, Nir TM, Schonfeld D, Jahanshad N, Hua X, Gongvatana A, Navia B, Cohen RA, Thompson PM. High-resolution shape analysis in HIV+ adults reveals associations between neurocognitive performance and subcortical morphometry. Organization for Human Brain Mapping (OHBM), Honolulu, Hawaii, 2015.

Ching CRK, Gutman BA, Sun D, Villalón-Reina JE, Qu X, Ragothaman A, Isaev D, Zavaliangos-Petropulu A, Lin A, Forsyth JK, Kushan L, Jonas RK, van Amelsvoort T, Bakker G, Kates WR, Campbell LA, McCabe KL, Daly E, Gudbrandsen M, Murphy C, Murphy D, Craig M, Vorstman J, Fiksinski A, Gras L, Ruparel K, Roalf D, Gur R, Schmitt JE, Simon TJ, Goodrich-Hunsaker NJ, Bassett AS, Chow EWC, Butcher N, Vila-Rodriguez F, Doherty J, Cunningham A, van den Bree M, Linden DE, Owen MJ, Moss H, Repetto GM, Crossley NA, Thompson PM, Bearden CE. Mapping Subcortical Brain Alterations in 22q11.2 deletion syndrome: effects of deletion size and convergence with idiopathic psychosis. In preparation to be submitted to The American Journal of Psychiatry

CRK, Hibar DP, McMahon K, de Zubicaray G, Martin N, Wright M, Thompson PM. Genetic clustering reveals thalamic regions with common genetic determination in 640 twins. Organization on Human Brain Mapping Conference, Seattle, WA, 2013.

Ching CRK, Rajagopalan P, Toga AW, Jack Jr CR, Weiner MW, Thompson PM (2012). Elderly people with lower vitamin B12 levels have smaller hippocampal and caudate volumes. Society for Neuroscience Annual Conference, New Orleans, LA, 2012.

Ching CRK, Hua X, Ward C, Gunter J, Bernstein M, Jack Jr CR, Weiner M, Thompson PM. Phantom-based MRI corrections and power to track brain change. ISBI 2012, Barcelona, Spain, May 2-5 2012.

Ching CRK, Hua X, Hibar DP, Ward CP, Gunter JL, Bernstein MA, Jack Jr CR, Weiner MW,

Thompson PM and the Alzheimer's Disease Neuroimaging Initiative (2012). MRI scan acceleration and power to track brain change, MICCAI NIBAD, Nice, France, Oct. 5, 2012.

Ching CR, Hua X, Hibar DP, Ward CP, Gunter JL, Bernstein MA, Jack CR, Jr., Weiner MW, Thompson PM. Does MRI scan acceleration affect power to track brain change? *Neurobiology of aging*. 2015;36 Suppl 1:S167-77. PMID: 4374606.

de Zwarte SMC, Brouwer RM, Agartz I, Alda M, Aleman A, Alpert KI, Bearden CE, Bertolino A, Bois C, Bonvino A, Bramon E, Buimer EEL, Cahn W, Cannon DM, Cannon TD, Caseras X, Castro-Fornieles J, Chen Q, Chung Y, De la Serna E, Di Giorgio A, Doucet GE, Eker MC, Erk S, Fears S, Foley SF, Frangou S, Frankland A, Fullerton JM, Glahn DC, Goghari VM, Gonul AS, Gruber O, de Haan L, Hajek T, Hawkins EL, Hillegers MHJ, Hulshoff HE, Hultman CM, Ingvar M, Jönsson EG, Kane F, Kempton M, Koenis MMG, Kopecek M, Krabbendam L, Krämer B, Lawrie SM, Lenroot RK, Marcelis M, Marsman JC, McDonald C, Michielse S, Mitchell PB, Moreno D, Murray RM, Mwangi B, Najt P, Neilson E, Newport J, van Os J, Overs B, Ozerdem A, Picchioni MM, Richter A, Roberts G, Aydogan AS, Schofield PR, Simsek R, Soares JC, Sugranyes G, Touloupoulou T, Walter H, Wang L, Weinberger DR, Yalin N, Andreassen OA, **Ching CRK**, van Erp TGM, Turner JA, Jahanshad N, Thompson PM, Kahn RS, van Haren NEM, for the ENIGMA Relatives Group. The association between familial risk and brain abnormalities is disease-specific: an ENIGMA–Relatives study of schizophrenia and bipolar disorder. **In review (Biological Psychiatry 2018)**.

Eyler LT, Thompson PM, **Ching CRK**, Andreassen OA, for the ENIGMA Bipolar Disorder Working Group. Advanced Brain Age and it's Clinical Correlates in Bipolar Disorder: A Global, Multi-Site Anlalysis Data from the ENIGMA Bipolar Disorder Working Group. **In preparation**

Favre P, Pauling P, Stout J, Hozer F, Sarrazin S, Abé C, Alda M, Alloza C, Alonso-Lana S, Andreassen OA, Baune BT, Benedetti F, Busatto GF, Caseras X, Chaim-Avancini MK, **Ching CRK**, Dannlowski U, Deppe M, Eyler LT, Fatjo-Vilas M, SF, Grotegerd D, Hajek T, Haukvik UK, Howells FM, Jahanshad N, Kugel H, Lagerberg TV, Lawrie SM, Linke JO, McIntosh A, Elisa M.T Melloni EMT, Mitchell PB, Pomarol-Clotet E, Repple J, Rosa PGP, Salvador R, Sarró

S, Schofield PR, Serpa MH, Sim K, Stein DJ, Sussmann JE, Temmingh HS, Thompson PM, Verdolini N, Vieta E, Wessa M, Whalley HC, Zanetti MV, Leboyer M, Mangin JF, Henry C, Duchesnay E, Houenou J, for the ENIGMA Bipolar Disorder Working Group. Widespread White Matter Microstructural Abnormalities in Bipolar Disorder: Evidence from mega, meta and machine learning analyses across 3033 individuals from the ENIGMA Bipolar Disorder Working Group. **In review (Biological Psychiatry 2018)**

Fouche J, Groenewold N, Heany S, Lochner C, Alonso P, Busatto GF, Cardoner N, Cath DC, **Ching CRK**, Denys D, Fukui K, Gutman B, Hoexter MQ, Jahanshad N, Jang JH, Jung WH, Kim SN, Kwon JS, Mataix-Cols D, Menchon JM, Migue EC, Nakamae T, Narumoto J, Nishida S, Phillips ML, Pujol J, Remijnse PL, Sakai Y, Sato JR, Schweren L, Shin NY, Soriano-Mas C, Thompson PM, Yamada K, Veltman DJ, van den Heuvel OA, Stein DJ. Shape analysis of subcortical structures in obsessive-compulsive disorder: a multi-site analysis of the OCD Brain Imaging Consortium. **Manuscript in preparation.**

Grasby KL, Jahanshad N, Painter JN, Colodro-Conde L, Bralten J, Hibar DP, Lind PA, Pizzagalli F, **Ching CR**, McMahon MA, Shatokhina N, Zsembik LCP, Agartz I, Alhusaini S, Almeida MA, Alnæs D, Amlien IK, Andersson M, Ard T, Armstrong NJ, Ashley-Koch A, Bernard M, Brouwer RM, Buimer EE, Bülow R, Bürger C, Cannon DM, Chakravarty M, Chen Q, Cheung JW, Couvy-Duchesne B, Dale AM, Dalvie S, de Araujo TK, de Zubicaray GI, de Zwarte SM, den Braber A, Doan NT, Dohm K, Ehrlich S, Engelbrecht H-R, Erk S, Fan CC, Fedko IO, Foley SF, Ford JM, Fukunaga M, Garrett ME, Ge T, Giddaluru S, Goldman AL, Groenewold NA, Grotegerd D, Gurholt TP, Gutman BA, Hansell NK, Harris MA, Harrison MB, Haswell CC, Hauser M, Herms S, Heslenfeld DJ, Ho NF, Hoehn D, Hoffmann P, Holleran L, Hoogman M, Hottenga J-J, Ikeda M, Janowitz D, Jansen IE, Jia T, Jockwitz C, Kanai R, Karama S, Kasperaviciute D, Kaufmann T, Kelly S, Kikuchi M, Klein M, Knapp M, Knodt AR, Krämer B, Lam M, Lancaster TM, Lee PH, Lett TA, Lewis LB, Lopes-Cendes I, Luciano M, Macciardi F, Marquand AF, Mathias SR, Melzer TR, Milaneschi Y, Mirza-Schreiber N, Moreira JC, Mühleisen TW, Müller-Myhsok B, Najt P, Nakahara S, Nho K, Olde Loohuis LM, Papadopoulos Orfanos D, Pearson JF, Pitcher TL, Pütz B, Ragothaman A, Rashid FM, Redlich R, Reinbold CS, Repple J, Richard G, Riedel BC, Risacher SL, Rocha CS, Roth Mota N, Salminen L, Saremi A,

Saykin AJ, Schlag F, Schmaal L, Schofield PR, Secolin R, Shapland CY, Shen L, Shin J, Shumskaya E, S nderby IE, Sprooten E, Strike LT, Tansey KE, Teumer A, Thalamuthu A, Thomopoulos SI, Tordesillas-Guti rrez D, Turner JA, Uhlmann A, Vallerga CL, van der Meer D, van Donkelaar MM, van Eijk L, van Erp TG, van Haren NE, Van Rooij D, van Tol M-J, Veldink JH, Verhoef E, Walton E, Wang M, Wang Y, Wardlaw JM, Wen W, Westlye LT, Whelan CD, Witt SH, Wittfeld K, Wolf C, Wolfers T, Yasuda CL, Zaremba D, Zhang Z, Zhu AH, Zwiers MP, Artiges E, Assareh AA, Ayesa-Arriola R, Belger A, Brandt CL, Brown GG, Cichon S, Curran JE, Davies GE, Degenhardt F, Dietsche B, Djurovic S, Doherty CP, Espiritu R, Garijo D, Gil Y, Gowland PA, Green RC, H usler AN, Heindel W, Ho B-C, Hoffmann WU, Holsboer F, Homuth G, Hosten N, Jack CR, Jang M, Jansen A, Kolsk r K, Koops S, Krug A, Lim KO, Luykx JJ, Mathalon DH, Mather KA, Mattay VS, Matthews S, Mayoral Van Son J, McEwen SC, Melle I, Morris DW, Mueller BA, Nauck M, Nordvik JE, N then MM, O'Leary DS, Opel N, Paill re Martinot M-L, Pike GB, Preda A, Quinlan EB, Ratnakar V, Reppermund S, Steen VM, Torres FR, Veltman DJ, Voyvodic JT, Whelan R, White T, Yamamori H, Adams HH, Bis JC, Debette S, Decarli C, Fornage M, Gudnason V, Hofer E, Ikram MA, Launer L, Longstreth WT, Lopez OL, Mazoyer B, Mosley TH, Roshchupkin GV, Satizabal CL, Schmidt R, Seshadri S, Yang Q, Alvim MK, Ames D, Anderson TJ, Andreassen OA, Arias-Vasquez A, Bastin ME, Baune BT, Blangero J, Boomsma DI, Brodaty H, Brunner HG, Buckner RL, Buitelaar JK, Bustillo JR, Cahn W, Calhoun V, Caseras X, Caspers S, Cavalleri GL, Cendes F, Corvin A, Crespo-Facorro B, Dalrymple-Alford JC, Dannlowski U, de Geus EJ, Deary IJ, Delanty N, Depondt C, Desriv eres S, Donohoe G, Espeseth T, Fern andez G, Fisher SE, Flor H, Forstner AJ, Francks C, Franke B, Glahn DC, Gollub RL, Grabe HJ, Gruber O, H berg AK, Hariri AR, Hartman CA, Hashimoto R, Heinz A, Hillegers MH, Hoekstra PJ, Holmes AJ, Hong LE, Hopkins WD, Hulshoff Pol HE, Jernigan TL, J nsson EG, Kahn RS, Kennedy MA, Kircher TT, Kochunov P, Kwok JB, Le Hellard S, Martin NG, Martinot J-L, McDonald C, McMahon KL, Meyer-Lindenberg A, Morey RA, Nyberg L, Oosterlaan J, Ophoff RA, Paus T, Pausova Z, Penninx BW, Polderman TJ, Posthuma D, Rietschel M, Roffman JL, Rowland LM, Sachdev PS, S mann PG, Schumann G, Sim K, Sisodiya SM, Smoller JW, Sommer IE, St Pourcain B, Stein DJ, Toga AW, Trollor JN, Van der Wee NJ, van't Ent D, V lzke H, Walter H, Weber B, Weinberger DR, Wright MJ, Zhou J, Stein JL, Thompson PM, Medland SE. The genetic architecture of the human cerebral cortex. **In Review (Nature 2018)**. BioRxiv

doi: <https://doi.org/10.1101/399402>

Gutman BA, Jahanshad N, **Ching CR**, Wang Y, Kochunov PV, Nichols TE, Thompson PM. Medial Demons Registration Localizes The Degree of Genetic Influence Over Subcortical Shape Variability: An N= 1480 Meta-Analysis. *Proc IEEE Int Symp Biomed Imaging*. 2015;2015:1402-6. PMID: 4578221.

Gutman BA, van Erp TGM, Alpert K, Isaev D, Zavaliangos-Petropulu A, Ragothaman A, Saremi A, Calhoun V, Glahn DC, Satterthwaite T, Andreassen OA, Borgwardt S, Howells F, Voineskos A, Radua J, Huang AJ, Weideman A, Potkin SG, Facorro BC, Shen L, Lebedeva I, Spalletta G, Donohoe G, Kochunov P, Trung Doan N, Agartz I, Harrisberger F, Stein DJ, Dickie EW, Canales-Rodriguez EJ, Roiz-Santiañez R, Cong S, Tomyshev A, Piras F, Wright M, McMahon KL, de Zubicaray G, **Ching CRK**, Jahanshad N, Thompson PM, Turner JA and Wang L for the ENIGMA Schizophrenia Working Group. A Meta-Analysis of Deep Brain Structural Shape Abnormalities in 2,763 Individuals with Schizophrenia Compared to 3,768 Healthy Volunteers via the ENIGMA Consortium. **Submitted (Molecular Psychiatry)**

Han LK, Dinga R, Hahn T, **Ching CRK**, Eyer L, Aftanas L, Aghajani M, Aleman A, Baune B, Berger K, Brak I, Busatto Filho G, Carballedo A, Connolly C, Couvy-Duchesne B, Cullen K, Dannlowski U, Davey C, Dima D, Duran F, Enneking V, Filimonova E, Frenzel S, Frodl T, Fu C, Godlewska B, Gotlib I, Grabe H, Groenewold N, Grotegerd D, Gruber O, Hall G, Harrison B, Hatton S, Hermesdorf M, Hickie I, Ho T, Hosten N, Jansen A, Kahler C, Kircher T, Klimes-Dougan B, Kramer B, Krug A, Lagopoulos J, Leenings R, MacMaster F, MacQueen G, McIntosh A, McLellan Q, McMahon K, Medland S, Mueller B, Mwangi B, Osipov E, Portella M, Pozzi E, Reneman L, Repple J, Rosa P, Sacchet M, Saemann P, Schnell K, Schranke A, Simulionyte E, Soares J, Sommer J, Stein D, Steinstrater O, Strike L, Thomopoulos S, van Tol M-J, Veer I, Vermeiren R, Walter H, van der Wee N, van der Werff S, Whalley H, Winter N, Wittfeld K, Wright M, Wu M-J, Volzke H, Yang T, Zannias V, de Zubicaray G, Zunta-Soares G, Abe C, Alda M, Andreassen O, Boen E, Bonnin C, Canales-Rodriguez E, Cannon D, Caseras X, Chaim-Avancini T, Elvsashagen T, Favre P, Foley S, Fullerton J, Goikolea J, Haarman B, Hajek T, Henry C, Houenou J, Howells F, Ingvar M, Kuplicki R, Lafer B, Landen M, Machado-Vieira

R, Malt U, McDonald C, Mitchell P, Nabulsi L, Otaduy M, Overs B, Polosan M, Pomarol-Clotet E, Radua J, Rive M, Roberts G, Ruhe H, Salvador R, Sarro S, Satterthwaite T, Savitz J, Schene A, Schofield P, Serpa M, Sim K, Soeiro-de-Souza M, Sutherland A, Temmingh H, Timmons G, Uhlmann A, Vieta E, Wolf D, Zanetti M, Jahanshad N, Thompson P, Veltman D, Penninx B, Marquand A, Cole J, Schmaal L. Brain Aging in Major Depressive Disorder: Results from the ENIGMA Major Depressive Disorder working group. **In submission (Lancet Psychiatry)**
BioRxiv doi: <https://doi.org/10.1101/560623>

Harrison TM, **Ching CR**, Andrews AM. A Model For Teaching Advanced Neuroscience Methods: A Student-Run Seminar to Increase Practical Understanding and Confidence. *J Undergrad Neurosci Educ.* 2016;15(1):A5-A10. PMID: 5105964

Haukvik UK, Gurholt TP, Nerland S, Thompson PM, **Ching CRK**, Andreassen OA, Agartz I, for the ENIGMA Bipolar Disorder Working Group. In vivo hippocampal subfield volumes in bipolar disorder: A multisite ENIGMA mega-approach. **In preparation (Molecular Psychiatry)**

Hibar DP, Stein JL, Renteria ME, Arias-Vasquez A, Desrivieres S, Jahanshad N, Toro R, Wittfeld K, Abramovic L, Andersson M, Aribisala BS, Armstrong NJ, Bernard M, Bohlken MM, Boks MP, Bralten J, Brown AA, Chakravarty MM, Chen Q, **Ching CR**, Cuellar-Partida G, den Braber A, Giddaluru S, Goldman AL, Grimm O, Guadalupe T, Hass J, Woldehawariat G, Holmes AJ, Hoogman M, Janowitz D, Jia T, Kim S, Klein M, Kraemer B, Lee PH, Olde Loohuis LM, Luciano M, Macare C, Mather KA, Mattheisen M, Milaneschi Y, Nho K, Pappmeyer M, Ramasamy A, Risacher SL, Roiz-Santianez R, Rose EJ, Salami A, Samann PG, Schmaal L, Schork AJ, Shin J, Strike LT, Teumer A, van Donkelaar MM, van Eijk KR, Walters RK, Westlye LT, Whelan CD, Winkler AM, Zwiers MP, Alhusaini S, Athanasiu L, Ehrlich S, Hakobjan MM, Hartberg CB, Haukvik UK, Heister AJ, Hoehn D, Kasperaviciute D, Liewald DC, Lopez LM, Makkinje RR, Matarin M, Naber MA, McKay DR, Needham M, Nugent AC, Putz B, Royle NA, Shen L, Sprooten E, Trabzuni D, van der Marel SS, van Hulzen KJ, Walton E, Wolf C, Almasy L, Ames D, Arepalli S, Assareh AA, Bastin ME, Brodaty H, Bulayeva KB, Carless MA, Cichon S, Corvin A, Curran JE, Czisch M, de Zubicaray GI, Dillman A, Duggirala R, Dyer TD, Erk S, Fedko IO, Ferrucci L, Foroud TM, Fox PT, Fukunaga M, Gibbs JR, Goring

HH, Green RC, Guelfi S, Hansell NK, Hartman CA, Hegenscheid K, Heinz A, Hernandez DG, Heslenfeld DJ, Hoekstra PJ, Holsboer F, Homuth G, Hottenga JJ, Ikeda M, Jack CR, Jr., Jenkinson M, Johnson R, Kanai R, Keil M, Kent JW, Jr., Kochunov P, Kwok JB, Lawrie SM, Liu X, Longo DL, McMahon KL, Meisenzahl E, Melle I, Mohnke S, Montgomery GW, Mostert JC, Muhleisen TW, Nalls MA, Nichols TE, Nilsson LG, Nothen MM, Ohi K, Olvera RL, Perez-Iglesias R, Pike GB, Potkin SG, Reinvang I, Reppermund S, Rietschel M, Romanczuk-Seiferth N, Rosen GD, Rujescu D, Schnell K, Schofield PR, Smith C, Steen VM, Sussmann JE, Thalamuthu A, Toga AW, Traynor BJ, Troncoso J, Turner JA, Valdes Hernandez MC, van 't Ent D, van der Brug M, van der Wee NJ, van Tol MJ, Veltman DJ, Wassink TH, Westman E, Zielke RH, Zonderman AB, Ashbrook DG, Hager R, Lu L, McMahon FJ, Morris DW, Williams RW, Brunner HG, Buckner RL, Buitelaar JK, Cahn W, Calhoun VD, Cavalleri GL, Crespo-Facorro B, Dale AM, Davies GE, Delanty N, Depondt C, Djurovic S, Drevets WC, Espeseth T, Gollub RL, Ho BC, Hoffmann W, Hosten N, Kahn RS, Le Hellard S, Meyer-Lindenberg A, Muller-Myhsok B, Nauck M, Nyberg L, Pandolfo M, Penninx BW, Roffman JL, Sisodiya SM, Smoller JW, van Bokhoven H, van Haren NE, Volzke H, Walter H, Weiner MW, Wen W, White T, Agartz I, Andreassen OA, Blangero J, Boomsma DI, Brouwer RM, Cannon DM, Cookson MR, de Geus EJ, Deary IJ, Donohoe G, Fernandez G, Fisher SE, Francks C, Glahn DC, Grabe HJ, Gruber O, Hardy J, Hashimoto R, Hulshoff Pol HE, Jonsson EG, Kloszewska I, Lovestone S, Mattay VS, Mecocci P, McDonald C, McIntosh AM, Ophoff RA, Paus T, Pausova Z, Ryten M, Sachdev PS, Saykin AJ, Simmons A, Singleton A, Soininen H, Wardlaw JM, Weale ME, Weinberger DR, Adams HH, Launer LJ, Seiler S, Schmidt R, Chauhan G, Satizabal CL, Becker JT, Yanek L, van der Lee SJ, Ebling M, Fischl B, Longstreth WT, Jr., Greve D, Schmidt H, Nyquist P, Vinke LN, van Duijn CM, Xue L, Mazoyer B, Bis JC, Gudnason V, Seshadri S, Ikram MA, Martin NG, Wright MJ, Schumann G, Franke B, Thompson PM, Medland SE. Common genetic variants influence human subcortical brain structures. *Nature*. 2015;520(7546):224-9. PMID: 4393366.

Hibar DP, Westlye LT, Doan NT, Jahanshad N, Cheung JW, **Ching CRK**, Versace A, Bilderbeck AC, Uhlmann A, Mwangi B, Kramer B, Overs B, Hartberg CB, Abe C, Dima D, Grotegerd D, Sprooten E, Boen E, Jimenez E, Howells FM, Delvecchio G, Temmingh H, Starke J, Almeida JRC, Goikolea JM, Houenou J, Beard LM, Rauer L, Abramovic L, Bonnin M, Ponteduro MF, Keil M, Rive MM, Yao N, Yalin N, Najt P, Rosa PG, Redlich R, Trost S,

Hagenaars S, Fears SC, Alonso-Lana S, van Erp TGM, Nickson T, Chaim-Avancini TM, Meier TB, Elvsashagen T, Haukvik UK, Lee WH, Schene AH, Lloyd AJ, Young AH, Nugent A, Dale AM, Pfennig A, McIntosh AM, Lafer B, Baune BT, Ekman CJ, Zarate CA, Bearden CE, Henry C, Simhandl C, McDonald C, Bourne C, Stein DJ, Wolf DH, Cannon DM, Glahn DC, Veltman DJ, Pomarol-Clotet E, Vieta E, Canales-Rodriguez EJ, Nery FG, Duran FLS, Busatto GF, Roberts G, Pearlson GD, Goodwin GM, Kugel H, Whalley HC, Ruhe HG, Soares JC, Fullerton JM, Rybakowski JK, Savitz J, Chaim KT, Fatjo-Vilas M, Soeiro-de-Souza MG, Boks MP, Zanetti MV, Otaduy MCG, Schaufelberger MS, Alda M, Ingvar M, Phillips ML, Kempton MJ, Bauer M, Landen M, Lawrence NS, van Haren NEM, Horn NR, Freimer NB, Gruber O, Schofield PR, Mitchell PB, Kahn RS, Lenroot R, Machado-Vieira R, Ophoff RA, Sarro S, Frangou S, Satterthwaite TD, Hajek T, Dannlowski U, Malt UF, Arolt V, Gattaz WF, Drevets WC, Caseras X, Agartz I, Thompson PM, Andreassen OA. Cortical abnormalities in bipolar disorder: an MRI analysis of 6503 individuals from the ENIGMA Bipolar Disorder Working Group. *Mol Psychiatry*. 2018;23(4):932-42. PMID: 5668195. doi:10.1038/mp.2017.73.

Hua X, **Ching CRK**, Mezher A, Gutman BA, Hibar DP, Bhatt P, Leow AD, Jack CR, Jr., Bernstein MA, Weiner MW, Thompson PM. MRI-based brain atrophy rates in ADNI phase 2: acceleration and enrichment considerations for clinical trials. *Neurobiology of aging*. 2016;37:26-37. PMID: 4827255.

Hua X, Hibar DP, **Ching CR**, Boyle CP, Rajagopalan P, Gutman BA, Leow AD, Toga AW, Jack CR, Jr., Harvey D, Weiner MW, Thompson PM. Unbiased tensor-based morphometry: improved robustness and sample size estimates for Alzheimer's disease clinical trials. *NeuroImage*. 2013;66:648-61. PMID: 3785376.

Jack CR, Jr., Barnes J, Bernstein MA, Borowski BJ, Brewer J, Clegg S, Dale AM, Carmichael O, **Ching C**, DeCarli C, Desikan RS, Fennema-Notestine C, Fjell AM, Fletcher E, Fox NC, Gunter J, Gutman BA, Holland D, Hua X, Insel P, Kantarci K, Killiany RJ, Krueger G, Leung KK, Mackin S, Maillard P, Malone IB, Mattsson N, McEvoy L, Modat M, Mueller S, Nosheny R, Ourselin S, Schuff N, Senjem ML, Simonson A, Thompson PM, Rettmann D, Vemuri P, Walhovd K, Zhao Y, Zuk S, Weiner M. Magnetic resonance imaging in Alzheimer's Disease

Neuroimaging Initiative 2. *Alzheimers Dement*. 2015;11(7):740-56. PMID: 4523217.

Looi JC, Rajagopalan P, Walterfang M, Madsen SK, Thompson PM, Macfarlane MD, **Ching C**, Chua P, Velakoulis D. Differential putaminal morphology in Huntington's disease, frontotemporal dementia and Alzheimer's disease. *Aust N Z J Psychiatry*. 2012;46(12):1145-58. PMID: 4113021

McMahon MAB, D Garijo, R Espiritu, F Rashid, M Jang, T Patted, V Knight, **CRK Ching**, V Ratnakar, Y Gil, PM Thompson, N Jahanshad. ENIGMA-ODS: A Platform for Global Neuroscience Collaborations in the ENIGMA Consortium, Society of Biological Psychiatry 2018, New York, May 2018.

Nir TM, Jahanshad N, **Ching CRK**, Cohen RA, Harezlak J, Schifitto G, Lam HY, Hua X, Zhong J, Zhu T, Taylor MJ, Campbell TB, Daar ES, Singer EJ, Alger JR, Thompson PM, Navia BA, On behalf of the HIV Neuroimaging Consortium. Progressive Brain Atrophy in Chronically Infected and Treated HIV+ Individuals. Accepted Journal of NeuroVirology January 2019

Nunes A, Schnack HG, **Ching CRK**, Agartz I, Akudjedu TN, Alda M, Alnaes D, Alonso-Lana S, Bauer J, Baune BT, Boen E, Bonnin CDM, Busatto GF, Canales-Rodriguez EJ, Cannon DM, Caseras X, Chaim-Avancini TM, Dannlowski U, Diaz-Zuluaga AM, Dietsche B, Doan NT, Duchesnay E, Elvsashagen T, Emden D, Eyler LT, Fatjo-Vilas M, Favre P, Foley SF, Fullerton JM, Glahn DC, Goikolea JM, Grotegerd D, Hahn T, Henry C, Hibar DP, Houenou J, Howells FM, Jahanshad N, Kaufmann T, Kenney J, Kircher TTJ, Krug A, Lagerberg TV, Lenroot RK, Lopez-Jaramillo C, Machado-Vieira R, Malt UF, McDonald C, Mitchell PB, Mwangi B, Nabulsi L, Opel N, Overs BJ, Pineda-Zapata JA, Pomarol-Clotet E, Redlich R, Roberts G, Rosa PG, Salvador R, Satterthwaite TD, Soares JC, Stein DJ, Temmingh HS, Trappenberg T, Uhlmann A, van Haren NEM, Vieta E, Westlye LT, Wolf DH, Yuksel D, Zanetti MV, Andreassen OA, Thompson PM, Hajek T. Using structural MRI to identify bipolar disorders - 13 site machine learning study in 3020 individuals from the ENIGMA Bipolar Disorders Working Group. *Mol Psychiatry*. 2018. doi:10.1038/s41380-018-0228-9.

Lin A, **Ching CRK**, Vajdi A, Sun D, Jonas RK, Jalbrzikowski M, Kushan-Wells L, Pacheco Hansen L, Krikorian E, Gutman B, Dokoru D, Helleman G, Thompson PM, Bearden CE. Mapping 22q11.2 Gene Dosage Effects on Brain Morphometry. *The Journal of Neuroscience*. 2017;37(26):6183-99. doi:10.1523/JNEUROSCI.3759-16.2017

Petrov D, Gutman BA, Yu SJ, van Erp TGM, Turner JA, Schmaal L, Veltman D, Wang L, Alpert K, Isaev D, Zavaliangos-Petropulu A, **Ching CRK**, Calhoun V, Glahn D, Satterthwaite TD, Andreasen OA, Borgwardt S, Howells F, Groenewold N, Voineskos A, Radua J, Potkin SG, Crespo-Facorro B, Tordesillas-Gutierrez D, Shen L, Lebedeva I, Spalletta G, Donohoe G, Kochunov P, Rosa PGP, James A, Dannlowski U, Baune BT, Aleman A, Gotlib IH, Walter H, Walter M, Soares JC, Ehrlich S, Gur RC, Doan NT, Agartz I, Westlye LT, Harrisberger F, Riecher-Rossler A, Uhlmann A, Stein DJ, Dickie EW, Pomarol-Clotet E, Fuentes-Claramonte P, Canales-Rodriguez EJ, Salvador R, Huang AJ, Roiz-Santianez R, Cong S, Tomyshev A, Piras F, Vecchio D, Banaj N, Ciullo V, Hong E, Busatto G, Zanetti MV, Serpa MH, Cervenka S, Kelly S, Grotegerd D, Sacchet MD, Veer IM, Li M, Wu MJ, Irungu B, Walton E, Thompson PM. Machine Learning for Large-Scale Quality Control of 3D Shape Models in Neuroimaging. *Mach Learn Med Imaging*. 2017;10541:371-8. PMID: 6049825.

Satizabal CL, Adams HHH, Hibar DP, White CC, Stein JL, Scholz M, Sargurupremraj M, Jahanshad N, Smith AV, Bis JC, Jian X, Luciano M, Hofer E, Teumer A, van der Lee SJ, Yang J, Yanek LR, Lee TV, Li S, Hu Y, Koh JY, Eicher JD, Desrivieres S, Arias-Vasquez A, Chauhan G, Athanasiu L, Renteria ME, Kim S, Hohn D, Armstrong NJ, Chen Q, Holmes AJ, den Braber A, Kloszewska I, Andersson M, Espeseth T, Grimm O, Abramovic L, Alhusaini S, Milaneschi Y, Pappmeyer M, Axelsson T, Ehrlich S, Roiz-Santianez R, Kraemer B, Haberg AK, Jones HJ, Pike GB, Stein DJ, Stevens A, Bralten J, Vernooij MW, Harris TB, Filippi I, Witte AV, Guadalupe T, Wittfeld K, Mosley TH, Becker JT, Doan NT, Hagenaars SP, Saba Y, Cuellar-Partida G, Amin N, Hilal S, Nho K, Karbalai N, Arfanakis K, Becker DM, Ames D, Goldman AL, Lee PH, Boomsma DI, Lovestone S, Giddaluru S, Le Hellard S, Mattheisen M, Bohlken MM, Kasperaviciute D, Schmaal L, Lawrie SM, Agartz I, Walton E, Tordesillas-Gutierrez D, Davies GE, Shin J, Ipser JC, Vinke LN, Hoogman M, Knol MJ, Jia T, Burkhardt R, Klein M, Crivello F, Janowitz D, Carmichael O, Haukvik UK, Aribisala BS, Schmidt H, Strike LT, Cheng

C-Y, Risacher SL, Putz B, Fleischman DA, Assareh AA, Mattay VS, Buckner RL, Mecocci P, Dale AM, Cichon S, Boks MP, Matarin M, Penninx BWJH, Calhoun VD, Chakravarty MM, Marquand A, Macare C, Masouleh SK, Oosterlaan J, Amouyel P, Hegenscheid K, Rotter JI, Schork AJ, Liewald DCM, De Zubicaray GI, Wong TY, Shen L, Samann PG, Brodaty H, Roffman JL, De Geus EJC, Tsolaki M, Erk S, Van Eijk KR, Cavalleri GL, Van der Wee NJA, McIntosh AM, Gollub RL, Bulayeva KB, Bernard M, Richards JS, Himali JJ, Loeffler M, Rommelse N, Hoffmann W, Westlye LT, Valdes Hernandez MC, Hansell NK, Van Erp TGM, Wolf C, Kwok JBJ, Vellas B, Heinz A, Olde Loohuis LM, Delanty N, Ho B-C, **Ching CRK**, Shumskaya E, Singh B, Hofman A, Van der Meer D, Homuth G, Psaty BM, Bastin M, Montgomery GW, Foroud TM, Reppermund S, Hottenga J-J, Simmons A, Meyer-Lindenberg A, Cahn W, Whelan CD, Van Donkelaar MMJ, Yang Q, Hosten N, Green RC, Thalamuthu A, Mohnke S, Hulshoff Pol HE, Lin H, Jack CR, Schofield PR, Muhleisen TW, Maillard P, Potkin SG, Wen W, Fletcher E, Toga AW, Gruber O, Huentelman M, Davey Smith G, Launer LJ, Nyberg L, Jonsson EG, Crespo-Facorro B, Koen N, Greve D, Uitterlinden AG, Weinberger DR, Steen VM, Fedko IO, Groenewold NA, Niessen WJ, Toro R, Tzourio C, Longstreth WT, Ikram MK, Smoller JW, Van Tol M-J, Sussmann JE, Paus T, Lemaitre H, Mazoyer B, Andreassen OA, Holsboer F, Depondt C, Veltman DJ, Turner JA, Pausova Z, Schumann G, Van Rooij D, Djurovic S, Deary IJ, McMahon KL, Muller-Myhsok B, Brouwer RM, Soininen H, Pandolfo M, Wassink TH, Cheung JW, Wolfers T, Martinot J-L, Zwiers MP, Nauck M, Melle I, Martin NG, Kanai R, Westman E, Kahn RS, Sisodiya SM, White T, Saremi A, van Bokhoven H, Brunner HG, Volzke H, Wright MJ, Van 't Ent D, Nothen MM, Ophoff RA, Buitelaar JK, Fernandez G, Sachdev PS, Rietschel M, Van Haren NEM, Fisher SE, Beiser AS, Francks C, Saykin AJ, Mather KA, Romanczuk-Seiferth N, Hartman CA, DeStefano AL, Heslenfeld DJ, Weiner MW, Walter H, Hoekstra PJ, Nyquist PA, Franke B, Bennett DA, Grabe HJ, Johnson AD, Chen C, van Duijn CM, Lopez OL, Fornage M, Wardlaw JA, Schmidt R, DeCarli C, De Jager PL, Villringer A, DeBette S, Gudnason V, Medland SE, Shulman JM, Thompson PM, Seshadri S, Ikram MA. Genetic Architecture of Subcortical Brain Structures in Over 40,000 Individuals Worldwide. **Submitted (Nature Genetics)**. BioRxiv doi: <https://doi.org/10.1101/173831>

Salminen LE, Wilcox R, Zhu AH, Riedel BC, **Ching CRK**, Boyle CP, Knight V, Saremi A, Rashid F, Thomopoulos SI, Harrison MB, Ragothaman A, Medland SE, Thompson PM,

Jahanshad N. Altered cortical brain structure and increased risk for disease seen decades after perinatal exposure to maternal smoking: A study of 9,000 adults in the UK Biobank. **Submitted (Accepted Cerebral Cortex March 2019)** BioRxiv doi: <https://doi.org/10.1101/471839>

Schmaal L, **Ching CRK**, McMahon AB, Jahanshad N, Thompson PM. Neuroimaging, Genetics and Personalized Psychiatry: Developments and Opportunities from the ENIGMA consortium. Submitted book chapter to “Personalized Psychiatry” edited by Dr. Bernhard Baune.

Sun D, **Ching CRK**, Lin A, Forsyth JK, Kushan L, Vajdi A, Jalbrzikowski M, Hansen L, Villalon-Reina JE, Qu X, Jonas RK, van Amelsvoort T, Bakker G, Kates WR, Antshel KM, Fremont W, Campbell LE, McCabe KL, Daly E, Gudbrandsen M, Murphy CM, Murphy D, Craig M, Vorstman J, Fiksinski A, Koops S, Ruparel K, Roalf DR, Gur RE, Schmitt JE, Simon TJ, Goodrich-Hunsaker NJ, Durdle CA, Bassett AS, Chow EWC, Butcher NJ, Vila-Rodriguez F, Doherty J, Cunningham A, van den Bree MBM, Linden DEJ, Moss H, Owen MJ, Murphy KC, McDonald-McGinn DM, Emanuel B, van Erp TGM, Turner JA, Thompson PM, Bearden CE. Large-scale mapping of cortical alterations in 22q11.2 deletion syndrome: Convergence with idiopathic psychosis and effects of deletion size. *Mol Psychiatry*. 2018. doi:10.1038/s41380-018-0078-5

Tao C, Nichols TE, Hua X, **Ching CRK**, Rolls ET, Thompson PM, Feng J. Generalized reduced rank latent factor regression for high dimensional tensor fields, and neuroimaging-genetic applications. *NeuroImage*. 2017;144(Pt A):35-57. PMID: 5798650.

Thompson PM, **Ching CRK**, Dennis EL, Salminen LE, Turner JA, van Erp TGM, Jahanshad N. Big data initiatives in psychiatry: Global neuroimaging studies. Submitted book chapter to “Neuroimaging in Schizophrenia” edited by Marek Kubicki and Martha E. Shenton (to be published by Springer Verlag 2019)

Thompson PM, Stein JL, Medland SE, Hibar DP, Vasquez AA, Renteria ME, Toro R, Jahanshad N, Schumann G, Franke B, Wright MJ, Martin NG, Agartz I, Alda M, Alhusaini S, Almasry L, Almeida J, Alpert K, Andreasen NC, Andreassen OA, Apostolova LG, Appel K, Armstrong NJ,

Aribisala B, Bastin ME, Bauer M, Bearden CE, Bergmann O, Binder EB, Blangero J, Bockholt HJ, Boen E, Bois C, Boomsma DI, Booth T, Bowman IJ, Bralten J, Brouwer RM, Brunner HG, Brohawn DG, Buckner RL, Buitelaar J, Bulayeva K, Bustillo JR, Calhoun VD, Cannon DM, Cantor RM, Carless MA, Caseras X, Cavalleri GL, Chakravarty MM, Chang KD, **Ching CR**, Christoforou A, Cichon S, Clark VP, Conrod P, Coppola G, Crespo-Facorro B, Curran JE, Czisch M, Deary IJ, de Geus EJ, den Braber A, Delvecchio G, Depondt C, de Haan L, de Zubicaray GI, Dima D, Dimitrova R, Djurovic S, Dong H, Donohoe G, Duggirala R, Dyer TD, Ehrlich S, Ekman CJ, Elvsashagen T, Emsell L, Erk S, Espeseth T, Fagerness J, Fears S, Fedko I, Fernandez G, Fisher SE, Foroud T, Fox PT, Francks C, Frangou S, Frey EM, Frodl T, Frouin V, Garavan H, Giddaluru S, Glahn DC, Godlewska B, Goldstein RZ, Gollub RL, Grabe HJ, Grimm O, Gruber O, Guadalupe T, Gur RE, Gur RC, Goring HH, Hagenaars S, Hajek T, Hall GB, Hall J, Hardy J, Hartman CA, Hass J, Hatton SN, Haukvik UK, Hegenscheid K, Heinz A, Hickie IB, Ho BC, Hoehn D, Hoekstra PJ, Hollinshead M, Holmes AJ, Homuth G, Hoogman M, Hong LE, Hosten N, Hottenga JJ, Hulshoff Pol HE, Hwang KS, Jack CR, Jr., Jenkinson M, Johnston C, Jonsson EG, Kahn RS, Kasperaviciute D, Kelly S, Kim S, Kochunov P, Koenders L, Kramer B, Kwok JB, Lagopoulos J, Laje G, Landen M, Landman BA, Lauriello J, Lawrie SM, Lee PH, Le Hellard S, Lemaitre H, Leonardo CD, Li CS, Liberg B, Liewald DC, Liu X, Lopez LM, Loth E, Lourdasamy A, Luciano M, Macciardi F, Machielsen MW, Macqueen GM, Malt UF, Mandl R, Manoach DS, Martinot JL, Matarin M, Mather KA, Mattheisen M, Mattingsdal M, Meyer-Lindenberg A, McDonald C, McIntosh AM, McMahan FJ, McMahan KL, Meisenzahl E, Melle I, Milanesechi Y, Mohnke S, Montgomery GW, Morris DW, Moses EK, Mueller BA, Munoz Maniega S, Muhleisen TW, Muller-Myhsok B, Mwangi B, Nauck M, Nho K, Nichols TE, Nilsson LG, Nugent AC, Nyberg L, Olvera RL, Oosterlaan J, Ophoff RA, Pandolfo M, Papalampropoulou-Tsiridou M, Papmeyer M, Paus T, Pausova Z, Pearlson GD, Penninx BW, Peterson CP, Pfennig A, Phillips M, Pike GB, Poline JB, Potkin SG, Putz B, Ramasamy A, Rasmussen J, Rietschel M, Rijpkema M, Risacher SL, Roffman JL, Roiz-Santianez R, Romanczuk-Seiferth N, Rose EJ, Royle NA, Rujescu D, Ryten M, Sachdev PS, Salami A, Satterthwaite TD, Savitz J, Saykin AJ, Scanlon C, Schmaal L, Schnack HG, Schork AJ, Schulz SC, Schur R, Seidman L, Shen L, Shoemaker JM, Simmons A, Sisodiya SM, Smith C, Smoller JW, Soares JC, Sponheim SR, Sprooten E, Starr JM, Steen VM, Strakowski S, Strike L, Sussmann J, Samann PG, Teumer A, Toga AW, Tordesillas-Gutierrez D, Trabzuni D, Trost S,

Turner J, Van den Heuvel M, van der Wee NJ, van Eijk K, van Erp TG, van Haren NE, van 't Ent D, van Tol MJ, Valdes Hernandez MC, Veltman DJ, Versace A, Volzke H, Walker R, Walter H, Wang L, Wardlaw JM, Weale ME, Weiner MW, Wen W, Westlye LT, Whalley HC, Whelan CD, White T, Winkler AM, Wittfeld K, Woldehawariat G, Wolf C, Zilles D, Zwiers MP, Thalamuthu A, Schofield PR, Freimer NB, Lawrence NS, Drevets W. The ENIGMA Consortium: large-scale collaborative analyses of neuroimaging and genetic data. *Brain Imaging Behav.* 2014;8(2):153-82. PMID: 4008818.

Villalón-Reina JE, Martínez K, Qu X, **Ching CRK**, Nir TM, Kothapalli D, Corbin C, Sun D, Lin A, Forsyth JK, Kushan L, Vajdi A, Jalbrzikowski M, Hansen L, Jonas RK, van Amelsvoort T, Bakker G, Kates WR, Antshel KM, Fremont W, Campbell LE, McCabe KL, Daly E, Gudbrandsen M, Murphy C, Murphy D, Craig M, Emanuel B, McDonald-McGinn D, Vorstman J, Fiksinski A, Koops S, Ruparel K, Roalf D, Gur RE, Schmitt JE, Simon TJ, Goodrich-Hunsaker NJ, Durdle CA, Doherty J, Cunningham AC, van den Bree M, Linden DEJ, Owen M, Moss H, Kelly S, Donohoe G, Murphy²⁶ KC, Arango C, Jahanshad N, Thompson PM, Bearden CE. Altered White Matter Microstructure in 22q11.2 Deletion Syndrome: A Multi-Site Diffusion Tensor Imaging Study. **In Review (Molecular Psychiatry 2018)**

Wilkes F, Abaryan Z; **Ching CRK**, Gutman B, Madsen S; Walterfang M; Velakoulis D, Stout J, Chua P, Egan G, Thompson PM; Looi J, Georgiou-Karistianis N. Striatal morphology and neurocognitive dysfunction in Huntington disease: The IMAGE-HD study. **In Review (Psychiatry Research: Neuroimaging 2019)**

Z Abaryan, F Wilkes, **CRK Ching**, BA Gutman, SK Madsen, M Walterfang, J Stout, A Churchyard, P Chua, D Velakoulis, G Egan, JCL Looi, PM Thompson, N Georgiou-Karistianis. Striatal shape differs before and after symptom onset in Huntington's disease and relates to clinical severity: the IMAGE HD study. Society for Neuroscience, 2015

In reference to IEEE copyrighted material, which is used with permission in this thesis,

the IEEE does not endorse any of UCLA's products or services. Internal or personal use of this

material is permitted. If interested in reprinting/republishing IEEE copyrighted material for advertising or promotional purposes or for creating new collective works for resale or redistribution, please go to http://www.ieee.org/publications_standards/publications/rights/rights_link.html to learn how to obtain a License from RightsLink. If applicable, University Microfilms and/or ProQuest Library, or the Archives of Canada may supply single copies of the dissertation.

VITA

- 2006 BA in Neuroscience and Philosophy, Pomona College
- 2007-2010 Staff Research Assistant: Center for Imaging of Neurodegenerative Diseases with Dr. Michael Weiner, UCSF
- 2011-present Co-author on 35 peer-review publications (17 in preparation/review), 4 peer-reviewed conference papers, 2 book chapters, and 74 conference abstracts.
- 2011 UCLA Eugene V. Cota-Robles Fellowship
- 2011 National Science Foundation Alliance for Graduate Education and the Professoriate Grant
- 2011-2015 UCLA Graduate Division Conference Travel Award
- 2012 UCLA Neuroimaging Training Program Fellowship, NIH R90 DA022768 and T90 DA023422
- 2013 National Science Foundation Graduate Research Fellowship Honorable Mention
- 2013 *NEUROSC 102 Introduction to the Functional Anatomy of the Central Nervous System* – Teaching Assistant
- 2013-2014 *Advanced Methods in Neuroscience Research* – Course developer, primary instructor and course advisor
- 2014-2016 UCLA Brain Research Center Society for Neuroscience Conference Travel Award
- 2015 Organization for Human Brain Mapping Merit Award Honolulu, Hawaii
- 2015 UCLA Neurobehavioral Genetics Predoctoral Fellowship, NIH/NIMH 5T32MH073526

2015-present Invited speaker for Society for Neuroscience (Chicago, 2015), UCLA Neurobehavioral Genetics Meeting (Los Angeles, 2017), Society of Biological Psychiatry (San Diego, 2017; New York, 2018), Conference on Mental Health and Addiction: Research Council of Norway, Norwegian Centre for Mental Disorders Research and the Norwegian Centre for Addiction Research (Oslo, 2018), and Society for Brain Mapping and Therapeutics (Los Angeles, 2019)

2016 Annual Conference on Retroviruses and Opportunistic Infections (CROI) Young Investigator Scholarship

CHAPTER 1

Introduction

1.1 Modern Brain Mapping

The 1990's have been termed the “Decade of the Brain” and were marked by an acceleration in the collection of neuroscientific data (Jones and Mendell, 2019). Growing access to MRI scanners led to widespread, noninvasive neuroimaging studies of the human brain. The power to relate MRI-based brain measures to clinical and behavioral features, as seen in early lesion studies, led to a flourishing brain mapping movement.

Early brain mapping was supported in large part by the development of semi-automated tools able to quantify aspects of brain images, thus making rigorous analyses and larger studies possible. Tools such as Statistical Parametric Mapping (Friston et al., 1995; Frackowiak, 1997), the FMRIB Software Library (FSL) (Jenkinson et al., 2012), FreeSurfer (Fischl et al., 2004) and other tools became widely adopted in the analysis of brain imaging data.

Around the time of early neuroimaging processing and analysis tool development, coordinated efforts such as the International Consortium for Brain Mapping began collecting neuroimaging data from around the world in order to establish brain mapping standards. These resources included tools such as average anatomical templates based on hundreds of brain scans. Software was developed to register study data to templates or atlases and thereby relate findings to existing data collections in a standardized coordinate space (Woods et al., 1993; Talairach et al., 1993; Collins et al., 1994; Ashburner et al., 1999; Jenkinson et al., 2002.). Thanks in part to these

early standardization efforts, researchers began to collect brain MRI data from clinical populations using consistent protocols.

One important consortium effort to collect and share brain imaging data was the Alzheimer's Disease Neuroimaging Initiative (ADNI) (Weiner et al., 2012). The first phase of ADNI involved a coordinated multisite effort to collect multimodal brain MRI scans along with in-depth neuropsychological and biological specimens on an unprecedented scale to study biomarkers of dementia. Importantly, ADNI data (now in Phase 3 of the study) is made freely available to researchers around the world. The ADNI database includes over 1,000 research subjects and has resulted in hundreds of peer-reviewed studies. Other consortia include the Brain Imaging Research Network (Potkin and Ford, 2009), IMAGEN (Schumann et al., 2010), CHARGE (Psaty, et al., 2009), and the Mind Clinical Imaging Consortium (Gollub, 2013).

However, coordinated large-scale efforts such as these are rare. Even today, typical neuroimaging studies collect fewer than one hundred subjects and challenges remain with regard to study power, replication and discovery in neuroimaging research. The effects of genetic variation and psychiatric disorders on brain structure and function are often subtle (Thompson et al., 2014). New approaches are thus necessary detect replicable and actionable structure/function relationships to empower future therapies and interventions. One way forward is in the aggregation of existing neuroimaging datasets to boost power and foster international collaboration.

In the next section I address some of the advantages and challenges inherent to large-scale

neuroimaging research. I focus on advances made by the Enhancing Neuro Imaging Genetics through Meta Analysis Consortium (ENIGMA) and my unique contributions to these large-scale, global neuroscience efforts during my graduate studies.

1.2 The Enhancing Neuro Imaging Genetics Through Meta Analysis Consortium (ENIGMA)

Large-scale, collaborative neuroimaging studies offer the potential to answer new questions as well as address older findings with greater confidence and rigor. In the last decade, attention has been drawn to a potential ‘crisis of reproducibility’ in biomedical research, where findings from smaller, underpowered studies have sometimes failed to replicate in independent samples (Button et al., 2013; Dumas-Mallet et al., 2017; Ioannidis et al., 2017). Historically, the large cost of collecting neuroimaging data meant that most studies assessed fewer than one hundred subjects. This resulted in underpowered studies that may have been unable to reliably detect the statistically subtle effects of psychiatric illness or to consistently identify disease modulators in the genome (Ioannidis, 2011; Turner et al., 2014). Early psychiatric genetics studies sometimes made assertions about candidate genes and their effects on the brain that later failed to replicate when tested in independent samples (Farrell et al., 2015). A recent paradigm shift has led to the formation of large-scale consortia efforts that pool resources from around the world to scan the genome for loci that consistently affect disease risk. Furthermore, a number of large-scale, international imaging consortia have recently formed to study brain structure and function in a wide range of psychiatric disorders (Okada et al., 2016; Thompson et al., 2017; Satizabal et al., 2017).

1.2.1 ENIGMA: Studying the effect of genetic variation on brain structure

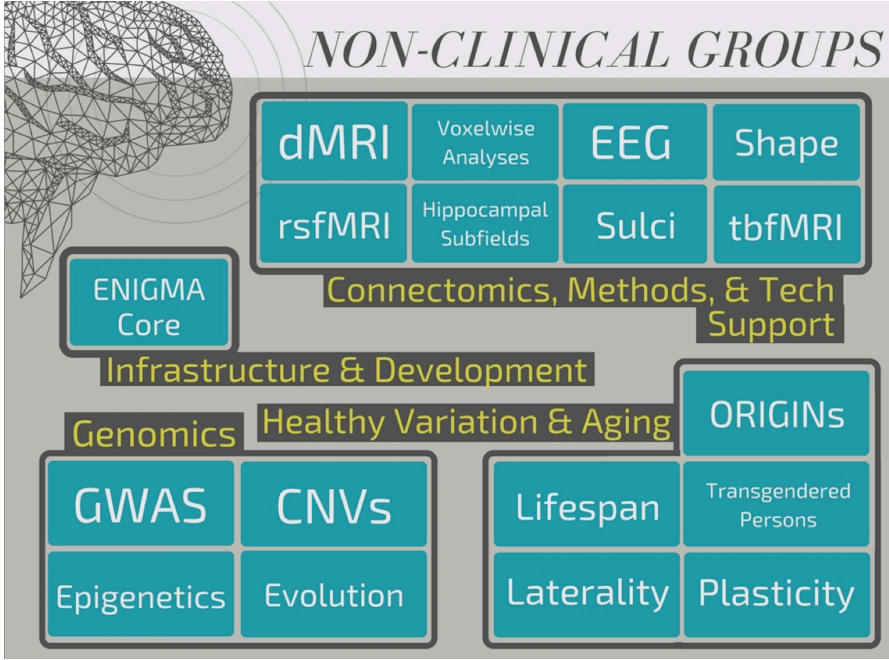
A growing number of loci along the human genome have been associated with increased risk for disorders such as schizophrenia, bipolar disorder, and major depression. The Psychiatric Genomics Consortium (PGC) is a prime example of the power of big data to drive discoveries in psychiatric genetics. The PGC has screened millions of genetic loci for associations with a range of disorders by aggregating effects across hundreds of thousands of samples. These efforts have uncovered hundreds of common variants that are over-represented in patients compared to controls (Schizophrenia Working Group of the Psychiatric Genomics Consortium, 2014; Bipolar Disorder and Schizophrenia Working Group of the Psychiatric Genomics Consortium, 2018, Wray et al., 2018). Large-scale genomics approaches such as these have also determined that there exists a significant overlap between disorders (Lee et al., 2013; Anttila et al., 2018; Gandal et al., 2018).

In the field of psychiatry, neuroimaging research has been proposed as a means to identify biological measures of disease that may be directly influenced by genetic variation — the so-called ‘endophenotype’ approach (14 Gottesman & Gould 2003). With the possible exception of *APOE4* — the major risk factor for Alzheimer's disease — a small (but growing) number of candidate genes have been found with reproducible effects on brain structure and function (Jahanshad et al., 2017). In 2009, in an effort led by Drs. Paul Thompson, Jason Stein and others, ENIGMA adopted the multi-site model similar to the PGC to perform genome-wide association studies (GWAS) on MRI-based brain measures in an effort to identify loci consistently associated with brain structure and function. To date, the ENIGMA consortium has published the largest genetic screens for human brain structures including hippocampal volume

(Stein et al., 2012; Hibar et al., 2017), other subcortical structures (Hibar et al., 2015), and intracranial volume (Adams et al., 2016). Furthermore, these studies were among the first to assess neuroimaging data from over 10,000 individuals.

1.2.2 ENIGMA methods and disease working groups

The success of the initial ENIGMA GWA studies led to the formation of allied ENIGMA methods and disease working groups (**Figure 1.2a**). There are currently over 30 working groups developing standardized protocols and studying a wide range of neurodegenerative and psychiatric disorders.



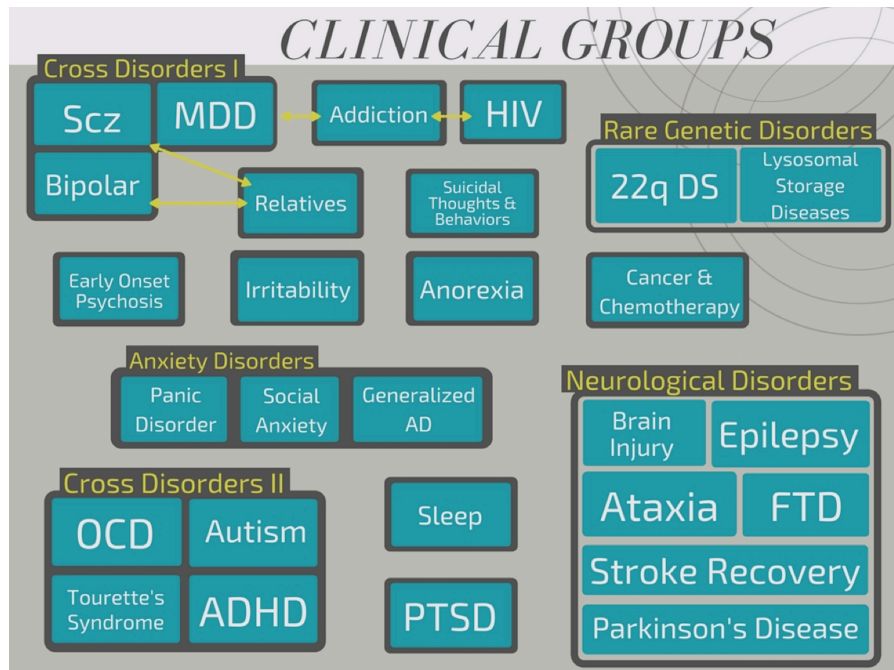


Figure 1.2a. ENIGMA methods and disease working groups

Working in parallel, and sharing protocols developed by the ENIGMA methods groups, the ENIGMA clinical working groups have been active in publishing the largest neuroimaging studies of bipolar disorder (Hibar et al., 2016; Hibar et al., 2018), major depressive disorder (Schmaal et al., 2016; Schmaal et al., 2017), schizophrenia (van Erp et al., 2016; van Erp et al., 2018), epilepsy (Whelan et al., 2018), obsessive compulsive disorder (Boedhoe et al., 2017; Boedhoe et al., 2018), autism spectrum disorder (van Rooij et al., 2018) and 22q11.2 deletion syndrome (Sun et al., 2018) (**Figure 1.2b**).

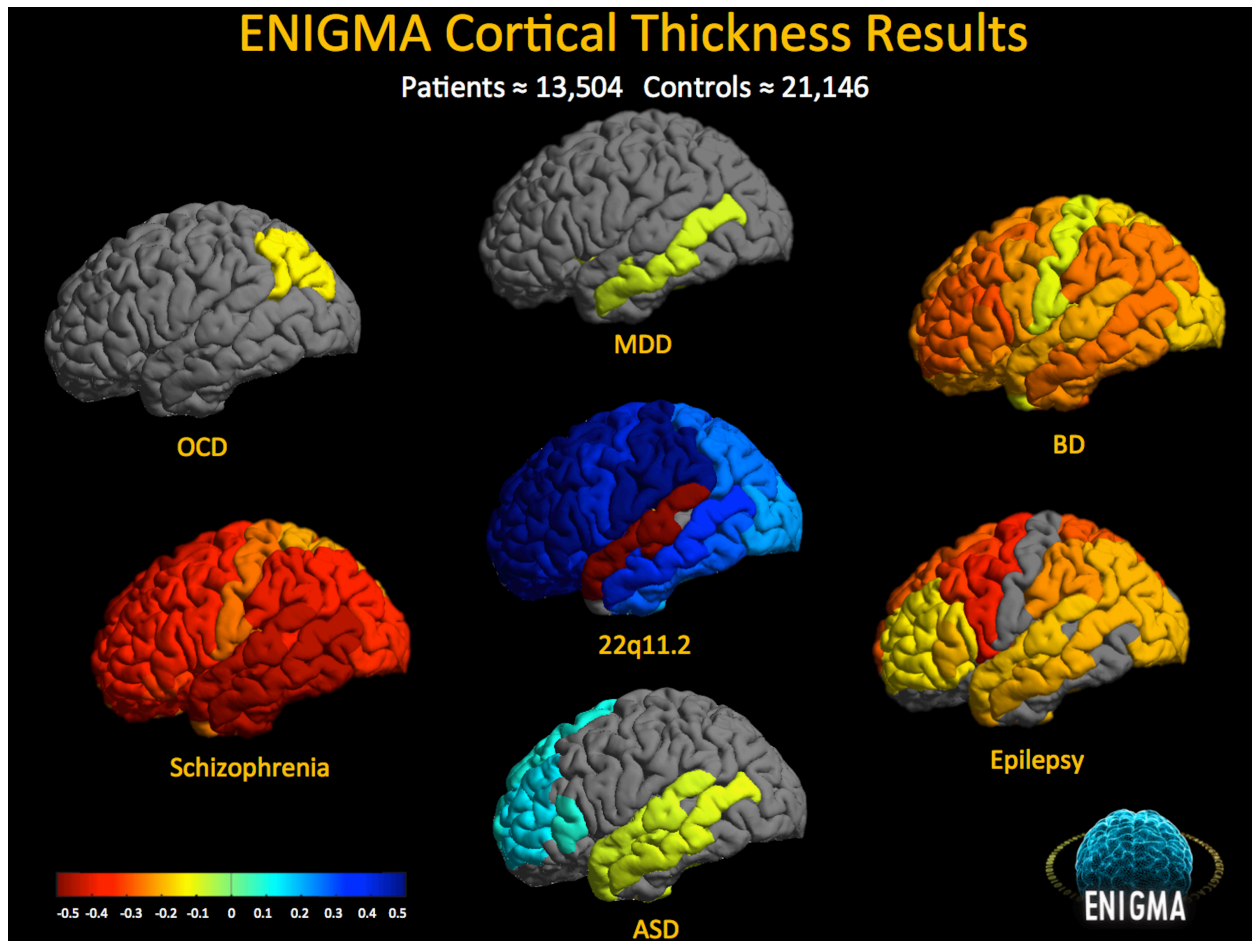


Figure 1.2b. Published case/control cortical thickness Cohen's d effect sizes from the ENIGMA psychiatric disorder working groups.

1.2.3 The ENIGMA Model: Advantages and challenges

A large-scale consortium effort presents advantages and challenges compared to previous smaller-scale studies. ENIGMA takes advantage of existing datasets, reutilizing studies that have often finished data collection and published their primary findings. The sheer cost of data collection means that most prospective large-scale neuroimaging initiatives are limited in the number of subjects that can be acquired. The Alzheimer's Disease Neuroimaging Initiative (ADNI) and the Parkinson's Progression Markers Initiative (PPMI) are two of the larger initiatives and have produced multisite samples in the neighborhood of 1,000 subjects. More recently, the epidemiological UK Biobank study aims to scan 100,000 participants, with

~15,000 scans currently available to researchers (Alfaro-Almagro et al. 2017). To date, the ENIGMA consortium has incorporated ~63,000 scans from a range of neurodegenerative and psychiatric disorders as well as healthy controls. ENIGMA currently includes over 700 scientists from 340 institutions, spanning 30 countries (**Figure 1.2c**). By taking advantage of existing data and utilizing parallel computing power across the world, ENIGMA has leveraged research resources that efficiently benefit to the wider research community at a relatively minimal cost.

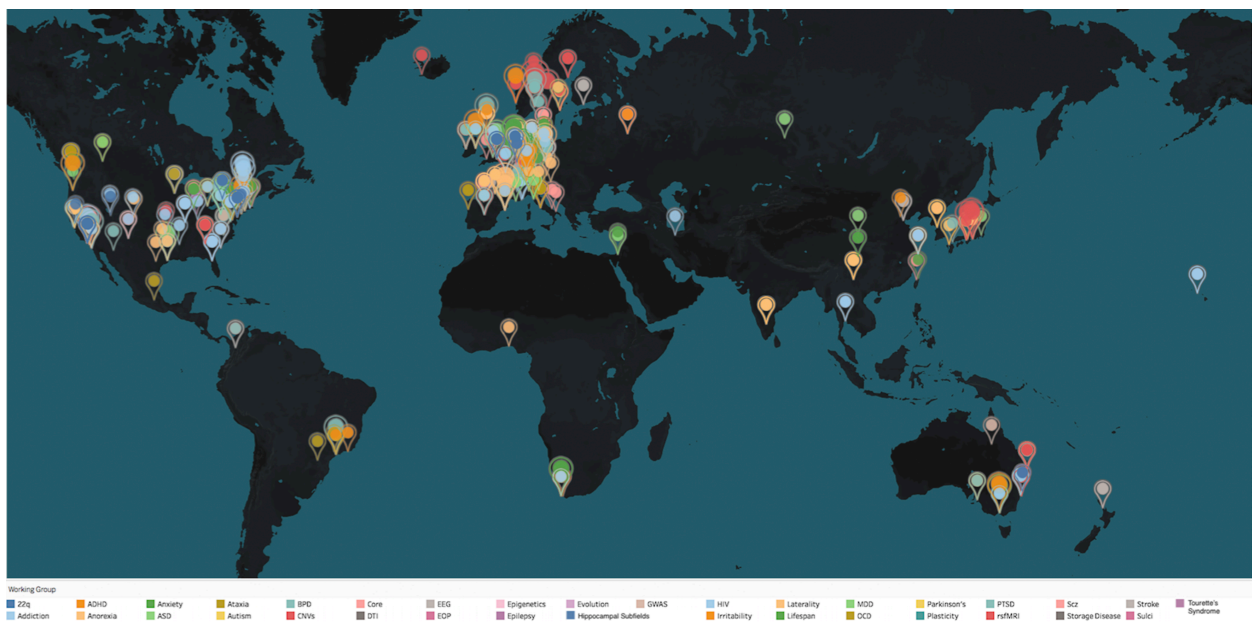


Figure 1.2c. The ENIGMA working groups around the world

1.2.4 Harmonized processing protocols for large samples

Unprecedented sample sizes have allowed ENIGMA to test hypotheses about nuanced effects of a disease or interventions on the brain. Subtle abnormalities that may have been undetectable in smaller studies have been identified as robust effects when data are aggregated from multiple centers.

One major strength of the ENIGMA approach over classic literature-based meta-analyses was the implementation of harmonized processing and analysis protocols. These procedures, validated and publicly available (<http://enigma.ini.usc.edu/protocols/>), make it possible to efficiently and consistently extract measures from MRI data and to perform robust statistical modeling that has reliably identified effects not detected within smaller cohorts. This approach also allows for the opportunity to compare results across ENIGMA working groups.

As imaging studies in psychiatry and neurology grow from hundreds to tens of thousands of subjects, several considerations arise that affect the feasibility of performing such large-scale research. Many of the algorithms that derive measures from MRI scans segment the brain into distinct regions, but this segmentation process is never perfect. Segmentation protocols typically require expert raters to identify algorithm failures or outliers. In **Chapter 2** I describe some of my contributions to harmonizing large-scale research efforts including contributions to the ENIGMA processing protocols that have been used by hundreds of researchers and applied to thousands of MRI scans from around the world.

1.2.5 Big Data: Heterogeneity as advantage and disadvantage

ENIGMA studies include varied ethnic/cultural populations, scanners, protocols, and enrollment criteria. While aggregating these types of data may result in higher subject heterogeneity, even in the case of harmonized reprocessing, it also results in more ecologically valid datasets. Even large, multisite, prospective studies such as ADNI and PPMI include possible site confounds. When handled appropriately, this heterogeneity allows researchers to determine common and distinct patterns of brain variation in a particular psychiatric disorder as they present across the

world. Furthermore, this type of data heterogeneity may make it possible to assert that results are somewhat invariant to minor differences in study protocol including factors such as educational level, socioeconomic status, and ethnic composition. However, special care must be made when analyzing international, multicenter cohorts, and while some skepticism remains about the aggregation of imaging data across multiple centers, a growing body of replicated psychiatric imaging and imaging genetics findings provide evidence for the validity and utility of this approach. Importantly, ENIGMA studies have detected genetic variants accounting for less than 1% of the variance in key brain measures as well as subtle effect sizes in psychiatric case/control comparisons, demonstrating that data heterogeneity does not obscure signals of interest. ENIGMA working groups test for confounds of processing method and study site and have found minimal influence of these factors on overall effect sizes (Hibar et al. 2016 and 2018; **Chapter 4**).

Important limitations are worth noting. Psychiatric disorders are clinically heterogeneous and study cohorts may differ more significantly in terms of demographic composition, duration of illness, treatment, age of onset, and other comorbid factors. When identifying common patterns of brain variation within a psychiatric disorder, there may be important subtypes within these overall patterns. Given the large individual variance in anatomy in both patients and controls, individual patients will not typically exhibit the exact distribution of brain variation seen in the group averages produced by such large-scale studies. Indeed, what the ENIGMA approach gains in power for replication and generalizability, it may lose with regard to subtle, subtype-specific effects.

In an effort to address some of these large-scale study limitations, the ENIGMA psychiatric disorder working groups support a growing list of parallel projects to resolve aspects of disorder subtype, disease risk and treatment effects. The ENIGMA bipolar disorder working group has performed analyses on medication effects and found brain alternations associated with common treatments such as lithium, anticonvulsants and antipsychotics. Extensive analyses have also been conducted on bipolar subtypes. For example, despite differences in clinical presentation, few detectable differences in brain structure or genetic background have been found between bipolar subtypes (**Chapter 4**). To evaluate disease risk, the ENIGMA relatives group studied discordant twins and first-degree relatives of patients across the ENIGMA bipolar and schizophrenia working groups. It's known that anatomical variations may not be specific to patients alone, and may also be evident, to a degree, in first-degree relatives (de Zwarte et al., 2019; **Chapter 4**).

The ENIGMA 22q11.2 deletion syndrome (22q11DS) working group is conducting a unique investigation into the risk and development of psychosis. This particular chromosomal abnormality leads to heightened risk for psychosis and has provided an important avenue to studying neurodevelopmental markers of schizophrenia. The 22q11.2 deletion working group has performed the largest analyses of cortical, subcortical and diffusion-weighted brain measures in this disorder. In close collaboration with the ENIGMA schizophrenia working group, this project is shedding light on unique and overlapping patterns of both 22q11DS-related psychosis and idiopathic schizophrenia (**Chapter 3**).

1.2.6 Meta- and mega-analysis

Both ENIGMA and the PGC have used meta-analysis techniques to sidestep some obstacles inherent to sharing primary brain measures or genetic data. In this approach, results from each ENIGMA cohort are combined by weighting statistical effects by the size of the cohort. Direct testing of the heterogeneity and reproducibility of the results within the full sample as well as across cohorts is reported. These techniques represent an important foundational principal of the ENIGMA consortium and were a significant factor in the initial success of the consortium. Early ENIGMA studies were based on the idea that no working group would ever be required to share any primary genetic or brain metrics. ENIGMA harmonized processing and analysis protocols could be run on site and effect size estimates would then be shared with the central analysis team to perform the necessary meta-analysis.

Meta-analyses such as those employed by ENIGMA come with limitations. When an effect size is analyzed across multiple cohorts, it may be easy to overlook important or influential factors that operate only in certain contexts. One example of this is the different profile of brain abnormalities seen in adult versus pediatric patients. Meta-analyses may also fail to detect the effects from factors that are strongly age-dependent. For instance, the effect on hippocampal volume of the major Alzheimer's risk allele, *APOE4*, is not the strongest locus in the genome-wide analysis of common variants that affect hippocampal volume (Stein et al., 2012). This limitation is important to consider, as some illness risk factors may not be reliably detected using this meta-analysis framework. To address some of these limitations, several of the ENIGMA working groups are now performing mega-analyses of individual level data in which primary brain measures are shared and analyzed jointly. These analyses allow for greater power and

modeling flexibility to detect subtle modulatory factors such as medication, sex differences, and environmental risk factors (**Chapters 3, 4 and 6**).

Most ENIGMA studies have applied relatively simple mass univariate analysis methods when studying imaging features. Combining multiple imaging modalities is likely to improve predictions about diagnosis and prognosis. In addition to classical multivariate approaches, machine learning models are being applied to neuroimaging data across a variety of brain disorders to predict diagnostic groups, treatment response, and soon to identify and characterize subtypes or clusters within highly heterogeneous diagnostic categories (**Chapter 5**). ENIGMA provides an opportunity to evaluate such machine learning models across large samples. Our initial efforts in the diagnostic classification of affective disorders show promise but their accuracy is likely to improve as more advanced metrics are added, including multimodal structural, functional, and in-depth clinical information (**Chapter 3 and 4**).

1.2.7 The future of ENIGMA

A key question in psychiatric neuroimaging research is the extent to which brain variations may be shared or differentiate major psychiatric disorders. Initial case control studies from the ENIGMA clinical working groups (**Figure 1.2b and 1.2d**) suggest interesting patterns of cortical and subcortical variation across disorders. Among the most striking findings from these studies were that schizophrenia case/control cortical effects were more widespread and greater in magnitude than those found in other ENIGMA studies. In line with prior hypotheses about the anatomical correlates of bipolar disorder versus major depressive disorder, frontal lobe systems showed greater deficits in bipolar patients, whereas limbic regions tended to show greater

deficits in major depressive disorder. Another key finding are the volumetric deficits in the hippocampus found across disorders (**Figure 1.2d**). Ongoing efforts to better characterize these effects include the examination of hippocampal subfield volumes and shape analysis of subcortical structures (**Chapters 3 and 4**).

Case-control Subcortical Effect Sizes Across ENIGMA Working Groups

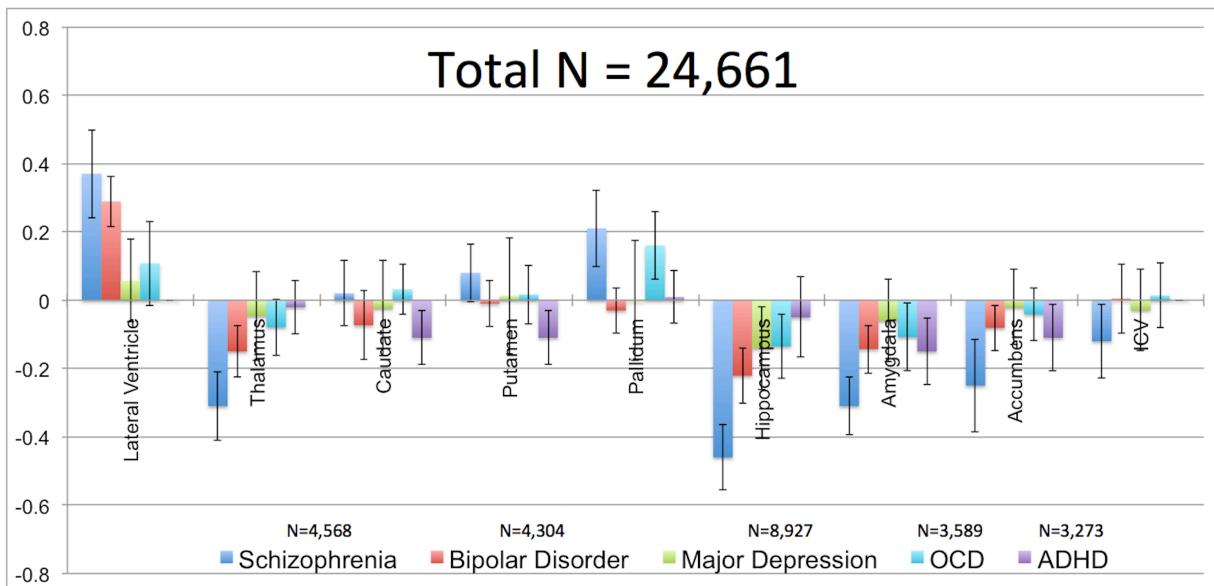


Figure 1.2d. Published case/control subcortical volume effect sizes from the ENIGMA psychiatric disorder working groups.

Psychiatric disorders, as currently defined by the major diagnostic manuals, represent syndromes or constellations of symptoms that broadly group individuals that share similar prognoses and respond to similar treatments. These diagnostic categories are inherently heterogeneous and can have seemingly vague boundaries between disorders with overlapping symptomatology (Carroll and Owen 2009). As noted earlier, growing evidence points to shared molecular markers across some psychiatric disorders (Gandal et al., 2018). As such, an important limitation of the early

ENIGMA analyses (and the majority of psychiatric neuroimaging studies to date) was the assessment of diagnostic categories rather than dimensional measures from specific symptom domains. The National Institutes of Health Research Domain Criteria (NIH RDoC) and other ongoing initiatives are motivating future studies to examine dimensional measures of cognitive and behavioral symptoms across classic diagnostic boundaries (Insel, 2014).

In **Chapter 5** I discuss ongoing work to directly compare harmonized brain measures from the ENIGMA bipolar, schizophrenia and major depression working groups. Of great interest will be whether those future analyses can discriminate between alternative patient groupings, such as those based on the presence of depressive or psychotic symptoms, disease severity, disease duration, substance use, and other shared characteristics across these three disorders.

A major challenge in the aggregation and comparison of the ENIGMA data are the range of symptom and cognitive measures that have been deployed across studies. Before direct comparisons can be made of data from the different clinical working groups, a dedicated effort is underway to assemble a dictionary of common data elements containing factors that influence brain development and disease (**Chapter 5, See Organic Data Science**). Through this effort it will also be possible to better distinguish the effects of common risk factors including comorbidities like depression and substance use on the expression of various psychiatric disorders.

An ever-present challenge for big data methods in psychiatry involves the need to relate imaging findings to cellular and molecular measures. A major barrier in psychiatric research is the

relative lack of histologic or molecular markers for psychiatric disorders. In **Chapter 3** I discuss associations between genetic deletion size and brain structure in 22q11DS. These analyses, the first of their kind, have implications for how we understand the differential risk and gene dosage in neurodevelopmental and psychotic disorders. In the near future, it's likely that connections will be made between neuroimaging measures and other types of high dimensional "omics" data such as plasma markers, metabolomic, epigenetic, gene expression, and other biological data.

While a thorough discussion of the application of diffusion-weighted imaging and fMRI in ENIGMA are beyond the scope of this dissertation, they represent important avenues of future work throughout the consortium and will lend insights into the structural and functional basis of psychiatric disorders.

ENIGMA studies will continue to be guided by the collective expertise of a strong network of neuroscientists, psychiatrists, data scientists, bioengineers and geneticists (Guglielmi, 2018). Big data consortia efforts such as these offer the opportunity to work cohesively on related research questions, bringing diverse sources of information to bear on converging neuroscientific problems, and will continue to provide valuable discoveries revealing consensus findings and informing future hypothesis-driven studies.

1.2.8 ENIGMA leadership

Paul M. Thompson and the team at the Imaging Genetics Center of The University of Southern California serve as the organizational core of the ENIGMA consortium. As an organizing member of the ENIGMA team, I have been involved in all stages of this worldwide, collaborative effort. This role has included design, implementation and support of harmonized

processing, analysis and quality control protocols. I currently co-chair the ENIGMA bipolar working group, the largest neuroimaging collaboration to ever study bipolar disorder, and I work closely with many of the ENIGMA clinical working groups (22q11DS, schizophrenia, major depression, PTSD, and others) to implement new study designs and projects.

1.3 Organization of the Dissertation

In **Chapter 2** I discuss neuroimaging tools and techniques that I have helped develop to empower large-scale, multisite MRI studies of health and disease. These efforts include techniques such as tensor-based morphometry to empower clinical trials, harmonized ENIGMA protocols to study cortical and subcortical brain morphometry, and an advanced technique to study high-resolution shape morphometry of subcortical structures (The ENIGMA Shape Analysis Pipeline).

In **Chapter 3** I present my work with the ENIGMA 22q11.2 deletion syndrome (22q11DS) working group, chaired by Dr. Carrie E. Bearden. This work encompasses multiple studies that aim to better characterize cortical, subcortical and white matter alterations in 22q11DS, highlighting important discoveries linking brain structure to deletion size and psychosis. Through close collaboration with the ENIGMA Schizophrenia working group, this work is an unprecedented effort (in technique and scale) to evaluate the overlap between 22q11DS-associated psychosis and idiopathic schizophrenia.

In **Chapter 4** I discuss findings from the ENIGMA bipolar disorder working group, the largest study of MRI-based markers of bipolar disorder ever conducted. As the co-chair and leader of

this effort, I focus special attention on subcortical shape variation as a follow-up to our original subcortical volumes study.

In **Chapter 5** I outline future directions that build off the presented dissertation work. Future ENIGMA cross-disorder studies are discussed including ongoing collaborations with the Psychiatric Genetics Consortium (PGC) and an effort I am leading to combine structural measures from the ENIGMA bipolar, schizophrenia and major depression working groups, which include over 35,000 subjects. These cross-disorder studies have important implications for probing some of the basic limitations of our current diagnostic systems and will provide important lessons for future psychiatric research.

In **Chapter 6** I provide two tensor-based morphometry studies of scan acceleration and phantom-based scaling outlining efforts to empower large-scale clinical trials. This work, while focused on aging and dementia, further represents my effort to develop robust methods to quantify brain structure across large, multisite studies. This work helped lead to more recent updates to the ADNI scanning protocol, the largest coordinated neuroimaging effort to study Alzheimer's disease.

In **Chapter 7** I provide an overview of related works accomplished during my graduate study not central to this dissertation thesis but important to the overall breadth of my research activities during my graduate studies. This brief section includes reference to the aforementioned organic data science projects important to cross-disorder clinical/behavioral scale harmonization as well as a publication summarizing a graduate neuroscience course that I developed with a classmate,

which continues to be a required course for first year students in the UCLA Interdepartmental Neuroscience PhD Program.

Chapter 1 includes work adapted from the following chapters/papers:

Thompson PM, **Ching CRK**, Dennis EL, Salminen LE, Turner JA, van Erp TGM, Jahanshad N. Big data initiatives in psychiatry: Global neuroimaging studies. Submitted book chapter to “Neuroimaging in Schizophrenia” edited by Marek Kubicki and Martha E. Shenton (to be published by Springer Verlag 2018).

Schmaal L, **Ching CRK**, McMahon AB, Jahanshad N, Thompson PM. Neuroimaging, Genetics and Personalized Psychiatry: Developments and Opportunities from the ENIGMA consortium. Submitted book chapter to “Personalized Psychiatry” edited by Dr. Bernhard Baune.

Thompson PM, Stein JL, Medland SE, Hibar DP, Vasquez AA, Renteria ME, Toro R, Jahanshad N, Schumann G, Franke B, Wright MJ, Martin NG, Agartz I, Alda M, Alhusaini S, Almasy L, Almeida J, Alpert K, Andreasen NC, Andreassen OA, Apostolova LG, Appel K, Armstrong NJ, Aribisala B, Bastin ME, Bauer M, Bearden CE, Bergmann O, Binder EB, Blangero J, Bockholt HJ, Boen E, Bois C, Boomsma DI, Booth T, Bowman IJ, Bralten J, Brouwer RM, Brunner HG, Brohawn DG, Buckner RL, Buitelaar J, Bulayeva K, Bustillo JR, Calhoun VD, Cannon DM, Cantor RM, Carless MA, Caseras X, Cavalleri GL, Chakravarty MM, Chang KD, **Ching CR**, ... (233 authors)... Drevets W. The ENIGMA Consortium: large-scale collaborative analyses of neuroimaging and genetic data. *Brain Imaging Behav.* 2014;8(2):153-82. PMID: 4008818.

1.4 Chapter 1 references

Adams HH, et al. Novel genetic loci underlying human intracranial volume identified through genome-wide association. *Nat Neurosci.* 2016;19(12):1569-82. PMID: 5227112.

Alfaro-Almagro F et al. Image processing and Quality Control for the first 10,000 brain imaging datasets from UK Biobank. *NeuroImage.* 2018;166:400-24. PMID: 5770339.

Anttila V et al. Analysis of shared heritability in common disorders of the brain. *Science.* 2018;360(6395). PMID: 6097237.

Bipolar Disorder and Schizophrenia Working Group of the Psychiatric Genomics Consortium. Genomic Dissection of Bipolar Disorder and Schizophrenia, Including 28 Subphenotypes. *Cell.* 2018;173(7):1705-15 e16.

Boedhoe PS et al. Distinct Subcortical Volume Alterations in Pediatric and Adult OCD: A Worldwide Meta- and Mega-Analysis. *Am J Psychiatry.* 2017;174(1):60-9. PMID: 5344782.

Boedhoe PSW et al. Cortical Abnormalities Associated With Pediatric and Adult Obsessive-Compulsive Disorder: Findings From the ENIGMA Obsessive-Compulsive Disorder Working Group. *Am J Psychiatry.* 2018;175(5):453-62.

Button KS et al. Power failure: why small sample size undermines the reliability of neuroscience. *Nat Rev Neurosci.* 2013;14(5):365-76.

de Zwarte et al. The association between familial risk and brain abnormalities is disease-specific: an ENIGMA–Relatives study of schizophrenia and bipolar disorder. In Review (*Biological Psychiatry* 2018)

Dumas-Mallet E et al. Low statistical power in biomedical science: a review of three human research domains. *R Soc Open Sci.* 2017;4(2):160254. PMID: 5367316.

Farrell MS et al. Evaluating historical candidate genes for schizophrenia. *Mol Psychiatry.* 2015;20(5):555-62. PMID: 4414705.

Fischl B et al. Automatically parcellating the human cerebral cortex. *Cerebral cortex.* 2004;14(1):11-22.

Frackowiak RSJ (1997). *Human Brain Function.* San Diego: Academic

Friston KJ et al. Analysis of fMRI time-series revisited. *NeuroImage.* 1995;2(1):45-53.

Gandal et al. Shared molecular neuropathology across major psychiatric disorders parallels polygenic overlap. *Science.* 2018;359(6376):693-7. PMID: 5898828.

Gollub et al. The MCIC collection: a shared repository of multi-modal, multi-site brain image

data from a clinical investigation of schizophrenia. *Neuroinformatics*. 2013;11(3):367-88. PMID: 3727653.

Gottesman, II, Gould TD. The endophenotype concept in psychiatry: etymology and strategic intentions. *Am J Psychiatry*. 2003;160(4):636-45.

Guglielmi, G. The world's largest set of brain scans are helping reveal the workings of the mind and how diseases ravage the brain. *Science* (2018). doi:10.1126/science.aat0994

Jahanshad N et al., Do candidate genes affect the brain's white matter microstructure? Large-scale evaluation of 6,165 diffusion MRI scans. *BioRxiv* doi:10.1101/107987

Hibar DP et al. Novel genetic loci associated with hippocampal volume. *Nat Commun*. 2017;8:13624. PMID: 5253632.

Hibar DP et al. Common genetic variants influence human subcortical brain structures. *Nature*. 2015;520(7546):224-9. PMID: 4393366.

Hibar DP et al. Subcortical volumetric abnormalities in bipolar disorder. *Mol Psychiatry*. 2016;21(12):1710-6. PMID: 5116479.

Hibar DP et al. Cortical abnormalities in bipolar disorder: an MRI analysis of 6503 individuals from the ENIGMA Bipolar Disorder Working Group. *Mol Psychiatry*. 2018;23(4):932-42. PMID: 5668195.

Insel TR. The NIMH Research Domain Criteria (RDoC) Project: precision medicine for psychiatry. *Am J Psychiatry*. 2014;171(4):395-7.

Ioannidis JP. Acknowledging and Overcoming Nonreproducibility in Basic and Preclinical Research. *Jama*. 2017;317(10):1019-20.

Ioannidis JP. Excess significance bias in the literature on brain volume abnormalities. *Arch Gen Psychiatry*. 2011;68(8):773-80.

Jenkinson M et al. *Fsl*. *NeuroImage*. 2012;62(2):782-90.

Jones EG, Mendell LM. Assessing the decade of the brain. *Science*. 1999;284(5415):739.

Lee et al. Genetic relationship between five psychiatric disorders estimated from genome-wide SNPs. *Nature genetics*. 2013;45(9):984-94. PMID: 3800159.

Okada N et al. Abnormal asymmetries in subcortical brain volume in schizophrenia. *Mol Psychiatry*. 2016;21(10):1460-6. PMID: 5030462.

Potkin SG, Ford JM. Widespread cortical dysfunction in schizophrenia: the FBIRN imaging consortium. *Schizophr Bull*. 2009;35(1):15-8. PMID: 2643955.

Psaty BM, Sitlani C. The Cohorts for Heart and Aging Research in Genomic Epidemiology (CHARGE) Consortium as a model of collaborative science. *Epidemiology*. 2013;24(3):346-8.

Satizabal CL et al. Genetic Architecture of Subcortical Brain Structures in Over 40,000 Individuals Worldwide. Submitted (Nature, 2018) *BioRxiv* <https://doi.org/10.1101/402255>

Schmaal L et al. Subcortical brain alterations in major depressive disorder: findings from the ENIGMA Major Depressive Disorder working group. *Mol Psychiatry*. 2016;21(6):806-12. PMID: 4879183.

Schmaal L et al. Cortical abnormalities in adults and adolescents with major depression based on brain scans from 20 cohorts worldwide in the ENIGMA Major Depressive Disorder Working Group. *Mol Psychiatry*. 2017;22(6):900-9. PMID: 5444023.

Schizophrenia Working Group of the Psychiatric Genomics Consortium. Biological insights from 108 schizophrenia-associated genetic loci. *Nature*. 2014;511(7510):421-7. PMID: 4112379.

Schumann G et al. The IMAGEN study: reinforcement-related behaviour in normal brain function and psychopathology. *Mol Psychiatry*. 2010;15(12):1128-39.

Stein JL et al. Identification of common variants associated with human hippocampal and intracranial volumes. *Nature genetics*. 2012;44(5):552-61. PMID: 3635491.

Sun D et al. Large-scale mapping of cortical alterations in 22q11.2 deletion syndrome: Convergence with idiopathic psychosis and effects of deletion size. *Mol Psychiatry*. 2018. PMID: 6292748.

Thompson PM et al. ENIGMA and the individual: Predicting factors that affect the brain in 35 countries worldwide. *NeuroImage*. 2017;145(Pt B):389-408. PMID: 4893347.

Turner JA. The rise of large-scale imaging studies in psychiatry. *Gigascience*. 2014;3:29. PMID: 4365768.

van Erp TG et al. Subcortical brain volume abnormalities in 2028 individuals with schizophrenia and 2540 healthy controls via the ENIGMA consortium. *Mol Psychiatry*. 2016;21(4):547-53. PMID: 4668237.

van Erp TGM et al. Cortical Brain Abnormalities in 4474 Individuals With Schizophrenia and 5098 Control Subjects via the Enhancing Neuro Imaging Genetics Through Meta Analysis (ENIGMA) Consortium. *Biol Psychiatry*. 2018;84(9):644-54. PMID: 6177304.

van Rooij D et al. Cortical and Subcortical Brain Morphometry Differences Between Patients With Autism Spectrum Disorder and Healthy Individuals Across the Lifespan: Results From the ENIGMA ASD Working Group. *Am J Psychiatry*. 2018;175(4):359-69.

Weiner MW et al. The Alzheimer's Disease Neuroimaging Initiative: a review of papers published since its inception. *Alzheimers Dement.* 2012;8(1 Suppl):S1-68. PMID: 3329969.

Whelan CD et al. Structural brain abnormalities in the common epilepsies assessed in a worldwide ENIGMA study. *Brain.* 2018;141(2):391-408. PMID: 5837616.

Wray NR et al. Genome-wide association analyses identify 44 risk variants and refine the genetic architecture of major depression. *Nature genetics.* 2018;50(5):668-81. PMID: 5934326.

CHAPTER 2

Harmonized protocols for large-scale brain MRI research

2.1 Overview

Chapter 2 provides an overview of the work I have completed to develop harmonized processing protocols for large-scale, multisite neuroimaging studies. These efforts include techniques such as Tensor-based morphometry to empower clinical trials (covered in more detail in **Chapter 6**), harmonized ENIGMA protocols to study brain anatomy, and an advanced technique to study high-resolution shape morphometry of subcortical structures.

2.2 Tensor-based morphometry

Since joining the Imaging Genetics Center, I have acted as tensor-based morphometry (TBM) processing lead, in charge of overseeing longitudinal brain change processing and analysis for the Alzheimer's Disease Neuroimaging Initiative (ADNI). This work has been aimed at developing neuroimaging metrics to empower clinical trials, combining imaging with multiscale disease biomarkers to improve disease detection. These robust TBM measures of Alzheimer's disease progression are provided to the wider research community through the LONI IDA (<https://ida.loni.usc.edu/login.jsp>). This work and relevant publications are further discussed in **Chapter 6**.

2.3 ENIGMA harmonized protocols for cortical/subcortical quality assurance

ENIGMA-harmonized protocols include a wide range of freely available neuroimaging processing pipelines. Quality assurance is an essential component of the ENIGMA processing pipelines and takes a crowd-sourcing approach. Individual sites are called upon to perform

quality inspection of ENIGMA-derived brain metrics. Sites submit quality rating based on standardized pass/fail criteria established by the ENIGMA methods team. I led a team responsible for processing and quality assurance for the ENIGMA cortical thickness and surface area method. We established standardized practices for processing, performing visual quality inspection, and results reporting. Code and resource guides, including visual quality rating criteria for 64 cortical regions of interest, are freely available and have been used by hundreds of groups around the world (<http://enigma.ini.usc.edu/protocols/imaging-protocols/>). Our recent GWA study of cortical brain structure, the largest study of the human cortex ever conducted (N>50,000 subjects), employed these methods (Grasby et al., 2018).

2.4. ENIGMA shape analysis pipeline: Development, quality control, and implementation

2.4.1 Rationale

Neurological disorders do not affect all brain regions equally. Patterns of variation may reveal region-specific vulnerabilities that are important for understanding the etiology of a disease process, including underlying cellular/molecular mechanisms (Strange et al., 2014). In order to reveal these patterns in the human brain, neuroimaging techniques have been used to noninvasively extract a variety of structural measures such as volumes, thickness, and surface areas. Here I review some of the current work I have conducted to perform finer mapping of subcortical structures in psychiatric disorders and beyond. The advanced shape analysis technique presented here, including demonstrated applications in **Chapters 3 and 4**, represent large-scale efforts to map the topographic burden of these disorders across the brain.

Many of the ENIGMA disease working groups begin with studies of subcortical structure. This includes extracting volumetric measures from structures such as the lateral ventricles, thalamus hippocampus, amygdala, nucleus accumbens, caudate, putamen, and pallidum using ENIGMA-harmonized segmentation pipelines. These studies utilize a single quality inspected gross volume from each structure. On average, subcortical results are relatively consistent across ENIGMA disease working groups. In **Chapter 3** we performed an analysis to show that subcortical findings (direction and magnitude of effect size) are correlated across certain ENIGMA working groups. The patterns found across these studies tend to show higher ventricular and lower subcortical volumes in patients versus controls, though some variation is observed depending on the structure. For example the ENIGMA schizophrenia working group reported larger globus pallidus volumes in patients (van Erp et al., 2016). The ENIGMA OCD working group also reported larger globus pallidus volumes in adults and larger thalamic volumes in pediatric patients (Boedhoe et al., 2017). In **Chapter 3** I report the more complex findings from the ENIGMA 22q11.2 deletion syndrome (22q11DS) working group and in **Chapter 4** I discuss the mostly lower volumes we find in the ENIGMA bipolar working group. Furthermore, volumetric alterations are known to be mediated by treatment. For example, we found higher volumes were associated with Lithium treatment and lower volumes associated with antiepileptic treatment in the largest neuroimaging study of bipolar disorder (Hibar et al., 2016).

In an effort to build from these early studies of gross volume, my work has moved toward finer mapping of disease effects across these subcortical structures of interest. Goals of this work include providing better resolution in mapping the distribution of these effects, to better understand the extent to which they may overlap underlying subregions (e.g. hippocampal

subfields), which may explain higher-level cognitive/behavioral deficits. Finer mapping may also serve to differentiate the overlapping gross volume effects we see across psychiatric disorders (e.g. smaller hippocampal volumes).

Over the past several years I have worked closely with Dr. Boris Gutman to standardize and validate a subcortical shape analysis protocol capable of high-throughput measurements of subcortical brain structure. I have helped lead efforts to implement this method across many of the ENIGMA working groups where both mega- and meta-analytic shape analyses are carried out on thousands of subjects across the world in a variety of neurodegenerative and psychiatric studies.

2.4.2 Shape analysis protocol

The ENIGMA Shape Analysis Pipeline quantifies thousands of shape characteristics across seven bilateral subcortical structures (left and right nucleus accumbens, amygdala, caudate, hippocampus, putamen, pallidum, and thalamus). Using FreeSurfer or FSL subcortical segmentations as the initial input, shape registration is based on existing shape templates and template medial models. The shape template, or the default ENIGMA shape atlas, was constructed by averaging surface models of 200 unrelated individuals from the Queensland Twin Imaging Study (100 males/100 females, mean age: 22.9, SD: 2.8years). The Euclidean average of these shapes served as the template surface, from which the template medial curve was computed. **Figure 2.4a** shows shape templates for all 7 bilateral subcortical volumes of interest as well as the hippocampus in higher definition.

Two point-wise measures of shape morphometry are derived. The first, termed *radial distance* (local thickness), is derived by a medial model approach (Gutman et al., 2012). For each point $p \in \mathcal{M}$ on the surface, and given a medial curve $c: [0,1] \rightarrow \mathbb{R}^3$, the radial distance is defined by

$$D(p) = \min\{\|c(t) - p\| \mid t \in [0,1]\}$$

The second, based on surface Tensor Based Morphometry (TBM), generalizes TBM from Euclidean spaces to surfaces (Gutman et al., 2012; Gutman et al., 2015). The differential map between the tangent spaces of two surfaces replaces the Jacobian:

$$J: T\mathcal{M}_t \rightarrow T\mathcal{M}$$

In our model, \mathcal{M}_t is the average template, and \mathcal{M} is the surface we wish to study. J is a linear mapping, and may be thought of as the restriction of the standard Jacobian to the tangent spaces of the template and study surfaces. Our model utilizes the Jacobian determinant, representing the surface dilation ratio between the template and the study subject. This measure can be interpreted as the dilation (surface dilation/contraction) required to match a small surface patch around a particular point of the template surface to the small patch of area around the corresponding point on the individual subject. A higher Jacobian value may suggest a larger volume for a corresponding subregion of the structure. Our final TBM measure is the logarithm of the Jacobian determinant, to obtain a distribution closer to Gaussian.

Both radial distance and the logarithm of the Jacobian determinant are calculated in native space for up to 2,502 homologous points across each subcortical structure, providing a detailed map of regional shape variation across subjects.

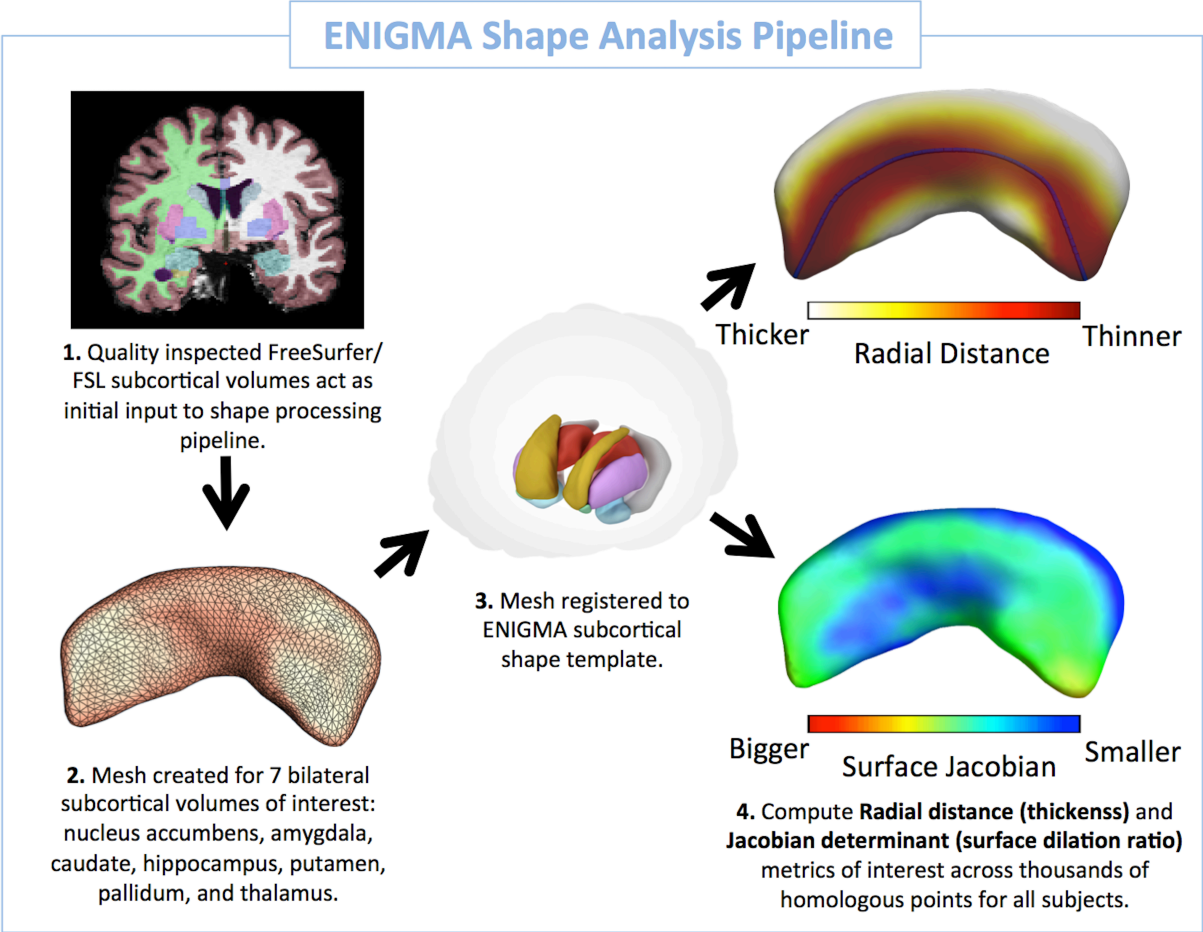


Figure 2.4a. The ENIGMA Subcortical Shape Analysis Pipeline at a glance

Current processing times allow for all 14 (7 bilateral) subcortical models to be created in less than 1 hour per subject. Parallel processing has made it possible to simultaneously run hundreds to thousands of subjects though the shape analysis pipeline on the scale of hours as opposed to days/weeks necessary for other neuroimaging processing pipelines.

We developed a standardized visual quality control rating system that has been successfully adopted by researchers around the world (**Figure 2.4b**). This process includes scripts to render three-dimensional shape models overlaid onto subjects' T1-weighted images. A comprehensive guide including example quality ratings for all structures of interest is provided with the pipeline. Failure rates across all structures tend to be <5% as long as initial segmentation inputs (FreeSurfer/FSL) are of moderate to good quality. Visual quality ratings are logged in a standardized manner and only those structures that pass visual inspection, conforming to T1-weighted MRI anatomical boundaries, are carried forward for statistical analysis.




ENIGMA Shape Analysis Pipeline

<http://enigma.ini.usc.edu/ongoing/enigma-shape-analysis/>



Guided Protocol



THE ENIGMA SUBCORTICAL SHAPE ANALYSIS PIPELINE

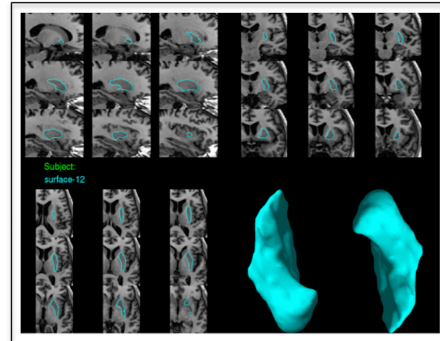
QUALITY CHECKING FREESURFER OUTPUT USING ENIGMA PROTOCOL
 Introduction
 Quality checking [FreeSurfer](#) outputs

GENERATING MESHES AND SHAPE DATA USING PERL SCRIPTS
 Introduction
 System and Program Requirements
 Setting up the program
 Running an individual subject
 Output
 Loading data into [Matlab](#) (see separate ENIGMA Shape Analysis Appendix)
 Visualization (see separate ENIGMA Shape Analysis Appendix)

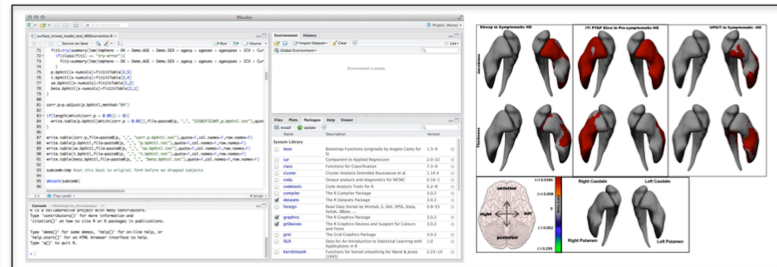
AUTOQA FOR SUBCORTICAL SURFACES (Kathryn Alpert and Arvin Sarem)
 Introduction
 System and Program Requirements
 Running the [AutoQA](#) (Streamlined)
 Script Outputs (Description)
 Reviewing Outputs
 Modifications (see separate ENIGMA Shape Analysis Appendix)
 Troubleshooting
 Rating shape outputs using example cases (separate QA guide with examples)
 Appendix

DATA EXTRACTION FOR ANALYSIS
 Introduction
 System and Program Requirements
 Running the Extraction Script
 Reviewing Script Output

Visual Quality Inspection



Statistical modeling and visualization



The screenshot displays a software interface with a code editor on the left, a central panel with various settings and options, and a right-hand panel showing multiple brain surface visualizations. The visualizations include a color scale legend and several brain slices with highlighted regions in red and cyan.

Figure 2.4b. The ENIGMA Shape Analysis Pipeline is freely available and comes with guided protocol steps, visual quality controls scripts, as well as statistical modeling and visualization resources.

2.4.3 Tracking disease-specific variation and genetic influence of subcortical structure

We have performed a number of studies showing that subcortical shape measures are highly sensitive to disease-specific changes in brain morphometry (Gutman et al., 2013). Vitamin B12 deficiency in the elderly is associated with poorer cognitive function, reduced overall brain volume and increased white matter hyperintensities. In a study of 600 ADNI subjects, we performed the largest investigation of the effects of B12 on the brain. Our shape analysis showed that lower vitamin B12 levels were associated smaller hippocampal and caudate volumes in both

Alzheimer's and mild cognitive impairment, even when adjusting for factors such as *APOE4* status and cognitive impairment (Ching et al., 2012) (**Figure 2.4c**).

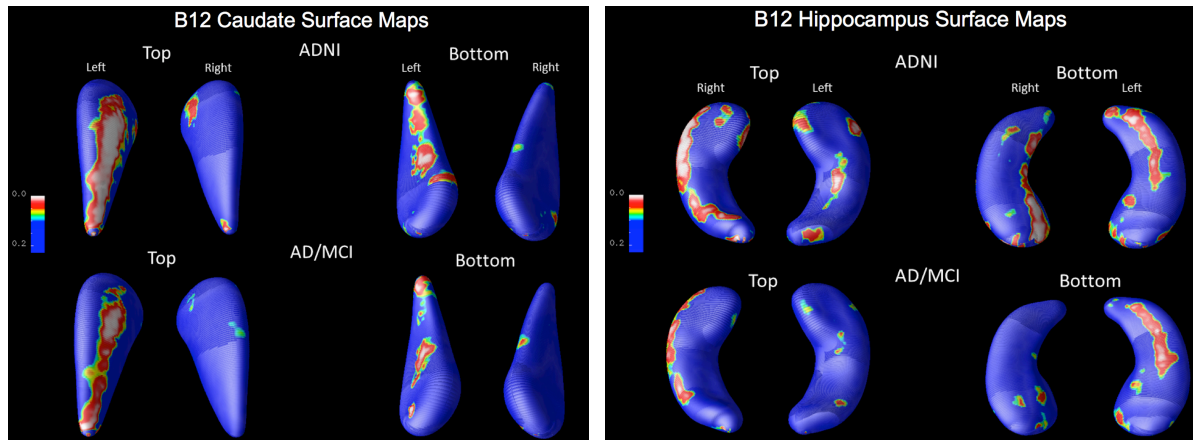


Figure 2.4c. Effect of Serum B12 levels (pg/ml) on 600 ADNI subjects including results from the full cohort and a subset containing Alzheimer's and mild cognitive impairment patients.

Radial atrophy maps showing regions of significant association between B12 and radial size after correcting for age and sex. Similar volumetric associations were found when correcting for age, sex, mini mental state score, Clinical Dementia Rating score (CDR Total), ApoE4 status, body mass index, systolic blood pressure, years of education, white matter hyperintensities and diagnosis (Ching et al., 2012).

Shape analysis has also proven sensitive in cohorts with both pronounced atrophy and those with more subtle effects. In a study of 36 presymptomatic and 37 symptomatic Huntington's disease subjects from the IMAGE-HD cohort, we found an intermediate patterns of local thinning and surface area reductions in presymptomatic versus symptomatic patients in caudate and putamen shape models. Lower regional thickness and surface area were associated with greater number of CAG sequence repeats, higher disease burden and rating scores (UHDRS), and fewer years to

onset (Abaryan et al., 2015; Wilkes et al., 2019) (**Figure 2.4d**). Here, shape analysis provided a better characterization of the spatial extent of (dorsal) striatal atrophy as patients progress toward symptom onset as well as how certain measures of disease severity map to atrophy in subcompartments of the caudate and putamen, structures undergoing significant atrophy in Huntington’s disease.

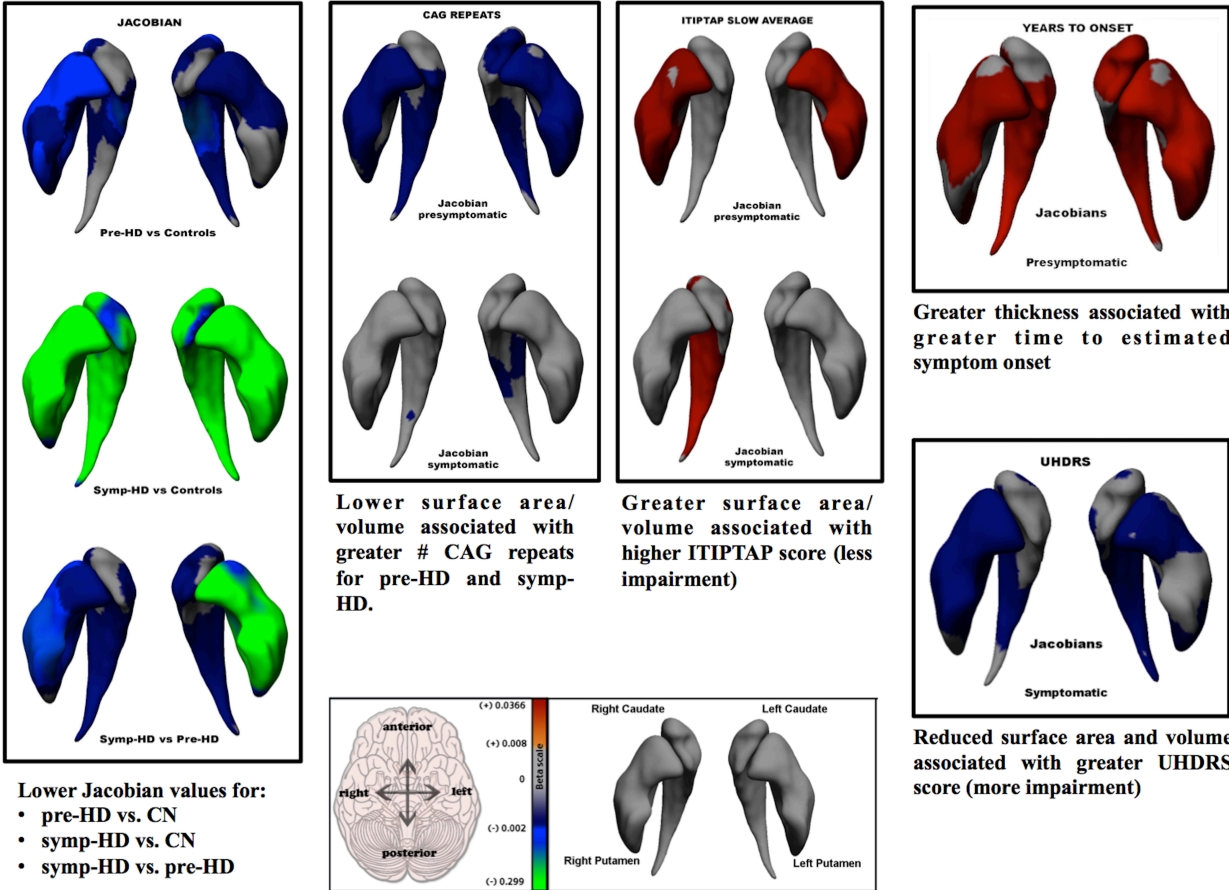


Figure 2.4d. Shape analysis of presymptomatic and symptomatic Huntington’s disease. Intermediate reductions in caudate and putamen surface area in presymptomatic versus symptomatic patients as well as associations with clinical risk such as number of CAG repeats, impairment and estimated time to symptom onset (in presymptomatic patients only) (Abaryan et al., 2015; Wilkes et al., 2019).

In disorders where brain atrophy is known to be less profound, such as HIV+ infection, shape analysis may reveal subtle brain changes that are missed by conventional volumetric analysis. In a study of 264 individuals from the HIV Neuroimaging Consortium (HIVNC) and HIV-associated brain dysfunction study at the Miriam Hospital and Brown University, we detected subtle but complex patterns of higher and lower local thickness associated with lower current and nadir CD4 lymphocyte count (a measure of disease severity) (**Figure 2.4e**). In a subset of individuals, we found lower local surface area in the thalamus, hippocampus and nucleus accumbens was associated with lower processing speed (Ching et al., 2015a; Ching et al., 2015b), a hallmark of HIV-associated neurocognitive disorders (HAND) that affects ~50% of HIV+ patients (Clifford, 2008). Importantly, these associations were not detected when performing more traditional volumetric analysis using single-value FreeSurfer segmentation volumes (**Figure 2.4f**).

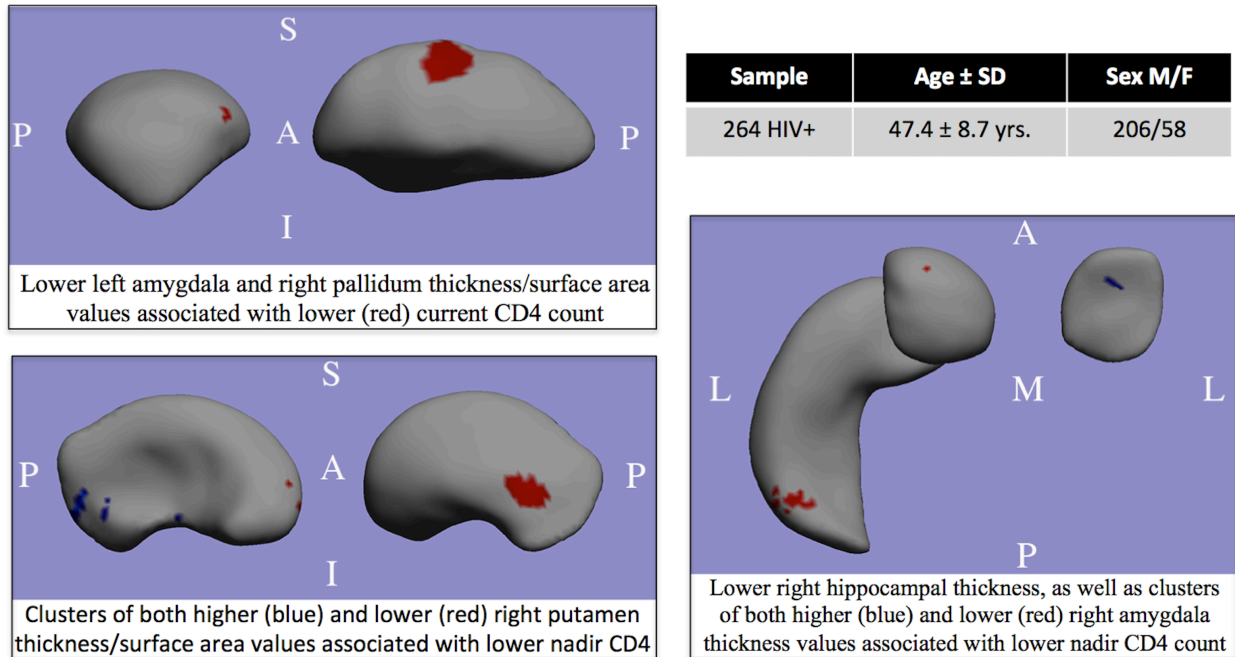


Figure 2.4e. Local thickness associations with current and nadir CD4-lymphocyte counts in a large population of HIV+ individuals. A: anterior; P: posterior; L: lateral; M: medial; S: superior; I: inferior (Ching et al., 2015a).

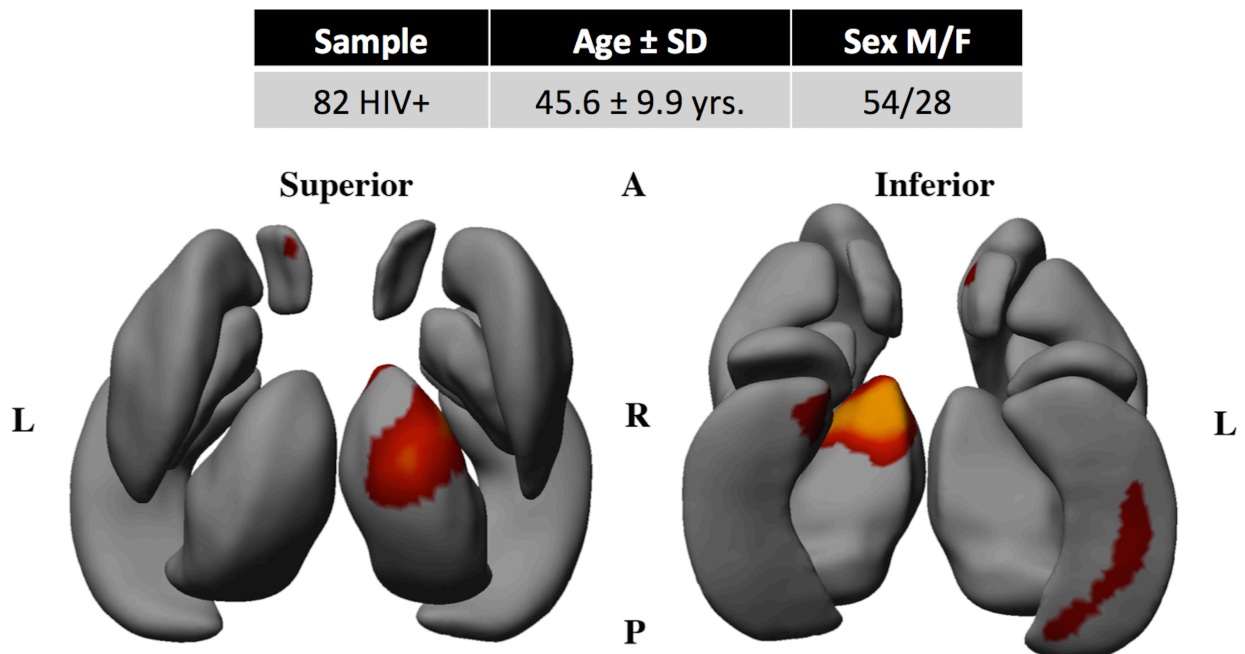


Figure 2.4f. Associations between subcortical Jacobian values and processing speed (PS)

showing β values for regions passing FDR correction ($q=0.05$). Red/Yellow regions indicate positive β values or regions where lower Jacobian values (lower surface area and volume) are associated with lower PS scores (greater impairment). Left Image: dorsal view; Right Image: ventral view; A: anterior; P: posterior; L: left; R: right (Ching et al., 2015b).

Human brain volumes derived from MRI are highly heritable (Blokland et al., 2012; Satizabal et al., 2019). To determine the heritability of the measures derived from the ENIGMA Shape Analysis pipeline, we studied the Jacobian and radial distance shape metrics of 1,400 subjects including both twins and siblings (Gutman et al., 2015). The heritability estimates were in line with previous studies using other measures of volume but provide a more detailed map of the heritability across subregions of each structure (**Figure 2.4g**). This was the first study to estimate heritability of vertex-wise features of subcortical structures and outperformed other shape analysis methods (SPHARM). The consistent genetic influence on these measures may be used in feature weighting for GWA studies of the brain.

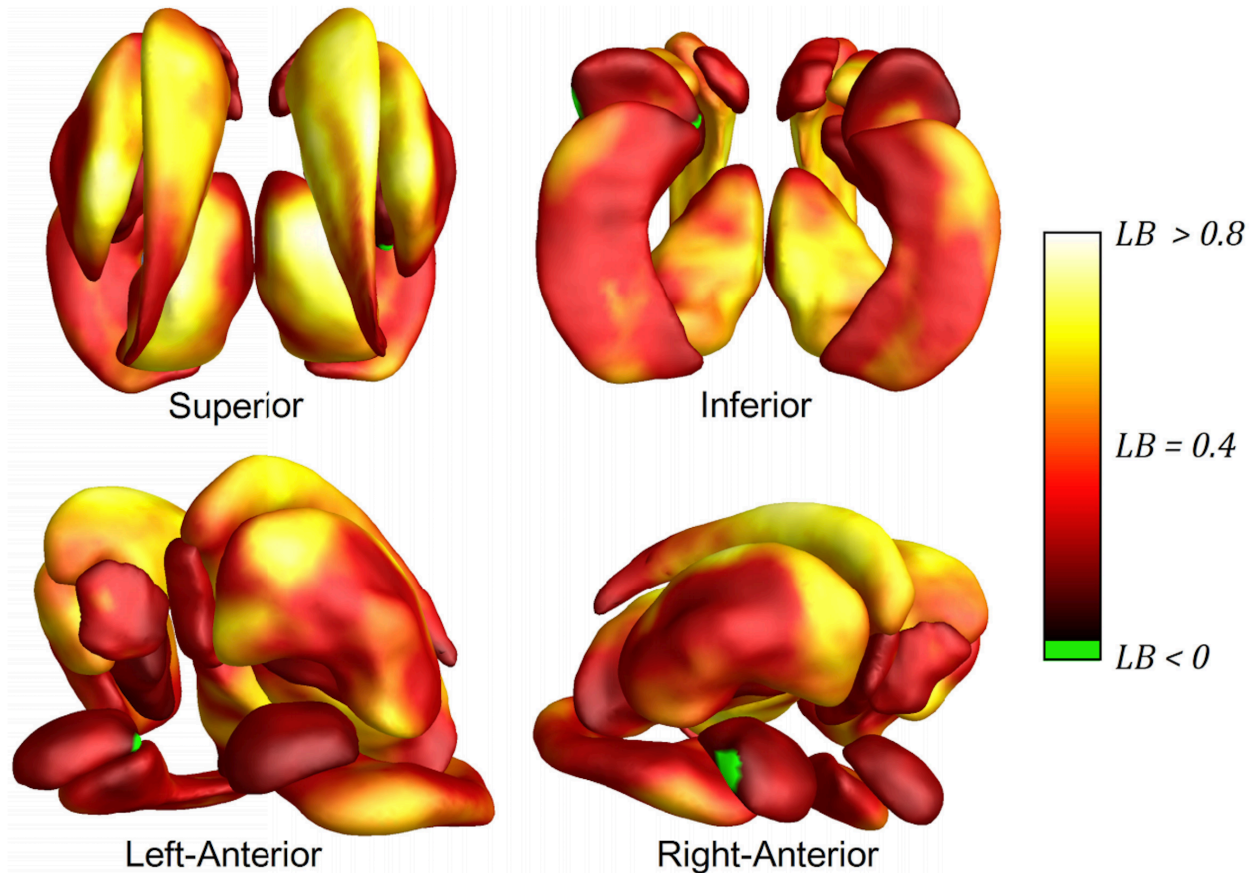


Figure 2.4g Meta-analysis of heritability estimates for surface Jacobian shape metric across 1,400 subjects. LB is the lower bound of heritability where an LB of $>.8$ represents regions where genetic variation explains more than 80% of the Jacobian (phenotypic) variation (Gutman et al., © 2015 IEEE).

In our recent study of common genetic variants influencing subcortical structure, we identified 5 novel genetic variants influencing caudate and putamen volume (Hibar et al., 2015). We mapped the strongest effects of a particular novel snp (rs945270) to the putamen using our shape analysis technique to understand the specific patterns of genetic influence that locus has across the surface of the putamen (**Figure 2.4h**). As expected, this locus does not affect the entire putamen volume uniformly. Instead, the shape analysis revealed a pattern of influence across

subcompartments, motivating future explorations into the underlying cellular and molecular makeup of these regions.

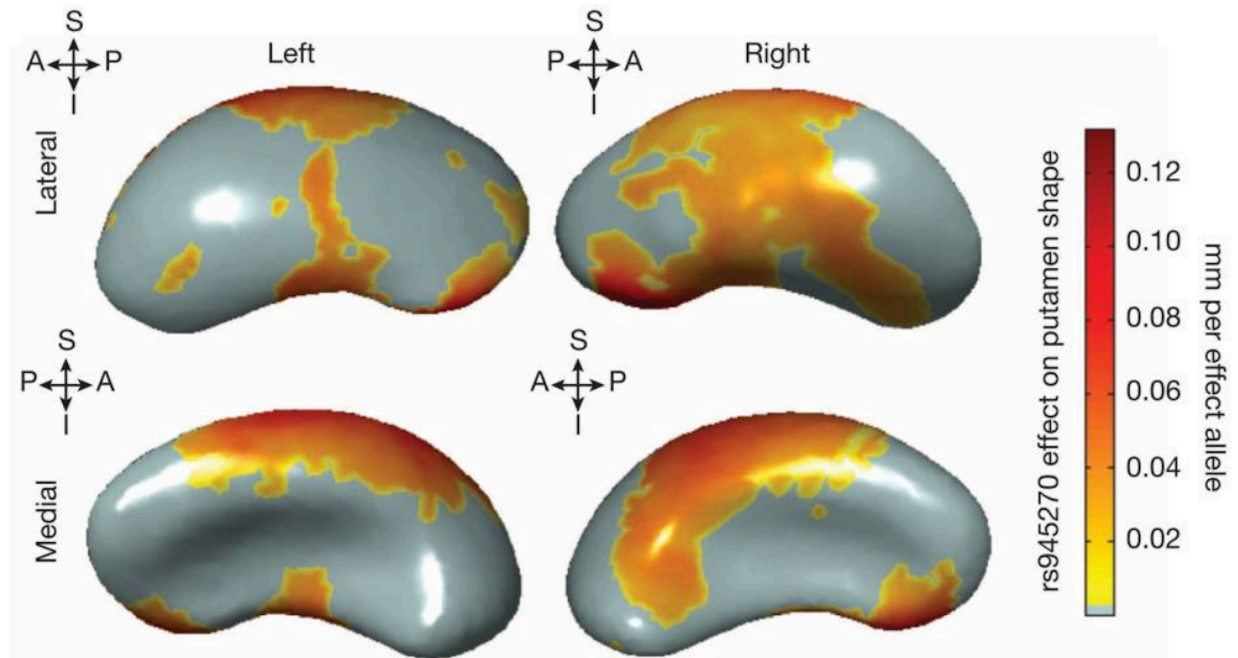


Figure 2.4h. A novel, genome-wide significant locus rs945270 was found to have a strong effect on putamen shape features as mapped in 1,541 subjects. Each copy of the rs945270-C allele was significantly associated with greater radial distance (warmer colors indicating greater local width of the putamen) (Hibar et al., 2015).

While our subcortical shape measures provide a better map of the local variations that affect volume, the dense sampling of local measures presents a challenge to GWA studies that must apply strict statistical adjustments in proportion to the number of testes performed. One solution would be to down sample the number of shape metrics. Another option is to perform genetic clustering to define subregions with common genetic influences that could then be tested in the GWAS framework. In the first genetic clustering analysis of thalamic shape models, we found

distinct clusters of genetically influenced morphology by applying X -means clustering (an iterative form of k -means) on genetic correlations between distances measures across the thalamic models (**Figure 2.4i**). Due to their consistent genetic determination, using these clusters as targets for genome-wide scans may boost power when searching for common variants affecting subcortical morphology by reducing the multiple comparisons problem (Ching et al., 2013).

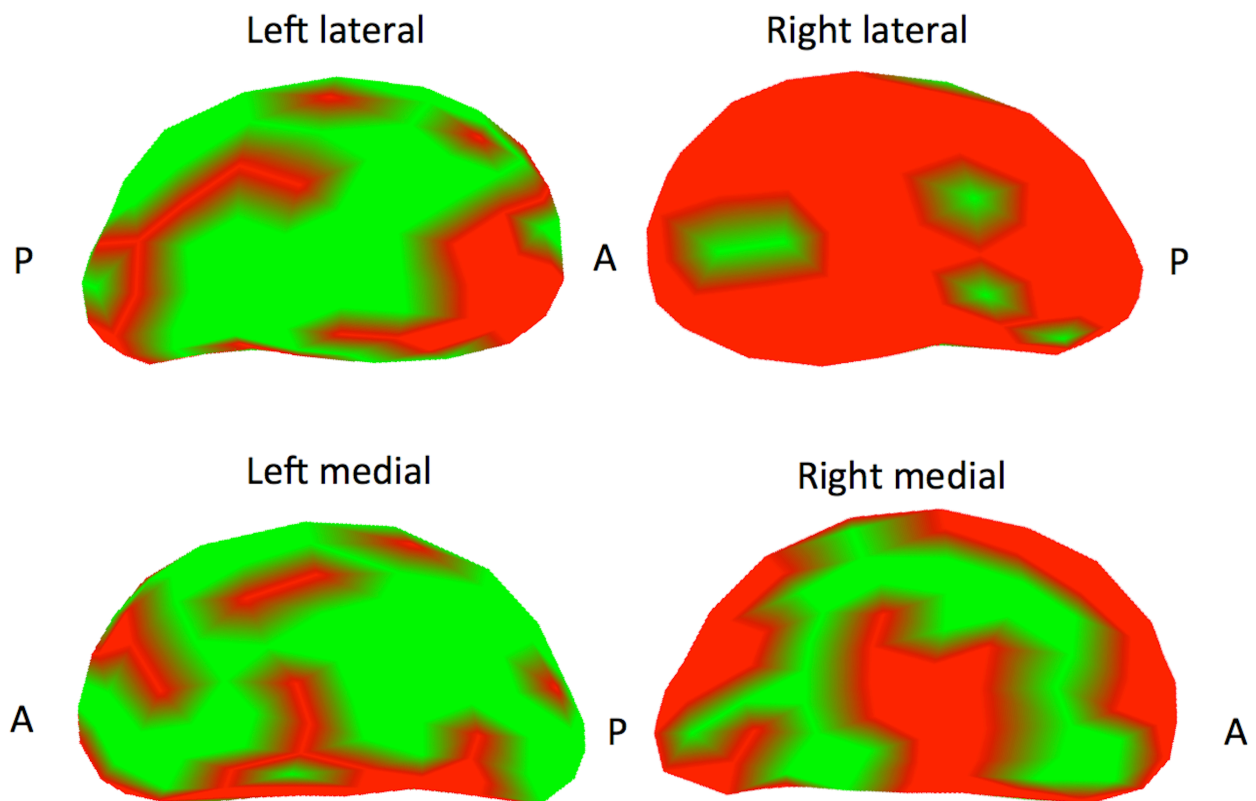


Figure 2.4i. Left and right thalamic clustering models including lateral and medial surfaces (A: anterior, P: posterior) with 2 main regions (red and green) found to have common genetic influence (Ching et al., 2013).

The ENIGMA Shape Analysis Pipeline has been widely applied across the ENIGMA disease working groups and now includes manuscripts in preparation and submission from the ENIGMA

schizophrenia (Gutman et al., 2019), major depression (Ho et al., 2019), obsessive compulsive (Fouche et al., 2019), 22q11.2 deletion syndrome (**Chapter 3**), and bipolar working groups (**Chapter 4**), lending new insights into the subregional burden of these psychiatric disorders across subcortical structures.

2.4.4 Advantages and limitations

The ENIGMA Shape Analysis technique has several key advantages and limitations that are worth mentioning explicitly. One key advantage is that the method offers measures that are sensitive to subtle variations in local morphometry that are related to underlying compartments (subregions or subfields) with known functions. The ability to directly sample the underlying thickness and surface area of these subcompartments may help to better explain a biological effect or represent a stronger marker of pathophysiology than more conventional volumetric approaches.

Degenerative and psychiatric disorders do not affect all brain structures in a uniform way. The disease-specific patterns detected by this method may provide a better understanding of the structure/function relationships, disease course and treatment response. Mapping of disease burden across subfields may also guide finer-grained investigations into specific cellular/molecular vulnerabilities and lead to more targeted therapeutics.

Importantly, our technique is also able to discern complex effects within a structure. As opposed to single volume measures that only detect effects in one direction, the ENIGMA shape analysis method can discern complex patterns of both higher and lower thickness or surface area that may

indicate differential affects across the structure. As in **Chapter 3**, in the context of 22q11.2 deletion syndrome, we see that the story of volumetric variation in a particular disorder is often made more complicated (or interesting) when viewed through the lens of shape analysis.

These shape measures may also drive new insights regarding effects on neighboring or interconnected brain structures. Future work aims to investigate the relationship between subcortical shape variation and cortical structure as well as measures of white matter connectivity. Altered subcortical structures do not act alone in the presentation of psychiatric illness, calling for a multimodal approach that relates shape measures to integrated structural and functional brain networks.

In terms of processing speed, the medial demons approach used by the ENIGMA Shape Pipeline is capable of processing subjects in less than 1 hour as opposed to hours or days in the case of other comparable techniques. The method also has good test-retest reliability with >0.81 ICC in unpublished tests. In terms of interpretability, the radial distance (local thickness) and surface Jacobian (local surface area dilation/contraction) metrics provide intuitive measures of local morphometry. However, more work is needed to relate ENIGMA shape metric variation to known underlying compartments such as hippocampal subfields (Mamah et al., 2016).

As visual quality inspection represents a significant (though not insurmountable) bottleneck in processing time for any neuroimaging technique, the ENIGMA Shape Pipeline provides guidance for quality assurance with visual inspections of a single structures taking less than 2 minutes in most cases. However, new machine learning approaches may significantly reduce the

amount of time spent on visual quality control. We have performed initial work applying machine learning techniques in the visual evaluation of subcortical shape models (Petrov et al., 2017). Initial findings, based on models derived from large samples of visually inspected shape data from across the ENIGMA consortium, indicate such machine learning techniques may reduce visual inspection times by as much as 50%.

Chapter 2 includes findings adapted from the following selected studies:

Cortical Quality Assurance

Grasby KL, Jahanshad N, Painter JN, Colodro-Conde L, Bralten, J, Hibar DP, Lind PA, Pizzagalli F, **Ching CRK**, ... (200+ authors)... Stein JL, Thompson PM, Medland SE. The genetic architecture of the human cerebral cortex. **Submitted (Nature 2018)** BioRxiv doi: <https://doi.org/10.1101/399402>

ENIGMA Shape Analysis Pipeline Development

Ching CRK, Hibar DP, McMahon K, de Zubicaray G, Martin N, Wright M, Thompson PM. Genetic clustering reveals thalamic regions with common genetic determination in 640 twins. Organization on Human Brain Mapping Conference, Seattle, WA, 2013.

Ching CRK, Gutman BA, Nir TM, Hua X, Jahanshad N, Harezlak J, Tate DF, Schifitto G, Gongvatana A, Zhong J, Zhu T, Taylor MJ, Campbell TB, Daar ES, Alger JR, Singer E, Cohen RA, Navia B, Thompson OM. High-resolution shape analysis reveals subcortical morphometry and lymphocyte relationships in HIV+. Organization for Human Brain Mapping (OHBM), Honolulu, Hawaii, June 14-18 2015.

Ching CRK, Gutman BA, Nir TM, Schonfeld D, Jahanshad N, Hua X, Gongvatana A, Navia B, Cohen RA, Thompson PM. High-resolution shape analysis in HIV+ adults reveals associations between neurocognitive performance and subcortical morphometry. Society for Neuroscience (SFN), Chicago, Illinois, October 17-21, 2015.

Ching CRK, Rajagopalan P, Toga AW, Jack Jr CR, Weiner MW, Thompson PM. Elderly people with lower vitamin B12 levels have smaller hippocampal and caudate volumes. Society for Neuroscience Annual Conference, New Orleans, LA, 2012.

Fouche J, Groenewold N, Heany S, Lochner C, Alonso P, Busatto GF, Cardoner N, Cath DC, **Ching CRK**, Denys D, Fukui K, Gutman B, Hoexter MQ, Jahanshad N, Jang JH, Jung WH, Kim SN, Kwon JS, Mataix-Cols D, Menchon JM, Migue EC, Nakamae T, Narumoto J, Nishida S, Phillips ML, Pujol J, Remijnse PL, Sakai Y, Sato JR, Schweren L, Shin NY, Soriano-Mas C, Thompson PM, Yamada K, Veltman DJ, van den Heuvel OA, Stein DJ. Shape analysis of subcortical structures in obsessive-compulsive disorder: a multi-site analysis of the OCD Brain Imaging Consortium. In preparation.

Gutman BA, Jahanshad N, **Ching CR**, Wang Y, Kochunov PV, Nichols TE, Thompson PM. Medial Demons Registration Localizes The Degree of Genetic Influence Over Subcortical Shape Variability: An N= 1480 Meta-Analysis. *Proc IEEE Int Symp Biomed Imaging*. 2015;2015:1402-6. PMID: 4578221. © 2015 IEEE.

Gutman BA, van Erp TGM, Alpert K, Isaev D, Zavaliangos-Petropulu A, Ragothaman A, Saremi A, Calhoun V, Glahn DC, Satterthwaite T, Andreassen OA, Borgwardt S, Howells F, Voineskos A, Radua J, Huang AJ, Weideman A, Potkin SG, Facorro BC, Shen L, Lebedeva I, Spalletta G, Donohoe G, Kochunov P, Trung Doan N, Agartz I, Harrisberger F, Stein DJ, Dickie EW, Canales-Rodriguez EJ, Roiz-Santiañez R, Cong S, Tomyshev A, Piras F, Wright M,

McMahon KL, de Zubicaray G, **Ching CRK**, Jahanshad N, Thompson PM, Turner JA and Wang L for the ENIGMA Schizophrenia Working Group. A Meta-Analysis of Deep Brain Structural Shape Abnormalities in 2,763 Individuals with Schizophrenia Compared to 3,768 Healthy Volunteers via the ENIGMA Consortium. Submitted (Molecular Psychiatry)

Hibar DP, Stein JL, Renteria ME, Arias-Vasquez A, Desrivieres S, Jahanshad N, Toro R, Wittfeld K, Abramovic L, Andersson M, Aribisala BS, Armstrong NJ, Bernard M, Bohlken MM, Boks MP, Bralten J, Brown AA, Chakravarty MM, Chen Q, **Ching CR**, ...(304 authors)... Thompson PM, Medland SE. Common genetic variants influence human subcortical brain structures. *Nature*. 2015;520(7546):224-9. PMID: 4393366.

Petrov D, Gutman BA, Yu SJ, van Erp TGM, Turner JA, Schmaal L, Veltman D, Wang L, Alpert K, Isaev D, Zavaliangos-Petropulu A, **Ching CRK**, Calhoun V, Glahn D, Satterthwaite TD, Andreasen OA, Borgwardt S, Howells F, Groenewold N, Voineskos A, Radua J, Potkin SG, Crespo-Facorro B, Tordesillas-Gutierrez D, Shen L, Lebedeva I, Spalletta G, Donohoe G, Kochunov P, Rosa PGP, James A, Dannlowski U, Baune BT, Aleman A, Gotlib IH, Walter H, Walter M, Soares JC, Ehrlich S, Gur RC, Doan NT, Agartz I, Westlye LT, Harrisberger F, Riecher-Rossler A, Uhlmann A, Stein DJ, Dickie EW, Pomarol-Clotet E, Fuentes-Claramonte P, Canales-Rodriguez EJ, Salvador R, Huang AJ, Roiz-Santianez R, Cong S, Tomyshev A, Piras F, Vecchio D, Banaj N, Ciullo V, Hong E, Busatto G, Zanetti MV, Serpa MH, Cervenka S, Kelly S, Grotegerd D, Sacchet MD, Veer IM, Li M, Wu MJ, Irungu B, Walton E, Thompson PM. Machine Learning for Large-Scale Quality Control of 3D Shape Models in Neuroimaging. *Mach Learn Med Imaging*. 2017;10541:371-8. PMID: 6049825.

Satizabal CL,... **Ching CRK**,... Genetic Architecture of Subcortical Brain Structures in Over 40,000 Individuals Worldwid. **Submitted (Nature Genetics)** BioRxiv doi: <https://doi.org/10.1101/173831>

Wilkes F, Abaryan Z; **Ching CRK**, Gutman B, Madsen S; Walterfang M; Velakoulis D, Stout J, Chua P, Egan G, Thompson PM; Looi J, Georgiou-Karistianis N. Striatal morphology and neurocognitive dysfunction in Huntington disease: The IMAGE-HD study. In Review (Psychiatry Research: Neuroimaging 2019)

Abaryan Z, Wilkes F, **Ching CRK**, Gutman BA, Madsen SK, Walterfang M, Stout J, Churchyard A, Chua P, Velakoulis D, Egan G, Looi JCL, Thompson PM, Georgiou-Karistianis N. Striatal shape differs before and after symptom onset in Huntington's disease and relates to clinical severity: the IMAGE HD study. Society for Neuroscience (SFN), Chicago, Illinois, October 17-21, 2015.

2.5 Chapter 2 references

Blokland et al. Genetic and environmental influences on neuroimaging phenotypes: a meta-analytical perspective on twin imaging studies. *Twin Res Hum Genet.* 2012;15(3):351-71. PMID: 4291185.

Boedhoe et al. Distinct Subcortical Volume Alterations in Pediatric and Adult OCD: A Worldwide Meta- and Mega-Analysis. *Am J Psychiatry.* 2017;174(1):60-9. PMID: 5344782.

Clifford DB. HIV-associated neurocognitive disease continues in the antiretroviral era. *Top HIV Med.* 2008;16(2):94-8.

Gutman et al. Maximizing power to track Alzheimer's disease and MCI progression by LDA-based weighting of longitudinal ventricular surface features. *NeuroImage.* 2013;70:386-401. PMID: 3942253.

Gutman et al. Shape Matching With Medial Curves and 1-D Group-Wise Registration. *Proc IEEE Int Symp Biomed Imaging.* 2012: 716-719. <https://doi.org/10.1109/ISBI.2012.6235648>

Hibar et al. Subcortical volumetric abnormalities in bipolar disorder. *Mol Psychiatry.* 2016;21(12):1710-6. PMID: 5116479.

Hibar et al. Common genetic variants influence human subcortical brain structures. *Nature.* 2015;520(7546):224-9. PMID: 4393366.

Mamah et al. Subcortical neuromorphometry in schizophrenia spectrum and bipolar disorders. *Neuroimage Clin.* 2016;11:276-86. PMID: 4781974.

Strange et al. Functional organization of the hippocampal longitudinal axis. *Nat Rev Neurosci.* 2014;15(10):655-69.

van Erp et al. Subcortical brain volume abnormalities in 2028 individuals with schizophrenia and 2540 healthy controls via the ENIGMA consortium. *Mol Psychiatry.* 2016;21(4):547-53. PMID: 4668237.

CHAPTER 3

22q11.2 Deletion Syndrome Brain Structure

3.1 Overview

There is increasing evidence that rare copy number variants (CNV) may play an important role in the etiology of psychosis and account for a larger proportion of cases than previously believed (Cantor and Geschwind, 2008; Sebat et al., 2009; Malhotra and Sebat, 2009; Gimán et al., 2011). Limited data exists on individuals carrying the same highly penetrant CNV, but studying cohorts with both genetically homogeneous and known etiology may provide an important framework to determine how genes within and/or outside CNV regions disrupt biological pathways that ultimately contribute to psychiatric phenotypes.

The 22q11.2 locus is an important region to investigate gene dosage effects on brain development as it's particularly susceptible to chromosomal rearrangements via non-allelic homologous recombination (McDonald-McGinn et al., 2012). 22q11.2 deletion syndrome (22q11DS) is a neurogenetic disorder resulting from a hemizygous microdeletion on the long arm of chromosome 22 and affects genes known to be involved in neurodevelopment. 22q11DS is associated with a wide range of physical abnormalities including craniofacial, cardiac, immune and neurocognitive defects. Over 60% of 22q11DS patients meet diagnostic criteria for a developmental neuropsychiatric disorder, including attention-deficit/hyperactivity, anxiety, mood and autism spectrum disorders (Drew et al., 2011; Jonas et al., 2014). With a prevalence of approximately 1 per 3,000-4,000 births, roughly 1 in 4 22q11DS patients develop a schizophrenia spectrum disorder in adolescence or early adulthood, making it the strongest known risk factor for schizophrenia (Murphy, 2002). Recent studies have also indicated a higher prevalence of early-onset Parkinson's disease in 22q11DS (Zaleski et al., 2009).

The 22q11.2 region is a neurodevelopmental hotspot. Out of 90 genes present in the typical 3Mb locus, there are ~50 protein coding, 10 noncoding RNA's and 27 pseudogenes, several of which are highly expressed in brain tissue. A number of these genes are widely studied, have been implicated in psychiatric disorders and are associated with intermediate phenotypes such as dopamine regulation, myelin, neural migration, and synaptic function (Jonas et al., 2014)

Roughly 85% of patients carry the same 3Mb microdeletion (A-D subtype), ~10% carry a 1.5Mb deletion (A-B subtype), with the remaining carrying other smaller atypical deletions. Variability in deletion length, breakpoint position, as well as aspects of the intact chromosome, likely plays a role in the highly heterogeneous clinical presentation (Jonas et al., 2014, McDonald-McGinn et al., 2015).

The pattern of 22q11DS burden on brain morphometry is far from understood. MRI-derived cortical and subcortical volume reductions have been reported by relatively small cohort studies and may follow an anterior to posterior gradient, with more pronounced brain volume reductions in more posterior brain regions (Kates et al., 2004; Bish et al., 2004; Tan et al., 2009; Bearden et al., 2008). Subcortical volume reductions are commonly reported, but many studies include relatively small samples, which may limit the power to detect complex brain change in 22q11DS. Mouse models of 22q11DS have found disrupted neurogenesis (Meechan et al., 2009), reduced hippocampal spine density (Stark et al., 2008), and reduced hippocampal-prefrontal synchrony (Sigurdsson 2010).

22q11.2 microduplications (22q11Dup) were first described clinically in 2003 (Ensenauer et al., 2003). Unlike 22q11DS, which tends to occur de novo, the duplication is frequently inherited (Ou et al., 2008). Less is known about the 22q11Dup phenotype, which is highly variable (Wentzel et al., 2008), but it appears to be associated with elevated rates of ASD and delays in language and psychomotor development (Wenger et al., 2016). There are few studies of 22q11Dup, but in a recent analysis of over 47,000 individuals, 22q11Dup was significantly less common in schizophrenia cases than in the general population (0.014% compared to 0.085%, OR=0.17), suggesting the first putative protective mutation for schizophrenia (Rees et al., 2014). This finding of lower schizophrenia incidence in 22q11Dup carriers has now been replicated in several independent studies (Marshall et al., 2016; Rees et al., 2016). In section 3.2 I present results from the first brain imaging study of 22q11Dup ever conducted.

This genetically-defined neurodevelopmental condition offers a biologically tractable framework to dissect genetic mechanisms underlying brain phenotypes associated with complex neuropsychiatric disorders. The ENIGMA 22q11.2 deletion syndrome working group, led by Dr. Carrie Bearden, is the largest brain imaging study of 22q11DS and 22q11Dup, including 11 international study samples and over 500 22q11DS, 35 22q11Dup and 330 healthy controls (6-56 yrs, 49% female). The ENIGMA 22q11DS working group is studying reproducible MRI markers of 22q11DS and 22q11Dup, and how these markers are associated deletion subtypes and psychosis. Furthermore, we are comparing the markers identified in 22q11DS against those discovered in the largest brain imaging studies of idiopathic psychosis in close collaboration with the ENIGMA Schizophrenia working group.

In our recently published paper of ENIGMA 22q11DS cortical structure (Sun et al., 2018), the largest brain imaging study ever conducted of 22q11DS, we detected robust differences between 22q11DS and controls (**Figure 3.1a**), associations with deletion size (**Figure 3.1b**), as well as a significant correlation between 22q11DS-related psychosis and idiopathic schizophrenia (**Figure 3.1c**).

When comparing 386 22q11DS patients to 315 healthy controls (HC), complex group differences emerged with a pattern of largely thicker cortex and lower surface area in 22q11DS compared to HC (**Figure 3.1a**). While the age range (6-56yrs) was an important strength of our study — few previous studies have investigated the effects of 22q11DS later in life — sparse age-by-group interactions were detected. Future large-scale longitudinal studies are needed to assess differential developmental trajectories in 22q11DS compared to typical brain development. Typically, cortical thinning initiates around year 2-4 and continues throughout life. Cortical surface area changes follow nonlinear trajectories starting in fetal development. And while the precise genetic mechanisms for disrupted cortical formations such as those detected here are unknown, several genes present in the 22q11.2 locus have been tied to early neural development. *RanBP1* is expressed in cortical progenitors from the ventricular/subventricular zone and is involved in rapidly dividing precursors, which may cause deficits in cortical radial glial progenitors leading to reduced cortical surface area. *DGCR8* is another candidate for altered cortical development and is widely expressed in cortical neurons. A preliminary classification analysis using cortical thickness and surface area alone (using support vector machines) provided an average case versus control classification accuracy of 93.8% (sensitivity: 94.2%; specificity: 93.3%). The regions most important to correct classification were surface areas of the left caudal

anterior cingulate, bilateral cuneus, and precentral gyrus, as well as thickness of the left insula. When the derived model was applied to two test datasets, containing only 22q11DS patients, all subjects were correctly classified as 22q11DS.

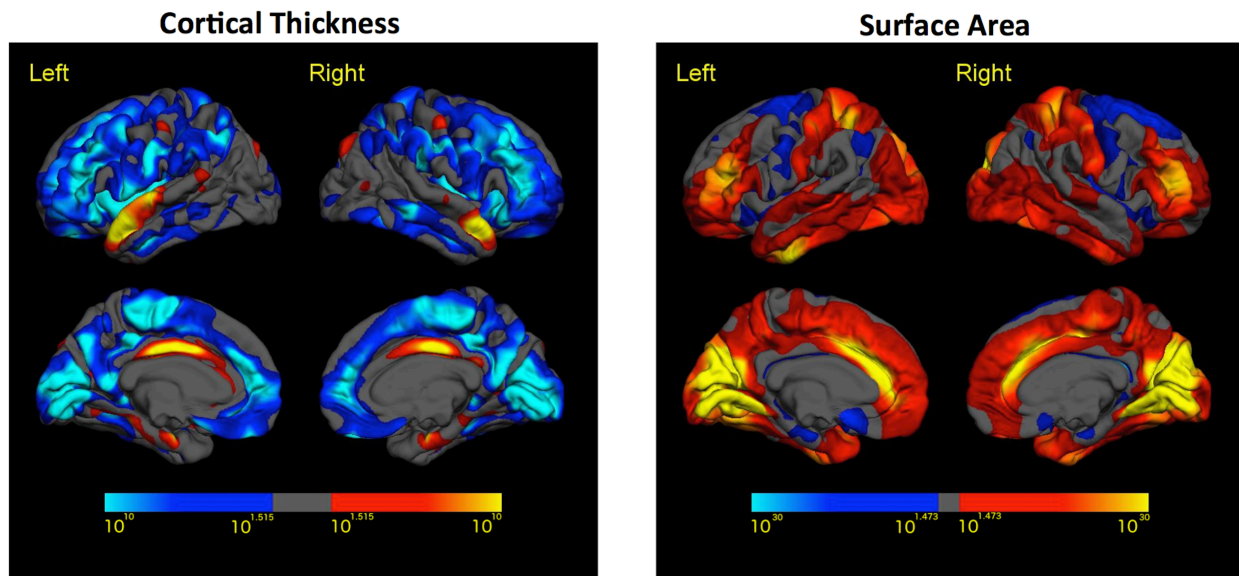


Figure 3.1a. Vertex-wise cortical thickness and surface area analysis showing differences between deletion patients and healthy controls. Thresholded p-values are displayed in regions that pass FDR correction. On the left the cooler blue colors represents thicker cortex in 22q11DS participants but the opposite effect was also detected, indicated by red/yellow in the medial temporal and cingulate regions where 22q11DS subjects were thinner compared to controls. On the right, surface area patterns are largely in the opposite direction, red/yellow indicating lower surface area in 22q11DS compared to controls, though some medial temporal, frontal and superior frontal regions showed the opposite effect (blue).

This study provides the first evidence for brain differences across deletion subtypes, with prior smaller studies unable to detect effects, likely due to challenges in recruiting (3Mb A-D deletion is present in ~85% of cases and the 1.5Mb A-B deletion present in ~10% of cases). Here, group

differences were detected across all comparisons of 108 A-D, 23 A-B, and 87 matched controls (across 11 study sites) (**Figure 3.1b**). Of particular interest was the widespread pattern of lower surface area in the more typical A-D deletion compared to the smaller AB deletion, a finding that may drive future insights into the heterogeneity of 22q11DS clinical presentation.

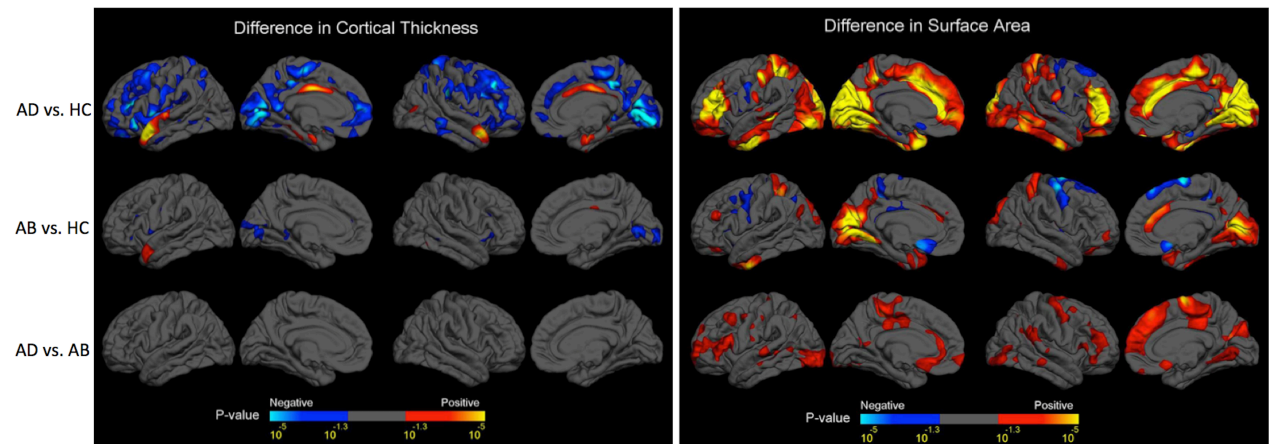


Figure 3.1b. Vertex-wise deletion subtype results comparing the most common 3Mb A-D deletion with the smaller less common 1.5Mb A-B deletion. Left panel includes cortical thickness, right panel includes surface area. The top row is A-D versus controls and looks quite similar to the 22q11DS versus HC comparison (as most 22q11DS have the A-D deletion subtype), showing largely thicker cortex and lower surface area in the A-D subjects. The second row shows the A-B versus HC, revealing a weaker but similar pattern to the A-D versus HC. The third row shows the first demonstrated evidence of brain difference between deletion subtypes, with A-D showing a widespread pattern of lower surface area compared to the smaller A-B deletion.

22q11DS-related psychosis and idiopathic schizophrenia are known to share core symptoms and course of illness. However, the extent to which underlying neuropathology overlaps between

conditions is far from understood. Here we show a significant correlation between cortical thickness results from the 22q11DS+psychosis versus –psychosis comparison and the ENIGMA schizophrenia working group case/control analysis (van Erp et al., 2018) (**Figure 3.1c**), lending evidence to concordant brain alterations in both disorders. Importantly, no significant correlation was observed between 22q11DS +/- psychosis effect sizes and results from the ENIGMA major depressive working group study of cortical structure. Given ENIGMA harmonized processing and analysis techniques, work is now underway to directly compare these cortical measures, as well as other harmonized neuroimaging metrics across the ENIGMA 22q11DS and schizophrenia working groups (**Chapter 5**).

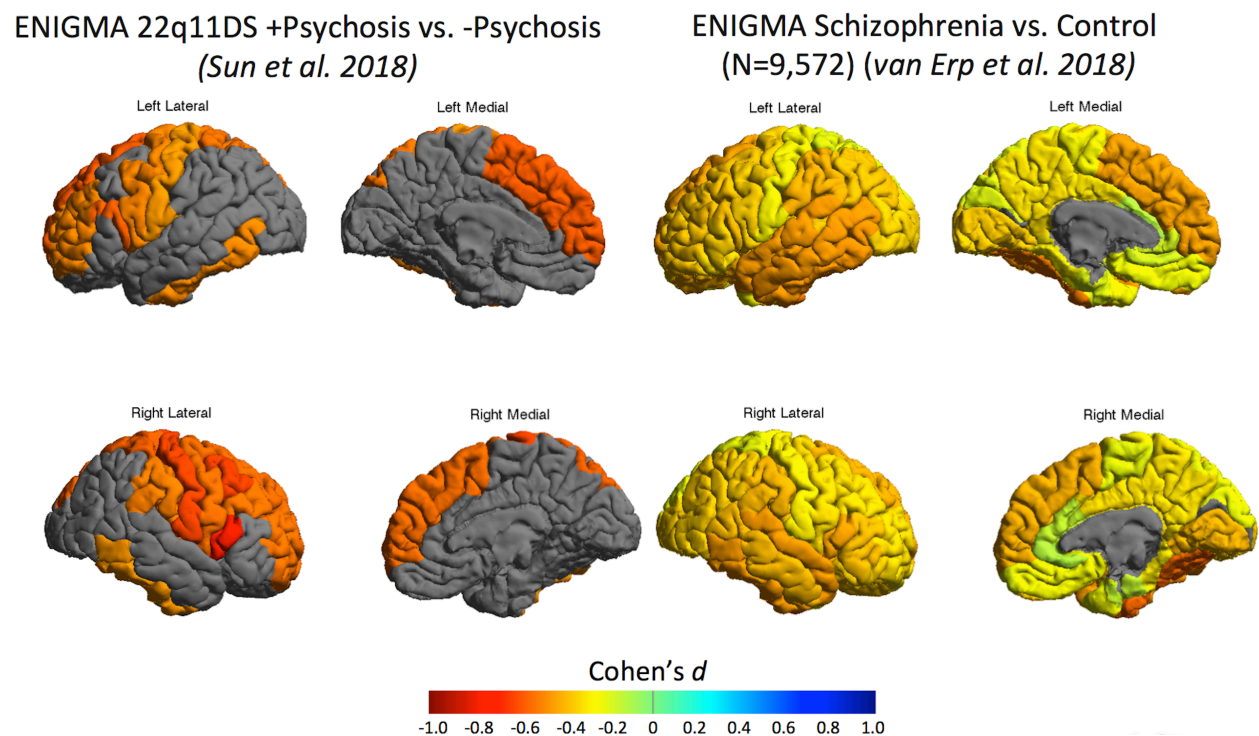


Figure 3.1c. Cortical thickness comparison between 22q11DS+psychosis versus –psychosis with results plotted on same effect size scale (Cohen's *d*) as those from the largest study of cortical structure ever conducted in idiopathic schizophrenia (ENIGMA SCZ working group). Results

here reflect cortical ROI analyses (average thickness across 34 bilateral ROIs). Warmer colors (red/yellow) indicate thinner cortical regions in both 22q11DS+psychosis (left) and schizophrenia (right).

In our recent ENIGMA 22q11DS study of diffusion-weighted metrics (Villalon et al. 2019), we found widespread white-matter alterations in 22q11DS compared to controls in the largest study of 22q11DS white matter ever completed. On average, 22q11DS displayed lower diffusivity compared to controls (mean diffusivity: a measure of total diffusion velocity, cellularity, edema, and necrosis; radial diffusivity: measure of inter-axonal spacing, de- myelination; axial diffusivity: a measure of axonal damage). Case versus control results from the analysis of fractional anisotropy (FA), an measure that likely reflects axonal packing, were more complex, with regions of both higher and lower FA in 22q11DS. Trends for lower diffusivity in A-D versus A-B deletion subtypes were observed but did not survive correction for multiple comparisons. 22q11DS-related psychosis was associated with lower diffusivity. Interestingly, these results did not significantly overlap with those from the ENIGMA schizophrenia working group DTI study in which they reported a widespread pattern of lower FA in schizophrenia patients, suggesting possible divergent white matter alterations across both disorders.

In the following sections I present work completed during my graduate studies focusing specifically on subcortical alterations in the 22q11DS brain and it's relationship to psychiatric disease.

Chapter 3 includes findings adapted from the following selected studies:

Lin A, **Ching CRK**, Vajdi A, Sun D, Jonas RK, Jalbrzikowski M, Kushan-Wells L, Pacheco Hansen L, Krikorian E, Gutman B, Dokoru D, Helleman G, Thompson PM, Bearden CE. Mapping 22q11.2 Gene Dosage Effects on Brain Morphometry. *The Journal of Neuroscience*. 2017;37(26):6183-99. doi:10.1523/JNEUROSCI.3759-16.2017

Sun D, **Ching CRK**, Lin A, Forsyth JK, Kushan L, Vajdi A, Jalbrzikowski M, Hansen L, Villalon-Reina JE, Qu X, Jonas RK, van Amelsvoort T, Bakker G, Kates WR, Antshel KM, Fremont W, Campbell LE, McCabe KL, Daly E, Gudbrandsen M, Murphy CM, Murphy D, Craig M, Vorstman J, Fiksinski A, Koops S, Ruparel K, Roalf DR, Gur RE, Schmitt JE, Simon TJ, Goodrich-Hunsaker NJ, Durdle CA, Bassett AS, Chow EWC, Butcher NJ, Vila-Rodriguez F, Doherty J, Cunningham A, van den Bree MBM, Linden DEJ, Moss H, Owen MJ, Murphy KC, McDonald-McGinn DM, Emanuel B, van Erp TGM, Turner JA, Thompson PM, Bearden CE. Large-scale mapping of cortical alterations in 22q11.2 deletion syndrome: Convergence with idiopathic psychosis and effects of deletion size. *Mol Psychiatry*. 2018. doi:10.1038/s41380-018-0078-5

Villalón-Reina JE, Martínez K, Qu X, **Ching CRK**, Nir TM, Kothapalli D, Corbin C, Sun D, Lin A, Forsyth JK, Kushan L, Vajdi A, Jalbrzikowski M, Hansen L, Jonas RK, van Amelsvoort T, Bakker G, Kates WR, Antshel KM, Fremont W, Campbell LE, McCabe KL, Daly E, Gudbrandsen M, Murphy C, Murphy D, Craig M, Emanuel B, McDonald-McGinn D, Vorstman J, Fiksinski A, Koops S, Ruparel K, Roalf D, Gur RE, Schmitt JE, Simon TJ, Goodrich-Hunsaker NJ, Durdle CA, Doherty J, Cunningham AC, van den Bree M, Linden DEJ, Owen M, Moss H, Kelly S, Donohoe G, Murphy26 KC, Arango C, Jahanshad N, Thompson PM, Bearden CE. Altered White Matter Microstructure in 22q11.2 Deletion Syndrome: A Multi-Site Diffusion Tensor Imaging Study. In Review (Molecular Psychiatry 2018)

Ching CRK, Gutman BA, Sun D, Villalón-Reina JE, Qu X, Ragothaman A, Isaev D, Zavaliangos-Petropulu A, Lin A, Forsyth JK, Kushan L, Jonas RK, van Amelsvoort T, Bakker G, Kates WR, Campbell LA, McCabe KL, Daly E, Gudbrandsen M, Murphy C, Murphy D, Craig M, Vorstman J, Fiksinski A, Gras L, Ruparel K, Roalf D, Gur R, Schmitt JE, Simon TJ, Goodrich-Hunsaker NJ, Bassett AS, Chow EWC, Butcher N, Vila-Rodriguez F, Doherty J, Cunningham A, van den Bree M, Linden DE, Owen MJ, Moss H, Repetto GM, Crossley NA, Thompson PM, Bearden CE. Mapping Subcortical Brain Alterations in 22q11.2 deletion syndrome: effects of deletion size and convergence with idiopathic psychosis. In preparation to be submitted to The American Journal of Psychiatry

3.2 UCLA 22q11.2 cohort subcortical findings

This section reproduces the subcortical study focusing on Dr. Bearden's 22q11DS UCLA cohort and includes subcortical shape analysis in both 22q11DS and the very first analysis of brain variation in 22q11Dup.

Lin A, **Ching CRK**, Vajdi A, Sun D, Jonas RK, Jalbrzikowski M, Kushan-Wells L, Pacheco Hansen L, Krikorian E, Gutman B, Dokoru D, Helleman G, Thompson PM, Bearden CE. Mapping 22q11.2 Gene Dosage Effects on Brain Morphometry. *The Journal of Neuroscience*. 2017;37(26):6183-99. doi:10.1523/JNEUROSCI.3759-16.2017

Mapping 22q11.2 Gene Dosage Effects on Brain Morphometry

Amy Lin,¹ Christopher R.K. Ching,^{1,2} Ariana Vajdi,¹ Daqiang Sun,¹ Rachel K. Jonas,¹ Maria Jalbrzikowski,³ Leila Kushan-Wells,¹ Laura Pacheco Hansen,¹ Emma Krikorian,¹ Boris Gutman,² Deepika Dokoru,¹ Gerhard Helleman,¹ Paul M. Thompson,² and Carrie E. Bearden^{1,4}

¹Department of Psychiatry and Biobehavioral Sciences, Semel Institute for Neuroscience and Human Behavior, University of California at Los Angeles, Los Angeles, California 90095, ²Imaging Genetics Center, Institute for Neuroimaging and Informatics, University of Southern California, Marina del Rey, California 90292, ³Department of Psychiatry, University of Pittsburgh, Pittsburgh, Pennsylvania 15213, and ⁴Department of Psychology, University of California at Los Angeles, Los Angeles, California 90095

Reciprocal chromosomal rearrangements at the 22q11.2 locus are associated with elevated risk of neurodevelopmental disorders. The 22q11.2 deletion confers the highest known genetic risk for schizophrenia, but a duplication in the same region is strongly associated with autism and is less common in schizophrenia cases than in the general population. Here we conducted the first study of 22q11.2 gene dosage effects on brain structure in a sample of 143 human subjects: 66 with 22q11.2 deletions (22q-del; 32 males), 21 with 22q11.2 duplications (22q-dup; 14 males), and 56 age- and sex-matched controls (31 males). 22q11.2 gene dosage varied positively with intracranial volume, gray and white matter volume, and cortical surface area (deletion < control < duplication). In contrast, gene dosage varied negatively with mean cortical thickness (deletion > control > duplication). Widespread differences were observed for cortical surface area with more localized effects on cortical thickness. These diametric patterns extended into subcortical regions: 22q-dup carriers had a significantly larger right hippocampus, on average, but lower right caudate and corpus callosum volume, relative to 22q-del carriers. Novel subcortical shape analysis revealed greater radial distance (thickness) of the right amygdala and left thalamus, and localized increases and decreases in subregions of the caudate, putamen, and hippocampus in 22q-dup relative to 22q-del carriers. This study provides the first evidence that 22q11.2 is a genomic region associated with gene-dose-dependent brain phenotypes. Pervasive effects on cortical surface area imply that this copy number variant affects brain structure early in the course of development.

Key words: autism spectrum disorder; chromosome 22; copy number variant; neurodevelopment; psychosis; structural neuroimaging

Significance Statement

Probing naturally occurring reciprocal copy number variation in the genome may help us understand mechanisms underlying deviations from typical brain and cognitive development. The 22q11.2 genomic region is particularly susceptible to chromosomal rearrangements and contains many genes crucial for neuronal development and migration. Not surprisingly, reciprocal genomic imbalances at this locus confer some of the highest known genetic risks for developmental neuropsychiatric disorders. Here we provide the first evidence that brain morphology differs meaningfully as a function of reciprocal genomic variation at the 22q11.2 locus. Cortical thickness and surface area were affected in opposite directions with more widespread effects of gene dosage on cortical surface area.

Introduction

Reciprocal chromosomal rearrangements represent powerful models to assess effects of copy number variation (CNV) on brain

morphology and associated neuropsychiatric outcomes. Gene dosage cannot be experimentally manipulated in humans as it can in animal or *in vitro* models, but a similar framework emerges

Received Nov. 30, 2016; revised April 7, 2017; accepted May 10, 2017.

Author contributions: B.G., P.M.T., and C.E.B. designed research; A.L., C.R.K.C., A.V., D.S., R.K.J., M.J., L.K.-W., L.P.H., E.K., B.G., D.D., and C.E.B. performed research; C.R.K.C., B.G., and G.H. contributed unpublished reagents/analytic tools; A.L., C.R.K.C., D.S., and R.K.J. analyzed data; A.L., C.R.K.C., R.K.J., P.M.T., and C.E.B. wrote the paper.

This work was supported by National Institute of Mental Health Grant R01MH085953 to C.E.B., Neurobehavioral Genetics Predoctoral Training Grant 5T32MH073526, and the Simons Foundation. ENIGMA was supported in part by National Institutes of Health Consortium Grant U54 EB020403 to P.M.T. (contributing to the Big Data to Knowledge

initiative), including the National Institute of Biomedical Imaging and Bioengineering and National Cancer Institute. These funding sources had no further role in study design, in the collection, analysis, and interpretation of data, in the writing of the report, nor in the decision to submit the paper for publication. We thank the participants and their families for being a part of our research; Danielle Denny and Khalima Bolden for conducting clinical assessments and administering neuropsychological measures to our participants; Giovanni Coppola for providing valuable support for qPCR and CNV breakpoint analysis; and Dmitry Isaev and Anjanibhargavi Ragathanam for contributing to the subcortical shape analysis pipeline.

via naturally occurring genetic variation. Such genomic imbalances confer some of the highest genetic risk factors for prevalent developmental neuropsychiatric disorders (Malhotra and Sebat, 2012; Hoeffding et al., 2017) and offer a quasi-experimental “reverse genetics” approach to elucidate how genes may impact neurodevelopmental phenotypes (Hiroi et al., 2013).

The 22q11.2 locus is a valuable region to investigate gene dosage effects on brain development, as it is particularly susceptible to chromosomal rearrangements due to nonallelic homologous recombination (Stankiewicz and Lupski, 2002). Occurring at nearly 1 in 2000 live births (Grati et al., 2015), the 22q11.2 deletion (22q-del), also known as DiGeorge or Velocardiofacial syndrome (OMIM #188400, #192430), results from a 1.5–3 Mb hemizygous deletion on the long arm of chromosome 22 (Shaikh et al., 2007). 22q-del is the largest known genetic risk factor for psychotic illness, associated with an ~30-fold increase in risk relative to population base rates (Bassett and Chow, 2008; Green et al., 2009; Schneider et al., 2014). It is also associated with heightened risk for other developmental neuropsychiatric disorders: attention deficit hyperactivity disorder, anxiety disorder, and autism spectrum disorders (ASDs) (Niklasson et al., 2001, 2009; Vorstman et al., 2006; Girirajan et al., 2011).

Duplications at the same locus (22q-dup) were first reported clinically in 2003 (Ensenauer et al., 2003). Unlike 22q-del, which tends to occur *de novo*, the duplication is frequently inherited (Ou et al., 2008). Less is known about the 22q-dup phenotype, which is highly variable (Wentzel et al., 2008), but it appears to be associated with elevated rates of ASD and delays in language and psychomotor development (Wenger et al., 2016). In an analysis of >47,000 individuals, the 22q-dup was significantly less common in schizophrenia cases than in the general population (0.014% compared with 0.085%, OR = 0.17), suggesting the first putative protective mutation for schizophrenia (Rees et al., 2014). This finding of lower schizophrenia incidence in 22q-dup carriers compared with noncarriers has now been replicated in independent studies (Li et al., 2016; Rees et al., 2016; CNV and Schizophrenia Working Groups of the Psychiatric Genomics Consortium, Psychosis Endophenotypes International Consortium, 2017).

Genes within the 22q11.2 locus are essential for cortical circuit formation (Meechan et al., 2015a), so it is not surprising that 22q-del carriers show aberrations in cortical anatomy. These abnormalities include widespread reductions in cortical volume, particularly in midline regions, relative to typically developing controls (Bearden et al., 2007; Jalbrzikowski et al., 2013; Schmitt et al., 2015). Mouse models of 22q-del show diminished frequency of projection neurons in layers II/III of the medial prefrontal cortex, which was in turn associated with the severity of executive function deficits (Meechan et al., 2015b).

Although no study has yet characterized how a 22q11.2 duplication affects brain morphometry, dose-dependent effects on human brain structure have recently been discovered for other reciprocal CNVs associated with neuropsychiatric phenotypes. Stefansson et al. (2014) first demonstrated dose-dependent effects of genes within the 15q11.2 locus for measures of regional brain volume that overlap with regions affected in idiopathic

psychosis. Similarly, reciprocal 16p11.2 deletions and duplications were found to have global, “mirror image” effects on brain structure, in which cortical surface area was differentially affected (Qureshi et al., 2014; Maillard et al., 2015).

We investigated cortical and subcortical anatomic variation at the 22q11.2 locus to test the hypothesis that reciprocal 22q11.2 deletions and duplications confer opposing effects on brain structure. We decomposed cortical volume into its constituent parts, cortical thickness (CT) and surface area (SA), which are thought to have distinct neurodevelopmental origins (Rakic, 1988; Panizzon et al., 2009; Winkler et al., 2010). Any differential effect of 22q11.2 variants on these measures may point to developmental processes that are disrupted during corticogenesis in distinct brain regions as a result of 22q11.2 gene dosage.

Materials and Methods

Participants. The sample consisted of 143 individuals: 66 with molecularly confirmed 22q11.2 deletions (32 males; 34 females), 21 with confirmed 22q11.2 duplications (14 males; 7 females), and 56 demographically matched, unrelated controls (31 males; 25 females; for demographics, see Table 1). Approximately 25% of the deletion carriers and controls were included in a prior publication (Jalbrzikowski et al., 2013). As such, the current study includes a substantially larger sample of 22q11.2 deletion carriers and controls, as well as a novel cohort of 22q11.2 duplication carriers. Patients were ascertained from either (1) the University of California at Los Angeles or Children’s Hospital, Los Angeles Pediatric Genetics, Allergy/Immunology and/or Craniofacial Clinics, or (2) local support groups and websites. Demographically comparable typically developing comparison subjects were recruited from the same communities as patients via web-based advertisements and by posting flyers and brochures at local schools, pediatric clinics, and other community sites.

Exclusion criteria for all study participants included significant neurological or medical conditions (unrelated to 22q11.2 mutation) that might affect brain structure, history of head injury with loss of consciousness, insufficient fluency in English, and/or substance or alcohol abuse or dependence within the past 6 months. Healthy controls additionally could not have significant intellectual disability or meet criteria for any major mental disorder with the exception of attention deficit-hyperactivity disorder or a past episode of depression, based on information gathered during the Structured Clinical Interview for the Diagnostic and Statistical Manual of Mental Disorders, Ed 4 (First and Gibbon, 2004) and/or Computerized Diagnostic Interview for Children (Shaffer et al., 2000). All participants underwent a verbal and written informed consent process. Participants under the age of 18 years provided written assent, while their parent or guardian completed written consent. The University of California at Los Angeles Institutional Review Board approved all study procedures and informed consent documents.

Psychiatric and cognitive assessment. Supervised clinical psychology doctoral students administered neurocognitive and psychodiagnostic evaluations (Structured Clinical Interview for the Diagnostic and Statistical Manual of Mental Disorders/Computerized Diagnostic Interview for Children, as described above) to study participants. Estimates of general intellectual functioning were obtained for all participants using the Wechsler Abbreviated Scale of Intelligence (Wechsler, 1999) or Wechsler Adult Intelligence Scale, Ed 4 (Wechsler et al., 2008). Diagnosis of ASD was based on the Autism Diagnostic Observation Schedule (Lord et al., 2000) and the Autism Diagnostic Interview-Revised (Lord et al., 1994). To obtain dimensional measures of ASD-relevant behavior, parents of study participants also completed the Social Responsiveness Scale (Constantino and Gruber, 2007), a quantitative measure of reciprocal social behavior that has been extensively validated in both clinically ascertained and population-based samples and the Repetitive Behavioral Scale (Lam and Aman, 2007) to capture patterns of restricted repetitive behavior often observed in ASD.

All diagnoses were determined by trained clinicians who participated in an ongoing quality assurance program (Ventura et al., 1998). Training, reliability, and ongoing quality assurance procedures for psychodiagnostic assessments are detailed in prior publications (Jalbrzikowski et al., 2013, 2016).

The authors declare no competing financial interests.

Correspondence should be addressed to Dr. Carrie E. Bearden, University of California at Los Angeles, Semel Institute for Neuroscience and Human Behavior, 760 Westwood Plaza, Room A7-436, Los Angeles, CA 90095. E-mail: CBearden@mednet.ucla.edu.

DOI:10.1523/JNEUROSCI.3759-16.2017

Copyright © 2017 the authors 0270-6474/17/376184-17\$15.00/0

Table 1. Participant demographics^a

	22q11.2 deletion participants (N = 66)	Healthy control participants (N = 56)	22q11.2 duplication participants (N = 21)
Scanner	34 BMC, 32 CCN	27 BMC, 29 CCN	21 CCN
Age (SD)	15.7 (7.55)	14.6 (6.93)	16.8 (12.00)
Males (% male)	32 (48.5%)	31 (55.4%)	14 (66.7%)
Race*, † (%)	59 white (89.4%), 1 black (1.5%), 6 multirace (9.1%)	33 white (58.9%), 7 black (12.5%), 5 Asian (8.9%), 11 multirace (19.6%)	21 white (100%)
Full-Scale IQ**, † (SD)	78.68 (12.53)	111.5 (18.98)	96.15 (20.42)
Verbal IQ**, † (SD)	76.2 (8.99)	113.3 (13.15)	93.3 (13.96)
Nonverbal IQ**, † (SD)	80.6 (10.91)	105 (10.11)	98.7 (14.41)
Highest parental education, years** (SD)	16.26 (2.52)	15.7 (3.18)	15.0 (2.25)
ASD (%)*, †	29 (43.9%)	0	13 (61.9%)
Psychotic disorder (%)**, †	4 (6.1%)	0	0
ADHD (%)*, †	27 (40.9%)	2 (3.6%)	6 (28.6%)
Social Responsiveness Scale*, † (SD)	70.07 (14.84)	49.29 (13.58)	72.31 (16.89)
Repetitive Behavioral Scale*, † (SD)	16.84 (22.77)	2.88 (7.16)	16.11 (19.44)
Current medication			
Psychostimulant*, ** (%)	6 (9.1%)	1 (1.8%)	6 (28.6%)
Antipsychotic† (%)	7 (10.6%)	0	1 (4.8%)
Antidepressant (SSRI)**, † (%)	11 (16.7%)	0	1 (4.8%)
Other (%)	4 (6.1%)	1 (1.8%)	2 (9.52%)
None*, † (%)	38 (57.6%)	52 (92.9%)	12 (57.1%)
CNV breakpoints			
A-B (%)	5 (7.6%)	—	5 (23.8%)
A-C (%)	1 (1.5%)	—	—
A-D (%)	56 (84.8%)	—	10 (47.6%)
B-D (%)	—	—	3 (14.3%)
C-E (%)	1 (1.5%)	—	1 (4.8%)
Other (%)	3 (4.5%)	—	2 (9.5%)

^aBMC, Brain Mapping Center; CCN, Center for Cognitive Neuroscience. One 22q-dup carrier was taking both an antipsychotic and psychostimulant. Family relatedness of the 22q-dup cohort: 4 singletons, 5 families with 2 members (3 parent-child pairs, 2 sibling pairs), 1 family with 3 members (siblings), 1 family with 4 members (1 parent, 3 children). CNV breakpoints: A-C deletion has additional C-D duplication, 3 Other deletions include D-F, D-G, and PRODH/DGCR8, 2 Other duplications include F-H and TOP3B. Data not available for the following: Full-Scale IQ/Verbal IQ: 1 22q-del, 2 controls, and 1 22q-dup; Nonverbal IQ: 2 controls and 1 22q-dup; Parental Education: 5 22q-del; Social Responsiveness Scale: 5 22q-dup, 6 22q-del, and 18 controls; Repetitive Behavioral Scale: 3 22q-del, 4 controls, and 2 22q-dup; Medication information for 2 controls.

*22q-dup/control difference (pairwise significance at uncorrected $p < 0.05$).

**22q-dup/22q-del difference (pairwise significance at uncorrected $p < 0.05$).

†22q-del/control difference (pairwise significance at uncorrected $p < 0.05$).

qRT-PCR. As an initial proof of principle to determine whether duplication and deletion carriers showed the expected increases or decreases, respectively, in gene dosage, we first investigated gene expression levels for three key genes in the 22q11.2 locus. Peripheral blood samples were drawn in two PAXgene tubes and were stored at 4°C. RNA was extracted using the PAXgene blood RNA kit (PreAnalytix, QIAGEN). We assessed RNA quantity using Nanodrop ND-1000 spectrophotometer (Nanodrop Technologies) and also quality with Agilent Bioanalyzer NanoChips.

qRT-PCR was conducted using TaqMan assays, as described by Coppola et al. (2006). Total RNA was converted into cDNA by SuperScript II kit (Invitrogen). The reactions were performed with a TaqMan Master Mix (Bio-Rad) in a 25 μ l volume. Assays were performed in triplicate and analyzed using a Roche Lightcycler. qPCR analyses were performed using the 2(-Delta Delta C(T)) method (2- $\Delta\Delta$ Ct). We assayed three genes within the 22q11.2 locus: catechol-O-methyltransferase (*comt*), DiGeorge Syndrome Critical Region Gene 8 (*dgc8*), and Zinc Finger DHHC-Type Containing 8 (*zdhc8*), using *gapdh* as a reference gene. Additionally, all 22q11.2 CNV carriers underwent multiplex ligation-dependent probe amplification (MLPA) (Sørensen et al., 2010) to determine specific breakpoint locations (Table 1).

MRI acquisition and preprocessing. Measures of brain structure were obtained with high-resolution structural MRI. Scanning was conducted on an identical 3 tesla Siemens Trio MRI scanner with a 12-channel head coil at the University of California at Los Angeles Brain Mapping Center or at the Center for Cognitive Neuroscience (Table 1). Each scan began with a 10 min acquisition of standard images used for determining regional anatomy, including a sagittal localizer image (TR/TE = 500/33 ms, 192 \times 256 matrix), a high-resolution T2-weighted axial image (TR/TE = 5000/33 ms, 128 \times 128 matrix, FOV = 200 \times 200 mm), and a sagittal 1 mm³ T1-weighted image. We used FreeSurfer to process 1 mm³ T1-weighted anatomical images acquired with an MPRAGE sequence.

The parameters for the MPRAGE were the following: TR = 2.3 s, TE = 2.91 ms, FOV = 256 mm, matrix = 240 \times 256, flip angle = 9°, slice thickness = 1.20 mm, 160 slices. The FreeSurfer image analysis suite (version 5.3.0; <http://surfer.nmr.mgh.harvard.edu>) surface-based processing pipeline was used to derive measures of volume, cortical thickness, and surface area. FreeSurfer is a well-validated processing package that has been previously described in detail (Dale et al., 1999; Fischl et al., 1999). We extracted cortical measures based on the Desikan FreeSurfer atlas (Desikan et al., 2006).

Quality assessment of MRI. Structural T1-weighted MRI brain scans were analyzed in an unbiased, whole-brain approach using well-validated analysis and quality control protocols developed for the ENIGMA consortium (Enhancing Neuroimaging Genetics through Meta-Analysis) (Thompson et al., 2014), which have previously been applied in large-scale studies of major depression (Schmaal et al., 2016), bipolar disorder (Hibar et al., 2016), and schizophrenia (van Erp et al., 2016). We used the ENIGMA quality assessment pipeline (Thompson et al., 2017) to determine scan quality. Segmented regions were visually inspected and statistically evaluated for outliers following standardized ENIGMA protocols (<http://enigma.ini.usc.edu/protocols/imaging-protocols>). Briefly, the pipeline includes three major steps: (1) extracting and organizing brain measures from FreeSurfer, (2) quality checking the outputs wherein a set of representative cross-sections from each subject are displayed with colored FreeSurfer segmentations, and (3) calculating population summary statistics of the cortical traits and related histograms. Visual inspections of ENIGMA snapshots were completed by 3 separate individuals who were blind to diagnostic status. Scans of 4 22q-dup participants, 3 control participants, and 5 22q-del participants failed the initial quality control assessment. The 22q-dup participant scans were then manually edited using standard procedures (detailed in Jalbrzikowski et al., 2013), after which they passed QC assessment.

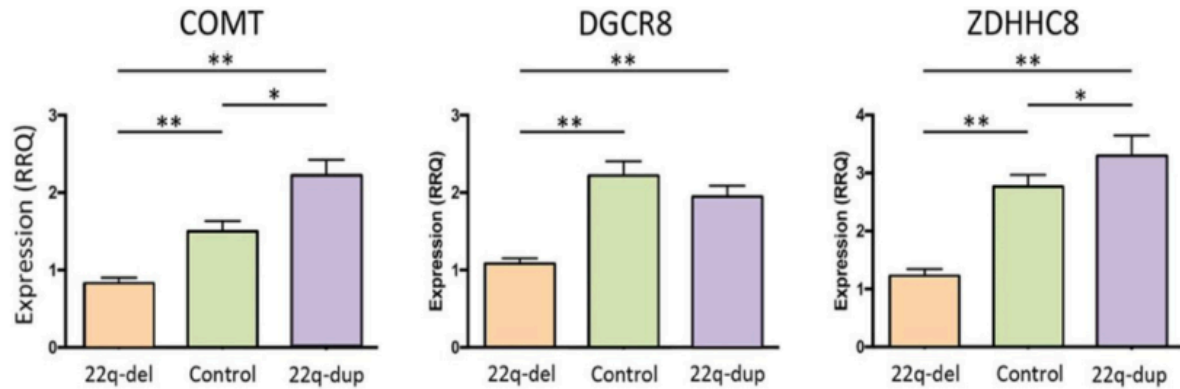


Figure 1. Gene expression. Relative Relative Quantification (RRQ) levels of *comt*, *dgcr8*, and *zdhhc8*. *comt* and *zdhhc8* expression levels were significantly different between all three cohorts, whereas *dgcr8* expression only showed significant differences between 22q-del carriers and controls as well as 22q-del carriers and 22q-dup carriers. * $p < 0.03$. ** $p < 0.001$.

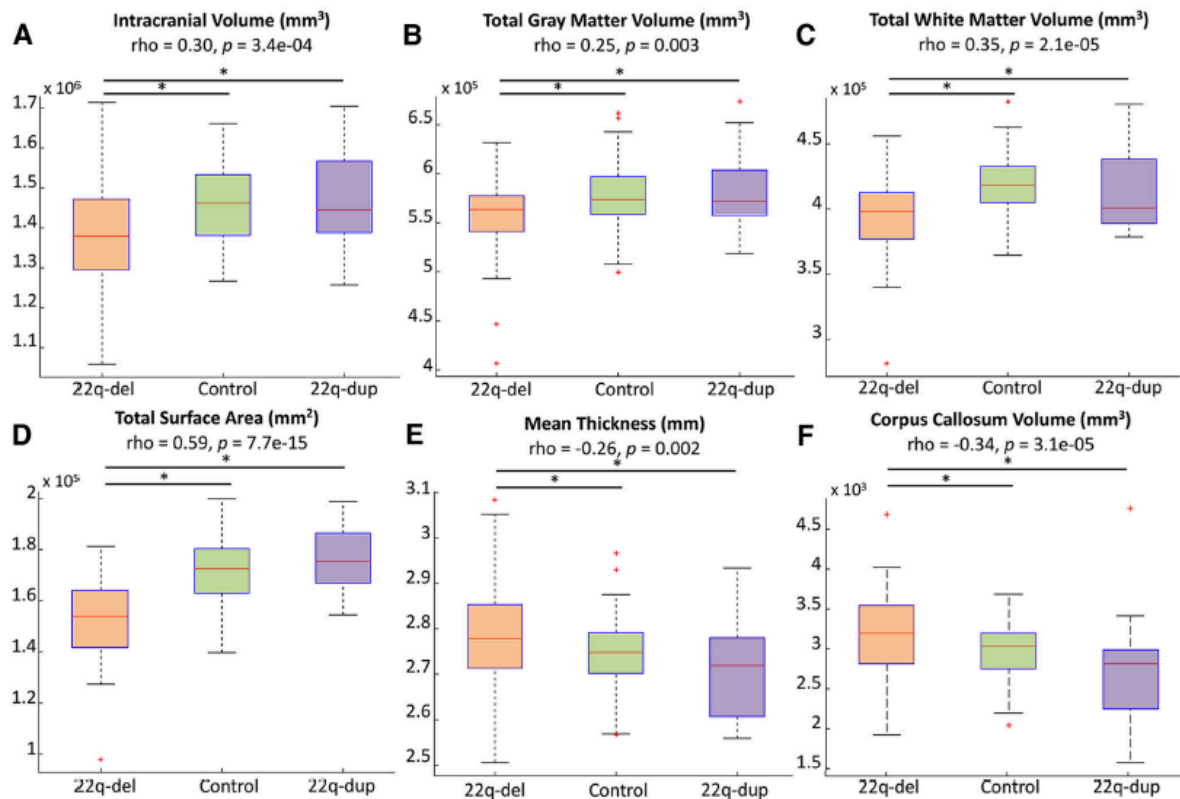


Figure 2. Global brain metrics for intracranial volume, total gray matter volume, total white matter volume, total surface area (SA), mean cortical thickness (CT), and corpus callosum volume. Boxplots of global brain metrics for each individual across groups adjusted for sex, age, and scanner location (as well as intracranial volume for volumetric measures). Spearman nonparametric correlations were performed for each measure, indicating significant gene dosage effects. For all measures, there were significant pairwise differences between 22q-del and controls that survive *post hoc* correction. * $p < 0.05$.

Subcortical shape analysis. As conventional subcortical volume analysis may obscure fine-grained differences in anatomical changes, a novel surface-based high-resolution parametric mapping technique was used to investigate shape differences across subjects for all subcortical regions of interest (ROIs) (Mamah et al., 2016). This technique is sensitive to subtle volumetric variations (Gutman et al., 2012, 2015) that may represent underlying subfield organization (Wang et al., 2008). It has recently shown high vertexwise heritability, suggesting that shape

indexes a biologically valid phenotype (Roshchupkin et al., 2016). A growing body of evidence indicates that different diseases have distinct effects on hippocampal subfields (Small et al., 2011); these localized patterns of disease effects may extend to other subcortical structures as well.

Using FreeSurfer segmentations as an initial input for creating the shape models, shape registration was based on existing shape templates and template “medial” models. The shape template was

Table 2. Global metrics: adjusted means, SEs, percentage difference from controls, and estimated 22q-dupN^a

Region	F	22q-del Mean (SE)	22q-del % difference from controls	Control, mean (SE)	22q-dup, mean (SE)	22q-dup % difference from controls	dupN
Corpus callosum volume ^{*,†,‡}	7.3	3195.5 (60.7)	7.6%	2969.3 (64.4)	2723.9 (113.5)	−8.3%	216
Cortical white matter volume ^{*,†,‡}	11.9	395,129.2 (3381.3)	−5.7%	418,977.0 (3587.9)	415,362.7 (6319.3)	−0.9%	695
Total gray matter ^{*,†,‡}	5.4	556,341.5 (4785.5)	−3.7%	577,545.6 (5080.0)	581,072.5 (8947.3)	0.6%	>1000
Mean thickness ^{*,†,‡}	4.6	2.78 (0.01)	1.5%	2.74 (0.01)	2.71 (0.02)	−1.1%	140
Total intracranial volume ^{*,†,‡}	7.1	1385812.3 (14058.4)	−4.9%	1,456,843.0 (15317.2)	1,466,356.0 (27086.6)	0.7%	403
Total area ^{*,†,‡}	35.4	152,415.5 (1760.0)	−11.1%	171,524.8 (1917.5)	176,466.1 (3390.9)	2.9%	208

^aAdjusted means are covaried for age, sex, and scanner location, as well as intracranial volume for volumetric measures.

^{**}Survives FDR correction ($p < 0.05$ threshold) at post hoc level for 22q-dup versus 22q-del.

[†]Survives FDR correction ($p < 0.05$ threshold) at post hoc level for 22q-del versus control.

[‡]Survives FDR correction ($p < 0.05$ threshold) at omnibus level.

Table 3. Regional cortical thickness adjusted means, and SEs^a

Region	F	22q-del, mean (SE)	Control, mean (SE)	22q-dup, mean (SE)	Region	F	22q-del, mean (SE)	Control, mean (SE)	22q-dup, mean (SE)
Left hemisphere					Right hemisphere				
Bank of superior temporal sulcus	2.4	2.65 (0.02)	2.70 (0.02)	2.75 (0.04)	Bank of superior temporal sulcus	0.8	2.83 (0.02)	2.85 (0.03)	2.89 (0.04)
Caudal anterior cingulate gyrus	4.8	2.83 (0.03)	2.95 (0.04)	3.03 (0.07)	Caudal anterior cingulate gyrus	2.7	2.70 (0.03)	2.82 (0.04)	2.78 (0.07)
Caudal middle frontal gyrus ^{*,**}	18.2	2.82 (0.02)	2.74 (0.02)	2.58 (0.04)	Caudal middle frontal gyrus ^{*,**}	12.7	2.75 (0.02)	2.66 (0.02)	2.55 (0.04)
Cuneus	3.3	2.13 (0.02)	2.05 (0.03)	2.04 (0.04)	Cuneus	3.6	2.17 (0.02)	2.11 (0.02)	2.05 (0.04)
Entorhinal cortex	1.6	3.48 (0.04)	3.55 (0.05)	3.38 (0.09)	Entorhinal cortex	1.5	3.81 (0.05)	3.80 (0.05)	3.63 (0.09)
Frontal pole	0.4	2.84 (0.04)	2.89 (0.05)	2.88 (0.09)	Frontal pole	0.8	2.83 (0.04)	2.76 (0.05)	2.84 (0.08)
Fusiform gyrus	0.2	2.90 (0.02)	2.90 (0.02)	2.88 (0.03)	Fusiform gyrus	2.2	3.00 (0.02)	2.95 (0.02)	2.98 (0.03)
Inferior parietal cortex	1.7	2.70 (0.02)	2.69 (0.02)	2.64 (0.03)	Inferior parietal cortex	3.4	2.74 (0.02)	2.70 (0.02)	2.64 (0.03)
Inferior temporal gyrus	0.0	2.88 (0.02)	2.88 (0.03)	2.88 (0.05)	Inferior temporal gyrus	1.0	3.05 (0.02)	3.01 (0.02)	3.03 (0.04)
Insula ^{*,†,‡}	23.3	3.42 (0.02)	3.25 (0.02)	3.21 (0.04)	Insula ^{†,‡}	7.5	3.42 (0.02)	3.30 (0.02)	3.29 (0.04)
Isthmus cingulate	1.7	2.78 (0.03)	2.76 (0.03)	2.67 (0.05)	Isthmus cingulate gyrus	0.8	2.65 (0.02)	2.68 (0.03)	2.61 (0.05)
Lateral occipital cortex	0.8	2.35 (0.02)	2.33 (0.02)	2.30 (0.03)	Lateral occipital cortex	1.4	2.42 (0.02)	2.41 (0.02)	2.36 (0.03)
Lateral orbitofrontal cortex	2.8	2.91 (0.02)	2.83 (0.03)	2.86 (0.04)	Lateral orbitofrontal cortex	2.1	2.76 (0.02)	2.70 (0.03)	2.80 (0.05)
Lingual gyrus ^{*,†}	9.9	2.30 (0.02)	2.23 (0.02)	2.16 (0.03)	Lingual gyrus ^{*,†}	8.3	2.38 (0.02)	2.29 (0.02)	2.24 (0.04)
Medial orbitofrontal cortex	6.7	2.70 (0.03)	2.57 (0.03)	2.52 (0.06)	Medial orbitofrontal cortex	6.1	2.55 (0.03)	2.43 (0.03)	2.39 (0.05)
Middle temporal gyrus	0.7	3.05 (0.02)	3.02 (0.02)	3.04 (0.04)	Middle temporal gyrus	2.3	3.15 (0.02)	3.08 (0.03)	3.09 (0.05)
Paracentral cortex ^{†,‡}	7.6	2.66 (0.02)	2.55 (0.02)	2.53 (0.04)	Paracentral gyrus ^{*,†}	8.9	2.70 (0.02)	2.62 (0.02)	2.51 (0.04)
Parahippocampal gyrus ^{*,†,‡}	13.0	2.70 (0.04)	2.94 (0.04)	3.02 (0.07)	Parahippocampal gyrus	0.7	2.95 (0.04)	3.01 (0.04)	2.99 (0.07)
Pars opercularis ^{*,†,‡}	15.2	2.89 (0.02)	2.77 (0.02)	2.75 (0.03)	Pars opercularis	3.3	2.82 (0.02)	2.73 (0.03)	2.73 (0.04)
Pars orbitalis	5.4	3.00 (0.03)	2.90 (0.03)	2.81 (0.06)	Pars orbitalis	2.1	2.83 (0.03)	2.73 (0.04)	2.78 (0.07)
Pars triangularis ^{*,†,‡}	14.2	2.76 (0.02)	2.61 (0.02)	2.56 (0.04)	Pars triangularis	2.9	2.64 (0.03)	2.53 (0.03)	2.55 (0.06)
Pericalcarine gyrus	5.4	1.85 (0.02)	1.78 (0.02)	1.71 (0.04)	Pericalcarine gyrus ^{†,‡}	9.7	1.87 (0.02)	1.75 (0.02)	1.72 (0.04)
Postcentral gyrus	6.8	2.28 (0.02)	2.19 (0.02)	2.17 (0.04)	Postcentral gyrus	5.3	2.28 (0.02)	2.20 (0.02)	2.14 (0.04)
Posterior cingulate gyrus	0.0	2.79 (0.02)	2.79 (0.02)	2.79 (0.04)	Posterior cingulate gyrus	2.9	2.72 (0.02)	2.78 (0.02)	2.72 (0.04)
Precentral gyrus ^{*,†}	9.9	2.76 (0.02)	2.70 (0.02)	2.61 (0.03)	Precentral gyrus	6.2	2.73 (0.02)	2.65 (0.02)	2.60 (0.04)
Precuneus	4.4	2.67 (0.02)	2.63 (0.02)	2.56 (0.03)	Precuneus ^{*,**}	11.3	2.70 (0.02)	2.66 (0.02)	2.50 (0.04)
Rostral anterior cingulate gyrus	0.6	3.18 (0.04)	3.14 (0.04)	3.10 (0.07)	Rostral anterior cingulate gyrus	1.9	2.83 (0.03)	2.92 (0.03)	2.92 (0.06)
Rostral middle frontal gyrus ^{*,†}	10.3	2.64 (0.02)	2.54 (0.02)	2.46 (0.04)	Rostral middle frontal gyrus ^{*,†}	9.4	2.46 (0.02)	2.35 (0.02)	2.29 (0.04)
Superior frontal gyrus ^{*,**}	14.7	3.05 (0.02)	3.00 (0.02)	2.84 (0.04)	Superior frontal gyrus ^{*,†}	10.1	2.93 (0.02)	2.88 (0.02)	2.74 (0.04)
Superior parietal cortex	2.7	2.41 (0.02)	2.37 (0.02)	2.32 (0.04)	Superior parietal cortex	3.4	2.40 (0.02)	2.34 (0.02)	2.30 (0.04)
Superior temporal gyrus	5.9	2.90 (0.02)	3.00 (0.02)	2.97 (0.04)	Superior temporal gyrus	0.2	2.99 (0.02)	2.99 (0.02)	3.02 (0.04)
Supramarginal gyrus ^{*,†}	9.0	2.86 (0.02)	2.77 (0.02)	2.71 (0.04)	Supramarginal gyrus ^{*,†}	15.0	2.90 (0.02)	2.79 (0.02)	2.70 (0.04)
Temporal pole	0.3	3.70 (0.04)	3.68 (0.05)	3.74 (0.08)	Temporal pole	0.3	3.92 (0.04)	3.91 (0.05)	3.84 (0.08)
Transverse temporal gyrus	0.5	2.58 (0.03)	2.62 (0.03)	2.57 (0.05)	Transverse temporal gyrus	1.8	2.68 (0.03)	2.60 (0.03)	2.68 (0.06)

^aAdjusted means are covaried for age, sex, and scanner location.

^{*}Survives FDR correction ($p < 0.05$ threshold) at post hoc level for 22q-dup versus control.

^{**}Survives FDR correction ($p < 0.05$ threshold) at post hoc level for 22q-dup versus 22q-del.

[†]Survives FDR correction ($p < 0.05$ threshold) at post hoc level for 22q-del versus control.

[‡]Survives FDR correction ($p < 0.05$ threshold) at omnibus level.

made by registering all subjects to a representative subject. The Euclidean average of these shapes served as the template surface, from which the template medial curve was computed. A pointwise measure of shape morphometry, radial distance, was derived for all 14 subcortical ROIs for each subject, using a medial model approach (Gutman et al., 2012, 2015). For each point $p \in \mathcal{M}$ on the surface, and given a medial curve $c: [0, 1] \rightarrow \mathbb{R}^3$, the radial distance is defined by the following:

$$D(p) = \min\{\|c(t) - p\| \mid t \in [0, 1]\}$$

In this way, radial distance (termed “thickness” henceforth) was calculated in native space for up to 2500 homologous points across each subcortical structure, providing a detailed index of regional shape differences across subjects. We included only those shape models that passed visual inspection and conformed to T1-weighted MRI anatomical

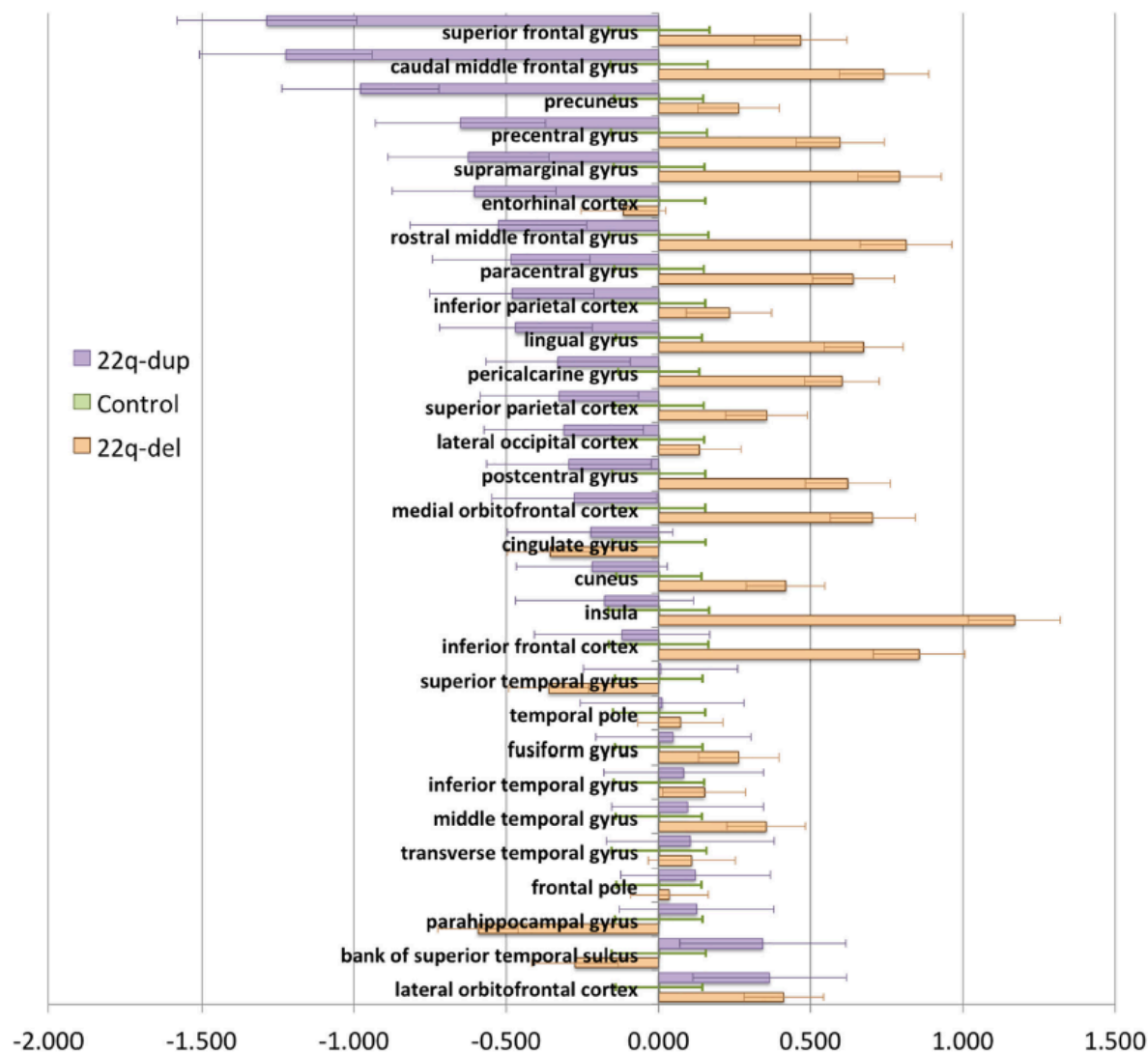


Figure 3. Cortical thickness z score plots of estimated marginal mean \pm SE. z scores are derived from individual subject means adjusted for sex, age, and scanner location using control mean and SD for each region. Then, z scores were submitted to the same primary statistical analysis to generate estimated marginal mean \pm SE. 22q-dup showed lower thickness relative to 22q-del patients in predominantly medial frontal and parietal regions, with controls showing an intermediate pattern.

boundaries using the ENIGMA Shape Analysis Quality Assessment Protocol (<http://enigma.ini.usc.edu/protocols/imaging-protocols/>).

Statistical analysis. The primary statistical analyses were performed in SPSS software version 24 (IBM; RRID: SCR_002865). Additional demographic comparisons and effect size calculations were done in either MATLAB version R2015a (The MathWorks; RRID: SCR_001622) or R 3.0.2 (R Core Team, 2016; RRID: SCR_000432). Statistical modeling for shape analyses was performed using the R *stats* package (<https://stat.ethz.ch/R-manual/R-devel/library/stats/html/lm.html>). We conducted independent samples *t* tests for continuous variables and χ^2 tests for categorical variables. For the analyses of relative gene expression differences, we conducted separate univariate ANCOVAs with gene expression level as the dependent variable, CNV status as the independent variable, and age, gender, and qRT-PCR batch as covariates.

Significance testing for our primary analyses was conducted in two steps. First, we determined whether 22q11.2 CNVs had an effect on standard FreeSurfer ROIs for CT and SA, as well as volumes of subcortical structures and global brain metrics (total intracranial volume, total gray,

and white matter volume, total SA, and average CT). For this omnibus test, we performed an ANCOVA and false discovery rate (FDR) correction at $q = 0.05$ (Benjamini and Hochberg, 1995) for the number of regions, for each brain metric. Group (22q-dup, 22q-del, or control) was used as the independent variable, and each ROI was included as the dependent variable with age, sex, and scanner location as covariates. Analyses of cortical and subcortical volume included intracranial volume (ICV) as an additional covariate. Given the considerable variance across different brain structures, we performed an ANCOVA for each ROI independently. Second, for regions that passed the FDR-corrected omnibus test, we conducted *post hoc* tests for each pairwise comparison, applying the same correction used for the initial omnibus test.

For subcortical shape analyses, a multiple linear regression model was used to assess surface-based thickness differences between 22q-del carriers, 22q-dup carriers, and controls after correcting for age, sex, ICV, and scanner location. The model was fitted at each point across the surface of each subcortical structure. As these values were calculated in native space, ICV was included as a covariate to regress out effects of head

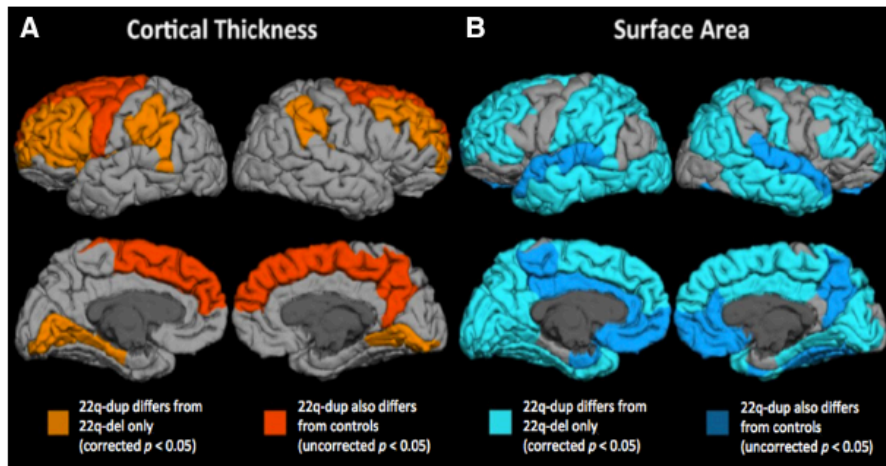


Figure 4. Neuroanatomic differences between 22q-dup carriers, 22q-del carriers, and controls. Cortical thickness and surface area. *A*, Light orange represents regions in which 22q-dup shows significant differences in cortical thickness relative to 22q-del (FDR-corrected, $q < 0.05$). Dark orange represents regions in which 22q-dup significantly differs from both 22q-del (corrected) and controls (uncorrected, nominal $p < 0.05$), with 22q-dup showing lower thickness relative to 22q-del and controls in frontal, inferior parietal, and parahippocampal regions. *B*, Light blue represents regions in which 22q-dup carriers differ in surface area from 22q-del carriers (FDR-corrected, $q < 0.05$). Dark blue represents regions where 22q-dup differs significantly from both 22q-del (corrected) and controls (uncorrected, nominal $p < 0.05$). 22q-dup carriers show greater surface area relative to 22q-del carriers and controls throughout most of the cortex, except for lateral orbitofrontal, middle frontal, inferior parietal, and right occipital regions.

size. To correct for multiple comparisons, a standard FDR correction was again applied at $q = 0.05$. Statistical models were fitted for the following comparisons of interest: 22q-del carriers versus controls, 22q-dup carriers versus controls, and 22q-dup carriers versus 22q-del carriers. All results described below are FDR-corrected unless otherwise indicated.

Sensitivity analyses. To determine whether group differences in brain structure are attributable to familial relationships between 22q-dup patients, a sensitivity analysis was conducted on a subset of the duplication cohort comprising only unrelated individuals ($N = 11$), in which we determined whether the parameter estimates for this subset differed from those obtained on the full cohort. Specifically, we tested whether the adjusted means calculated for unrelated subjects were within 2 SEs of the adjusted means of the full cohort. 22q-dup patients in the subset were selected with the aim of maintaining similar mean age and sex ratios to the control and 22q-del group.

We conducted a similar secondary analysis to rule out the effect of antipsychotic medication on brain structure, in which 8 participants (7 22q-del carriers and 1 22q-dup carrier) who were taking antipsychotic medication at the time of visit were excluded. This approach was chosen as the small sample size of the subgroup precluded a mixed model analysis that explicitly accounted for family structure. Similarly, the confounding of medication use and group made a direct analysis of the effects of antipsychotic medication difficult to interpret. These sensitivity analyses are designed to show that the inclusion/exclusion of these participants does not bias the results.

Additionally, we conducted secondary analyses in which we covaried for: (1) race and (2) global brain metrics (mean cortical thickness and total cortical surface area).

Results

Neuropsychiatric and cognitive findings

There were significant differences in Full Scale IQ between groups: 22q-del carriers had the lowest IQ scores, followed by 22q-dup carriers, then control participants had the highest IQ scores (Table 1). The same pattern persisted for the Verbal IQ domain; however, for Nonverbal IQ (as measured by Matrix Reasoning), 22q-del carriers performed significantly more poorly than 22q-dup carriers and controls, who did not differ from each other. Four 22q-del carriers and no 22q-dup carriers were diagnosed with a psychotic disorder, but rates of ASD were elevated in

both groups. 22q-del and 22q-dup carriers had similarly elevated scores on dimensional measures of autism-relevant symptomatology (Social Responsiveness Scale and Repetitive Behavioral Scale scales) relative to control participants.

mRNA expression

As shown in Figure 1, qRT-PCR analyses revealed a linear effect of gene dosage on mRNA expression levels of COMT and ZD-HHC8, but not DGCR8 (Fig. 1).

Gene dosage effects on global brain metrics

There were no significant main effects of scanner location, but significant effects of group were found for total intracranial volume ($F_{(2,137)} = 7.12, p = 0.001$), total gray matter volume ($F_{(2,136)} = 5.43, p = 0.005$), cortical white matter volume ($F_{(2,136)} = 11.88, p = 1.76e-5$), total cortical SA ($F_{(2,137)} = 35.37, p = 4.1e-13$), mean CT ($F_{(2,137)} = 4.60, p = 0.01$), and the corpus callosum ($F_{(2,136)} = 7.32, p = 9.6e-4$; Fig. 2A–F). Effects of gene dosage appeared generally proportional in magnitude relative to controls for callosal volume and cortical thickness, although for total intracranial, gray and white matter volume and SA, the percentage reduction in deletion carriers was more substantial than the relative increase seen in duplication carriers (Table 2; Fig. 2). Further, as shown in Figure 2, the effects of this CNV on brain structure did not appear to be accounted for by a subset of severely affected individuals, but rather, the entire distribution was shifted, suggesting a highly penetrant effect (Qureshi et al., 2014). *Post hoc* pairwise contrasts revealed that the significant effect of group was driven by patterns of differences between 22q-del and 22q-dup carriers, as well as 22q-del carriers and controls.

Effects of reciprocal 22q11.2 variation on cortical thickness

Omnibus ANCOVA revealed a significant effect of group for 20 ROIs (Table 3). Across cortical regions, 22q-dup tended to show lower thickness compared with 22q-del with controls showing an intermediate pattern (Fig. 3). *Post hoc* pairwise *t* tests revealed that, compared with controls, 22q-del showed significantly greater thickness in 8 ROIs and significantly lower thickness in 1

Table 4. Regional SA adjusted means and SEs^a

Region	F	22q-del, mean (SE)	Control, mean (SE)	22q-dup, mean (SE)	Region	F	22q-del, mean (SE)	Control, mean (SE)	22q-dup, mean (SE)
Left hemisphere					Righthemisphere				
Bank of superior temporal sulcus**,+†,††	16.1	941.0 (19.9)	1049.5 (21.7)	1169.4 (38.3)	Bank of superior temporal sulcus**,+†,††	24.6	882.7 (16.2)	1031.1 (17.6)	1062.8 (31.2)
Caudal anterior cingulate gyrus**,+†,††	37.5	511.8 (15.4)	665.7 (16.8)	756.9 (29.6)	Caudal anterior cingulate**,+†,††	18.2	626.0 (19.5)	785.1 (21.3)	800.5 (37.6)
Caudal middle frontal gyrus	4.5	2172.4 (47.1)	2342.8 (51.3)	2422.2 (90.7)	Caudal middle frontal gyrus	3.4	1936.7 (49.6)	2103.6 (54.1)	2143.2 (95.6)
Cuneus**,+†,††	59.7	1139.3 (23.8)	1479.2 (25.9)	1550.7 (45.8)	Cuneus**,+†,††	43.6	1213.9 (24.5)	1522.3 (26.6)	1553.4 (47.1)
Entorhinal cortex**,+†	6.2	340.5 (10)	369.6 (10.9)	414.1 (19.2)	Entorhinal cortex	5.1	288.0 (8.8)	326.8 (9.6)	328.0 (17)
Frontal pole**,+†	6.9	203.2 (3.9)	212.8 (4.3)	234.6 (7.5)	Frontal pole**,+†	11.6	270.9 (5.4)	292.4 (5.9)	325.5 (10.4)
Fusiform gyrus**,+†,††	28.8	2909.4 (46.1)	3386.8 (50.3)	3416.9 (88.9)	Fusiform gyrus**,+†,††	29.0	2807.8 (48.4)	3298.0 (52.7)	3374.1 (93.2)
Inferior parietal cortex	5.5	4415.6 (70.2)	4758.8 (76.5)	4621.3 (135.3)	Inferior parietal cortex**,+†,††	13.1	5129.4 (86)	5715.1 (93.7)	5808.7 (165.6)
Inferior temporal gyrus**,+†,††	32.0	2832.7 (50.7)	3402.2 (55.3)	3371.4 (97.7)	Inferior temporal gyrus**,+†,††	19.0	2746.9 (57)	3237.9 (62.1)	3223.3 (109.9)
Insula	2.5	2020.5 (28.2)	2056.6 (30.7)	2156.5 (54.2)	Insula	0.7	2070.9 (32.7)	2032.4 (35.6)	2112.2 (68.1)
Isthmus cingulate**,+†	8.8	960.2 (19.9)	1012.1 (21.7)	1140.5 (38.3)	Isthmus cingulate	4.4	904.4 (19.5)	920.9 (21.3)	1030.1 (37.7)
Lateral occipital cortex**,+†,††	21.5	4315.6 (67)	4851.8 (73)	5082.6 (129.1)	Lateral occipital cortex†,††	13.5	4155.7 (76.2)	4708.4 (83)	4688.1 (146.8)
Lateral orbitofrontal cortex	4.2	2403.1 (38.2)	2551.7 (41.6)	2571.2 (73.6)	Lateral orbitofrontal cortex	3.2	2310.9 (40.6)	2444.1 (44.2)	2475.3 (78.2)
Lingual gyrus**,+†,††	43.5	2497.2 (49.2)	3090.4 (53.6)	3238.2 (94.7)	Lingual gyrus**,+†,††	57.2	2478.1 (45.7)	3121.8 (49.8)	3246.1 (88.1)
Medial orbitofrontal cortex**,+†	9.9	1599.7 (28.5)	1715.3 (31.1)	1860.7 (54.9)	Medial orbitofrontal cortex**,+†,††	11.8	1656.8 (25.3)	1783.0 (27.6)	1898.7 (48.7)
Middle temporal gyrus**,+†,††	22.3	2719.2 (46.5)	3131.5 (50.7)	3198.6 (89.6)	Middle temporal gyrus**,+†,††	15.1	3070.4 (52.6)	3448.2 (57.3)	3531.6 (101.4)
Paracentral gyrus**,+†,††	18.1	1222.9 (22.3)	1369.4 (24.3)	1479.8 (42.9)	Paracentral gyrus**,+†,††	14.8	1343.5 (29.5)	1559.0 (32.1)	1585.4 (56.8)
Parahippocampal gyrus	4.6	696.3 (14.6)	730.4 (15.9)	790.9 (28.2)	Parahippocampal gyrus**,+†	7.3	633.2 (11)	683.1 (12)	708.9 (21.3)
Pars opercularis	1.8	1634.4 (32.7)	1715.0 (35.6)	1731.9 (63)	Pars opercularis	0.3	1348.7 (27.7)	1381.2 (30.2)	1367.4 (53.3)
Pars orbitalis	1.7	602.8 (10.6)	623.3 (11.5)	641.1 (20.4)	Pars orbitalis	3.4	731.5 (12.7)	777.0 (13.8)	777.3 (24.4)
Pars triangularis**,+†,††	10.0	1201.2 (25.3)	1345.2 (27.5)	1388.8 (48.7)	Pars triangularis**,+†,††	15.5	1328.8 (28.4)	1536.1 (30.9)	1578.3 (54.7)
Pericalcarine gyrus**,+†,††	35.5	1070.8 (25.7)	1361.9 (28)	1398.2 (49.6)	Pericalcarine gyrus**,+†,††	38.4	1193.6 (26.1)	1514.1 (28.4)	1499.0 (50.3)
Postcentral gyrus**,+†,††	17.4	3819.5 (55.9)	4260.0 (61)	4323.3 (107.8)	Postcentral gyrus**,+†,††	28.8	3576.2 (58.4)	4170.3 (63.7)	4247.1 (112.6)
Posterior cingulate**,+†,††	14.0	1108.8 (21.1)	1226.8 (23)	1326.2 (40.7)	Posterior cingulate gyrus**,+†,††	14.1	1093.6 (23.7)	1256.2 (25.8)	1297.5 (45.6)
Precentral gyrus	1.3	4737.2 (63.4)	4795.0 (69.1)	4960.8 (122.1)	Precentral gyrus	1.4	4722.6 (63.7)	4878.9 (69.4)	4820.4 (122.8)
Precuneus**,+†,††	36.3	3296.2 (53.3)	3893.8 (58.1)	4009.7 (102.7)	Precuneus**,+†,††	30.6	3427.1 (60.4)	3990.3 (65.8)	4273.1 (116.4)
Rostral anterior cingulate**,+†,††	33.7	641.6 (19)	807.5 (20.6)	942.8 (36.5)	Rostral anterior cingulate gyrus**,+†,††	15.7	580.8 (16.1)	670.0 (17.5)	761.4 (31)
Rostral middle frontal gyrus**,+†,††	26.3	4919.1 (88.9)	5784.2 (96.8)	5892.9 (171.2)	Rostral middle frontal gyrus**,+†,††	34.6	5009.6 (88.6)	6005.9 (96.5)	6101.4 (170.6)
Superior frontal cortex**,+†,††	15.2	6670.0 (95.9)	7369.3 (104.5)	7495.3 (184.9)	Superior frontal gyrus**,+†,††	11.4	6533.1 (98.5)	7113.8 (107.4)	7344.0 (189.9)
Superior parietal cortex**,+†,††	47.0	4657.2 (72.2)	5651.2 (78.6)	5539.0 (139)	Superior parietal cortex**,+†,††	45.2	4696.4 (66.5)	5536.5 (72.4)	5670.4 (128.1)
Superior temporal gyrus**,+†	11.8	3512.4 (51.6)	3756.9 (56.2)	4017.4 (99.4)	Superior temporal gyrus**,+†,††	20.8	3241.9 (44.1)	3569.5 (48)	3765.9 (84.9)
Supramarginal gyrus**,+†	7.1	3684.9 (60.5)	3958.8 (65.9)	4089.0 (116.5)	Supramarginal gyrus†,†	12.7	3414.5 (61.4)	3671.1 (66.9)	4063.7 (118.3)
Temporal pole**,+†,††	18.6	426.2 (7)	483.3 (7.6)	490.2 (13.4)	Temporal pole**,+†,††	10.8	381.3 (7.3)	427.2 (8)	432.5 (14.1)
Transverse temporal gyrus**,+†	10.6	424.6 (8.6)	463.9 (9.4)	504.0 (16.6)	Transverse temporal gyrus†,†	9.1	302.3 (6.7)	341.2 (7.3)	344.2 (12.9)

^aAdjusted means are covaried for age, sex, and scanner location.**Survives FDR correction ($p < 0.05$ threshold) at post hoc level for 22q-dup versus 22q-del.†Survives FDR correction ($p < 0.05$ threshold) at post hoc level for 22q-del versus control.††Survives FDR correction ($p < 0.05$ threshold) at omnibus level.

ROI. In contrast, 22q-dup carriers had significantly lower CT relative to controls, specifically in 3 lateral frontal and parietal ROIs: the left caudal and superior frontal gyrus, and the right precuneus (Table 3). 22q-dup carriers also showed cortical thinning relative to controls at a nominal uncorrected $p < 0.05$ level in predominantly frontal and sensorimotor regions (Fig. 4A). As shown in Figure 3, the decreases in 22q-dup carriers in regional cortical thickness measures are proportional to the increases observed in 22q-del carriers, albeit in somewhat different cortical regions; specifically, increased CT in 22q-del carriers was greatest in the insula and inferior frontal regions, whereas reductions of CT in 22q-dup were greatest in frontoparietal regions.

Opposing effects on cortical surface area

Pervasive effects of gene dosage were observed for cortical SA with significant effects of group for 52 ROIs (Table 4). Cortical SA showed a pattern opposite to that observed for CT: 22q-dup carriers largely showed greater SA compared with 22q-del carriers and controls mostly intermediate (Fig. 5). No differences between 22q-dup and controls survived correction, but 16 ROIs showed nominally significant differences at an uncorrected $p < 0.05$ level (Fig. 4B). These regions included most of the cortex

with differences of greatest magnitude observed in medial frontal cortex, the cingulate, superior temporal gyrus, and bank of the superior temporal sulcus (Fig. 5), notably, key components of social cognitive neural circuitry (Lieberman, 2007).

Moreover, there was a notable divergence in the brain regions predominantly affected by the deletion versus duplication. Although reductions of cortical SA were of greatest magnitude in parietal regions for 22q-del carriers, SA increases in the duplication group were greatest in frontotemporal and midline regions (i.e., cingulate cortex).

Effect size plots for 22q-dup carriers versus controls confirmed a global divergent pattern between CT and SA: SA was larger in 22q-dup carriers relative to controls (median effect size: Cohen's $d = -0.22$) with a negative value indicating larger cortical SA in 22q-dup carriers (Fig. 6B). Effects on CT, although more localized, were generally in the opposite direction. 22q-dup carriers showed lower thickness relative to controls (median effect size: Cohen's $d = 0.20$), most notably in superior frontal regions (Fig. 6A).

Post hoc power analysis for regional cortical thickness and surface area

Maps of *post hoc* power calculations, estimating the sample size needed to achieve a significant group difference in 22q-dup car-

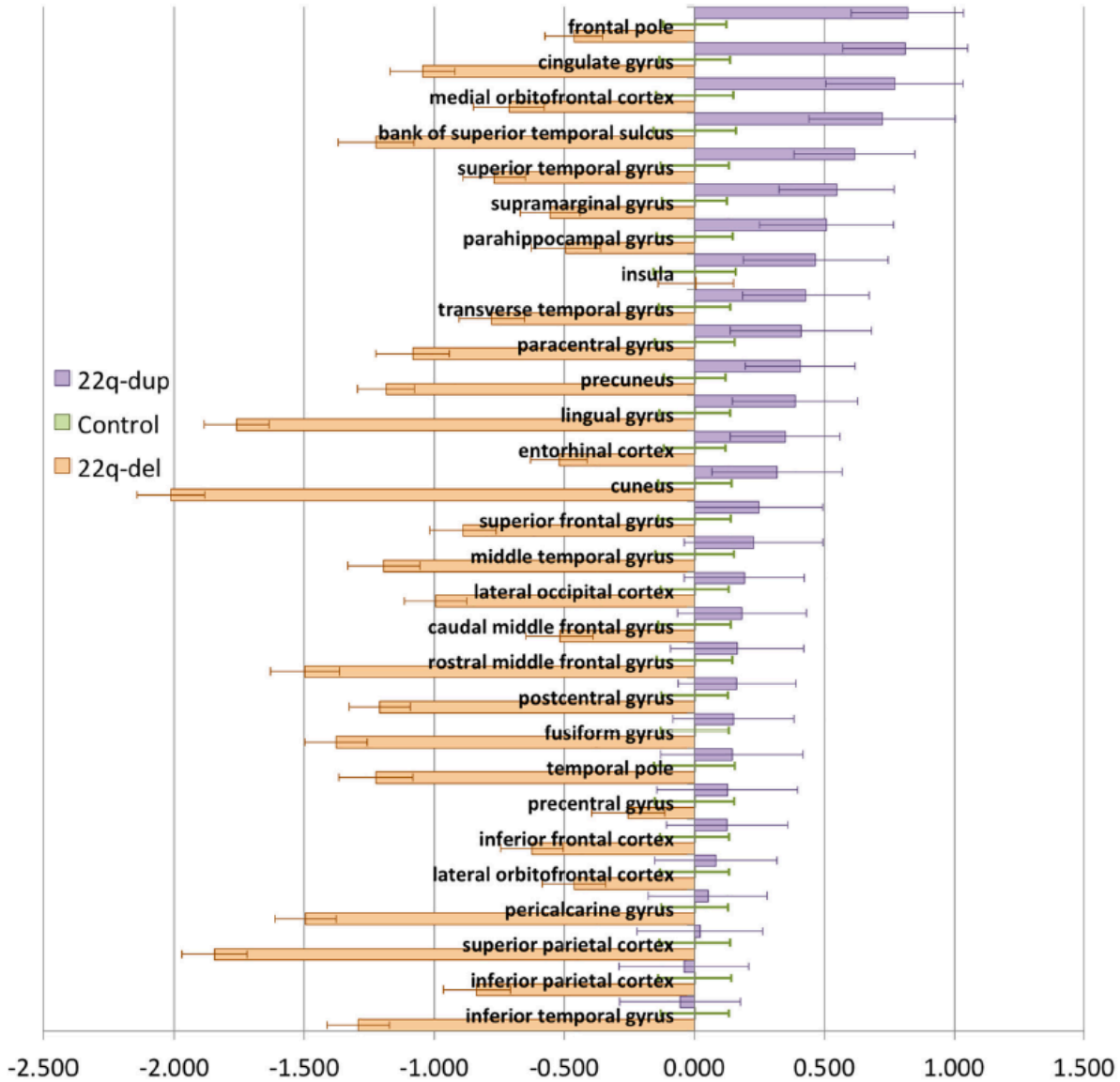


Figure 5. Cortical surface area z score plots of estimated marginal mean \pm SE. z scores are derived from individual subject means adjusted for sex, age, and scanner location using control mean and SD for each region. Then, z scores were submitted to the same primary statistical analysis to generate estimated marginal mean \pm SE. 22q-dup showed greater surface area relative to 22q-del patients in predominantly medial frontal and superior temporal regions, with controls showing an intermediate pattern.

riers versus controls across cortical regions (Fig. 6C,D), indicate that there is substantial regional variability in the effects of the 22q11.2 duplication on brain structure. With a sample size approximately equivalent to that of our deletion and control groups, we would also be likely to find significant thickness differences in additional frontoparietal regions in the duplication cohort (i.e., the bilateral supramarginal, precentral and postcentral gyrus, and left entorhinal cortex and insula). However, much larger samples would be required to observe thickness differences in temporal structures, as indicated by the smaller effect sizes in these regions. The regional distribution of effect sizes differs somewhat for cortical SA (Fig. 6D). With comparable sample sizes to our deletion and control groups, we would likely identify significant differences in SA in midline and right lateral parietal

regions, as well as the frontal pole and left temporal regions (entorhinal cortex, bank of the superior temporal sulcus) in duplication carriers versus controls. However, in other regions, the effects were quite small, likely requiring several hundred subjects to detect a significant group difference.

Patterns extend to subcortical structures: volume and morphometry

Significant effects of group extended into subcortical structures. Although pairwise differences between 22q-dup carriers and controls did not survive multiple comparisons correction for global subcortical volumes or local shape metrics, there were significant differences between 22q-dup and 22q-del carriers. Pairwise significant differences, indicating lower volume in 22q-del carriers com-

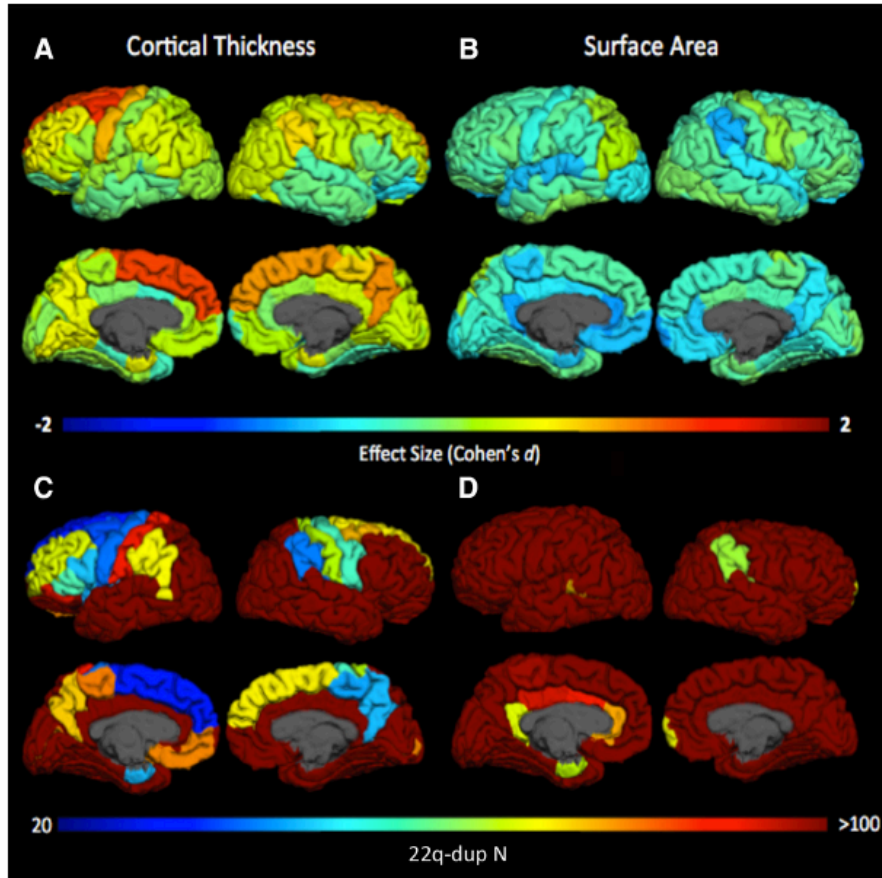


Figure 6. Effect size maps for 22q-dup carriers versus controls. *A, B*, Cohen's *d* is displayed for each ROI adjusted for age, sex, and scanner for 22q-dup carriers and controls. Cooler colors represent regions in which 22q-dup carriers show greater thickness or area. Warmer colors represent regions in which controls show greater thickness or area. For thickness, effect sizes ranged from -0.5 to 1.4 (median: 0.2), with controls showing greater thickness particularly in medial frontal regions. 22q-dup carriers showed widespread increases in surface area relative to controls, across multiple cortical regions (median effect size: -0.22 ; range -0.82 to 0.24). *C, D*, Estimated number of 22q-dup carriers needed to achieve a statistically significant difference from controls with 80% power, for each ROI. Raw values (not adjusted for any covariates) and Bonferroni correction for the number of regions were used to reduce model assumptions, resulting in conservative estimates.

Table 5. Subcortical volume: adjusted means, SEs, and estimated 22q-dupN^a

Region	<i>F</i>	22q-del, mean (SE)	Control, mean (SE)	22q-dup, mean (SE)	dupN	Region	<i>F</i>	22q-del, mean (SE)	Control, mean (SE)	22q-dup, mean (SE)	dupN
Left hemisphere						Right hemisphere					
Accumbens	2.7	852.7 (15.0)	803.6 (15.9)	807.2 (28.0)	>1000	Accumbens	5.8	815.7 (13.1)	749.6 (13.9)	774.3 (24.5)	>1000
Caudate	4.9	4058.0 (54.2)	3872.5 (57.5)	3729.0 (101.2)	363	Caudate**,†,††	10.5	4423.3 (55.8)	4091.8 (59.3)	3997.7 (104.4)	435
Hippocampus†,††	8.6	3790.8 (56.3)	4132.8 (59.8)	4054.5 (105.3)	>1000	Hippocampus**,†,††	8.2	3789.8 (53.9)	4074.8 (57.2)	4147.3 (100.7)	155
Inferior lateral ventricle**,†,††	17.6	505.4 (26.2)	295.9 (27.8)	263.8 (48.9)	>1000	Inferior lateral ventricle**,†,††	19.0	483.9 (27.7)	239.1 (29.4)	265.1 (51.7)	417
Lateral ventricle†,††	9.4	8339.6 (510.4)	5042.0 (541.6)	6534.2 (953.9)	189	Lateral ventricle†,††	15.0	7967.4 (475.7)	4094.3 (504.7)	6062.3 (888.9)	80
Pallidum	0.4	1787.5 (35.4)	1834.2 (37.5)	1817.2 (66.1)	>1000	Pallidum	0.4	1654.4 (25.0)	1670.5 (26.5)	1704.9 (46.6)	>1000
Putamen	1.0	6468.2 (87.2)	6558.3 (92.5)	6302.9 (162.9)	465	Putamen	1.6	6053.1 (75.0)	6247.9 (79.5)	6092.9 (140.1)	384
Thalamus	1.3	7269.6 (75.4)	7421.2 (80.0)	7484.6 (141.0)	658	Thalamus	1.8	7325.2 (73.2)	7295.5 (77.7)	7033.2 (136.8)	892

^aAdjusted means are covaried for age, sex, scanner location, and intracranial volume.
^{**}Survives FDR correction ($p < 0.05$ threshold) at post hoc level for 22q-dup versus 22q-del.
[†]Survives FDR correction ($p < 0.05$ threshold) at post hoc level for 22q-del versus control.
^{††}Survives FDR correction ($p < 0.05$ threshold) at omnibus level.

pared with 22q-dup carriers, were found for the right hippocampus (Table 5). In contrast, the right caudate displayed an opposite pattern: 22q-del carriers showed greater volume, whereas 22q-dup showed a decrease in volume compared with controls.

Novel shape analysis methods revealed a widespread and complex pattern of differences in local thickness measures

between 22q-del and 22q-dup carriers in subcortical regions (Fig. 7). Compared with 22q-del carriers, 22q-dup carriers had predominantly greater local thickness in bilateral hippocampal, left thalamus, and right amygdala structures. However, some smaller subregions of the hippocampi showed the opposite effect. Based on prior surface-based mapping of hippocampal subfields (Mamah

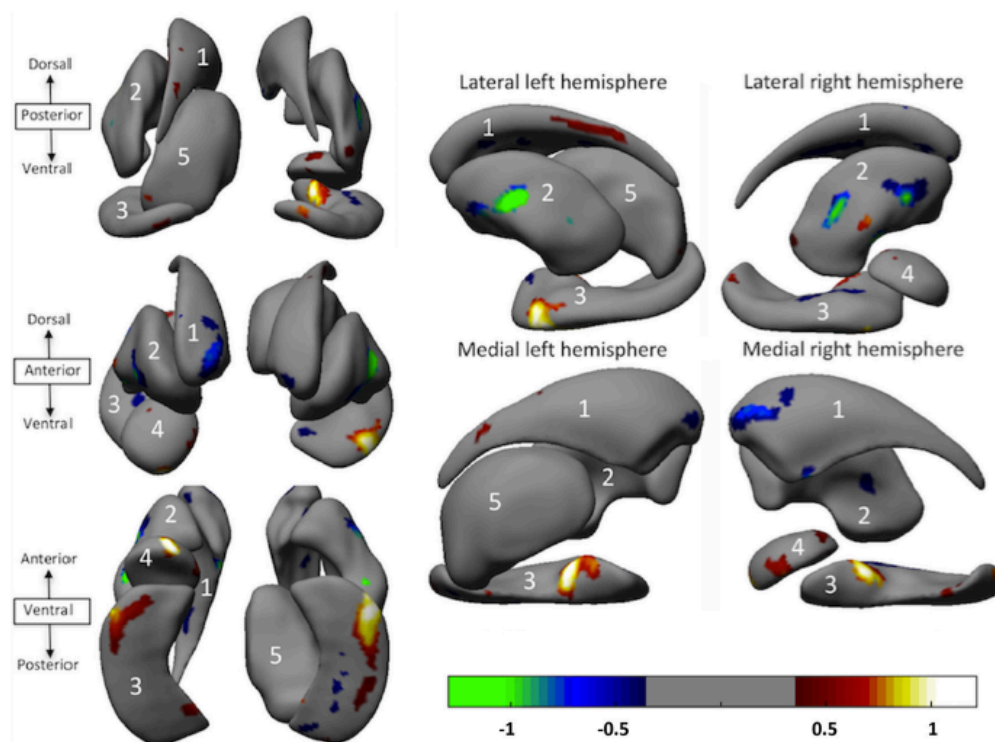


Figure 7. Subcortical shape differences. Radial distance maps for 22q-dup versus 22q-del carriers, showing β values, adjusted for sex, age, scanner, and intracranial volume, for regions passing correction for multiple comparisons at $q < 0.05$. Cooler colors represent negative β values (regions of lower local thickness or volume in 22q-dup vs 22q-del). Warmer colors represent positive β values (regions of greater local thickness or volume in 22q-dup vs 22q-del). Only structures that showed differences between 22q-dup and 22q-del that survive correction are displayed, as no significant differences were found between 22q-dup and controls. 1, Caudate; 2, putamen; 3, hippocampus; 4, amygdala; 5, thalamus.

et al., 2016), regions of greater thickness in the 22q-dup carriers approximately correspond to subiculum and CA1 regions, whereas decreased thickness in 22q-dup carriers approximately corresponds to CA2–4/dentate subfield regions. In contrast, largely lower local thickness measures were found in bilateral putamen and caudate structures in 22q-dup relative to 22q-del carriers with small localized regions of greater thickness.

Sensitivity analyses

Sensitivity analyses revealed that neither familial relatedness nor antipsychotic medication generally influenced the parameter estimates of interest. For the subsample of unrelated individuals, the estimated effects for all global metrics, as well as the ROIs showing significant 22q-dup versus control differences, were all within 2 SEs of the estimated effects in the primary analyses (Table 6). Similarly, the results of the analyses excluding participants on antipsychotics were within 2 SEs of the estimates obtained in the primary analyses for all ROIs.

Moreover, covarying for race did not alter our overall pattern of findings. Specifically, significant 22q-dup versus control differences in cortical thickness in all previously identified ROIs (the left caudal and superior frontal gyrus, and the right precuneus) remained significant, and an additional region, the right superior frontal gyrus, was also found to be significantly different.

Finally, after adjusting for mean thickness (Table 7), 7 of the 17 ROIs remained significant for 22q-del versus 22q-dup differences. The 3 ROIs in which we observed 22q-dup versus control differences remained significant, regardless of whether average

Table 6. Full dataset versus unrelated 22q-dup patients: adjusted means and SEs

Measure	Full dataset 22q-dup adjusted, mean (SE)	Unrelated 22q-dup adjusted, mean (SE)	Within 2 SEs?
Corpus callosum volume	2723.9 (113.5)	2737.4 (149.7)	Yes
Cortical white matter volume	415,362.7 (6319.3)	411,210.5 (8372.5)	Yes
Total gray matter	581,072.5 (8947.3)	5738,25.4 (11956.8)	Yes
Mean thickness	2.71 (0.02)	2.70 (0.03)	Yes
Total intracranial volume	1,466,356.0 (27086.6)	1,466,689.9 (35730.6)	Yes
Total area	176,466.1 (3390.9)	174,713.5 (4522.6)	Yes
Left caudal middle frontal gyrus	2.58 (0.04)	2.56 (0.05)	Yes
Left superior frontal gyrus	2.84 (0.04)	2.83 (0.05)	Yes
Right precuneus	2.50 (0.04)	2.49 (0.05)	Yes

cortical thickness was included as a covariate or not, indicating localized effects of the 22q11.2 CNV on thickness. In contrast, covarying for total SA reduced the magnitude of deletion-duplication differences in regional SA measures. Specifically, only 8 of the 50 previously identified ROIs remained significantly different for 22q-del versus 22q-dup comparisons (Table 8), suggesting that our SA results should be interpreted as a diffuse, global surface deficit in 22q11.2 deletion carriers with additional regional accentuation in occipitoparietal and cingulate regions.

Discussion

22q11.2 copy number variation was associated with global opposing effects on brain structure, involving widespread cortical SA reductions in deletion carriers with corresponding enlargement in duplication carriers. CT showed an opposite, more lo-

Table 7. Regional cortical thickness: adjusted means and SEs with additional mean thickness covariate^a

Region	F	22q-del, mean (SE)	Control, mean (SE)	22q-dup, mean (SE)	Region	F	22q-del, mean (SE)	Control, mean (SE)	22q-dup, mean (SE)
Left hemisphere					Right hemisphere				
Bank of superior temporal sulcus ^{**} ,††	9.3	2.63 (0.02)	2.72 (0.02)	2.8 (0.04)	Bank of superior temporal sulcus	4.9	2.81 (0.02)	2.87 (0.02)	2.94 (0.04)
Caudal anterior cingulate gyrus ^{**} ,††	9.1	2.81 (0.03)	2.97 (0.04)	3.08 (0.06)	Caudal anterior cingulate gyrus	6.4	2.68 (0.03)	2.84 (0.03)	2.84 (0.06)
Caudal middle frontal gyrus ^{**} ,††,‡	14.4	2.8 (0.01)	2.76 (0.02)	2.63 (0.03)	Caudal middle frontal gyrus ^{**} ,††,‡	7.7	2.73 (0.02)	2.68 (0.02)	2.6 (0.03)
Cuneus	1.0	2.11 (0.02)	2.07 (0.02)	2.09 (0.04)	Cuneus	0.8	2.15 (0.02)	2.12 (0.02)	2.1 (0.04)
Entorhinal cortex	1.9	3.46 (0.04)	3.57 (0.05)	3.44 (0.08)	Entorhinal cortex	0.8	3.78 (0.05)	3.82 (0.05)	3.69 (0.09)
Frontal pole	2.3	2.81 (0.04)	2.92 (0.04)	2.96 (0.08)	Frontal pole	1.1	2.8 (0.04)	2.78 (0.04)	2.92 (0.08)
Fusiform gyrus	1.1	2.89 (0.01)	2.91 (0.02)	2.93 (0.03)	Fusiform gyrus	1.9	2.99 (0.01)	2.97 (0.01)	3.03 (0.03)
Inferior parietal cortex	0.9	2.69 (0.01)	2.71 (0.01)	2.69 (0.02)	Inferior parietal cortex	0.4	2.72 (0.01)	2.71 (0.01)	2.69 (0.02)
Inferior temporal gyrus	1.7	2.86 (0.02)	2.9 (0.02)	2.94 (0.04)	Inferior temporal gyrus	1.4	3.03 (0.02)	3.03 (0.02)	3.09 (0.03)
Insula ^{**} ,†,†,‡	18.6	3.4 (0.02)	3.26 (0.02)	3.26 (0.03)	Insula	3.9	3.4 (0.02)	3.32 (0.02)	3.35 (0.04)
Isthmus cingulate	0.7	2.77 (0.03)	2.78 (0.03)	2.71 (0.05)	Isthmus cingulate	1.5	2.64 (0.02)	2.69 (0.02)	2.66 (0.04)
Lateral occipital cortex	0.2	2.33 (0.01)	2.34 (0.02)	2.35 (0.03)	Lateral occipital cortex	0.6	2.4 (0.02)	2.43 (0.02)	2.4 (0.03)
Lateral orbitofrontal cortex	2.1	2.89 (0.02)	2.86 (0.02)	2.93 (0.03)	Lateral orbitofrontal cortex	6.2	2.73 (0.02)	2.73 (0.02)	2.86 (0.04)
Lingual gyrus	5.3	2.29 (0.02)	2.24 (0.02)	2.2 (0.03)	Lingual gyrus	4.0	2.37 (0.02)	2.31 (0.02)	2.29 (0.03)
Medial orbitofrontal cortex	3.2	2.67 (0.03)	2.59 (0.03)	2.57 (0.05)	Medial orbitofrontal cortex	2.3	2.52 (0.02)	2.46 (0.02)	2.45 (0.04)
Middle temporal gyrus	0.8	3.03 (0.02)	3.03 (0.02)	3.08 (0.04)	Middle temporal gyrus	0.9	3.12 (0.02)	3.1 (0.02)	3.15 (0.04)
Paracentral gyrus	3.9	2.65 (0.02)	2.57 (0.02)	2.58 (0.04)	Paracentral gyrus	4.8	2.68 (0.02)	2.64 (0.02)	2.55 (0.04)
Parahippocampal gyrus ^{**} ,†,†,‡	17.5	2.68 (0.04)	2.95 (0.04)	3.06 (0.07)	Parahippocampal gyrus	2.0	2.93 (0.04)	3.02 (0.04)	3.04 (0.07)
Pars opercularis [†] ,†,‡	11.4	2.87 (0.01)	2.78 (0.01)	2.8 (0.02)	Pars opercularis	1.1	2.79 (0.02)	2.76 (0.02)	2.8 (0.04)
Pars orbitalis	2.0	2.98 (0.03)	2.93 (0.03)	2.88 (0.05)	Pars orbitalis	1.4	2.8 (0.03)	2.75 (0.03)	2.86 (0.06)
Pars triangularis [†] ,†,‡	9.6	2.74 (0.02)	2.63 (0.02)	2.63 (0.03)	Pars triangularis	1.2	2.61 (0.03)	2.56 (0.03)	2.62 (0.05)
Pericalcarine gyrus	2.6	1.84 (0.02)	1.79 (0.02)	1.75 (0.04)	Pericalcarine gyrus	6.5	1.86 (0.02)	1.76 (0.02)	1.74 (0.04)
Postcentral gyrus	3.0	2.26 (0.02)	2.21 (0.02)	2.23 (0.03)	Postcentral gyrus	1.6	2.26 (0.02)	2.22 (0.02)	2.19 (0.04)
Posterior cingulate	0.8	2.78 (0.02)	2.81 (0.02)	2.82 (0.04)	Posterior cingulate	3.9	2.71 (0.02)	2.79 (0.02)	2.75 (0.04)
Precentral gyrus	5.3	2.74 (0.01)	2.72 (0.01)	2.65 (0.02)	Precentral gyrus	2.0	2.71 (0.02)	2.67 (0.02)	2.65 (0.03)
Precuneus	1.3	2.65 (0.01)	2.65 (0.01)	2.61 (0.02)	Precuneus ^{**} ,††,‡	8.5	2.68 (0.02)	2.68 (0.02)	2.56 (0.03)
Rostral anterior cingulate	0.2	3.15 (0.03)	3.17 (0.03)	3.18 (0.06)	Rostral anterior cingulate	6.2	2.81 (0.03)	2.94 (0.03)	2.98 (0.06)
Rostral middle frontal gyrus	5.3	2.62 (0.02)	2.56 (0.02)	2.53 (0.03)	Rostral middle frontal gyrus	4.6	2.44 (0.02)	2.37 (0.02)	2.36 (0.03)
Superior frontal cortex ^{**} ,††,‡	12.1	3.03 (0.01)	3.02 (0.01)	2.89 (0.03)	Superior frontal cortex	6.3	2.91 (0.01)	2.9 (0.02)	2.8 (0.03)
Superior parietal cortex	0.1	2.39 (0.02)	2.39 (0.02)	2.38 (0.03)	Superior parietal cortex	0.3	2.38 (0.02)	2.36 (0.02)	2.35 (0.03)
Superior temporal gyrus [†] ,†,‡	23.0	2.87 (0.02)	3.01 (0.02)	3.03 (0.03)	Superior temporal gyrus	4.2	2.97 (0.02)	3.01 (0.02)	3.08 (0.03)
Supramarginal gyrus	4.1	2.84 (0.01)	2.79 (0.02)	2.76 (0.03)	Supramarginal gyrus ^{**} ,†,†,‡	11.1	2.87 (0.01)	2.81 (0.01)	2.76 (0.02)
Temporal pole	1.1	3.67 (0.04)	3.69 (0.05)	3.8 (0.08)	Temporal pole	0.1	3.9 (0.04)	3.92 (0.05)	3.89 (0.08)
Transverse temporal gyrus	2.8	2.55 (0.03)	2.64 (0.03)	2.63 (0.05)	Transverse temporal gyrus	1.9	2.66 (0.03)	2.62 (0.03)	2.73 (0.05)

^aAdjusted means are covaried for age, sex, scanner location, and mean thickness.

^{**}Survives FDR correction ($p < 0.05$ threshold) at post hoc level for 22q-dup versus 22q-del.

[†]Survives FDR correction ($p < 0.05$ threshold) at post hoc level for 22q-del versus control.

^{††}Survives FDR correction ($p < 0.05$ threshold) at omnibus level.

[‡]FDR-corrected omnibus effect as well as FDR-corrected del-dup or dup-con difference that remain significant with inclusion of mean thickness covariate.

calized pattern. These findings were not accounted for by a subset of individuals, but rather the entire distribution was shifted, suggesting a highly penetrant effect of gene dosage.

22q11.2 gene dosage implications for neuropsychiatric disorders

There is now replicated evidence that duplications at 22q11.2 are substantially less common in schizophrenia cases than in the general population, but reciprocal deletions are an established strong risk factor for schizophrenia (Rees et al., 2014, 2016). Our findings suggest a possible underlying neurobiological basis for these divergent behavioral phenotypes. We found opposing effects of CT and SA in in 22q-del versus 22q-dup in medial temporal and frontal brain regions strongly implicated in idiopathic schizophrenia (Palaniyappan et al., 2011; Shepherd et al., 2012), suggesting relevant underlying brain mechanisms that may be selective for schizophrenia. Alternatively, because both 22q-del and 22q-dup confer increased risk for ASD, opposing effects in common brain regions implicated in autism (Ecker et al., 2013; Wallace et al., 2015; Ohta et al., 2016) (e.g., decreased vs increased SA in medial frontal regions in 22q-del and 22q-

dup, respectively) may result in similar downstream phenotypic effects on traits, such as language delay and reciprocal social behavior deficits. Future, prospective longitudinal brain-behavior investigations in these two groups are necessary to test these hypotheses.

22q11.2 gene dosage effects on brain structure

Critical to our study framework, we separately measured CT and SA, two cortical measures that likely have different phylogenetic and ontogenetic origins (Rakic, 1995; Panizzon et al., 2009) and distinct developmental trajectories (Raznahan et al., 2011; Wierenga et al., 2014). Our findings of opposing directions of effect, as well as more pervasive effects of the 22q11 CNV on SA relative to CT, suggest that different mechanisms may be involved. In particular, increased progenitor cell production during early embryonic development predominantly influences SA expansion (Rakic, 1988); thus, widespread SA decreases in 22q-del may reflect reduced production of progenitor cells in multiple cortical areas, implying that these divergent phenotypes arise early in the course of development. Nevertheless, these effects were not entirely proportional in magnitude, as deletions conferred a rela-

Table 8. Regional SA: adjusted means and SEs with additional total area covariate^a

Region	F	22q-del, mean (SE)	Control, mean (SE)	22q-dup, mean (SE)	Region	F	22q-del, mean (SE)	Control, mean (SE)	22q-dup, mean (SE)
Left hemisphere					Right hemisphere				
Bank of superior temporal sulcus	3.0	1012.1 (19.2)	1003.3 (19.2)	1092.9 (33.8)	Bank of superior temporal sulcus	2.3	944 (15.2)	991.3 (15.3)	996.9 (26.8)
Caudal anterior cingulate gyrus ^{**} ,†,‡	9.5	562.7 (15.3)	632.6 (15.3)	702.1 (26.9)	Caudal anterior cingulate gyrus	3.2	674.4 (20.8)	753.7 (20.8)	748.4 (36.6)
Caudal middle frontal gyrus	1.6	2347.8 (44.7)	2229 (44.8)	2233.6 (78.7)	Caudal middle frontal gyrus	2.3	2122.7 (47)	1982.9 (47.1)	1943.2 (82.7)
Cuneus ^{**} ,†,‡	21.4	1207.1 (24.6)	1435.2 (24.7)	1477.9 (43.4)	Cuneus†,‡	9.2	1315.4 (21.9)	1456.4 (21.9)	1444.3 (38.5)
Entorhinal cortex	1.4	361 (10.9)	356.3 (10.9)	392 (19.2)	Entorhinal cortex	1.1	298.1 (10)	320.3 (10)	317.1 (17.6)
Frontal pole	3.0	208 (4.4)	209.6 (4.4)	229.4 (7.8)	Frontal pole	4.0	280.2 (6)	286.3 (6)	315.4 (10.5)
Fusiform gyrus	3.8	3089.4 (42.8)	3269.9 (42.8)	3223.2 (75.3)	Fusiform gyrus	1.7	3039.8 (38.2)	3147.4 (38.3)	3124.6 (67.2)
Inferior parietal cortex ^{**} ,†,‡	8.9	4753.7 (55.1)	4539.3 (55.2)	4257.6 (97)	Inferior parietal cortex	0.4	5522.2 (71.2)	5460 (71.4)	5386.2 (125.4)
Inferior temporal gyrus	4.8	3060.1 (42.8)	3254.6 (42.8)	3126.8 (75.3)	Inferior temporal gyrus	1.1	3016.1 (45.8)	3063.2 (45.8)	2933.7 (80.6)
Insula†,‡	12.9	2150.5 (23.1)	1972.2 (23.1)	2018.4 (40.7)	Insula†,‡	12.0	2188.7 (31.5)	1955.9 (31.6)	1965.4 (55.5)
Isthmus cingulate	5.5	1035.8 (18.7)	962.9 (18.7)	1059.1 (32.9)	Isthmus cingulate†,‡	11.2	987.4 (17.2)	867.1 (17.2)	940.8 (30.3)
Lateral occipital cortex	0.9	4603.4 (58.5)	4665 (58.6)	4773 (102.9)	Lateral occipital cortex	1.4	4513.9 (61.4)	4475.9 (61.5)	4302.8 (108.1)
Lateral orbitofrontal cortex ^{**} ,†,‡	12.7	2602.7 (26.8)	2422.1 (26.8)	2356.5 (47.1)	Lateral orbitofrontal cortex ^{**} ,†,‡	8.7	2504 (32.2)	2318.7 (32.3)	2267.5 (56.8)
Lingual gyrus ^{**} ,†,‡	9.3	2691.7 (45.2)	2964.1 (45.3)	3028.9 (79.6)	Lingual gyrus ^{**} ,†,‡	16.1	2663.8 (41.4)	3001.2 (41.5)	3046.4 (72.9)
Medial orbitofrontal cortex	2.7	1712.5 (26.2)	1642 (26.3)	1739.3 (46.2)	Medial orbitofrontal cortex	2.2	1767.2 (21.8)	1711.4 (21.8)	1779.9 (38.4)
Middle temporal gyrus	0.3	2947.1 (35.8)	2983.6 (35.8)	2953.5 (62.9)	Middle temporal gyrus	1.5	3349.2 (36)	3267.2 (36)	3231.7 (63.3)
Paracentral gyrus	1.8	1311.3 (20.5)	1312 (20.5)	1384.8 (36.1)	Paracentral gyrus	0.2	1466.5 (26.3)	1479.2 (26.3)	1453.1 (46.2)
Parahippocampal gyrus	1.6	735.3 (15.4)	705 (15.4)	748.9 (22.7)	Parahippocampal gyrus	0.4	672.3 (10.7)	657.8 (10.7)	666.9 (18.9)
Pars opercularis	3.3	1750.8 (31.7)	1639.5 (31.7)	1606.7 (55.7)	Pars opercularis ^{**} ,†,‡	9.8	1458.5 (25.4)	1309.9 (25.5)	1249.2 (44.8)
Pars orbitalis	4.1	641.3 (10.1)	598.3 (10.2)	599.6 (17.8)	Pars orbitalis	2.1	777.3 (12.2)	747.3 (12.2)	728.1 (21.5)
Pars triangularis	0.0	1290.9 (24.5)	1287 (24.6)	1292.4 (43.2)	Pars triangularis	0.7	1425.3 (28)	1473.4 (28)	1474.5 (49.2)
Pericalcarine gyrus†,‡	8.3	1153.1 (25.9)	1308.5 (25.9)	1309.6 (45.6)	Pericalcarine gyrus†,‡	10.2	1279.5 (26)	1458.4 (26.1)	1406.7 (45.8)
Postcentral gyrus	0.1	4075.6 (46.3)	4093.8 (46.4)	4047.8 (81.5)	Postcentral gyrus	2.1	3845.7 (48)	3995.4 (48.1)	3957.2 (84.5)
Posterior cingulate	1.5	1190 (19.7)	1174.1 (19.8)	1238.9 (34.7)	Posterior cingulate	0.0	1196.4 (20.5)	1189.4 (20.5)	1186.8 (36)
Precentral gyrus†,‡	14.8	5030.1 (52)	4604.7 (52.1)	4645.7 (91.5)	Precentral gyrus ^{**} ,†,‡	21.7	5049.7 (45.9)	4666.6 (46)	4468.5 (80.8)
Precuneus	4.5	3542.2 (43.8)	3734 (43.9)	3745 (77.1)	Precuneus	2.5	3733.5 (44.3)	3791.4 (44.4)	3943.5 (78)
Rostral anterior cingulate	6.8	729.4 (15.5)	750.5 (15.5)	848.3 (27.2)	Rostral anterior cingulate	2.5	638.4 (15.5)	632.6 (15.6)	699.4 (27.3)
Rostral middle frontal gyrus	0.6	5387.4 (61.3)	5480.1 (61.4)	5389.1 (108)	Rostral middle frontal gyrus	3.1	5473.6 (61.8)	5704.7 (61.9)	5602.3 (108.7)
Superior frontal cortex	2.3	7192.6 (62)	7030 (62.1)	6933.1 (109.2)	Superior frontal cortex	5.6	7073.8 (62.7)	6762.8 (62.8)	6762.4 (110.4)
Superior parietal cortex†,‡	13.6	4941.4 (66.6)	5466.6 (66.7)	5233.2 (117.2)	Superior parietal cortex†,‡	10.6	4952 (62.1)	5370.5 (62.2)	5395.4 (109.4)
Superior temporal gyrus	6.4	3776 (37.4)	3585.7 (37.5)	3733.8 (65.9)	Superior temporal gyrus	1.3	3457.6 (33.9)	3429.4 (34)	3533.8 (59.7)
Supramarginal gyrus	1.3	3933 (54.4)	3797.7 (54.5)	3822.2 (95.8)	Supramarginal gyrus	5.2	3682.6 (52.9)	3497 (53)	3775.3 (93.1)
Temporal pole	3.7	442.6 (7.5)	472.7 (7.5)	472.6 (13.2)	Temporal pole	2.9	391.3 (8.3)	420.7 (8.3)	421.8 (14.6)
Transverse temporal gyrus	1.5	451.3 (8.7)	446.5 (8.7)	475.2 (15.4)	Transverse temporal gyrus	0.3	321.5 (7)	328.7 (7)	323.6 (12.2)

^aAdjusted means are covaried for age, sex, scanner location, and total area.^{**}Survives FDR correction ($p < 0.05$ threshold) at post hoc level for 22q-dup versus 22q-del.[†]Survives FDR correction ($p < 0.05$ threshold) at post hoc level for 22q-del versus control.[‡]Survives FDR correction ($p < 0.05$ threshold) at omnibus level.[‡]FDR-corrected omnibus effect as well as FDR-corrected del-dup or dup-con difference that remain significant with inclusion of total area covariate.

tively larger “hit” to SA and to global brain volume metrics than did duplications. This pattern is consistent with the relatively milder effect of 22q-dup on cognition, which aligns with epidemiological findings that duplication CNVs tend to have less deleterious effects on cognition (Männik et al., 2015). Widespread SA reductions in 22q-del, with more subtle increases for 22q-dup, may be a potential mechanism underlying differential deficits in cognition associated with deletions at this locus. However, regional CT decreases in 22q-dup were proportional to the increases observed in deletion carriers, albeit in somewhat different cortical regions.

While deletion-duplication differences in SA were widespread throughout the cortex, including frontotemporal regions critical for language (Friederici and Gierhan, 2013) and medial and lateral frontal and parietal regions implicated in self-referential thought and social perception (Kennedy and Adolphs, 2012), effects on CT were more localized. Despite the notable divergence in the specific brain regions predominantly affected by the deletion versus duplication, regions with the greatest magnitude of effects are notable in their shared role in social-cognitive neural circuitry (Lieberman, 2007; Adolphs, 2009).

The overall patterns detected in the cortex persisted into subcortical regions, previously shown to be affected by 22q-del (Bish et al., 2004; Kates et al., 2004), suggesting global effects of 22q11.2 CNV on brain development. Our novel shape analysis revealed localized patterns of subcortical alteration, which may correspond to underlying anatomic subfields that cannot be resolved by conventional volumetric approaches (Mamah et al., 2016). We found largely higher local thickness in 22q-dup relative to 22q-del carriers in bilateral hippocampal, left thalamus, and right amygdala structures; the opposite pattern was observed for bilateral putamen and caudate structures, which together form the dorsal striatum and importantly contain the same types of neurons and circuits (Alexander and Crutcher, 1990). Local and global hippocampal reductions in 22q-del are consistent with findings in a mouse model, indicating decreased density of dendritic spines and glutamatergic synapses as well as impaired dendritic growth, in primary hippocampal neurons (Mukai et al., 2008). To our knowledge, no preclinical models of the reciprocal duplication have yet been developed; thus, it is unclear the extent to which our human findings are recapitulated in animal models. Future work aims to map known subfields to subcortical surface

models so that stronger inferences may be made regarding the underlying compartmental effects detected by this shape analysis technique.

Genes critical for cortical circuit formation in the 22q11.2 locus

The 22q11.2 region houses many genes highly conserved in model organisms and expressed in the developing brain. Some 22q11.2 genes are selectively expressed in cortical progenitors in the ventricular/subventricular zones (e.g., *ranbp1* and *cdc45l*), whereas others, including *dgcr8*, a microRNA processing cofactor, are more broadly expressed in cortical neurons (Meechan et al., 2015a). As many of these genes are expressed early in development, diminished dosage of multiple 22q11.2 genes may lead to compromised proliferative and neurogenic capacity of neuronal precursors.

Although the function of individual 22q11.2 genes in the developing cortex remains poorly understood, *ranbp1* gene dosage remains a candidate mechanism as a regulator of early nervous system development (Paronett et al., 2015). *ranbp1* homozygous null mouse embryos are either exencephalic or microcephalic at early stages. *ranbp1* plays a role in rapidly dividing precursors in the developing cortex, loss of which may compromise the overall pool of cortical radial glial progenitors, resulting in a smaller brain. *ranbp1*^{-/-} embryos were found to have selectively disrupted layer 2/3 cortical projection neuron generation, suggesting an important role in cortical circuit development. In addition, a haplotype block including the *ranbp1* and *dgcr8* genes was associated with idiopathic schizophrenia (Liu et al., 2002). Thus, targeted studies of the effects of overexpression and underexpression of *Ranbp1* and other key neurodevelopmental genes in the locus are warranted.

Gene-dosage effects in other reciprocal CNVs

Notably, dose-dependent effects of two other neuropsychiatric CNVs (15q11.2 BP1-BP2 and 16p11.2) on brain structure have recently been discovered. Our findings of similar diametric patterns in the 22q11.2 locus suggest that this anthropometric variation may be regulated by multiple, distinct genomic regions. Consistent with our 22q11.2 findings, in the Icelandic population Stefansson et al. (2014) found a positive gene dosage effect of 15q11.2 on gray matter volume, whereas corpus callosum size was lower in 15q11.2 duplication relative to deletion carriers. Further, convergent findings across 16p11.2 mouse and human studies indicate pervasive effects of gene dosage across cortical and subcortical structures, suggesting the role of genes important in early development (Horev et al., 2011; Qureshi et al., 2014). Similar to our results, reciprocal variation at 16p11.2 revealed widespread alterations in SA (Qureshi et al., 2014); intriguingly, however, the pattern of findings was in the opposite direction (deletion > control > duplication). Thus, while gene dosage is associated with opposing brain phenotypes across these “neuropsychiatric” CNVs, deletion or duplication of genomic material does not consistently determine the direction of effect. Finally, in a zebrafish model, Golzio et al. (2012) identified a single gene at the 16p11.2 locus, *KCTD13*, that is likely responsible for the opposing brain phenotypes, as it causes microcephaly when overexpressed and macrocephaly when suppressed. It is not yet known whether the patterns observed for 22q11.2 are attributable to a single gene or an oligogenic effect.

Study limitations

Several limitations of our study must be noted, such as the modest sample size of our 22q-dup group. As the first study to inves-

tigate effects of reciprocal genomic variation in this region, these results should be confirmed in subsequent, larger investigations. Additionally, given the duplication's inheritance pattern (Wentzel et al., 2008), many participants in this group were related. Although effect sizes for our main findings did not substantively change when removing related individuals, we could not entirely disentangle familial effects from those of the duplication itself. Additionally, the two CNV groups contained a greater proportion of subjects of European ancestry than the control group; nevertheless, covarying for race did not alter the significant findings. Further, although 22q-dup carriers did not differ in nonverbal IQ from controls, it was not possible to match nonverbal IQ of duplication to deletion carriers. Crucially, however, our sample was highly representative of the phenotypic spectrum of 22q11.2 disorders in the broader population (McDonald-McGinn et al., 2015; Tang et al., 2016).

In conclusion, elucidating the pathophysiology of developmental neuropsychiatric disorders remains a major challenge, due to considerable heterogeneity at both the genetic and phenotypic level (Geschwind and Flint, 2015). The robust, opposing effects on brain structure described here highlight the utility of investigating the influence of reciprocal chromosomal imbalances on neural processes and how these may ultimately contribute to disease pathogenesis. Prospective longitudinal studies are underway to track divergent neurodevelopmental trajectories over time in CNV carriers. Finally, *in vitro* modeling of reciprocal CNVs at the 22q11.2 locus offers an avenue to directly characterize associated cellular phenotypes.

References

- Adolphs R (2009) The social brain: neural basis of social knowledge. *Annu Rev Psychol* 60:693–716. [CrossRef Medline](#)
- Alexander GE, Crutcher MD (1990) Functional architecture of basal ganglia circuits: neural substrates of parallel processing. *Trends Neurosci* 13:266–271. [CrossRef Medline](#)
- Bassett AS, Chow EW (2008) Schizophrenia and 22q11.2 deletion syndrome. *Curr Psychiatry Rep* 10:148–157. [CrossRef Medline](#)
- Bearden CE, van Erp TG, Dutton RA, Tran H, Zimmermann L, Sun D, Geaga JA, Simon TJ, Glahn DC, Cannon TD, Emanuel BS, Toga AW, Thompson PM (2007) Mapping cortical thickness in children with 22q11.2 deletions. *Cereb Cortex* 17:1889–1898. [CrossRef Medline](#)
- Benjamini Y, Hochberg Y (1995) Controlling the false discovery rate: a practical and powerful approach to multiple testing. *J R Stat Soc B Met* 57:289–300.
- Bish JP, Nguyen V, Ding L, Ferrante S, Simon TJ (2004) Thalamic reductions in children with chromosome 22q11.2 deletion syndrome. *Neuroreport* 15:1413–1415. [CrossRef Medline](#)
- CNV and Schizophrenia Working Groups of the Psychiatric Genomics Consortium, Psychosis Endophenotypes International Consortium (2017) Contribution of copy number variants to schizophrenia from a genome-wide study of 41,321 subjects. *Nat Genet* 49:27–35. [Medline](#)
- Constantino JN, Gruber CP (2007) Social Responsiveness Scale (SRS). Los Angeles: Western Psychological Services.
- Coppola G, Choi SH, Santos MM, Miranda CJ, Tentler D, Wexler EM, Pandolfo M, Geschwind DH (2006) Gene expression profiling in frataxin deficient mice: microarray evidence for significant expression changes without detectable neurodegeneration. *Neurobiol Dis* 22:302–311. [CrossRef Medline](#)
- Dale AM, Fischl B, Sereno MI (1999) Cortical surface-based analysis: I. Segmentation and surface reconstruction. *Neuroimage* 9:179–194. [CrossRef Medline](#)
- Desikan RS, Ségonne F, Fischl B, Quinn BT, Dickerson BC, Blacker D, Buckner RL, Dale AM, Maguire RP, Hyman BT, Albert MS, Killiany RJ (2006) An automated labeling system for subdividing the human cerebral cortex on MRI scans into gyral based regions of interest. *Neuroimage* 31:968–980. [CrossRef Medline](#)

- Ecker C, Ginestet C, Feng Y, Johnston P, Lombardo MV, Lai MC, Suckling J, Palaniyappan L, Daly E, Murphy CM, Williams SC, Bullmore ET, Baron-Cohen S, Brammer M, Murphy DG (2013) Brain surface anatomy in adults with autism: the relationship between surface area, cortical thickness, and autistic symptoms. *JAMA Psychiatry* 70:59–70. [CrossRef Medline](#)
- Ensenauer RE, Adeyinka A, Flynn HC, Michels VV, Lindor NM, Dawson DB, Thorland EC, Lorentz CP, Goldstein JL, McDonald MT, Smith WE, Simon-Fayard E, Alexander AA, Kulharya AS, Ketterling RP, Clark RD, Jalal SM (2003) Microduplication 22q11.2, an emerging syndrome: clinical, cytogenetic, and molecular analysis of thirteen patients. *Am J Hum Genet* 73:1027–1040. [CrossRef Medline](#)
- First MB, Gibbon M (2004) The Structured Clinical Interview for DSM-IV Axis I Disorders (SCID-I) and the Structured Clinical Interview for DSM-IV Axis II Disorders (SCID-II). In: *Comprehensive handbook of psychological assessment, Vol. 2: Personality assessment* (Hilsenroth MJ, Segal DL, eds), pp 134–143. Hoboken, NJ: Wiley.
- Fischl B, Sereno MI, Dale AM (1999) Cortical surface-based analysis. II: Inflation, flattening, and a surface-based coordinate system. *Neuroimage* 9:195–207. [CrossRef Medline](#)
- Friederici AD, Gierhan SM (2013) The language network. *Curr Opin Neurobiol* 23:250–254. [CrossRef Medline](#)
- Geschwind DH, Flint J (2015) Genetics and genomics of psychiatric disease. *Science* 349:1489–1494. [CrossRef Medline](#)
- Girirajan S, Brkanac Z, Coe BP, Baker C, Vives L, Vu TH, Shafer N, Bernier R, Ferrero GB, Silengo M, Warren ST, Moreno CS, Fichera M, Romano C, Raskind WH, Eichler EE (2011) Relative burden of large CNVs on a range of neurodevelopmental phenotypes. *Plos Genet* 7:e1002334. [CrossRef Medline](#)
- Golzio C, Willer J, Talkowski ME, Oh EC, Taniguchi Y, Jacquemont S, Raymond A, Sun M, Sawa A, Gusella JF, Kamiya A, Beckmann JS, Katsanis N (2012) KCTD13 is a major driver of mirrored neuroanatomical phenotypes of the 16p11.2 copy number variant. *Nature* 485:363–367. [CrossRef Medline](#)
- Grati FR, Molina Gomes D, Ferreira JC, Dupont C, Alesi V, Gouas L, Horelli-Kuitunen N, Choy KW, Garcia-Herrero S, de la Vega AG, Piotrowski K, Genesio R, Queipo G, Malvestiti B, Hervé B, Benzacken B, Novelli A, Vago P, Piippo K, Leung TY, et al. (2015) Prevalence of recurrent pathogenic microdeletions and microduplications in over 9500 pregnancies. *Prenatal Diag* 35:801–809. [CrossRef Medline](#)
- Green T, Gothelf D, Glaser B, Debbane M, Frisch A, Kotler M, Weizman A, Eliez S (2009) Psychiatric disorders and intellectual functioning throughout development in velocardiofacial (22q11.2 deletion) syndrome. *J Am Acad Child Adolesc Psychiatry* 48:1060–1068. [CrossRef Medline](#)
- Gutman BA, Wang YL, Rajagopalan P, Toga AW, Thompson PM (2012) Shape matching with medial curves and 1-D group-wise registration, pp 716–719. 9th IEEE International Symposium on Biomedical Imaging, Barcelona, Spain, May 2–5, 2012.
- Gutman BA, Jahanshad N, Ching CR, Wang YL, Kochunov PV, Nichols TE, Thompson PM (2015) Medial demons registration localizes the degree of genetic influence over subcortical shape variability: an N = 1480 meta-analysis. *Proc EIII Int Symp Biomed Imaging* 2015:1402–1406.
- Hibar DP, et al. (2016) Subcortical volumetric abnormalities in bipolar disorder. *Mol Psychiatry* 21:1710–1716. [CrossRef](#)
- Hiroi N, Takahashi T, Hishimoto A, Izumi T, Boku S, Hiramoto T (2013) Copy number variation at 22q11.2: from rare variants to common mechanisms of developmental neuropsychiatric disorders. *Mol Psychiatry* 18:1153–1165. [CrossRef](#)
- Hoefding LK, Trabjerg BB, Olsen L, Mazin W, Sparsø T, Vangkilde A, Mortensen PB, Pedersen CB, Werge T (2017) Risk of psychiatric disorders among individuals with the 22q11.2 deletion or duplication: a Danish nationwide, register-based study. *JAMA Psychiatry* 74:282–290. [CrossRef Medline](#)
- Horev G, Ellegood J, Lerch JP, Son YE, Muthuswamy L, Vogel H, Krieger AM, Buja A, Henkelman RM, Wigler M, Mills AA (2011) Dosage-dependent phenotypes in models of 16p11.2 lesions found in autism. *Proc Natl Acad Sci U S A* 108:17076–17081. [CrossRef Medline](#)
- Jalbrzikowski M, Jonas R, Senturk D, Patel A, Chow C, Green MF, Bearden CE (2013) Structural abnormalities in cortical volume, thickness, and surface area in 22q11.2 microdeletion syndrome: relationship with psychotic symptoms. *Neuroimage Clin* 3:405–415. [CrossRef Medline](#)
- Jalbrzikowski M, Ahmed KH, Patel A, Jonas R, Kushan L, Chow C, Bearden CE (2017) Categorical versus dimensional approaches to autism-associated intermediate phenotypes in 22q11.2 microdeletion syndrome. *Biol Psychiatry Cogn Neurosci Neuroimaging* 2:53–65. [CrossRef Medline](#)
- Kates WR, Burnette CP, Besette BA, Folley BS, Strunge L, Jabs EW, Pearlson GD (2004) Frontal and caudate alterations in velocardiofacial syndrome (deletion at chromosome 22q11.2). *J Child Neurol* 19:337–342. [CrossRef Medline](#)
- Kennedy DP, Adolphs R (2012) The social brain in psychiatric and neurological disorders. *Trends Cogn Sci* 16:559–572. [CrossRef Medline](#)
- Lam KS, Aman MG (2007) The repetitive behavior scale-revised: independent validation in individuals with autism spectrum disorders. *J Autism Dev Disord* 37:855–866. [CrossRef Medline](#)
- Li Z, Chen J, Xu Y, Yi Q, Ji W, Wang P, Shen J, Song Z, Wang M, Yang P, Wang Q, Feng G, Liu B, Sun W, Xu Q, Li B, He L, He G, Li W, Wen Z, et al. (2016) Genome-wide analysis of the role of copy number variation in schizophrenia risk in Chinese. *Biol Psychiatry* 80:331–337. [CrossRef Medline](#)
- Lieberman MD (2007) Social cognitive neuroscience: a review of core processes. *Annu Rev Psychol* 58:259–289. [CrossRef Medline](#)
- Liu H, Abecasis GR, Heath SC, Knowles A, Demars S, Chen YJ, Roos JL, Rapoport JL, Gogos JA, Karayiorgou M (2002) Genetic variation in the 22q11 locus and susceptibility to schizophrenia. *Proc Natl Acad Sci U S A* 99:16859–16864. [CrossRef Medline](#)
- Lord C, Rutter M, Le Couteur A (1994) Autism diagnostic interview-revised: a revised version of a diagnostic interview for caregivers of individuals with possible pervasive developmental disorders. *J Autism Dev Disord* 24:659–685. [CrossRef Medline](#)
- Lord C, Risi S, Lambrecht L, Cook EH Jr, Leventhal BL, DiLavore PC, Pickles A, Rutter M (2000) The Autism Diagnostic Observation Schedule-Generic: a standard measure of social and communication deficits associated with the spectrum of autism. *J Autism Dev Disord* 30:205–223. [CrossRef Medline](#)
- Maillard AM, Ruef A, Pizzagalli F, Migliavacca E, Hippolyte L, Adaszewski S, Dukart J, Ferrari C, Conus P, Männik K, Zazhytska M, Siffrédi V, Maeder P, Kutalik Z, Kherif F, Hadjikhani N, Beckmann JS, Raymond A, Dragan-ski B, Jacquemont S (2015) The 16p11.2 locus modulates brain structures common to autism, schizophrenia and obesity. *Mol Psychiatry* 20:140–147. [CrossRef Medline](#)
- Malhotra D, Sebat J (2012) CNVs: harbingers of a rare variant revolution in psychiatric genetics. *Cell* 148:1223–1241. [CrossRef Medline](#)
- Mamah D, Alpert KI, Barch DM, Csernansky JG, Wang L (2016) Subcortical neuromorphometry in schizophrenia spectrum and bipolar disorders. *Neuroimage Clin* 11:276–286. [CrossRef Medline](#)
- Männik K, Mägi R, Macé A, Cole B, Guyatt AL, Shihab HA, Maillard AM, Alavere H, Kolk A, Reigo A, Mihailov E, Leitsalu L, Ferreira AM, Nõukas M, Teumer A, Salvi E, Cusi D, McGue M, Iacono WG, Gaunt TR, et al. (2015) Copy number variations and cognitive phenotypes in unselected populations. *JAMA* 313:2044–2054. [CrossRef Medline](#)
- McDonald-McGinn DM, Sullivan KE, Marino B, Philip N, Swillen A, Vorstman JA, Zackai EH, Emanuel BS, Vermeesch JR, Morrow BE, Scambler PJ, Bassett AS (2015) 22q11.2 deletion syndrome. *Nat Rev Dis Primers* 1:15071. [CrossRef Medline](#)
- Meehan DW, Maynard TM, Tucker ES, Fernandez A, Karpinski BA, Rothblat LA, LaMantia AS (2015a) Modeling a model: mouse genetics, 22q11.2 deletion syndrome, and disorders of cortical circuit development. *Prog Neurobiol* 130:1–28. [CrossRef Medline](#)
- Meehan DW, Rutz HL, Fralish MS, Maynard TM, Rothblat LA, LaMantia AS (2015b) Cognitive ability is associated with altered medial frontal cortical circuits in the LgDel mouse model of 22q11.2DS. *Cereb Cortex* 25:1143–1151. [CrossRef Medline](#)
- Mukai J, Dhilla A, Drew LJ, Stark KL, Cao L, MacDermott AB, Karayiorgou M, Gogos JA (2008) Palmitoylation-dependent neurodevelopmental deficits in a mouse model of 22q11 microdeletion. *Nat Neurosci* 11:1302–1310. [CrossRef Medline](#)
- Niklasson L, Rasmussen P, Oskarsdóttir S, Gillberg C (2001) Neuropsychiatric disorders in the 22q11 deletion syndrome. *Genet Med* 3:79–84. [CrossRef Medline](#)
- Niklasson L, Rasmussen P, Oskarsdóttir S, Gillberg C (2009) Autism, ADHD, mental retardation and behavior problems in 100 individuals with 22q11 deletion syndrome. *Res Dev Disabil* 30:763–773. [CrossRef Medline](#)

- Ohta H, Nordahl CW, Iosif AM, Lee A, Rogers S, Amaral DG (2016) Increased surface area, but not cortical thickness, in a subset of young boys with autism spectrum disorder. *Autism Res* 9:232–248. [CrossRef Medline](#)
- Ou Z, Berg JS, Yonath H, Enciso VB, Miller DT, Picker J, Lenzi T, Keegan CE, Sutton VR, Belmont J, Chinault AC, Lupski JR, Cheung SW, Roeder E, Patel A (2008) Microduplications of 22q11.2 are frequently inherited and are associated with variable phenotypes. *Genet Med* 10:267–277. [CrossRef Medline](#)
- Palaniyappan L, Mallikarjun P, Joseph V, White TP, Liddle PF (2011) Regional contraction of brain surface area involves three large-scale networks in schizophrenia. *Schizophr Res* 129:163–168. [CrossRef Medline](#)
- Panizzon MS, Fennema-Notestine C, Eyler LT, Jernigan TL, Prom-Wormley E, Neale M, Jacobson K, Lyons MJ, Grant MD, Franz CE, Xian H, Tsuang M, Fischl B, Seidman L, Dale A, Kremen WS (2009) Distinct genetic influences on cortical surface area and cortical thickness. *Cereb Cortex* 19:2728–2735. [CrossRef Medline](#)
- Paronetti EM, Meechan DW, Karpinski BA, LaMantia AS, Maynard TM (2015) Ranbp1, deleted in DiGeorge/22q11.2 deletion syndrome, is a microcephaly gene that selectively disrupts layer 2/3 cortical projection neuron generation. *Cereb Cortex* 25:3977–3993. [CrossRef Medline](#)
- Qureshi AY, Mueller S, Snyder AZ, Mukherjee P, Berman JJ, Roberts TP, Nagarajan SS, Spiro JE, Chung WK, Sherr EH, Buckner RL (2014) Opposing brain differences in 16p11.2 deletion and duplication carriers. *J Neurosci* 34:11199–11211. [CrossRef Medline](#)
- R Core Team (2016) R: a language and environment for statistical computing. Vienna: R Foundation for Statistical Computing.
- Rakic P (1988) Specification of cerebral cortical areas. *Science* 241:170–176. [CrossRef Medline](#)
- Rakic P (1995) A small step for the cell, a giant leap for mankind: a hypothesis of neocortical expansion during evolution. *Trends Neurosci* 18:383–388. [CrossRef Medline](#)
- Raznahan A, Shaw P, Lalonde F, Stockman M, Wallace GL, Greenstein D, Clasen L, Gogtay N, Giedd JN (2011) How does your cortex grow? *J Neurosci* 31:7174–7177. [CrossRef Medline](#)
- Rees E, Kirov G, Sanders A, Walters JT, Chambert KD, Shi J, Szatkiewicz J, O’Dushlaine C, Richards AL, Green EK, Jones I, Davies G, Legge SE, Moran JL, Pato C, Pato M, Genovese G, Levinson D, Duan J, Moy W, et al. (2014) Evidence that duplications of 22q11.2 protect against schizophrenia. *Mol Psychiatry* 19:37–40. [CrossRef](#)
- Rees E, Kendall K, Pardiñas AF, Legge SE, Pocklington A, Escott-Price V, MacCabe JH, Collier DA, Holmans P, O’Donovan MC, Owen MJ, Walters JT, Kirov G (2016) Analysis of intellectual disability copy number variants for association with schizophrenia. *JAMA Psychiatry* 73:963–969. [CrossRef Medline](#)
- Roshchupkin GV, Gutman BA, Vernooij MW, Jahanshad N, Martin NG, Hofman A, McMahon KL, van der Lee SJ, van Duijn CM, de Zubicaray GI, Uitterlinden AG, Wright MJ, Niessen WJ, Thompson PM, Ikram MA, Adams HH (2016) Heritability of the shape of subcortical brain structures in the general population. *Nat Commun* 7:13738. [CrossRef Medline](#)
- Schmaal L, Veltman DJ, van Erp TG, Sämann PG, Frodl T, Jahanshad N, Loehrer E, Tiemeier H, Hofman A, Niessen WJ, Vernooij MW, Ikram MA, Wittfeld K, Grabe HJ, Block A, Hegenscheid K, Völzke H, Hoehn D, Czisch M, Lagopoulos J, et al. (2016) Subcortical brain alterations in major depressive disorder: findings from the ENIGMA Major Depressive Disorder working group. *Mol Psychiatry* 21:806–812. [CrossRef Medline](#)
- Schmitt JE, Vandekar S, Yi J, Calkins ME, Ruparel K, Roalf DR, Whinna D, Souders MC, Satterwaite TD, Prabhakaran K, McDonald-McGinn DM, Zuckai EH, Gur RC, Emanuel BS, Gur RE (2015) Aberrant cortical morphometry in the 22q11.2 deletion syndrome. *Biol Psychiatry* 78:135–143. [CrossRef Medline](#)
- Schneider M, Debbané M, Bassett AS, Chow EW, Fung WL, van den Bree M, Owen M, Murphy KC, Niarchou M, Kates WR, Antshel KM, Fremont W, McDonald-McGinn DM, Gur RE, Zuckai EH, Vorstman J, Duijff SN, Klaassen PW, Swillen A, Gothelf D, et al. (2014) Psychiatric disorders from childhood to adulthood in 22q11.2 deletion syndrome: results from the International Consortium on Brain and Behavior in 22q11.2 Deletion Syndrome. *Am J Psychiatry* 171:627–639. [CrossRef Medline](#)
- Shaffer D, Fisher P, Lucas CP, Dulcan MK, Schwab-Stone ME (2000) NIMH Diagnostic Interview Schedule for Children Version IV (NIMH DISC-IV): description, differences from previous versions, and reliability of some common diagnoses. *J Am Acad Child Psychiatry* 39:28–38. [CrossRef Medline](#)
- Shaikh TH, O’Connor RJ, Pierpont ME, McGrath J, Hacker AM, Nimmakayalu M, Geiger E, Emanuel BS, Saitta SC (2007) Low copy repeats mediate distal chromosome 22q11.2 deletions: sequence analysis predicts breakpoint mechanisms. *Genome Res* 17:482–491. [CrossRef Medline](#)
- Shaw P, Gogtay N, Rapoport J (2010) Childhood psychiatric disorders as anomalies in neurodevelopmental trajectories. *Hum Brain Mapp* 31:917–925. [CrossRef Medline](#)
- Shepherd AM, Laurens KR, Matheson SL, Carr VJ, Green MJ (2012) Systematic meta-review and quality assessment of the structural brain alterations in schizophrenia. *Neurosci Biobehav Rev* 36:1342–1356. [CrossRef Medline](#)
- Small SA, Schobel SA, Buxton RB, Witter MP, Barnes CA (2011) A pathophysiological framework of hippocampal dysfunction in ageing and disease. *Nat Rev Neurosci* 12:585–601. [CrossRef Medline](#)
- Sørensen KM, Agergaard P, Olesen C, Andersen PS, Larsen LA, Ostergaard JR, Schouten JP, Christiansen M (2010) Detecting 22q11.2 deletions by use of multiplex ligation-dependent probe amplification on DNA from neonatal dried blood spot samples. *J Mol Diagn* 12:147–151. [CrossRef Medline](#)
- Stankiewicz P, Lupski JR (2002) Genome architecture, rearrangements and genomic disorders. *Trends Genet* 18:74–82. [CrossRef Medline](#)
- Stefansson H, Meyer-Lindenberg A, Steinberg S, Magnusdottir B, Morgen K, Arnarsdottir S, Bjornsdottir G, Walters GB, Jonsdottir GA, Doyle OM, Tost H, Grimm O, Kristjansdottir S, Snorrason H, Davidsdottir SR, Gudmundsson LJ, Jonsson GF, Stefansson B, Helgadóttir I, Haraldsson M, et al. (2014) CNVs conferring risk of autism or schizophrenia affect cognition in controls. *Nature* 505:361. [Medline](#)
- Sullivan PF, Daly MJ, O’Donovan M (2012) Genetic architectures of psychiatric disorders: the emerging picture and its implications. *Nat Rev Genet* 13:537–551. [CrossRef Medline](#)
- Tang SX, Moore TM, Calkins ME, Yi JJ, Savitt A, Kohler CG, Souders MC, Zuckai EH, McDonald-McGinn DM, Emanuel BS, Gur RC, Gur RE (2016) The psychosis spectrum in 22q11.2 deletion syndrome is comparable to that of nondeleteds youths. *Biol Psychiatry*. Advance online publication. Retrieved Sep 8, 2016. doi: 10.1016/j.biopsych.2016.08.034. [CrossRef Medline](#)
- Thompson PM, Stein JL, Medland SE, Hibar DP, Vasquez AA, Renteria ME, Toro R, Jahanshad N, Schumann G, Franke B, Wright MJ, Martin NG, Agartz I, Alda M, Alhusaini S, Almasy L, Almeida J, Alpert K, Andreassen NC, Andreassen OA, et al. (2014) The ENIGMA Consortium: large-scale collaborative analyses of neuroimaging and genetic data. *Brain Imaging Behav* 8:153–182. [Medline](#)
- Thompson PM, Andreassen OA, Arias-Vasquez A, Bearden CE, Boedhoe PS, Brouwer RM, Buckner RL, Buitelaar JK, Bulayeva KB, Cannon DM, Cohen RA, Conrod PJ, Dale AM, Deary IJ, Dennis EL, de Reus MA, Desrivieres S, Dima D, Donohoe G, Fisher SE, et al. (2017) ENIGMA and the individual: predicting factors that affect the brain in 35 countries worldwide. *Neuroimage* 145:389–408. [CrossRef Medline](#)
- van Erp TG, Hibar DP, Rasmussen JM, Glahn DC, Pearlson GD, Andreassen OA, Agartz I, Westlye LT, Haukvik UK, Dale AM, Melle I, Hartberg CB, Gruber O, Kraemer B, Zilles D, Donohoe G, Kelly S, McDonald C, Morris DW, Cannon DM, et al. (2016) Subcortical brain volume abnormalities in 2028 individuals with schizophrenia and 2540 healthy controls via the ENIGMA consortium. *Mol Psychiatry* 21:547–553. [CrossRef Medline](#)
- Ventura J, Liberman RP, Green MF, Shaner A, Mintz J (1998) Training and quality assurance with the Structured Clinical Interview for DSM-IV (SCID-I/P). *Psychiatry Res* 79:163–173. [CrossRef Medline](#)
- Vorstman JA, Morcus ME, Duijff SN, Klaassen PW, Heineman-de Boer JA, Beemer FA, Swaab H, Kahn RS, van Engeland H (2006) The 22q11.2 deletion in children: high rate of autistic disorders and early onset of psychotic symptoms. *J Am Acad Child Adolesc Psychiatry* 45:1104–1113. [CrossRef Medline](#)
- Wallace GL, Eisenberg IW, Robustelli B, Dankner N, Kenworthy L, Giedd JN, Martin A (2015) Longitudinal cortical development during adolescence and young adulthood in autism spectrum disorder: increased cortical

- thinning but comparable surface area changes. *J Am Acad Child Psychiatry* 54:464–469. [CrossRef Medline](#)
- Wang L, Mamah D, Harms MP, Karnik M, Price JL, Gado MH, Thompson PA, Barch DM, Miller MI, Csernansky JG (2008) Progressive deformation of deep brain nuclei and hippocampal-amygdala formation in schizophrenia. *Biol Psychiatry* 64:1060–1068. [CrossRef Medline](#)
- Wechsler D (1999) WASI manual. San Antonio: Psychological Corporation.
- Wechsler D, Coalson DL, Raiford SE (2008) WAIS-IV: Wechsler Adult Intelligence Scale. San Antonio: Pearson.
- Wenger TL, Miller JS, DePolo LM, de Marchena AB, Clements CC, Emanuel BS, Zackai EH, McDonald-McGinn DM, Schultz RT (2016) 22q11.2 duplication syndrome: elevated rate of autism spectrum disorder and need for medical screening. *Mol Autism* 7:27. [CrossRef Medline](#)
- Wentzel C, Fernström M, Ohrner Y, Annerén G, Thureson AC (2008) Clinical variability of the 22q11.2 duplication syndrome. *Eur J Med Genet* 51:501–510. [CrossRef Medline](#)
- Wierenga LM, Langen M, Oranje B, Durston S (2014) Unique developmental trajectories of cortical thickness and surface area. *Neuroimage* 87:120–126. [CrossRef Medline](#)
- Winkler AM, Kochunov P, Blangero J, Almasy L, Zilles K, Fox PT, Duggirala R, Glahn DC (2010) Cortical thickness or grey matter volume? The importance of selecting the phenotype for imaging genetics studies. *Neuroimage* 53:1135–1146. [CrossRef Medline](#)
- Yu S, Cox K, Friend K, Smith S, Buchheim R, Bain S, Liebelt J, Thompson E, Bratkovic D (2008) Familial 22q11.2 duplication: a three-generation family with a 3-Mb duplication and a familial 1.5-Mb duplication. *Clin Genet* 73:160–164. [CrossRef Medline](#)

3.3 ENIGMA 22q11DS subcortical volume and shape findings

Building off the work in the UCLA cohort (Chapter 3.2) we performed the following study of subcortical volume and shape analysis across the ENIGMA 22q11DS cohort. The goal of this study was look at FreeSurfer-derived subcortical volumes across the larger ENIGMA 22q11DS working group and to map 22q11DS-related brain variation using our subcortical shape analysis technique to gain a better understanding of the distribution of those effects across the ROIs of interest. Comparisons between deletion subtypes, 22q11DS psychosis, and relationship to idiopathic schizophrenia (as well as comparisons to effects across all published ENIGMA subcortical studies) are presented. This work has extended our understanding of the topographic burden of 22q11DS on subcortical brain structures.

Ching CRK, Gutman BA, Sun D, Villalón-Reina JE, Qu X, Ragothaman A, Isaev D, Zavaliangos-Petropulu A, Lin A, Forsyth JK, Kushan L, Jonas RK, van Amelsvoort T, Bakker G, Kates WR, Campbell LA, McCabe KL, Daly E, Gudbrandsen M, Murphy C, Murphy D, Craig M, Vorstman J, Fiksinski A, Gras L, Ruparel K, Roalf D, Gur R, Schmitt JE, Simon TJ, Goodrich-Hunsaker NJ, Bassett AS, Chow EWC, Butcher N, Vila-Rodriguez F, Doherty J, Cunningham A, van den Bree M, Linden DE, Owen MJ, Moss H, Repetto GM, Crossley NA, Thompson PM, Bearden CE. Mapping Subcortical Brain Alterations in 22q11.2 deletion syndrome: effects of deletion size and convergence with idiopathic psychosis. In preparation to be submitted to The American Journal of Psychiatry

Abstract

Objective: 22q11.2 deletion syndrome (22q11DS) is among the strongest known genetic risk factors for schizophrenia. Prior 22q11DS neuroimaging studies report variable alterations in subcortical brain structures. To elucidate the nature of subcortical changes in 22q11DS,

including modulating effects of clinical and genetic heterogeneity, we studied a large multicenter neuroimaging cohort from the ENIGMA 22q11.2 Deletion Syndrome Working Group.

Method: Subcortical structures were measured using ENIGMA-harmonized protocols for gross volume and subcortical shape morphometry, in 533 patients with 22q11DS and 330 healthy controls (HC) (age: 6-56 years, 49% female).

Results: Subjects with 22q11DS showed lower intracranial volume (ICV), thalamus, putamen, pallidum, hippocampus, and amygdala volumes and greater lateral ventricle, caudate, and accumbens volumes compared to HC (Cohen's $d = -0.90 - 0.93$). Shape analyses revealed complex differences in 22q11DS across all subcortical structures, affecting subregions with projections to frontal, cingulate, and association cortices. The larger A-D deletion was associated with more extensive shape alterations compared to the smaller A-B deletion. 22q11DS subjects with psychosis (22q+Psy) showed lower ICV, hippocampus, amygdala, caudate and thalamic volumes (Cohen's $d = -0.53 - -0.91$) compared to 22q11DS subjects without psychosis. Shape analysis revealed lower thickness and surface area across subregions of these structures. By comparing profiles of subcortical abnormalities across diseases studied by the ENIGMA Consortium, we identified significant overlaps between 22q+Psy with schizophrenia, major depression and obsessive compulsive disorder.

Conclusions: Widespread alterations to subcortical brain structures were observed in 22q11DS, which depended on deletion subtype and psychotic symptoms. Furthermore, findings indicate convergence between 22q11DS-associated psychosis, idiopathic schizophrenia, and other neuropsychiatric illnesses.

Introduction

22q11.2 deletion (22q11DS) — the most common cause of DiGeorge syndrome, velocardiofacial syndrome and conotruncal anomaly face syndrome — is a multisystem disorder resulting from a hemizygous microdeletion on the long arm of chromosome 22, affecting multiple genes involved in development. 22q11DS results in physical and medical comorbidities, including craniofacial abnormalities, cardiac malformations, immune and endocrine alterations, as well as neurocognitive deficits (1). 22q11DS has a prevalence of ~1 in 2,000-4,000 live births. Roughly 1 in 4 patients will develop a schizophrenia spectrum disorder in adolescence or early adulthood, making the deletion one of the strongest known genetic risk factors for schizophrenia (2; 3). Over 60% of individuals with 22q11DS meet diagnostic criteria for a developmental neuropsychiatric disorder, including attention deficit hyperactivity disorder (ADHD), anxiety or mood disorders, or autism spectrum disorders (2; 4; 5). 22q11DS offers a genetically homogeneous framework to study how known microdeletions disrupt biological and neural pathways that contribute to developmental and psychiatric disorders.

Individuals with 22q11DS who ultimately develop a schizophrenia spectrum disorder largely overlap in symptoms with patients who have idiopathic schizophrenia (6). In the largest coordinated analysis of subcortical brain volumes in schizophrenia to date, hippocampal volume showed the greatest reduction in patients relative to matched controls, but there were also deficits in intracranial volume (ICV), amygdala, thalamus and accumbens, and larger ventricle and pallidum volumes (7). However, the extent to which variations in underlying subcortical structure overlap between 22q11DS and idiopathic schizophrenia is not well understood, in part because of the lack of large, well-characterized cohorts with each condition.

In addition, the size of the microdeletion may affect subcortical brain structural alterations. Microdeletion breakpoints tend to occur within four regions of low copy repeats lying within the 22q11.2 region. The most common deletion subtype — found in ~85% of 22q11DS cases — involves the loss of ~3 megabases (Mb) of DNA, and is known as the A-D deletion. A smaller 1.5Mb deletion, termed the A-B deletion, is the next most common subtype, found in ~10% of cases (3).

Mouse models of the 22q11.2 deletion show disrupted neurogenesis (8), altered brain development along the anterior-posterior axis (in a rostral to caudal gradient) and anomalies of midline brain structures (9; 10; 11). Consistent with this, subcortical volume reductions are reported in human 22q11DS (12; 13; 14) with greater volumetric reductions in more posterior brain regions (15) and thinning in midline structures (16). Even so, most published studies examine small samples, typically ascertained at a single site, limiting the power to detect subtle brain abnormalities and determine how consistently they are found.

Most neuroimaging studies examine regional brain volumes, but the 22q11.2 deletion may differentially impact subregions of subcortical structures, in a profile that may be obscured when considering only the overall volume of the structure (14). High-resolution shape analysis of subcortical structures has been used to map fine-grained brain alterations in Alzheimer's disease (17), psychopathy (18), and psychiatric disorders including ADHD and schizophrenia (19; 20; 21; 22), offering insights into specific subregions and circuitry that may be affected in each particular disease or disorder.

To address limitations of smaller, single site studies of 22q11DS, we performed a coordinated analysis of the largest MRI dataset to date, ascertained by the ENIGMA 22q11.2 Deletion Syndrome Working Group. To map abnormalities at a finer scale than is possible with regional volumetry, we used a fine-scale surface mapping approach (the ENIGMA Shape Analysis Pipeline) which is sensitive to subtle variations in subcortical morphometry (23; 24; 25).

We assessed overall subcortical brain volumes and pointwise shape differences across the entire surface of each structure, to answer 3 questions:

1. What is the spatial distribution of subcortical differences between 22q11DS and HC?
2. Do differences in subcortical structure depend on the genetic deletion size?
3. Do subcortical differences exist between 22q11DS subjects with a history of psychosis (22q+Psy) versus those without (22q11-Psy)? And do those 22q+Psy-related subcortical patterns overlap with those found in other harmonized large-scale studies of idiopathic schizophrenia and related neuropsychiatric disorders?

Methods

Data Sample

After removing related individuals and those with poor quality MRI scans, a total of 863 subjects (22q11DS = 533, HC = 330) from 11 study sites were included. Participant demographics are listed in **Table 3.3**. All individual participating research studies had obtained approval from their

local ethics committees and/or institutional review boards and written informed consent (and/or assent for minors) was obtained from all participants.

	Healthy Control (HC)	22q11DS
N	330	533
Age mean (sd)	18.14 (9.24)	17.85 (8.60)
IQ mean (sd)	110.64 (15.35)	74.95 (12.53)
Sex = Female (%)	148 (44.8)	275 (51.6)
Psychotic Disorder (%)	0	73 (13.8)
Deletion Type (%)		
A-B	0	28 (8.0)
A-C	0	6 (1.7)
A-D	0	311 (88.6)
B-D	0	3 (0.9)
C-E	0	1 (0.3)
D-F	0	1 (0.3)
D-G	0	1 (0.3)
Current Medication (%)		
Typical Antipsychotic	0 (0.0)	15 (3.0)
Atypical Antipsychotic	0 (0.0)	72 (14.5)
Lithium	0 (0.0)	4 (0.8)
Anticonvulsant	1 (0.4)	31 (6.3)
Antidepressant	5 (1.8)	95 (19.2)
Psychostimulant	5 (1.8)	65 (13.1)

Table 3.3. Full Cohort Demographics

Subcortical Segmentation

All T1-weighted scans were segmented using the FreeSurfer software, version 5.3.0 (26) to derive subcortical volumes for 8 bilateral regions of interest (ROIs): lateral ventricle, nucleus accumbens, amygdala, caudate, hippocampus, putamen, pallidum, and thalamus (16 total structures per scan) along with intracranial volume (ICV).

Subcortical Shape Analysis

As subtle and complex variations in local volume may be undetectable by gross volume measures, we applied a novel surface-based high-resolution parametric mapping technique, the ENIGMA Subcortical Shape Analysis Pipeline (23; 24; 25), to investigate high-resolution shape variation within 14 ROIs: the hippocampus, amygdala, caudate, putamen, pallidum, thalamus and nucleus accumbens, in each brain hemisphere. We recently applied this technique in a previous single-site study of reciprocal 22q11.2 CNVs (22).

Briefly, using the subcortical FreeSurfer segmentations as inputs, two measures of shape morphometry were derived for each subject. The first, ‘radial distance’ (which we will subsequently refer to as ‘thickness’) is the distance from each surface vertex to a medial curve, and represents a measure of local thickness. (Note that each structure is computationally represented as a mesh of triangular tiles, and the points on the surface are known as vertices that form the overall 3D mesh). The second measure - the logarithm of the Jacobian determinant (‘Jacobian’ or surface area dilation/contraction from now on) - is the surface dilation ratio between the template and the individual subject’s structure. The Jacobian can be interpreted as areal dilation or contraction of the ROIs’ surface; higher Jacobian measures suggest larger local surface area.

Both thickness and surface dilation measures were calculated in native space for up to 2,502 homologous points across each of the 14 subcortical shape models to index regional shape differences in detail across subjects.

Quality Control

Visual quality inspection was performed by a rater trained in neuroanatomy for each subcortical volume and shape model, with standardized rating criteria based on fidelity to known anatomical boundaries ([overlaid](#) on T1-weighted MRI). ENIGMA standardized processing and quality control protocols for FreeSurfer and ENIGMA Shape Analysis pipelines are freely available online (<http://enigma.ini.usc.edu/protocols/imaging-protocols/>). Only those ROIs passing visual quality inspection were used in the analysis.

Statistical Analysis

Analyses were conducted using multiple linear regression. The dependent variable was ROI volume for gross volumetric analysis and either thickness or regional surface area for vertex-wise shape analysis. Primary analyses were run on left and right structures separately. The independent variable was the grouping variable of interest (e.g., diagnosis, deletion subtype, or history of psychosis) while adjusting for appropriate covariates.

Basic covariate adjustments included those for age, age², sex and ICV. Age effects were modeled with both a linear and quadratic term based on model fit. Sex was included as a covariate as it is associated with ROI volume, as was ICV. No age-by-sex interactions on ROI volume were detected. Handedness was largely not associated with ROI volumes and therefore not used as covariate in follow-up models, in line with our prior large-scale studies of handedness and brain laterality (27). IQ was available in a subset of subjects (22q11DS = 506, HC = 233); as IQ and

related measures have repeatedly been found to be associated with brain volume, IQ was included in follow-up analyses.

Medications use at the time of scan acquisition were classified into 5 groups: typical (1st generation) antipsychotics, atypical (2nd generation) antipsychotics, lithium, anticonvulsants, antidepressants, and psychostimulants. Medications found to have significant associations with subcortical volume were added as covariates in secondary statistical analyses, and included typical and atypical antipsychotics, anticonvulsants and antidepressants.

Cohen's d effect size estimates were computed from the t -statistic of the group variable from the regression models (28; 29). To correct for multiple comparisons, a standard false discovery rate (FDR) correction was applied at the conventionally accepted level of 5% ($q=0.05$) (30). FDR-corrected p -values below 0.05 were considered significant.

For vertex-wise Jacobian and thickness analyses, the multiple linear regression model was fit at each point across the surface. As these values were calculated in native space (i.e., without scaling the image), ICV was used to adjust for effects of head size. While subcortical volumes often scale with overall brain size (ICV) (i.e., a larger overall brain correlates with larger overall subcortical structures), we fit alternative models for the shape analyses in which the volume of each structure was used as a covariate instead of ICV. For example, models fit at each vertex of the left hippocampus are adjusted for total left hippocampal volume (instead of ICV); this step is performed to identify any regionally selective effects on structures beyond those accounted for

by overall volume. Linear regressions were carried out using the *lm* function in the R statistical environment, version 3.1.3 (31; 32).

22q11.2 Deletion Carriers vs. Healthy Controls

Group differences between the 437 participants with 22q11DS and 330 HC were assessed using multiple linear regression. 22q11DS subjects from the Utrecht and Toronto2 sites were withheld from this analysis as they lacked matched HC data. The independent variable was group, and adjustments were made for age, age², sex, intracranial volume (ICV), and scan site. Follow up analyses assessed diagnosis-by-age and diagnosis-by-sex interactions, and medication effects. Additional models treating scanner as a random variable in a linear mixed model approach were also assessed using the *nlme* library in R.

Effects of Deletion Size

Microdeletion size was measured from peripheral blood samples using a multiplex ligation-dependent probe amplification (MLPA) (33) and a comparison of the two most common deletion subtypes (A-D vs. A-B) was carried out on matched samples. Demographic matching provided a cohort of 106 22q11DS subjects with A-D deletions, 23 22q11DS subjects with A-B deletions, and 86 HC. Within site, 22q11DS participants with the A-B deletion were matched with 4-5 subjects with A-D deletions and 4-5 HC of comparable sex and age, as in our study of cortical structure in 22q11DS (34). Regional brain volumes were compared across all three groups using an analysis of covariance (ANCOVA), controlling for age, age², sex, ICV, and scan site. Multiple linear regressions were fit for all pairwise comparisons of A-D, A-B and HC, adjusting

for age, age², sex, ICV, and scan site. Follow-up analyses adjusting for medication effects were also conducted.

Effects of Psychosis

A diagnosis of psychosis was assessed by structured clinical interview at each study site, with diagnoses validated across sites using a consensus procedure (35). Sixty-four subjects with 22q11DS with a history of psychotic disorder diagnosis (22q+Psy) were compared to 64 subjects without a history of psychotic symptoms (22q-Psy) by matching +/-Psy participants within each site, with the same sex, and the nearest possible age. This sample also largely overlaps with the matched sample from our study of cortical brain structure in 22q11DS (34). Multiple linear regression models were fit comparing 22q+Psy and 22q-Psy groups, adjusting for age, age², sex, ICV, and scan site. Follow-up analyses adjusting for medication effects were also conducted.

Cross-Disorder Comparison of 22q-Psychosis, Idiopathic Schizophrenia and Other Neuropsychiatric Disorders

As most previously published ENIGMA studies of subcortical volume analyzed averaged left and right volumes (instead of the bilateral analyses here), an additional analysis was conducted in which 22q11DS versus HC models were fit on averaged left and right ROI volumes, which again served as the dependent variable, adjusting for age, age², sex, ICV and scan site. 22q+Psy versus 22q-Psy averaged ROI models were fit adjusting for age, age², sex and scan site given that ICV was significantly lower in 22q+Psy individuals (see results).

To compare the pattern of 22q+Psy to that of idiopathic schizophrenia, Spearman rank correlations were used to correlate the set of Cohen's *d* effect size estimates from the 22q+Psy versus 22q-Psy analysis with comparable case-control analyses from the ENIGMA Schizophrenia Working Group (SCZ). The ENIGMA SCZ study is the largest study to date of subcortical volume in schizophrenia, based on 4,474 participants with schizophrenia and 5,098 healthy controls (36). Spearman rank correlations were conducted using the R function, *rcorr*. To assess the specificity of this correlation, 22q+/-Psy effect sizes were compared to the case-control subcortical effect size data from the ENIGMA major depressive disorder (37), bipolar disorder (38), obsessive compulsive disorder (39), autism spectrum disorder (40), and attention deficit hyperactivity disorder (41) working group studies. Each of these studies constitutes the largest investigation of subcortical structure to date, in their respective disorders. All of these studies used the same harmonized ENIGMA subcortical processing and quality control protocols enabling a cross-disorder comparison of subcortical structure, albeit with some inevitable limitations (see Discussion).

Results

22q11.2 Deletion vs. Healthy Controls

Gross volumetric analysis revealed significant group differences across most of the ROIs (15/17), with moderate to large effects (**Figure 3.3a**). The pattern of effects includes significantly lower volumes, on average, in 22q11.2DS, for the thalamus, putamen, pallidum, hippocampal, amygdala and ICV, and greater ventricular, caudate and accumbens volumes.

These results (in terms of both pattern and effect sizes) remained essentially the same when adjusting for medication, IQ, and when treating scanning site as a random effect.

In addition, a diagnosis-by-age interaction was detected for the bilateral caudate, pallidum and left thalamus. Whereas the left thalamus and bilateral caudate volumes tended to be lower in 22q11DS with increasing age, the pattern was flipped for the pallidum (i.e., higher pallidum volume with increased age in 22q11DS). No sex-by-diagnosis interactions were detected for any ROI. IQ data was available for a subset of patients; as expected, IQ was significantly lower in 22q11DS subjects compared to HC ($p = 1.7 \times 10^{-136}$). IQ was highly associated with regional brain volumes.

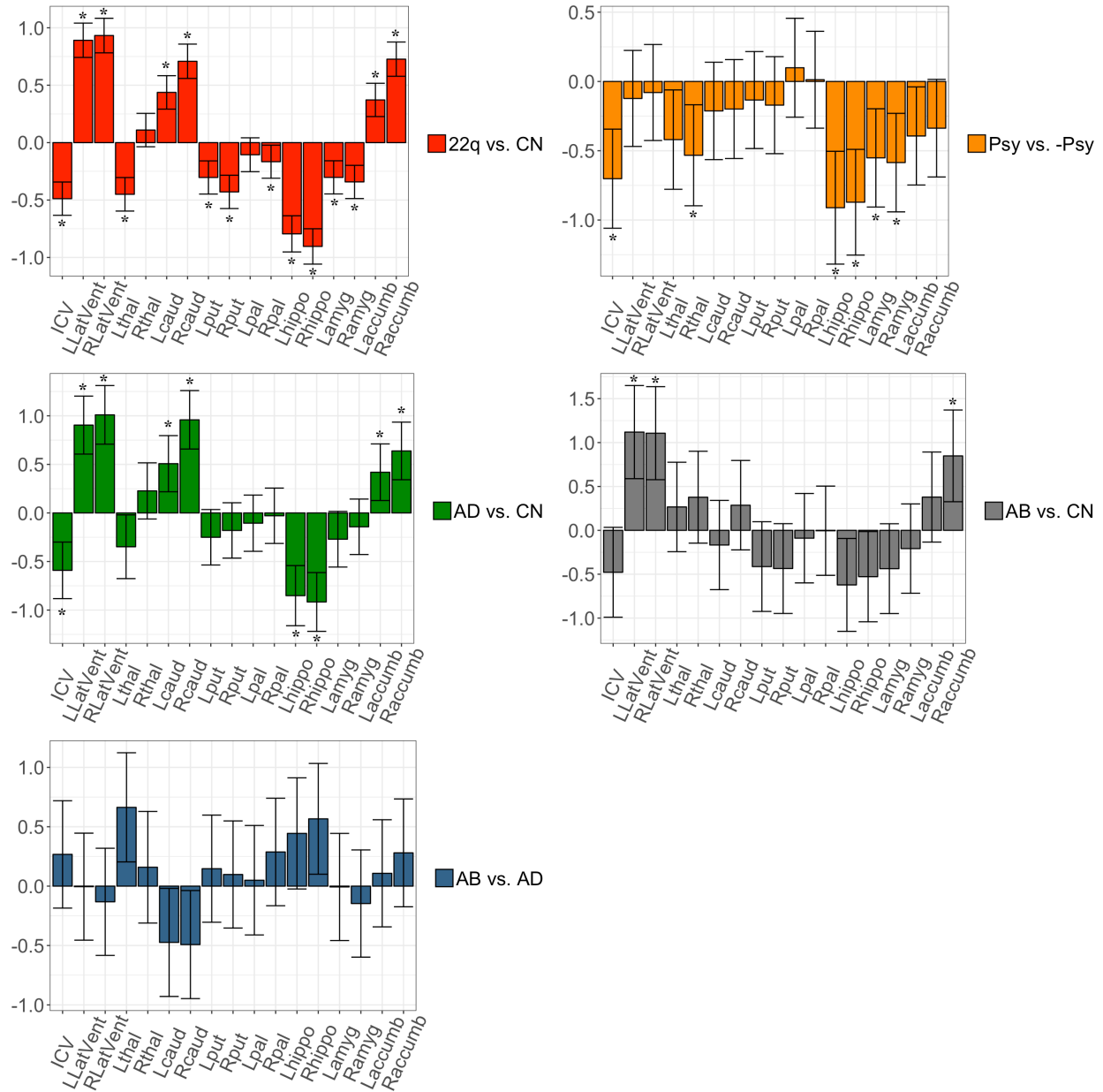


Figure 3.3a. Cohen's *d* effect size (with 95% confidence intervals) plotted for major pairwise volumetric comparisons. An asterisk (*) indicates significant group difference after correction for multiple comparisons for cases versus controls (group listed first = case, group listed second = control). FDR corrected P-values < 0.05 were considered significant. 22q11DS vs. HC, A-D vs. HC, A-B vs. HC and A-B vs. A-D models were adjusted for age, age², sex, ICV, and scan site. 22q+Psy vs. -Psy models were adjusted for age, age², sex, and scan site. Abbreviations:

L/R, left/right; *LatVent*, lateral ventricle; *thal*, thalamus; *caud*, caudate; *put*, putamen; *pal*, pallidum; *hippo*, hippocampus; *amyg*, amygdala; *accumb*, accumbens; *ICV*, intracranial volume.

Subcortical shape analysis revealed complex group differences between 22q11DS and HC: most structures exhibited some subregions with higher – and others with lower – thickness and Jacobian values in 22q11DS subjects relative to HC (**Figure 3.3b**). In particular, local thickness measures revealed greater thickness in the head of the caudate, thalamus, and medial hippocampal regions, but thinner regions in the caudate body and lateral hippocampal subregions. The Jacobian metric, a measure of local surface area dilation/contraction, revealed surface contraction across large portions of the putamen, amygdala, and hippocampus, and dilation across anterior/lateral regions of the caudate and most of the nucleus accumbens. These effects were robust to adjustment for medication and ROI volume.

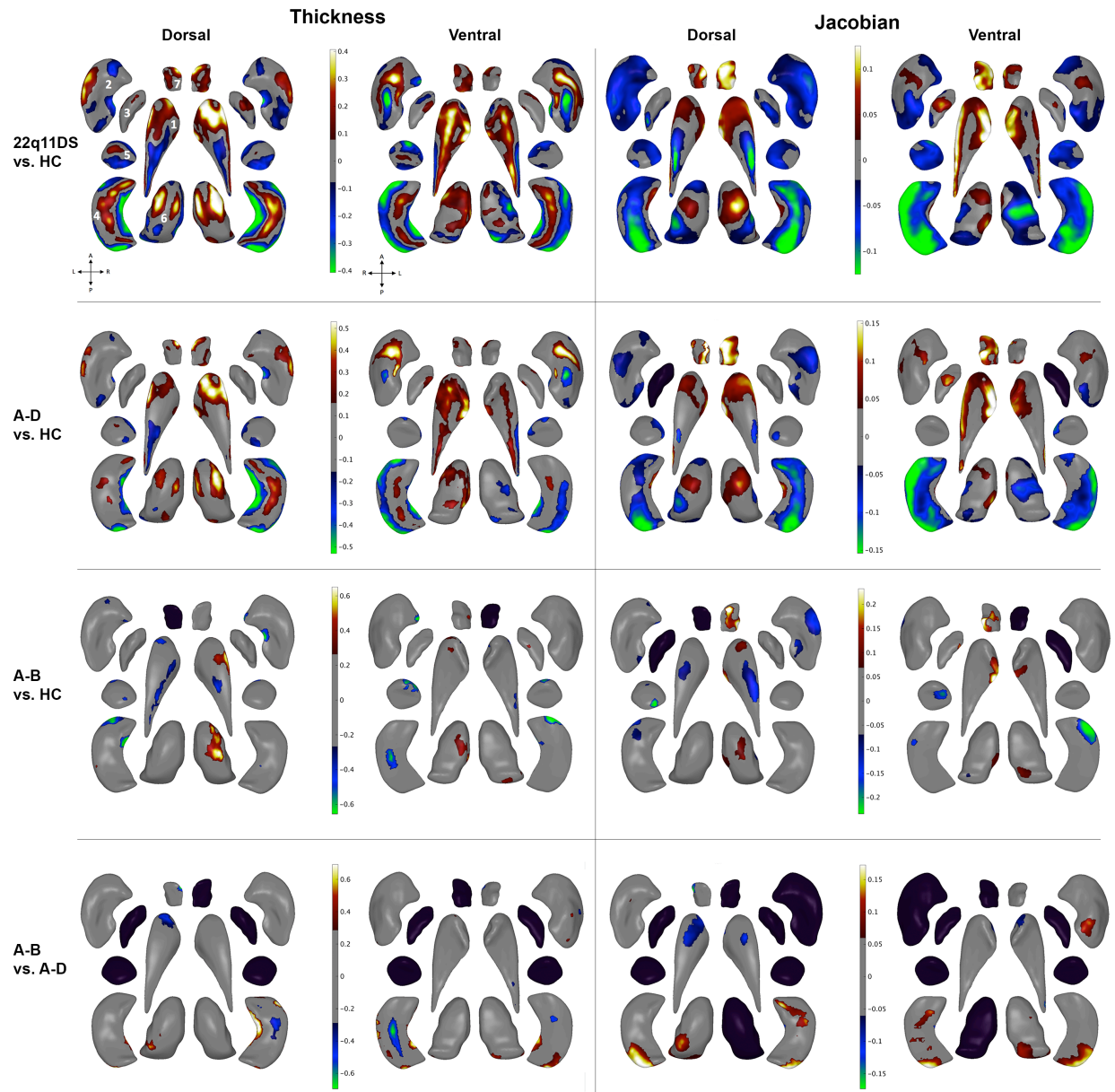


Figure 3.3b. Shape analysis with regression coefficient values plotted in regions passing correction for multiple comparisons ($FDR < 0.05$). Blue/green colors indicate negative coefficient values, or regions of lower thickness or Jacobian measures in cases versus controls (group listed first = case, group listed second = control). Red/yellow colors indicate positive coefficient values, or regions of greater thickness or Jacobian values in cases versus controls. The left two columns include thickness results; the right two columns include Jacobian map results.

Thickness represents local radial distance and Jacobian represents local surface area dilation/contraction. Dorsal and ventral views of the structures are provided: *A*, anterior; *P*, posterior; *L*, left; *R*, right. 1. Caudate; 2. Putamen; 3. Globus Pallidus; 4. Hippocampus; 5. Amygdala; 6. Thalamus; 7. Nucleus Accumbens. Gray regions indicate areas of no significant difference after correction for multiple comparisons. Black structures are those for which no vertex-wise test was significant after correction for multiple comparisons.

Effects of Deletion Size

ANCOVA results indicated a significant difference between ROIs across A-D, A-B, and HC matched samples.

Large A-D Deletion vs. HC Comparison

Pairwise comparisons of A-D versus HC subjects revealed a similar pattern of ROI differences to that of the full 22q11DS versus HC comparison (**Figure 3.3a**), likely because ~89% of the 22q11DS sample carried the more common 3Mb A-D deletion subtype. Compared to HC, A-D subjects had larger ventricle, caudate, and accumbens volumes, and smaller hippocampal and ICV volumes. These results were largely replicated when adjusting for current medication.

Subcortical shape analysis revealed a pattern of both higher and lower local thickness and Jacobian measures, similar to 22q11DS versus HC comparison, but with lesser magnitude (**Figure 3.3b**). These effects were robust when adjusted for medication and ROI volume.

A-B vs. HC Comparison

Subjects with an A-B deletion showed significantly higher ventricle and right accumbens volumes compared to matched HC (**Figure 3.3a**). Effects across all ROIs were largely in the same direction as those from the A-D versus HC and 22q11DS versus HC comparisons, indicating similar, though much attenuated group differences, likely driven somewhat by the much smaller A-B sample size (N=18). When adjusting for medication, no significant group differences passed correction for multiple comparisons.

Subcortical shape analysis results showed a more extensive, though subtle, pattern of differences between A-B and HC (**Figure 3.3b**). The shape analysis revealed that higher accumbens volumes were likely driven by higher Jacobian (surface dilation) in A-B subjects. Results were diminished when correcting for ROI volume and medication, though, given the small sample size, this was somewhat expected.

A-B vs. A-D Comparison

There were no global volume differences between matched A-B and A-D subjects that passed correction for multiple comparisons (Figure 1). However, shape analysis showed that A-B deletion subjects had higher hippocampal, thalamic, and putamen Jacobian measures (higher surface area), and lower caudate and accumbens thickness/Jacobian measures compared to A-D (Figure 3.3b). The hippocampus showed somewhat complex effects of thickness, with medial/lateral aspects being thicker and dorsal/ventral regions being thinner in A-B versus A-D. These results remained stable when adjusting for ROI and medication.

22q11.2 Deletion Psychosis Analysis

The 22q+Psy and -Psy groups were largely matched in demographics. However, as expected, 22q+Psy subjects had a higher rate of typical/atypical antipsychotic and anticonvulsant treatment, and lower IQ compared to the -Psy group. A significant psychosis-by-age interaction was observed for the left and right caudate, in which 22q+Psy had higher caudate volumes with increased age compared to 22q-Psy.

22q+Psy showed significantly smaller hippocampal, amygdala, right thalamus and ICV volumes compared to the matched 22q-Psy cohort (**Figure 3.3a**). These effects were largely replicated when adjusting for medication and IQ. However, when additionally adjusting for ICV, no group differences survived correction for multiple comparisons, likely due to significantly lower ICV volumes in the 22q+Psy group.

When adjusting for age, age², sex, and scan site, subcortical shape analysis revealed lower thalamus, hippocampal, amygdala and nucleus accumbens thickness and Jacobian surface area measures in 22q+Psy subjects compared to 22q-Psy. There was one region along the left dorsal putamen where the reverse pattern was observed (higher thickness/surface area in 22q+Psy subjects) (**Figure 3.3c**). When adjusting for medication, effects were diminished but exhibited a similar pattern of lower thickness and surface area in 22q+Psy. When also adjusting for ICV, only two regions continued to pass correction for multiple comparisons: higher surface area of the left putamen and lower surface area of the right hippocampus. When adjusting for both ICV

and medication, no significant shape measure differences survived correction for multiple comparisons.

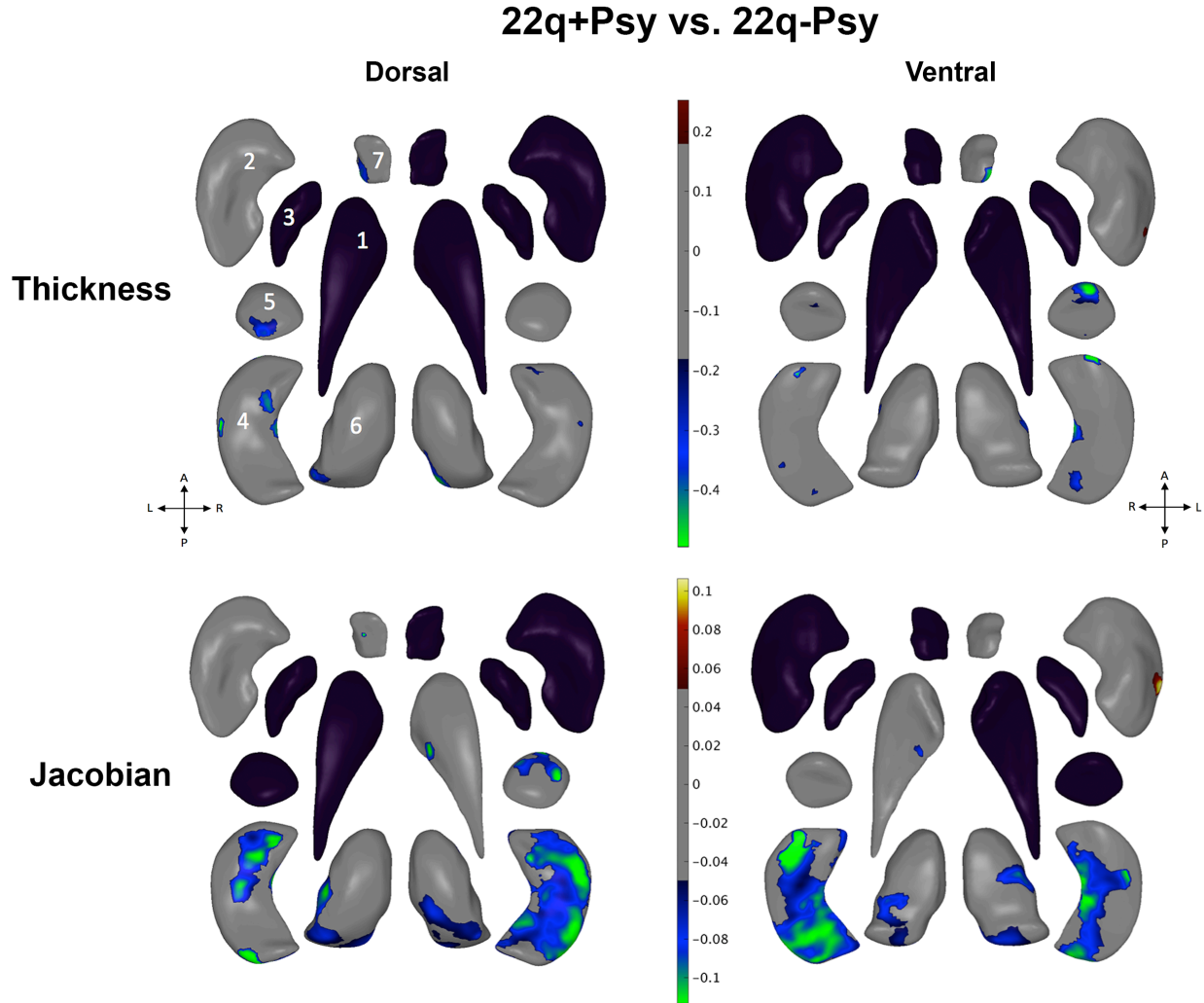


Figure 3.3c. Shape analysis with regression coefficients plotted in regions passing correction for multiple comparisons ($FDR < 0.05$). Blue/green colors indicate negative coefficient values, or regions of lower thickness or Jacobian measures in cases versus controls. Red/yellow colors indicate positive coefficient values, or regions of greater thickness (i.e., local radial distance) or Jacobian values (i.e., local surface area dilation/contraction) in cases versus controls. The top row includes thickness results; the bottom row includes Jacobian results. Dorsal and ventral

views of the structures are provided: *A*, anterior; *P*, posterior; *L*, left; *R*, right. 1. Caudate; 2. Putamen; 3. Globus Pallidus; 4. Hippocampus; 5. Amygdala; 6. Thalamus; 7. Nucleus Accumbens. Gray regions indicate areas of no significant difference after correction for multiple comparisons. Black structures are those for which no vertex-wise test was significant after correction for multiple comparisons.

22q11DS Psychosis Cross-Disorder Comparisons

22q+Psy versus 22q-Psy subcortical ROI volume Cohen's *d* effect sizes were significantly correlated with those from the ENIGMA schizophrenia, major depression and obsessive compulsive disorder studies. 22q+Psy effect sizes were not significantly correlated with those from the ENIGMA bipolar, autism spectrum and attention deficit hyperactivity disorder case-control studies (**Figure 3.3d**).

22q11DS versus HC effect sizes were not significantly correlated with any other ENIGMA study.

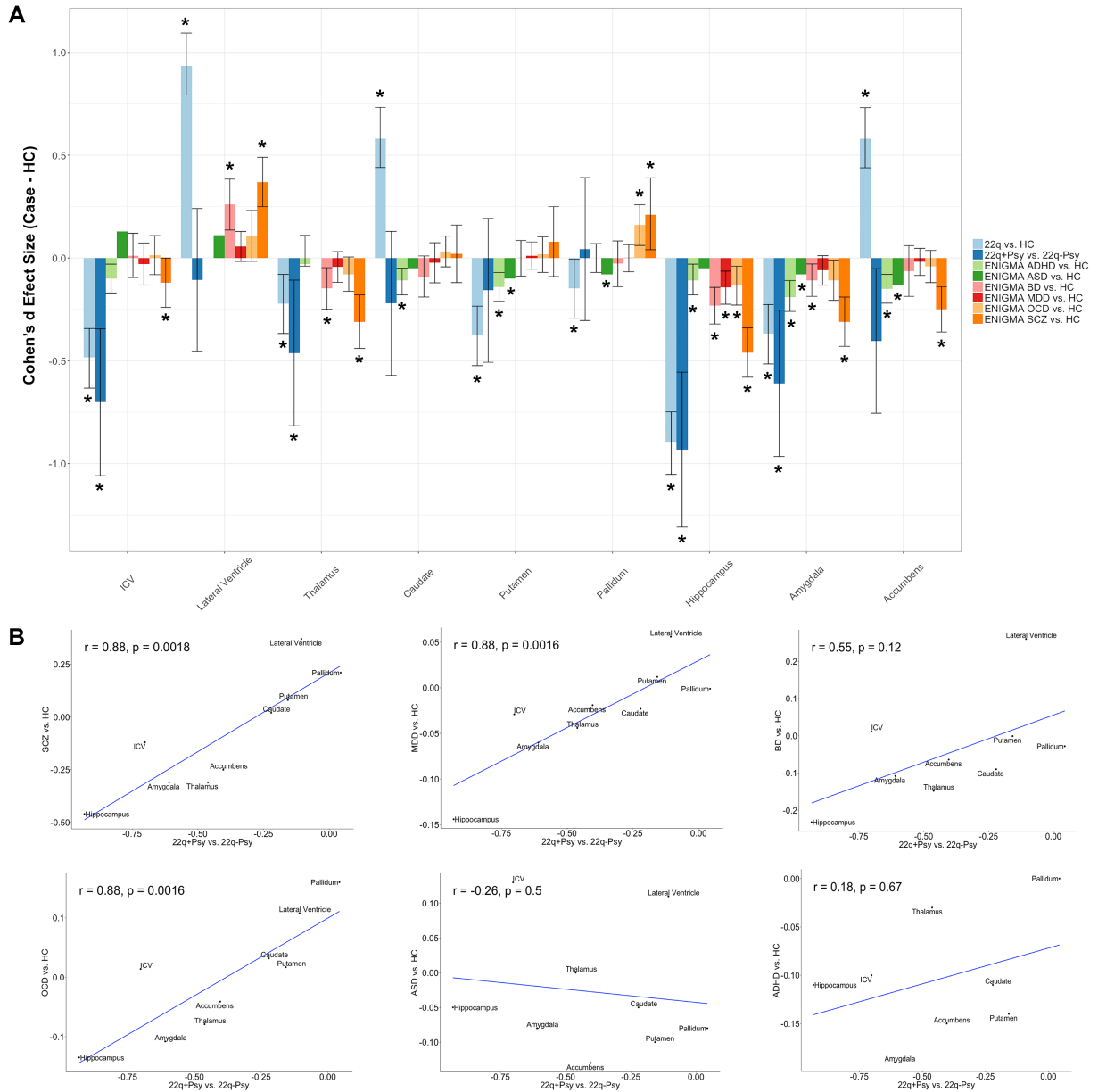


Figure 3.3d. Cross-Disorder comparisons from the ENIGMA clinical working group subcortical studies. **A.** Case-control Cohen's *d* effect size estimates are shown, from the ENIGMA schizophrenia (7), major depressive disorder (37), bipolar disorder (38), obsessive compulsive disorder (39), autism spectrum disorders (40), and attention deficit hyperactivity disorder (41) working group JCV studies, which all used comparable analysis methods to the current study. An asterisk (*) indicates a significant group difference in the respective study and include 95%

confidence intervals from original study publication. Note that the ENIGMA autism group did not report 95% confidence intervals in their published report, and the ENIGMA attention deficit hyperactivity disorder group did not assess lateral ventricle volume in their subcortical studies. **B.** Spearman rank correlations between 22q+Psy vs. 22q-Psy effect size estimates and those from other ENIGMA working groups. Significant correlations were found between 22q+Psy and the ENIGMA schizophrenia, major depressive disorder and obsessive compulsive disorder working group studies.

Discussion

This study represents the largest neuroimaging investigation to date of subcortical brain structure in 22q11DS and provides 4 key findings:

1. We detected robust group differences between groups of individuals with 22q11DS and HC using conventional gross volumetric measures.
2. Shape analysis revealed complex local differences across most subcortical ROIs and subtle differences as a function of deletion size. Significant differences between deletion subtypes were detected by shape analysis.
3. 22q11DS subjects with a history of psychosis had lower ICV, thalamic, hippocampal, and amygdala volumes compared to 22q11DS subjects without history of psychosis; these effects were driven largely by contracted surface area across subregions of these structures.

22q11DS psychosis effects significantly overlapped with those from the largest study of subcortical structure in schizophrenia, major depression and OCD but differed from bipolar disorder, autism spectrum disorder, and ADHD. Subcortical effect sizes for 22q11DS were generally greater than those found in most other ENIGMA studies.

Based on volumetric analysis, 22q11DS subjects had significant differences in nearly all ROIs studied, with moderate to large effect sizes. Our large multisite sample revealed overlapping but more extensive group differences than were previously detected in data from single site studies of 22q11DS (22). Shape analysis revealed 22q11DS effects to be complex in nature, with most structures exhibiting patterns of both higher (in some regions) and lower (in other regions) local thickness and surface area compared to HC. Interestingly, our vertex-wise cortical analysis of 22q11DS also found somewhat complex thickness and surface area variations compared to HC (34). A general pattern of regionally lower cortical surface area with gyral thickening was flipped in some regions (thinner superior temporal, cingulate and parahippocampal regions), similar to complex opposing effects seen in the larger subcortical structures (caudate, putamen, hippocampus and thalamus).

With respect to the complex group differences in the hippocampus, the 22q11DS group showed lateral/medial thinning and dorsal/ventral thickening compared to HC. Based on prior surface-based mapping of hippocampal subfields (21), the thinning along the lateral/medial axis may correspond to CA1 and subiculum subfields, whereas the dorsal/ventral thickening may

correspond to CA2-4 subfields as well as parts of the subiculum. The Jacobian maps indicate a more extensive pattern of contracted surface area across large portions of the hippocampus.

Subjects with 22q11DS had thicker and greater surface area for thalamic subregions, roughly corresponding to anterior, dorsomedial and ventral lateral nuclei. The anterior thalamic nucleus receives input from the mammillothalamic tract and hippocampus, and projects to the cingulate gyrus. The dorsomedial nucleus receives input from and projects back to the prefrontal cortex. The ventral lateral nucleus receives input from the basal ganglia and cerebellum and projects back to motor areas of the cortex. Subjects with 22q11DS also appear to have lower thickness and surface area in the pulvinar, a region that receives input from – and projects to – the parietal, occipital and temporal lobes. Both the pulvinar and the dorsomedial nucleus make up the principal association nuclei of the thalamus, with projections to cortical association areas that mediate many higher order mental functions shown to be altered in 22q11DS individuals.

With respect to the caudate, 22q11DS subjects had, on average, greater thickness and surface area in more anterior (head) and lateral portions of the caudate, and lower thickness and surface area in more posterior (tail) regions compared to HC. The caudate receives most of its inputs from cortical association areas, especially from the prefrontal cortex (42). Differential alterations to these caudate subregions may be related to frontal cortex alterations associated with the executive functioning deficits previously reported in functional studies of 22q11DS (43).

As in our study of cortical structure from the ENIGMA 22q11DS cohort (34), subcortical differences between A-B versus HC appeared similar, though diminished, compared to patterns in the A-D versus HC and 22q11DS versus HC comparisons. While there were no significant differences between A-B versus A-D subtypes with respect to gross volume, shape analysis revealed regions of higher surface area in the hippocampus, putamen and thalamus as well as lower caudate surface area and thickness in A-B compared to A-D. This pattern was seen to some extent in our cortical study, where A-B subjects had higher cortical surface area compared to A-D, which may point to overlapping neurodevelopmental mechanisms affecting both cortical and subcortical structures.

22q+Psy was associated with lower ICV, hippocampal, amygdala and right thalamic volumes, all results that overlap with the ENIGMA schizophrenia study. Shape analysis revealed that lower gross volumes were driven primarily by contracted surface area across these structures. Mouse models of 22q11DS have revealed decreased dendritic spine density and reduced glutamatergic synapses in hippocampal neurons (44). Copy number variations in genes located in the 22q11.2 region such as *COMT* or *Tbx1* have been shown to disrupt adult neural stem and progenitor cells in the hippocampus and prevent normal working memory capacity in mouse models (45). Mice haploinsufficient for the gene *Zdhhc8* – another gene within the homologous 22q11.2 region – suffer from deficits in spatial working memory and functional connectivity (46), all deficits that are well documented in schizophrenia and ASD. Together, these structural and functional deficits could explain the generally smaller hippocampal volumes we observed in 22q11DS, and particularly in those with psychosis.

Our cortical study found that 22q+Psy was marked by a pattern of mostly thinner frontal, temporal and lateral occipital regions compared to 22q-Psy. Functionally, altered hippocampal-prefrontal connectivity has been found to be associated with working memory impairments in 22q11DS mice (47), and may underlie disrupted frontal-temporal connectivity in patients with idiopathic schizophrenia.

ICV was significantly lower in 22q11DS and 22q+Psy, findings that overlap with previous studies of 22q11DS (10), and schizophrenia (48; 7). *RANBPI*, a gene found in the 22q11.2 region, plays an important role in cortical progenitor cells and has been shown to regulate brain development. Loss of *RANBPI* may affect the overall quantity of radial glial progenitors, resulting in smaller brain volumes. A haplotype block including both *DGCR8* and *RANBPI* have been implicated in schizophrenia susceptibility (49).

The significant correlation between 22q+Psy effect sizes with those from the ENIGMA schizophrenia working group suggest a structural concordance with idiopathic schizophrenia that we also found at the cortical level in the same cohort (34). Interestingly, 22q+Psy subcortical effect sizes were also correlated with those from the ENIGMA major depressive disorder and OCD studies, but not those from the bipolar, ASD and ADHD studies. While these findings suggest this set of psychiatric disorders may exhibit similar profiles of subcortical alterations, the ENIGMA consortium creates the opportunity for direct comparison of these harmonized brain measures across disorders. Common abnormalities in subcortical structure across psychiatric populations further motivates the use of our subcortical shape analysis technique, yielding

detailed information on topographic effects that may offer greater contrast between psychiatric populations (either with respect to classical diagnostic groupings or in relation to research domain criteria).

The ENIGMA Shape Analysis Pipeline is currently being applied in the ENIGMA schizophrenia, major depressive disorder and OCD working groups to determine the spatial distribution of effects reported in their initial large-scale studies of conventional gross subcortical volumes and to study whether variations may be more complex, as we found in 22q11DS. These analyses may help reveal patterns of disease burden and disrupted development across known subcortical subregions with distinct cytoarchitecture and functional connectivity (50). Furthermore, the ENIGMA harmonized processing and analysis protocols facilitate direct comparisons of such shape metrics across disorders.

Several limitations must be noted. Shape analysis offers a sensitive measure of local morphometric variation across subcortical structures. The thickness and Jacobian measures convey complementary but subtly different information with respect to underlying gross volumetric change. The relationship between subregional shape measures and underlying cytoarchitecture is not yet known. Ongoing work is investigating the correspondence of such shape variations to changes in underlying subfields and gene expression.

We cannot rule out that some subjects with 22q11DS with no history of psychosis may later develop a schizophrenia spectrum disorder, which may have attenuated the group differences we

report here. Further investigation of 22q11DS comorbidities such as immune system, cardiac, and autism spectrum disorders was outside the scope of the current study, but will be pursued in future.

Here, we have shown robust differences in subcortical structure between 22q11DS and demographically comparable healthy controls, with more extreme alterations in those with the larger deletions, and in those with psychotic illness. The pattern of 22q11DS psychosis effects overlaps those from the largest study to date of subcortical structure in idiopathic schizophrenia. This adds evidence to the notion that 22q11DS serves as a biologically applicable framework for understanding brain mechanisms that underlie of psychosis. Interestingly, subcortical effects overlapped across several major neuropsychiatric conditions, suggesting common subcortical alterations that will be explored in future cross-disorder shape and genetic analyses.

References

1. McDonald-McGinn DM, Sullivan KE, Marino B, et al.: 22q11.2 deletion syndrome. *Nat Rev Dis Primers* 2015; 1:15071
2. Schneider M, Debbané M, Bassett AS, et al.: Psychiatric disorders from childhood to adulthood in 22q11.2 deletion syndrome: results from the International Consortium on Brain and Behavior in 22q11.2 Deletion Syndrome. *Am J Psychiatry* 2014; 171:627–39
3. Bassett AS, Chow EW: Schizophrenia and 22q11.2 deletion syndrome. *Curr Psychiatry Rep* 2008; 10:148–57
4. Jonas RK, Montojo CA, Bearden CE: The 22q11.2 deletion syndrome as a window into complex neuropsychiatric disorders over the lifespan. *Biol Psychiatry* 2014; 75:351–60
5. Drew LJ, Crabtree GW, Markx S, et al.: The 22q11.2 microdeletion: fifteen years of insights into the genetic and neural complexity of psychiatric disorders. *Int J Dev Neurosci* 2011; 29:259–81
6. Bassett AS, Chow EW, AbdelMalik P, et al.: The schizophrenia phenotype in 22q11 deletion syndrome. *Am J Psychiatry* 2003; 160:1580–6
7. van ETG, Hibar DP, Rasmussen JM, et al.: Subcortical brain volume abnormalities in 2028 individuals with schizophrenia and 2540 healthy controls via the ENIGMA consortium. *Mol Psychiatry* 2016; 21:585
8. Meechan DW, Tucker ES, Maynard TM, et al.: Diminished dosage of 22q11 genes disrupts neurogenesis and cortical development in a mouse model of 22q11 deletion/DiGeorge syndrome. *Proc Natl Acad Sci U S A* 2009; 106:16434–45
9. Gothelf D, Schaer M, Eliez S: Genes, brain development and psychiatric phenotypes in velo-cardio-facial syndrome. *Dev Disabil Res Rev* 2008; 14:59–68

10. Tan GM, Arnone D, McIntosh AM, et al.: Meta-analysis of magnetic resonance imaging studies in chromosome 22q11.2 deletion syndrome (velocardiofacial syndrome). *Schizophr Res* 2009; 115:173–81
11. Toyoda R, Assimacopoulos S, Wilcoxon J, et al.: FGF8 acts as a classic diffusible morphogen to pattern the neocortex. *Development* 2010; 137:3439–48
12. Kates WR, Burnette CP, Bessette BA, et al.: Frontal and caudate alterations in velocardiofacial syndrome (deletion at chromosome 22q11.2). *J Child Neurol* 2004; 19:337–42
13. Bish JP, Nguyen V, Ding L, et al.: Thalamic reductions in children with chromosome 22q11.2 deletion syndrome. *Neuroreport* 2004; 15:1413–5
14. Flahault A, Schaer M, Ottet MC, et al.: Hippocampal volume reduction in chromosome 22q11.2 deletion syndrome (22q11.2DS): a longitudinal study of morphometry and symptomatology. *Psychiatry Res* 2012; 203:1–5
15. Frank DU, Fotheringham LK, Brewer JA, et al.: An Fgf8 mouse mutant phenocopies human 22q11 deletion syndrome. *Development* 2002; 129:4591–603
16. Bearden CE, van ETG, Dutton RA, et al.: Alterations in midline cortical thickness and gyrification patterns mapped in children with 22q11.2 deletions. *Cereb Cortex* 2009; 19:115–26
17. Gutman BA, Hua X, Rajagopalan P, et al.: Maximizing power to track Alzheimer’s disease and MCI progression by LDA-based weighting of longitudinal ventricular surface features. *Neuroimage* 2013; 70:386–401
18. Boccardi M, Ganzola R, Rossi R, et al.: Abnormal hippocampal shape in offenders with psychopathy. *Hum Brain Mapp* 2010; 31:438–47

19. Wang L, Mamah D, Harms MP, et al.: Progressive deformation of deep brain nuclei and hippocampal-amygdala formation in schizophrenia. *Biol Psychiatry* 2008; 64:1060–8
20. Seymour KE, Tang X, Crocetti D, et al.: Anomalous subcortical morphology in boys, but not girls, with ADHD compared to typically developing controls and correlates with emotion dysregulation.. *Psychiatry Res Neuroimaging* 2017; 261:20–28
21. Mamah D, Alpert KI, Barch DM, et al.: Subcortical neuromorphometry in schizophrenia spectrum and bipolar disorders.. *Neuroimage Clin* 2016; 11:276–286
22. Lin A, Ching CRK, Vajdi A, et al.: Mapping 22q11.2 Gene Dosage Effects on Brain Morphometry.. *J Neurosci* 2017; 37:6183–6199
23. Roshchupkin GV, Gutman BA, Vernooij MW, et al.: Heritability of the shape of subcortical brain structures in the general population.. *Nat Commun* 2016; 7:13738
24. Gutman BA, Fletcher PT, Cardoso MJ, et al.: A Riemannian Framework for Intrinsic Comparison of Closed Genus-Zero Shapes.. *Inf Process Med Imaging* 2015; 24:205–18
25. Gutman BA, Jahanshad N, Ching CR, et al.: Medial Demons Registration Localizes The Degree of Genetic Influence Over Subcortical Shape Variability: An N= 1480 Meta-Analysis.. *Proc IEEE Int Symp Biomed Imaging* 2015; 2015:1402–1406
26. Fischl B, Salat DH, Busa E, et al.: Whole brain segmentation: automated labeling of neuroanatomical structures in the human brain.. *Neuron* 2002; 33:341–55
27. Kong XZ, Mathias SR, Guadalupe T, et al.: Mapping cortical brain asymmetry in 17,141 healthy individuals worldwide via the ENIGMA Consortium.. *Proc Natl Acad Sci U S A* 2018; 115:E5154–E5163

28. Cohen J: A power primer. [Internet]. *Psychological Bulletin* 1992; 112:155–159 Available from: <https://doi.org/10.1037%2F0033-2909.112.1.155>
29. Nakagawa S, Cuthill IC: Effect size confidence interval and statistical significance: a practical guide for biologists [Internet]. *Biological Reviews* 2007; 82:591–605 Available from: <https://doi.org/10.1111%2Fj.1469-185x.2007.00027.x>
30. Benjamini Y, Hochberg Y: Controlling the false discovery rate: a practical and powerful approach to multiple testing. *Journal of the royal statistical society Series B (Methodological)* 1995; 289–300
31. R Core Team: R: A Language and Environment for Statistical Computing. Vienna, Austria: R Foundation for Statistical Computing; 2014. R Foundation for Statistical Computing 2016
32. LM Function Available from: <https://stat.ethz.ch/R-manual/R-devel/library/stats/html/lm.html>
33. Sørensen KM, Agergaard P, Olesen C, et al.: Detecting 22q11.2 deletions by use of multiplex ligation-dependent probe amplification on DNA from neonatal dried blood spot samples. *J Mol Diagn* 2010; 12:147–51
34. Sun D, Ching CRK, Lin A, et al.: Large-scale mapping of cortical alterations in 22q11.2 deletion syndrome: Convergence with idiopathic psychosis and effects of deletion size. *Mol Psychiatry* 2018
35. Gur RE, Bassett AS, McDonald-McGinn DM, et al.: A neurogenetic model for the study of schizophrenia spectrum disorders: the International 22q11.2 Deletion Syndrome Brain Behavior Consortium. *Mol Psychiatry* 2017; 22:1664–1672

36. van Erp TGM, Hibar DP, Rasmussen JM, et al.: Subcortical brain volume abnormalities in 2028 individuals with schizophrenia and 2540 healthy controls via the ENIGMA consortium. *Mol Psychiatry* 2016; 21:585
37. Schmaal L, Hibar DP, Sämann PG, et al.: Cortical abnormalities in adults and adolescents with major depression based on brain scans from 20 cohorts worldwide in the ENIGMA Major Depressive Disorder Working Group. *Mol Psychiatry* 2017; 22:900–909
38. Hibar DP, Westlye LT, van Erp TGM, et al.: Subcortical volumetric abnormalities in bipolar disorder. *Mol Psychiatry* 2016; 21:1710–1716
39. Boedhoe PS, Schmaal L, Abe Y, et al.: Distinct Subcortical Volume Alterations in Pediatric and Adult OCD: A Worldwide Meta- and Mega-Analysis. *Am J Psychiatry* 2017; 174:60–69
40. van Rooij D, Anagnostou E, Arango C, et al.: Cortical and Subcortical Brain Morphometry Differences Between Patients with Autism Spectrum Disorder and Healthy Individuals Across the Lifespan: Results from the ENIGMA ASD Working Group. *Am J Psychiatry* 2018; 175:359–369
41. Hoogman M, Bralten J, Hibar DP, et al.: Subcortical brain volume differences in participants with attention deficit hyperactivity disorder in children and adults: a cross-sectional mega-analysis. *Lancet Psychiatry* 2017; 4:310–319
42. Kotz SA, Anwander A, Axer H, et al.: Beyond cytoarchitectonics: the internal and external connectivity structure of the caudate nucleus. *PLoS One* 2013; 8:e70141
43. Jonas RK, Jalbrzikowski M, Montojo CA, et al.: Altered Brain Structure-Function Relationships Underlie Executive Dysfunction in 22q11.2 Deletion Syndrome. *Mol Neuropsychiatry* 2015; 1:235–46
44. Mukai J, Dhillon A, Drew LJ, et al.: Palmitoylation-dependent neurodevelopmental deficits in a mouse model of 22q11 microdeletion. *Nat Neurosci* 2008; 11:1302–10

45. Boku S, Izumi T, Abe S, et al.: Copy number elevation of 22q11.2 genes arrests the developmental maturation of working memory capacity and adult hippocampal neurogenesis. *Mol Psychiatry* 2017
46. Mukai J, Tamura M, Fénelon K, et al.: Molecular substrates of altered axonal growth and brain connectivity in a mouse model of schizophrenia. *Neuron* 2015; 86:680–95
47. Sigurdsson T, Stark KL, Karayiorgou M, et al.: Impaired hippocampal prefrontal synchrony in a genetic mouse model of schizophrenia [Internet]. *Nature* 2010; 464:763–767 Available from: <https://doi.org/10.1038/nature08855>
48. Haijma SV, Van HN, Cahn W, et al.: Brain volumes in schizophrenia: a meta-analysis in over 18 000 subjects. *Schizophr Bull* 2013; 39:1129–38
49. Liu H, Abecasis GR, Heath SC, et al.: Genetic variation in the 22q11 locus and susceptibility to schizophrenia [Internet]. *Proceedings of the National Academy of Sciences* 2002; 99:16859–16864 Available from: <https://doi.org/10.1073/pnas.232186099>
50. Small SA, Schobel SA, Buxton RB, et al.: A pathophysiological framework of hippocampal dysfunction in ageing and disease. *Nat Rev Neurosci* 2011; 12:585–601

3.4 Chapter 3 references

Bearden et al. Alterations in midline cortical thickness and gyrification patterns mapped in children with 22q11.2 deletions. *Cerebral cortex*. 2009;19(1):115-26. PMID: 2733329.

Bish et al. Thalamic reductions in children with chromosome 22q11.2 deletion syndrome. *Neuroreport*. 2004;15(9):1413-5.

Cantor and Geschwind. Schizophrenia: genome, interrupted. *Neuron*. 2008;58(2):165-7.

Drew et al. The 22q11.2 microdeletion: fifteen years of insights into the genetic and neural complexity of psychiatric disorders. *International journal of developmental neuroscience : the official journal of the International Society for Developmental Neuroscience*. 2011;29(3):259-81. PMID: 3074020.

Ensenauer et al. Microduplication 22q11.2, an emerging syndrome: clinical, cytogenetic, and molecular analysis of thirteen patients. *American journal of human genetics*. 2003;73(5):1027-40. PMID: 1180483.

Gilman et al. Rare de novo variants associated with autism implicate a large functional network of genes involved in formation and function of synapses. *Neuron*. 2011;70(5):898-907. PMID: 3607702.

Jonas et al. The 22q11.2 deletion syndrome as a window into complex neuropsychiatric disorders over the lifespan. *Biol Psychiatry*. 2014;75(5):351-60. PMID: 3875621.

Kates et al. Frontal and caudate alterations in velocardiofacial syndrome (deletion at chromosome 22q11.2). *J Child Neurol*. 2004;19(5):337-42.

Kelly et al. Widespread white matter microstructural differences in schizophrenia across 4322 individuals: results from the ENIGMA Schizophrenia DTI Working Group. *Mol Psychiatry*. 2018;23(5):1261-9. PMID: 5984078.

Marshall et al. Contribution of copy number variants to schizophrenia from a genome-wide study of 41,321 subjects. *Nature genetics*. 2017;49(1):27-35. PMID: 5737772.

Malhotra and Sebat. CNVs: harbingers of a rare variant revolution in psychiatric genetics. *Cell*. 2012;148(6):1223-41. PMID: 3351385.

McDonald-McGinn et al. 22q11.2 deletion syndrome. *Nature reviews Disease primers*. 2015;1:15071. PMID: 4900471.

Meechan et al. Diminished dosage of 22q11 genes disrupts neurogenesis and cortical development in a mouse model of 22q11 deletion/DiGeorge syndrome. *P Natl Acad Sci USA*. 2009;106(38):16434-45. PMID: 2752572.

- Murphy KC. Schizophrenia and velo-cardio-facial syndrome. *Lancet*. 2002;359(9304):426-30.
- Ou et al. Microduplications of 22q11.2 are frequently inherited and are associated with variable phenotypes. *Genet Med*. 2008;10(4):267-77.
- Rees et al. Evidence that duplications of 22q11.2 protect against schizophrenia. *Mol Psychiatry*. 2014;19(1):37-40. PMID: 3873028.
- Rees et al. Analysis of Intellectual Disability Copy Number Variants for Association With Schizophrenia. *JAMA Psychiatry*. 2016;73(9):963-9. PMID: 5014093.
- Sebat et al. Rare structural variants in schizophrenia: one disorder, multiple mutations; one mutation, multiple disorders. *Trends Genet*. 2009;25(12):528-35. PMID: 3351381.
- Sigurdsson et al. Impaired hippocampal-prefrontal synchrony in a genetic mouse model of schizophrenia. *Nature*. 2010;464(7289):763-7. PMID: 2864584.
- Stark et al. Altered brain microRNA biogenesis contributes to phenotypic deficits in a 22q11-deletion mouse model. *Nature genetics*. 2008;40(6):751-60.
- Tan et al. Meta-analysis of magnetic resonance imaging studies in chromosome 22q11.2 deletion syndrome (velocardiofacial syndrome). *Schizophr Res*. 2009;115(2-3):173-81.
- van Erp et al. Cortical Brain Abnormalities in 4474 Individuals With Schizophrenia and 5098 Control Subjects via the Enhancing Neuro Imaging Genetics Through Meta Analysis (ENIGMA) Consortium. *Biol Psychiatry*. 2018;84(9):644-54. PMID: 6177304.
- Wenger et al. 22q11.2 duplication syndrome: elevated rate of autism spectrum disorder and need for medical screening. *Mol Autism*. 2016;7:27. PMID: 4859984.
- Wentzel et al. Clinical variability of the 22q11.2 duplication syndrome. *Eur J Med Genet*. 2008;51(6):501-10.
- Zaleski et al. The co-occurrence of early onset Parkinson disease and 22q11.2 deletion syndrome. *Am J Med Genet A*. 2009;149A(3):525-8. PMID: 3295831.

CHAPTER 4

The ENIGMA Bipolar Disorder Working Group: Large-scale studies in bipolar disorder brain structure

4.1 Overview

Bipolar disorder (BD) consists of a spectrum of related mental illnesses that involve the neural circuitry of emotional and reward processing where patients present with a range of behavioral symptoms including mania and depression (Merikangas et al., 2011; Strakowski et al., 2012). BD is a leading cause of disability and affects 1-3% of the adult population worldwide (Grande et al., 2016). BD is highly heritable (McGuffin et al., 2003; Wray and Gottesman, 2012) and despite significant advances the understanding of the disorder, the underlying mechanisms are far from understood. Current psychiatric diagnostic criteria are based on descriptions of behavioral symptoms, leading to inaccurate and often delayed diagnosis of BD (Ghaemi et al., 1999; Duffy et al., 2009; Bschor et al., 2012). Delayed diagnosis is estimated to be, on average, 5-10 years between symptom onset and first treatment and has important implications for prognosis. While mania and depression are the most characteristic features of the disorder, complex presentation and comorbid factors contribute to difficult management with the majority of patients suffering long-term impairment (Conus et al., 2014). Given the global impact of this complex illness, there is an urgent need for objective biomarkers to improve diagnosis, track treatment effects, and inform future investigations into the cellular/molecular mechanisms of BD.

A large number of brain-based MRI studies have reported a range of alterations in BD, implicating cortical regions such as the precentral, middle frontal, inferior frontal and fusiform gyri (Hajek et al., 2013; Ganzola and Duchesne, 2017). Alterations of subcortical structures such

as the thalamus, hippocampus and amygdala have also been tied to BD (Hajek et al., 2009; Hajek et al., 2012). However, previous studies have also offered conflicting volumetric results, ranging from volume increases and decreases in BD patients compared to controls (Phillips and Swartz, 2014). Such discrepancies are likely due to patient heterogeneity, treatment effects and small sample sizes. Furthermore, many studies tend to only compare one BD subtype to healthy controls.

The high cost of MRI data collection has led to underpowered studies whose findings often fail to replicate, cannot adequately model confounds, and lack the power to pick up key factors that modulate disease progression or recovery. Global initiatives such as the ENIGMA bipolar disorder working group aim to offer detailed, reproducible, and reliable data on brain changes in BD.

The ENIGMA bipolar working group is co-chaired by myself and Dr. Ole A. Andreassen, professor of Medicine at the University of Oslo and the director of The Norwegian Centre for Mental Disorders (NORMENT). Dr. Andreassen also leads the Psychiatric Genetics Consortium working group on bipolar disorder. To date, the ENIGMA bipolar working group includes a growing sample of 44 international cohorts (**Figure 4.1a**) with multimodal neuroimaging data from over 3,000 BD subjects and 8,000 healthy controls, making it by far the largest neuroimaging consortia effort to ever study BD.

ENIGMA Bipolar Disorder Working Group



Figure 4.1a. Map of ENIGMA bipolar disorder working group study sites

The bipolar working group recently completed 3 large-scale meta- and mega-analyses of subcortical volume (Hibar et al., 2016), cortical thickness (Hibar et al., 2018), and machine learning classification (Nunes et al., 2018). There are 15 additional projects in various stages of completion led by an international team of researchers, all of which represent the largest studies of their kind (**Figure 4.1b**).

Bipolar Working Group Studies

1. **Subcortical Volume** – Derrek Hibar (USA) *Published
2. **Cortical Thickness and Surface Area** – Derrek Hibar (USA) *Published
3. **Bipolar Classification: Cortical/Subcortical Machine Learning** – Tomas Hajek (Canada) *Published
4. **ENIGMA Relatives (BD and SCZ)** – Neeltje van Haren, Rachel Brouwer, Sonja de Zwarte (Netherlands) *In review
5. **DTI** – Josselin Houenou, Pauline Favre, Melissa Pauling (France) *In review
6. **Bipolar Classification: DTI and clinical metrics** – Josselin Houenou, Pauline Favre (France) *In submission
7. **Hippocampal Subfields** – Ingrid Agartz and Unn Haukvik (Norway) *In preparation
8. **Subcortical Shape Analysis** – Christopher Ching (USA) *In preparation
9. **Structural brain aging in bipolar disorder** – Lisa Eyler (USA) *In preparation
10. **Genotyping: Polygenic Risk in Collaboration with the PGC** – Ole Andreassen (Norway) *Underway
11. **H1-MRS** – Márcio Gerhardt Soeiro-de-Souza (Brazil) *Underway
12. **Subcortical Morphometry and Polypharmacy** – Colm McDonald (Ireland) *Underway
13. **Longitudinal Brain Change** – Christoph Abé, Mikael Landen (Sweden) *Underway
14. **Virtual Histology (Gene expression and the Allen Brain Atlas)** – Tomas Paus (Canada) *Underway
15. **White Matter Connectivity** – Dara Cannon, Leila Nabulsi (Ireland) *Underway
16. **Multimodal Imaging and Intelligence** – Tristram Lett and Henrik Walter (Germany) *Underway
17. **Obesity/BMI** – Tomas Hajek (Canada) *Underway
18. **Cross Disorder (BD, MDD, and SCZ)** – Christopher Ching (USA) *Underway



Figure 4.1b. All ENIGMA bipolar disorder working group projects

4.2 Recent findings from the ENIGMA bipolar working group

4.2.1 Subcortical Volumes

The ENIGMA bipolar working group's first study was a large-scale meta-analysis of 1,710 BD patients and 4,304 healthy controls (HC). Higher bilateral ventricular volumes and lower hippocampal, amygdala and thalamic volumes were detected in BD patients versus HC (**Figure 4.2a**) (Hibar et al., 2016). These group differences may reflect either accelerated atrophy in patients or chronic effects of the illness or medication. Importantly, previous meta-analyses were unable to detect case/control differences in amygdala volume and smaller studies reported both higher and lower amygdala volume (Altshuler et al., 2000; Chang et al., 2005).

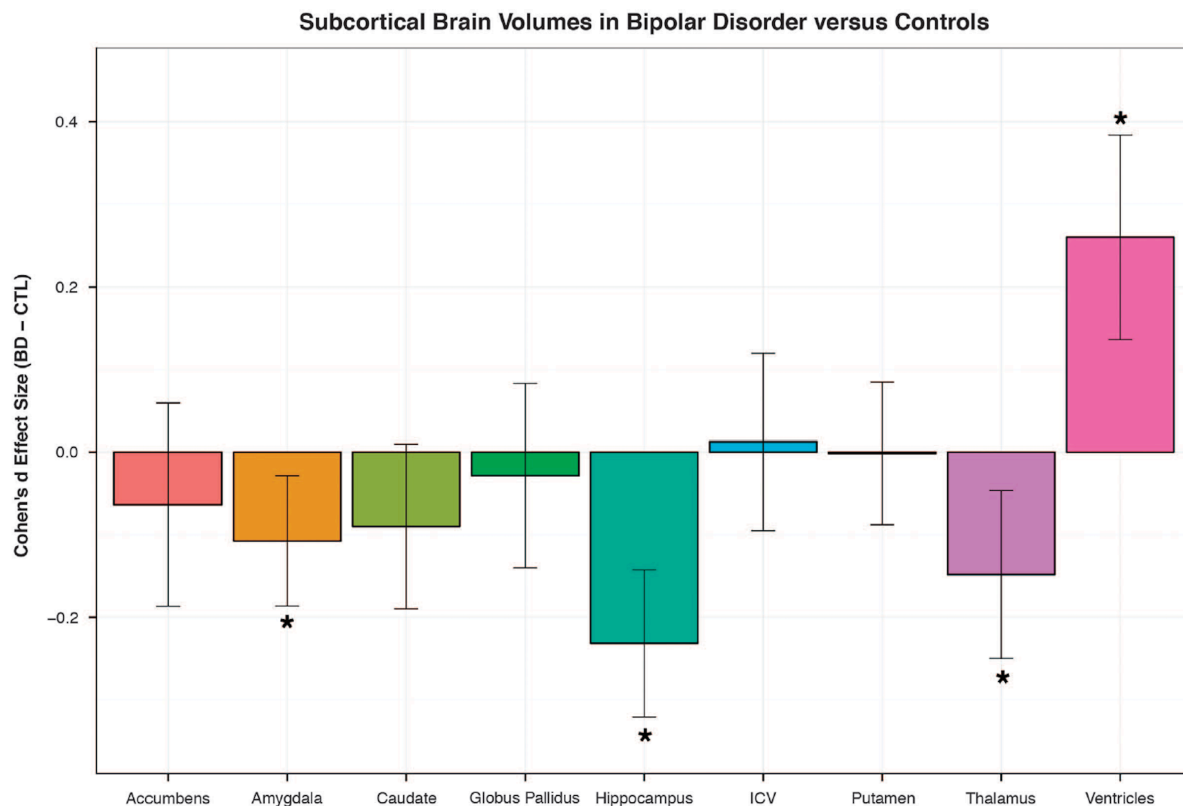


Figure 4.2a. Cohen's *d* effect size estimates for all BD patients versus controls using ENIGMA-harmonized FreeSurfer volumes. Statistical model accounts for age, sex, and intracranial volume. Error bars indicate mean effect size \pm s.e.m. Results passing study-wide significance threshold ($P < 4.91 \times 10^{-3}$) are indicated by (*) (Hibar et al., 2016).

No differences between BD subtype (BD1, BD2 and BD-NOS) nor between BD subtype and HC were detected. Lithium treatment was associated with larger thalamic volumes compared to non-treated BD patients (when adjusting for the effect of other medication). When compared to controls, BD patients taking Lithium had smaller hippocampal and thalamic volumes and larger lateral ventricles. On average, BD patients taking anticonvulsants had smaller hippocampal volumes compared to non-treated BD patients. As medication is one of the most debated sources

of patient variability in the literature, and has widely focused on Lithium treatment, we were able to isolate specific effects of Lithium and anticonvulsants on subcortical volume. These results should be interpreted with caution as medication status likely interacts with illness characteristics (such as symptom severity). Furthermore, a simple binary coding (prescribed/not prescribed) was used to determine medication status at the time of scan. A future study led by Dr. Colm McDonald from the ENIGMA bipolar working group aims to study more detailed measures of medication such as history, dose, and serum level in order to delve into interactions between different pharmacological agents and their effect on brain structure across the cohort.

4.2.2 Cortical thickness and surface area

Previous meta-analyses have reported lower cortical thickness in the anterior cingulate, paracingulate, superior temporal gyrus and prefrontal regions. Surface area findings have been far more variable. In our recent study of BD cortical structure, the largest of its kind (2,447 BD and 4,056 healthy controls) and using ENIGMA harmonized measures of cortical thickness and surface area, we reported significant alterations in the cortex of BD patients (Hibar et al., 2018).

Compared to controls, BD patients exhibited a widespread pattern of thinner cortex (**Figure 4.2b**). Interestingly, no case/control differences were detected for cortical surface area. Again, as in the subcortical study, no significant differences were detected between BD subtypes. Longer illness duration was associated with a pattern of lower cortical thickness but not with surface area.

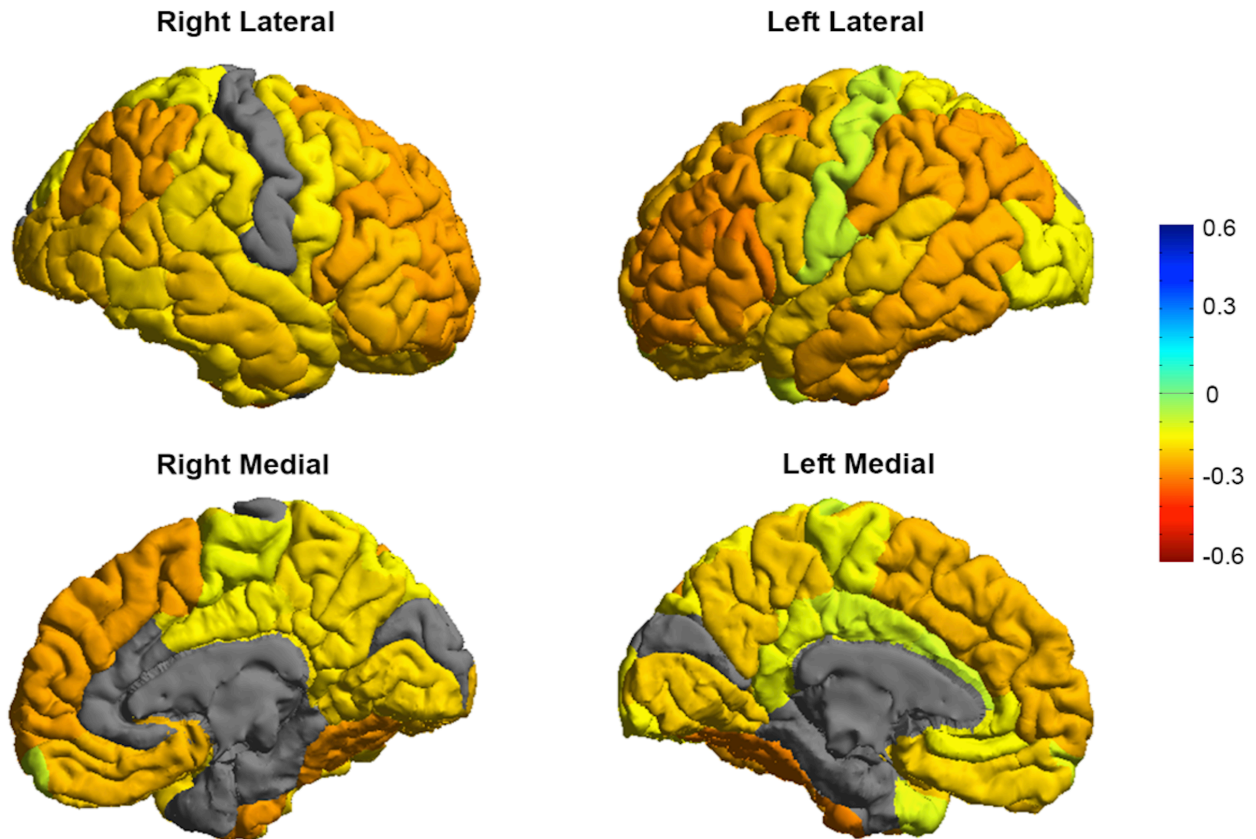


Figure 4.2b. A widespread pattern of thinner cortex in BD adult patients versus controls. Colors indicate Cohen's d effect sizes after correction for multiple comparisons (Hibar et al., 2018).

We found significantly higher cortical thickness in BD patients taking Lithium, with the largest effects located in the left paracentral gyrus (**Figure 4.2c**). Anticonvulsant treatment was associated with lower cortical thickness, with the highest effects observed in the left and right lateral occipital gyrus. Typical (first generation) antipsychotics were associated with higher cortical surface area in the left inferior parietal gyrus and atypical (second generation) antipsychotics were associated with lower surface area in the rostral middle frontal gyrus.

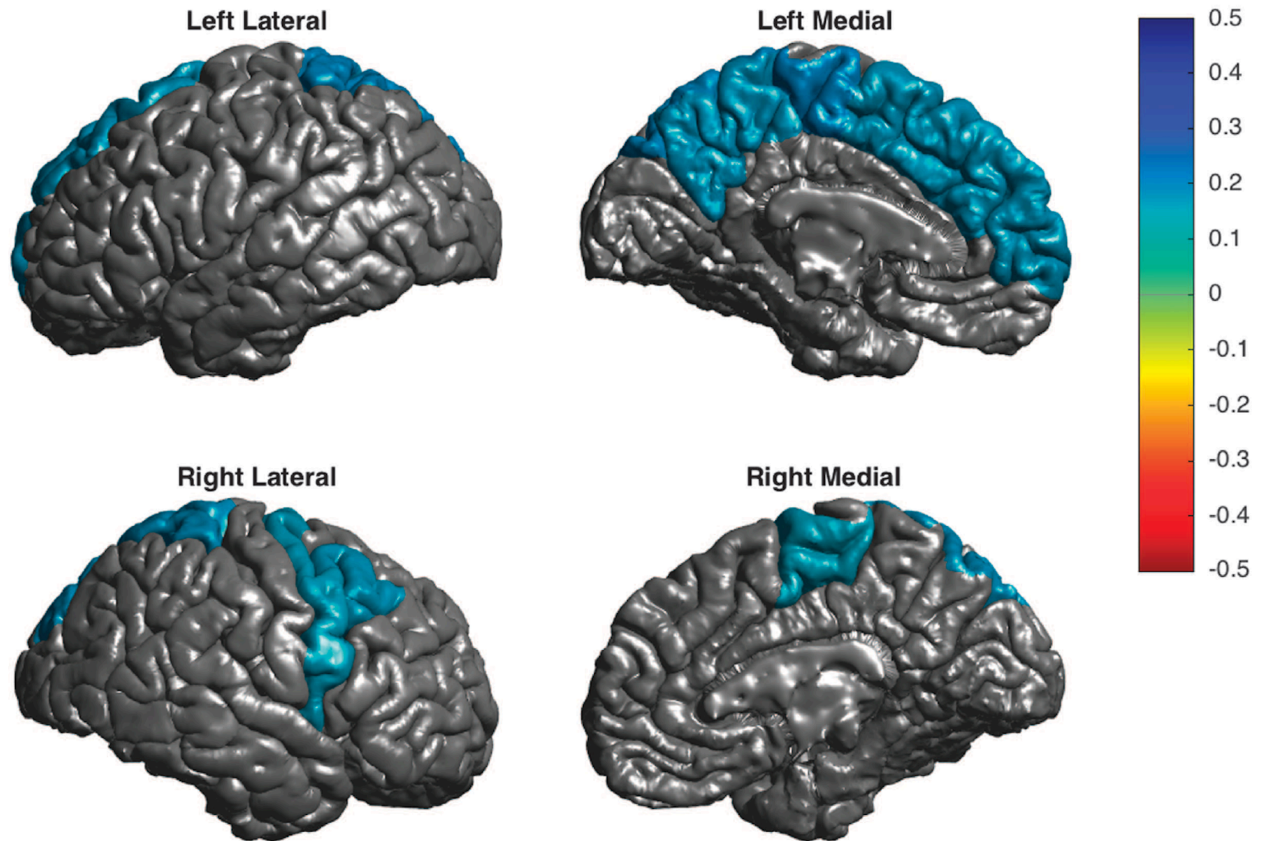


Figure 4.2c. Thicker cortex in BD patients on Lithium at time of scan. Cohen's d effect sizes plotted in regions passing correction for multiple comparisons (Hibar et al., 2018).

In summary, the cortical findings were largely in line with prior reports of thinner frontal and temporal cortices. Notably, regions with the largest case/control differences were the ventrolateral prefrontal cortex, an area that has been long implicated in the pathophysiology of BD. Important new contributions include the observation of lower thickness in inferior parietal, fusiform, and inferior temporal regions in adult BD patients. Structural deficits in these regions have been tied to disruptions in sensorimotor integration and language and may be tied altered emotion perception and rapid mood changes in BD.

Recently, the ENIGMA relatives project studied first-degree relatives (FDRs) of patients across the ENIGMA bipolar disorder and schizophrenia working groups. FDRs of BD subjects were found to have significantly larger ICV compared to controls. Higher ICV explained other whole-brain enlargements seen in the FDRs-BD group (total volume, surface area, cortical gray matter). The effect sizes were quite small suggesting that familial brain risk in BD is subtle, though enlargements in ICV may represent a form of resilience to developing BD, as suggested in a report of hippocampal volume in non-affected co-twins (van Erp et al., 2012).

4.2.3 Machine learning classification using cortical and subcortical measures

We recently performed the largest machine learning study of BD, including 853 BD and 2,167 controls across 13 international sites. In this study we applied a support vector machine technique to ENIGMA-harmonized measures of subcortical volume, and cortical thickness and surface area. The goal of the study was to differentiate BD patients from controls, interrogate alternate data handling strategies and determine the features most important for case/control classification (Nunes et al., 2018).

A linear kernel, support vector machine (SVM) (without hyperparameter optimization) was used in the primary analysis. SVM fit to data pooled across all sites outperformed two other techniques: meta-analysis of site-level analyses and a leave-one-site-out cross validation procedure. The pooled (aggregate) model performed significantly above chance with the ROC-AUC of 71.49% (**Figure 4.2d**) with an accuracy of 65.23%. Anatomical features driving classification were both biologically relevant and consistent across the 13 cohorts.

Anticonvulsant treatment and age were associated with the greatest odds of accurate classification.

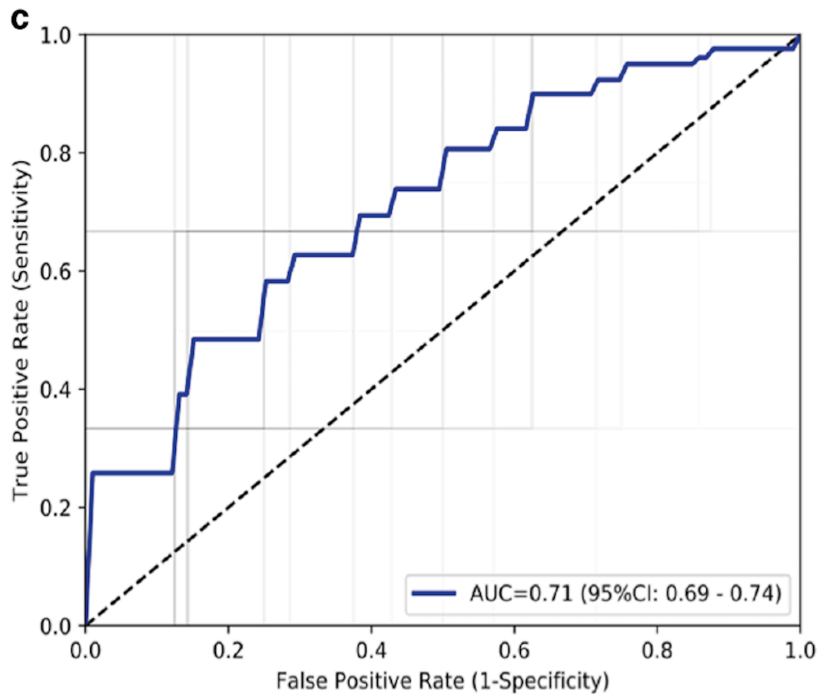


Figure 4.2d. ROC curves for pooled (aggregate) analysis. Faint gray lines indicate ROC curves for validation folds and the blue line represent the mean ROC curve (Nunes et al., 2018).

While a classification accuracy of 65% sounds low, it's important to note that the Cohen's kappa reliability (inter-rater agreement) for BD-1 diagnosis is ~ 0.56 and can range as low as ~ 0.40 for BD-2 (Regier et al., 2013). Furthermore, the classification of BD from controls is not the end goal of this line of research. While falling short of the 80% accuracy mark set as clinically relevant (Savitz et al., 2013), these results show proof of concept that large-scale, multisite brain imaging data can be useful in such classification problems. The addition of other deeper phenotyping data, like those being collected through the ENIGMA cross-disorder project I'm leading now (**Chapter 5**), along with more advanced methods such as deep learning (requiring

sharing of raw data), may greatly improve classification and tackle more clinically interesting problems such as discerning treatment responders, BD subtypes, suicidal ideation, and more.

*This study was listed a 2018 Leading Research Achievement by the Brain and Behavior Research Foundation (<https://www.bbrfoundation.org/2018-research-highlights>).

4.3 Subcortical shape morphometry: A single site study

Building off our initial study of BD subcortical structure (Hibar et al., 2016) and to address some of the limitations of previous BD studies of subcortical volumes, we analyzed a large cohort of patients with BD subtypes I and II (BD1, BD2) and not otherwise specified (BD NOS), assessing overall volumes and point-wise shape differences. We hypothesized that our novel shape analysis of these structures would reveal regional differences between BD and controls not detected by measures of gross volume. Shape analysis might also reveal subtle difference between BD subtype and associations with subcortical regions involved in emotional and reward processing.

SHAPE MODELING MAY OUTPERFORM GROSS VOLUMETRICS IN DETECTING SUBCORTICAL DIFFERENCES IN BIPOLAR DISORDER

Christopher R. K. Ching^{1,2}, Boris A. Gutman², Derrek P. Hibar², Neda Jahanshad²,
Benson Mwangi³, Jair C. Soares³, Paul M. Thompson^{2,4}

1. Graduate Interdepartmental Program in Neuroscience, UCLA School of Medicine, CA, USA

2. Imaging Genetics Center, University of Southern California, CA, USA

3. Department of Psychiatry and Behavioral Sciences, University of Texas Medical School, Houston, TX, USA

4. Departments of Neurology, Psychiatry, Radiology, Engineering, Pediatrics and Ophthalmology, University of Southern California, CA, USA

ABSTRACT

Shape analysis of subcortical brain structures derived from magnetic resonance imaging (MRI) provides sensitive markers of structural abnormalities in psychiatric and neurological disorders. Here we apply a novel, automated shape analysis technique, including surface-based Jacobian and local thickness maps, to a large cohort of 286 patients with bipolar disorder (BD) and 174 healthy controls (CN). No volumetric differences were detected between bipolar subtypes and controls for 7 widely segmented subcortical structures. Even so, subcortical shape models revealed significant BD-specific differences in distinct regions of several subcortical structures. Our model provided detailed metrics of regional shape morphology that were more sensitive to disease effects than traditional volumetric analysis. This shape mapping method may be useful for large-scale meta-analysis of neurological and psychiatric disorders in which patients exhibit subtle brain structure abnormalities.

Index Terms— Magnetic Resonance Imaging, Surface Modeling, Shape Analysis, Bipolar Disorder, Neuroimaging

1. INTRODUCTION

Bipolar disorder (BD) consists of a spectrum of related mental illnesses that involve the neural circuitry of emotional and reward processing; patients have a range of behavioral symptoms including mania and depression [1, 2]. Many studies have attempted to characterize underlying neurophysiological mechanisms that may give rise to BD, but a consensus is far from clear. A large number of magnetic resonance imaging (MRI) studies have reported conflicting volumetric abnormalities in BD, ranging from volume increases and decreases in BD patients compared to controls [3]. Discrepancies among different volumetric studies are likely due to patient heterogeneity, treatment effects and small sample sizes. Furthermore, many studies only compare one or two BD subtypes to healthy controls.

The Enhancing Neuro Imaging Genetics Through Meta-Analysis consortium (ENIGMA) recently performed a very large study of 1,745 BD patients and 2,613 healthy controls, finding consistent volume reductions for BD patients in a number of subcortical regions [4].

Even so, small effect sizes lead to large sample requirements, making it advantageous to test other metrics of structural abnormality, beyond simple volumetrics. High-resolution shape analysis of subcortical structure is a sensitive marker of progression in degenerative diseases such as Alzheimer's disease, and has detected brain abnormalities in psychiatric conditions that gross volume analyses might miss [5], including studies of blind versus sighted controls, and in psychopathy patients versus controls [6, 7].

To address some of the limitations of previous BD studies of subcortical volumes, we analyzed a large cohort of patients with BD subtypes I and II (BD1, BD2) and not otherwise specified (BD NOS), assessing overall volumes and point-wise shape differences, building on prior work analyzing hippocampal shape in smaller bipolar cohorts [8]. We hypothesized that BD subtype would be associated with subcortical differences in regions involved in emotional and reward processing. We also hypothesized that our novel shape analysis of these structures would reveal regional differences between BD subtypes not detected by gross volume analysis alone.

2. METHODS

2.1 Data sample

High-resolution T1-weighted brain MRI data were analyzed from retrospective samples supported by the NIMH Grant RO1 085667 to Jair C. Soares. The sample included all three BD subtypes and controls with an age range from 8-66 years (BD1=180, BD2=64, BD NOS=42, CN=174). Patient demographics broken down by diagnosis are listed in Table 1. Patients were scanned at 4 sites: patient numbers and scanner information for each site are listed in Table 2.

Group	Male/Female	Age (SD)
BD1	73/107	29.9 (13.5)
BD2	21/43	29.3 (13.4)
BD NOS	23/19	21.9 (15.9)
CN	79/95	24.4 (14.9)

Table 1: Total sample sizes listing numbers of men and women, average age in years (SD: standard deviation), separated by diagnosis.

	Site 1	Site 2	Site 3	Site 4
BD1	37/58	5/3	24/32	7/14
BD2	15/27	0/0	6/16	0/0
BD NOS	5/5	1/0	17/14	0/0
CN	38/46	2/7	37/34	2/8
Total	95/136	8/10	84/96	9/22

Table 2: Sample sizes (male/female) by scan site. Site 1: Philips Gyroscan Intera 1.5T - MPRAGE/3D SPGR; Site 2: Siemens Trio 3T - MPRAGE; Site 3: Siemens Allegra 3T - MPRAGE; Site 4: Philips Intera 3T - 3D T1 PRESENSE.

2.2 Subcortical segmentation

All T1-weighted scans were segmented using the FreeSurfer software package, version 5.3 [9]. The 7 subcortical volumes of interest were: left and right nucleus accumbens, amygdala, caudate, hippocampus, putamen, pallidum, and thalamus. We analyzed only segmentations that passed visual quality inspection. Processing and quality control protocols are found online as provided by the ENIGMA consortium [10].

2.3 Subcortical shape modeling

A surface-based parametric mapping technique developed by our group was used to detect shape differences across subjects. Using FreeSurfer segmentations, shape registration was based on existing shape templates and template medial models. The shape template was made by registering all subjects to a representative subject. The Euclidean average then served as the template surface, on which the template medial curve was computed. Figure 1 shows shape templates for all 7 bilateral subcortical volumes of interest.

Two point-wise measures of shape morphometry were derived. The first, termed radial distance, was derived by a medial model approach [11] where for each point $p \in \mathcal{M}$ on the surface, and given a medial curve $c: [0,1] \rightarrow \mathbb{R}^3$, the radial distance is defined by

$$D(p) = \min(\|c(r) - p\| \mid r \in [0,1]) \quad (1)$$

The second, based on surface Tensor Based Morphometry (TBM), generalizes TBM on Euclidean spaces to surfaces [12]. The differential map between the tangent spaces of two surfaces replaces the Jacobian

$$J: T\mathcal{M}_i \rightarrow T\mathcal{M}. \quad (2)$$

In our model, \mathcal{M}_i is the average template, and \mathcal{M} is the surface we wish to study. J is a linear mapping, and may be thought of as the restriction of the standard Jacobian to the tangent spaces of the template and study surfaces. While analysis of the full tensor using Log-Euclidean metrics on SPD matrices is possible [12], such analyses are difficult to interpret. Instead, our model considers the Jacobian determinant, representing the surface dilation ratio between the template and the study subject. An interpretation of this measure is that of a ratio of the area of a small surface patch around a particular point of the subject surface and the small patch of area around the corresponding point on the template. A higher Jacobian may indicate larger volume of a structure's subfield corresponding to the region. Our final TBM measure is the logarithm of the Jacobian determinant, to obtain a distribution closer to Gaussian.

In this way, both radial size (termed *thickness* from now on) and the logarithm of the Jacobian determinant (termed simply *Jacobian* from now on) were calculated in native space for up to 2,500 points across each subcortical structure, providing a sensitive index of regional shape differences across subjects.



Figure 1: Subcortical surface templates for all 7 structures of interest: left and right nucleus accumbens, amygdala, caudate, hippocampus, putamen, pallidum, and thalamus. *Left image: inferior view; right image: anterior/lateral view*

2.4 Statistics

A linear mixed effects model was used to assess gross volume, as well as surface-based Jacobian and thickness differences within and between BD subtypes and controls after correcting for age, sex, age², age*sex, age²*sex and intracranial volume (ICV) as fixed effects, and scan site as a random effect. Statistical modeling was carried out using the R package *nlme* version 3.1-111. For gross volume, p -values were corrected for multiple comparisons using matrix spectral decomposition to estimate the number of independent tests based on the correlation matrix of all gross subcortical volume measures as implemented in the following references [13,14]. For point-wise Jacobian and thickness analyses of the subcortical shape models, the aforementioned linear mixed effects model was fitted at each point across the surface for which there was a thickness or Jacobian value. Because these values were calculated in

native space, ICV was used to regress out the effects of head size. To correct for multiple comparisons, a standard false discovery rate (FDR) correction was applied at the conventionally accepted level of 5% ($q=0.05$) as implemented in the R function *p.adjusted* [15]. Statistical models were fitted for the following comparisons of interest: BDall vs. CN (collapsing all BD subtypes 1, 2 and NOS into one group); BD1 vs. CN; BD2 vs. CN; BD NOS vs. CN; BD1 vs. BD2; BD1 vs. BD NOS; BD2 vs. BD NOS.

3. RESULTS

After correcting for multiple comparisons, no significant differences were detected in overall subcortical volumes within BD subtypes or between BD subtypes and CN.

However, subcortical shape modeling detected several differences between BD subtypes and controls. **Figure 2** and **3** show Jacobian and thickness differences (respectively) between BD1 and CN. In both cases, BD1 showed regionally higher Jacobian values and greater thickness compared to CN.

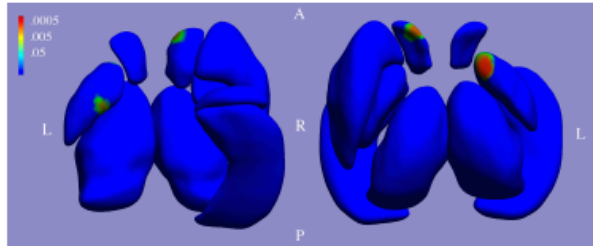


Figure 2: FDR corrected P -value maps show differences between BD1 and CN Jacobian values (*left image: inferior view; right: superior view*). Non-blue colors represent areas of significance and were associated with positive β values indicating greater Jacobian values in the anterior right accumbens and left pallidum for BD1 patients compared to CN. Some structures are not shown to make significant associations easier to see. *L: left; R: right; A: anterior; P: posterior.*

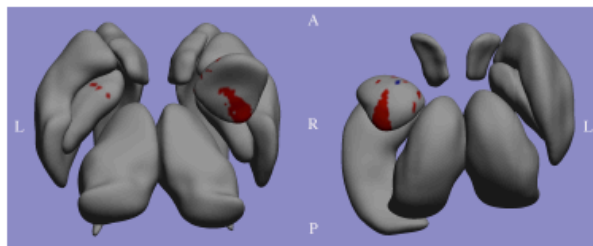


Figure 3: BD1 versus CN thickness comparison showing β values for regions passing FDR correction ($q = 0.05$). *Red* indicates positive β values (the majority of significant differences across the right amygdala and left pallidum), whereas *Blue* indicates negative β values (one small patch of points on the superior surface of the right amygdala). *Left image: inferior view; right image: superior view. L: left; R: right; A: anterior; P: posterior.*

When combining all BD subtypes, Jacobian values were significantly higher for patients versus controls in anterior

portions of the right accumbens compared to controls (**Figure 4**).

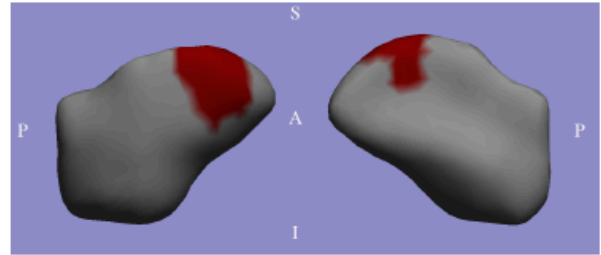


Figure 4: All BD subtypes combined versus CN Jacobian comparison, showing β values for the right accumbens passing FDR correction ($q = 0.05$). *Red* indicates positive β values. *Left image: medial view; right image: lateral view. A: anterior; P: posterior; S: superior; I: inferior.*

When comparing BD1 and BD2 groups, the BD1 group showed significantly lower Jacobian values in the superior and inferior surface of the left pallidum compared to BD2 (**Figure 5**).

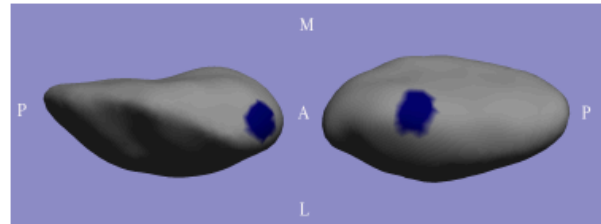


Figure 5: BD1 versus BD2 Jacobian map comparison showing β values for regions of the left pallidum passing FDR correction ($q = 0.05$). *Blue* indicates negative β values. *Left image: superior view; right image: inferior view. A: anterior; P: posterior; M: medial; L: lateral.*

Direct comparisons of BD1 and BD2 groups revealed significantly lower thickness in superior portions of the right accumbens for BD1 patients (**Figure 6**).

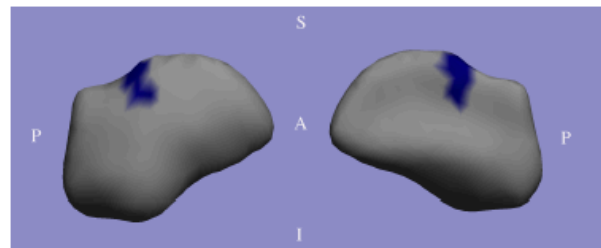


Figure 6: BD1 versus BD2 thickness comparison showing β values for regions of the right accumbens passing FDR correction ($\alpha = 0.05$). *Blue* indicates negative β values. *Left image: medial view; right image: lateral view. A: anterior; P: posterior; S: superior; I: inferior.*

Finally, the BD1 group showed significantly lower thickness measures in both lateral and medial aspects of the anterior

portion of the right caudate, compared to BD NOS (Figure 7).

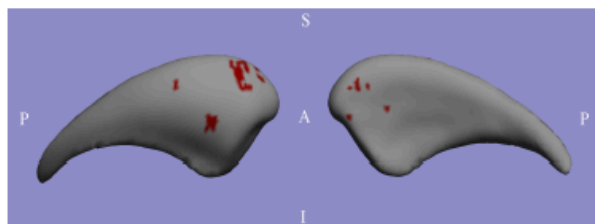


Figure 7: BD1 versus BD NOS group thickness comparison showing β values for right caudate regions passing FDR correction ($q = 0.05$). Red indicates positive β values. *Left image: medial view; right image: lateral view. A: anterior; P: posterior; S: superior; I: inferior.*

Table 3 summarizes the non-significant overall volume trends ($P < 0.05$, uncorrected) and significant differences detected in the shape analysis by highlighting the correspondence in the sign of β values for both analyses. Not only was the shape analysis more sensitive to subcortical differences, the results were in the same direction as trends found in the overall volume analysis (+/- indicates the sign of the β value).

	BDall vs. CN	BD1 vs. CN	BD2 vs. CN	BD1 vs. BD2	BD1 vs. BD3
L Acc					
L Hippo					
L Pall		T (+) J (+)		J (-)	
L Thal					
R Acc	J (+)	J (+)		T (-)	
R Amyg		T (+/-)			
R Caud					T (+)

Table 3: Colored squares represent non-significant trends from gross volume analysis (red: positive β ; blue: negative β). Significant differences detected by shape analysis are represented by the letters J: Jacobian and T: thickness, with positive/negative β values in parentheses. The sign of the β value (+/-) from the significant shape analysis findings always corresponded to the sign of the β in the gross volume analysis trend (red/blue). *BDall: all BD subtypes combined; Acc: accumbens; Hippo: hippocampus; Pall: pallidum; Thal: thalamus; Amyg: amygdala; Caud: caudate.*

4. CONCLUSION

Our study had two key findings. First, we detected no significant differences within BD subtype or between BD subtypes and CN when comparing gross subcortical volume for any of the 7 subcortical structures of interest. Second, our novel subcortical shape modeling technique was able to pick up statistically significant regional morphological differences within BD subtypes and between BD subtypes and CN. The direction of these significant differences corresponded to the sign of the β 's from the non-significant

trends in the gross volumetric analysis. In other words, the shape analyses confirmed trends from the gross volumetric analysis but were more sensitive to the pattern of alterations across the surfaces of these structures.

These findings, in the largest shape analysis that we know of in BD, demonstrate that subcortical shape analysis may be more sensitive to subtle brain alterations associated with BD. There are conflicting reports regarding subcortical volume alterations in BD and few studies have compared neuroimaging measures across BD1, BD2 and BD NOS. As there are many gross volumetric studies in the BD literature, shape analyses such as these may lead to more stable and replicable findings across studies, as well as more efficient detection of differences in smaller cohorts. Furthermore, significant regional differences between BD subtypes in specific subcortical structures may help elucidate mechanisms implicated in the spectrum of BD disorders.

5. ACKNOWLEDGEMENTS

This study was supported by NIMH Grant RO1 085667, The Dunn Foundation and the Pat Rutherford, Jr. Endowed Chair in Psychiatry (Jair C. Soares). This research was also supported in part by NIH 'Big Data to Knowledge' (BD2K) Center of Excellence grant U54 EB020403, funded by a cross-NIH consortium including NIBIB and NCI.

6. REFERENCES

- [1] Merikangas KR, et al. (2011) Prevalence and correlates of bipolar spectrum disorder in the world mental health survey initiative. *Arch Gen Psychiatry* 68(3):241-251.
- [2] Strakowski SM et al. (2012) The functional neuroanatomy of bipolar disorder: a consensus model. *Bipolar Disorders* 14(4):313-325.
- [3] Phillips ML et al. (2014) A critical appraisal of neuroimaging studies of bipolar disorder: toward a new conceptualization of underlying neural circuitry and a road map for future research. *Am J Psychiatry* 171(8):829-43.
- [4] Hibar DP et al. (2014) Robust subcortical volumetric abnormalities in bipolar disorder: findings from the ENIGMA Bipolar Disorder Working Group. Submitted to *Molecular Psychiatry* (October 2014).
- [5] Gutman B et al. (2013) Maximizing power to track Alzheimer's disease and MCI progression by LDA-based weighting of longitudinal ventricular surface features. *NeuroImage* 70:386-401.
- [6] Laporé N et al. (2009) Pattern of Hippocampal Shape and Volume Differences in Blind Subjects. *NeuroImage* 46(4):949-957.
- [7] Boccardi M et al. (2010) Abnormal hippocampal shape in offenders with psychopathy. *Hum Brain Mapp* 31(3):438-47.
- [8] Bearden CE et al. (2008) Three-dimensional mapping of hippocampal anatomy in unmedicated and lithium-treated patients with bipolar disorder. *Neuropsychopharmacology* 33(6):1229-38.
- [9] Fischl B et al. (2002) Whole brain segmentation: Automated labeling of neuroanatomical structures in the human brain. *Neuron* 33(3):341-355.
- [10] <http://enigma.ini.usc.edu/protocols/>

- [11] Gutman B et al. (2012) Shape matching with medial curves and 1-D group-wise registration. 9th IEEE International Symposium on Biomedical Imaging, 716–719.
- [12] Wang Y et al. (2011) Surface-based TBM boosts power to detect disease effects on the brain: an N=804 ADNI study. *Neuroimage* 56(4):1993-2010.
- [13] Li J et al. (2005) Adjusting multiple testing in multilocus analyses using the eigenvalues of a correlation matrix. *Heredity* 95:221-227.
- [14] <http://gump.qmir.edu.au/general/daleN/matSpD>
- [15] Benjamini Y et al. (1995) Controlling the False Discovery Rate: a Practical and Powerful Approach to Multiple Testing. *Journal of the Royal Statistical Society* 57(1), 289-300.

4.4 Subcortical shape morphometry: Results from the ENIGMA bipolar working group

As a follow-up to our study of gross volumes (Hibar et al., 2016), we have applied the high-resolution ENIGMA shape analysis techniques to a large, multicenter cohort (N=3,488) to better characterize the localized patterns of morphometric variation we detected in that initial study of subcortical structure. We hypothesized that BD subjects would have generally lower hippocampal, amygdala and thalamus volumes compared to healthy controls (HC) and that shape analysis would reveal patterns of morphometric differences between groups not detected by our prior work. This ongoing subcortical shape analysis from the wider ENIGMA BD working group currently includes 13 international study samples with 1,272 BD and 2,216 HC (**Table 4.4**).

Sample	Country	BD	HC	% Male	Age Mean (SD)
Cardiff	UK	78	53	32	39 (\pm 23)
Frankfurt	Germany	34	32	51	39 (\pm 10)
KCL	UK	23	22	33	42 (\pm 14)
Paris	France	36	55	50	37 (\pm 12)
Penn	USA	58	88	45	34 (\pm 13)
Tulsa	USA	68	90	31	35 (\pm 11)
UCSD	USA	42	78	39	50 (\pm 13)
Yale	USA	195	604	40	36 (\pm 13)
Japan	Japan	158	573	36	46 (\pm 16)
TOP	Norway	192	303	48	35 (\pm 10)
MALT	Norway	44	44	34	33 (\pm 8)
Sydney	Australia	58	100	41	23 (\pm 4)
Houston	USA	286	174	42	26 (\pm 14)

Table 4.4. Demographics from ENIGMA BD subcortical shape analysis (Ching et al., manuscript in preparation)

As described in **Chapter 2**, two measures of shape morphometry are computed along left and

right nucleus accumbens, amygdala, caudate, hippocampus, putamen, pallidum, and thalamus shape models. The radial distance (thickness) metric represents the distance between up to 2,502 surface points and a medial curve. The Jacobian measure is based on surface Tensor Based Morphometry and represents the surface dilation ratio between a surface template and study subject, where larger Jacobian values indicate larger local volume and surface area. A multiple linear regression model was fit at each homologous thickness and Jacobian value across the surface to assess differences between BD and HC groups while adjusting for age, sex, and intracranial volume. A vertex-wise random-effects meta-analysis (metafor R package) was used to combine results from all study samples. All results were corrected for multiple comparisons (FDR $q=0.05$).

This ongoing analysis has several important preliminary findings (Ching et al., manuscript in preparation). Subcortical shape analysis has indicated mostly lower subcortical shape measures in BD compared to HC (**Figure 4.4**). Local thickness and surface area measures were smaller for bilateral hippocampal, thalamic, amygdala, and nucleus accumbens structures after correction for multiple comparisons. More complex patterns of both higher and lower thickness and surface area measures were found in bilateral putamen structures for BD subjects compared to HC. No significant differences in BD subtype (BDI versus BDII) or association with medication at the time of scan were detected after correction for multiple comparisons.

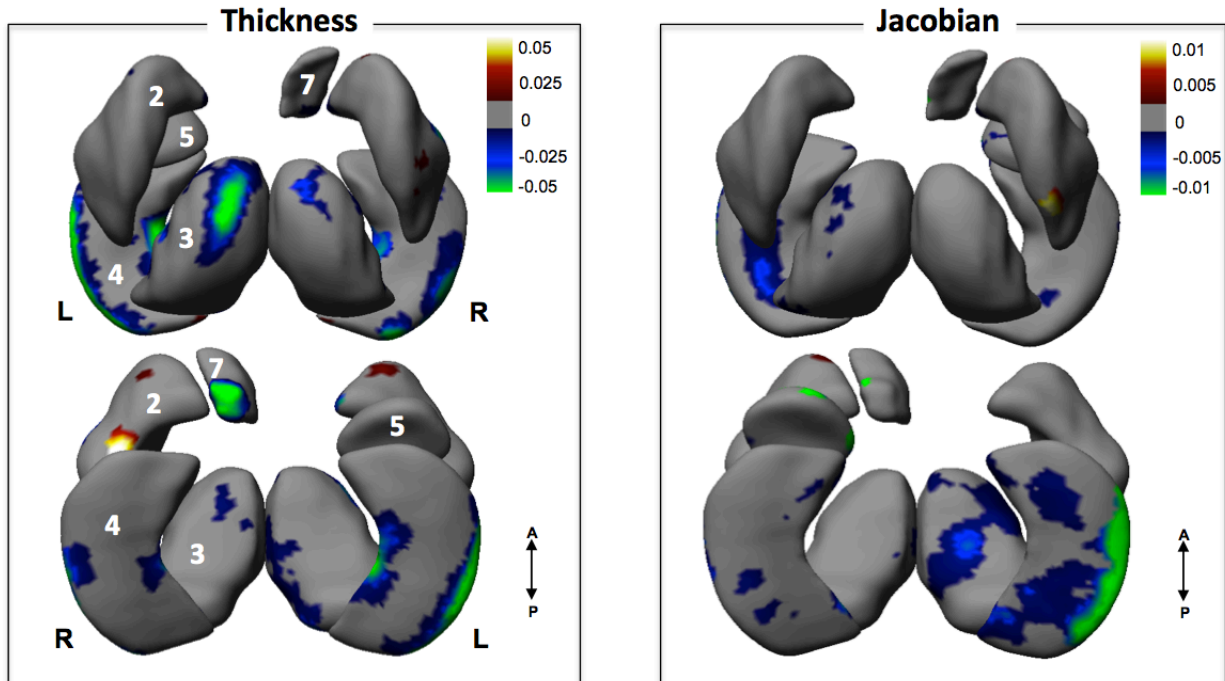


Figure 4.4. Shape meta-analysis with regression coefficient values plotted in regions passing correction for multiple comparisons. **A.** BD vs. HC thickness results: Blue/Green indicate regions of *lower* thickness in BD vs. HC. Red/Yellow indicate regions of *greater* thickness in BD vs. HC. Top: dorsal view; Bottom: ventral view. **B.** BD vs. HC Jacobian results: Blue/Green indicate regions of *lower* surface area in BD vs. HC. Red/Yellow indicate regions of *greater* surface area in BD vs. HC. Top: dorsal view; Bottom: ventral view. 2. putamen; 3. thalamus; 4. hippocampus; 5. amygdala; 7. nucleus accumbens.

In the most current form of the analysis, subcortical shape findings were largely in line with our prior study of single-value measures of subcortical volume (Hibar et al., 2016). There, we reported lower hippocampus, thalamus and amygdala volumes. Here, our shape analysis has revealed patterns of subtle variation in local morphometry, which may provide a more detailed profile of BD-related burden across these subcortical structures. Furthermore, a complex pattern of both higher and lower volume and surface area in bilateral putamen models is found here that

was not reported in our prior work. Shape analysis also revealed a pattern of lower local thickness and surface area of the right nucleus accumbens, again a structure that was not implicated in our previous study of left and right averaged gross volumes.

Patterns of lower hippocampal thickness and surface area appear to conform to possible boundaries of the subiculum/presubiculum as well as CA1-3 subfields. Interestingly, an ENIGMA bipolar working group effort focused on analyzing hippocampal subfields has reported preliminary findings indicating lower volumes in these same subfields in a highly overlapping sample of BD subjects and HC (Haukvik et al., 2019; Haukvik et al., 2019 in preparation).

Lower thalamic thickness and surface area measures in BD compared to HC may overlap with anterior and dorsomedial nuclei. The anterior thalamic nucleus receives inputs from the mammillothalamic tract and hippocampus and sends projections to the cingulate gyrus. The dorsomedial nucleus receives input from prefrontal and limbic areas and projects to the prefrontal cortex. Alterations to the underlying cellular, molecular, or functional connectivity of these thalamic subregions could be related to known alterations in the frontal cortex (Dickstein et al., 2005; Blumberg et al., 2006; Hibar et al., 2018) and cingulate cortices (Gogtay et al., 2007), which have been tied to known deficits of emotional processing and executive behavior in BD (LeDoux, 1995).

If such variations in shape morphometry do map to known underlying subfields as previously reported (Mamah et al. 2016), our findings may help guide more mechanistic investigations of distinct neuronal populations in these structures.

To our knowledge, our study represents the largest investigation of subcortical shape morphometry in BD and marks an unprecedented effort between BD researchers across the world to use harmonized processing and analysis protocols to study the complex subcortical alterations driving BD pathophysiology.

Chapter 4 includes findings adapted from the following studies:

Ching CRK, Gutman BA, Hibar DP, Jahanshad N, Mwangi B, Soares JC, Thompson PM, Andreassen OA for The ENIGMA Bipolar Disorder Working Group. Shape modeling may outperform gross volumetrics in detecting subcortical differences in bipolar disorder. In Preparation

Ching CRK, Gutman BA, Hibar DP, Thompson PM, Andreassen OA for The ENIGMA Bipolar Disorder Working Group. Subcortical Shape Morphometry in Bipolar disorder: An ENIGMA Bipolar Disorder Working Group Study. In preparation

Hibar DP, Westlye LT, Doan NT, Jahanshad N, Cheung JW, **Ching CRK**, Versace A, Bilderbeck AC, Uhlmann A, Mwangi B, Kramer B, Overs B, Hartberg CB, Abe C, Dima D, Grotegerd D, Sprooten E, Boen E, Jimenez E, Howells FM, Delvecchio G, Temmingh H, Starke J, Almeida JRC, Goikolea JM, Houenou J, Beard LM, Rauer L, Abramovic L, Bonnin M, Ponteduro MF, Keil M, Rive MM, Yao N, Yalin N, Najt P, Rosa PG, Redlich R, Trost S, Hagenaaers S, Fears SC, Alonso-Lana S, van Erp TGM, Nickson T, Chaim-Avancini TM, Meier TB, Elvsashagen T, Haukvik UK, Lee WH, Schene AH, Lloyd AJ, Young AH, Nugent A, Dale AM, Pfennig A, McIntosh AM, Lafer B, Baune BT, Ekman CJ, Zarate CA, Bearden CE, Henry C, Simhandl C, McDonald C, Bourne C, Stein DJ, Wolf DH, Cannon DM, Glahn DC, Veltman DJ, Pomarol-Clotet E, Vieta E, Canales-Rodriguez EJ, Nery FG, Duran FLS, Busatto GF, Roberts G, Pearlson GD, Goodwin GM, Kugel H, Whalley HC, Ruhe HG, Soares JC, Fullerton JM, Rybakowski JK, Savitz J, Chaim KT, Fatjo-Vilas M, Soeiro-de-Souza MG, Boks MP, Zanetti MV, Otaduy MCG, Schaufelberger MS, Alda M, Ingvar M, Phillips ML, Kempton MJ, Bauer M, Landen M, Lawrence NS, van Haren NEM, Horn NR, Freimer NB, Gruber O, Schofield PR, Mitchell PB, Kahn RS, Lenroot R, Machado-Vieira R, Ophoff RA, Sarro S, Frangou S, Satterthwaite TD, Hajek T, Dannlowski U, Malt UF, Arolt V, Gattaz WF, Drevets WC, Caseras X, Agartz I, Thompson PM, Andreassen OA. Cortical abnormalities in bipolar disorder: an MRI analysis of 6503 individuals from the ENIGMA Bipolar Disorder Working Group. *Mol Psychiatry*. 2018;23(4):932-42. PMID: 5668195. doi:10.1038/mp.2017.73.

Nunes A, Schnack HG, **Ching CRK**, Agartz I, Akudjedu TN, Alda M, Alnaes D, Alonso-Lana S, Bauer J, Baune BT, Boen E, Bonnin CDM, Busatto GF, Canales-Rodriguez EJ, Cannon DM, Caseras X, Chaim-Avancini TM, Dannlowski U, Diaz-Zuluaga AM, Dietsche B, Doan NT, Duchesnay E, Elvsashagen T, Emden D, Eyler LT, Fatjo-Vilas M, Favre P, Foley SF, Fullerton JM, Glahn DC, Goikolea JM, Grotegerd D, Hahn T, Henry C, Hibar DP, Houenou J, Howells FM, Jahanshad N, Kaufmann T, Kenney J, Kircher TTJ, Krug A, Lagerberg TV, Lenroot RK, Lopez-Jaramillo C, Machado-Vieira R, Malt UF, McDonald C, Mitchell PB, Mwangi B, Nabulsi L, Opel N, Overs BJ, Pineda-Zapata JA, Pomarol-Clotet E, Redlich R, Roberts G, Rosa PG, Salvador R, Satterthwaite TD, Soares JC, Stein DJ, Temmingh HS, Trappenberg T, Uhlmann A, van Haren NEM, Vieta E, Westlye LT, Wolf DH, Yuksel D, Zanetti MV, Andreassen OA, Thompson PM, Hajek T. Using structural MRI to identify bipolar disorders - 13 site machine learning study in 3020 individuals from the ENIGMA Bipolar Disorders Working Group. *Mol Psychiatry*. 2018. doi:10.1038/s41380-018-0228-9.

Favre P, Pauling P, Stout J, Hozer F, Sarrazin S, Abé C, Alda M, Alloza C, Alonso-Lana S, Andreassen OA, Baune BT, Benedetti F, Busatto GF, Caseras X, Chaim-Avancini MK, **Ching CRK**, Dannlowski U, Deppe M, Eyler LT, Fatjo-Vilas M, SF, Grotegerd D, Hajek T, Haukvik UK, Howells FM, Jahanshad N, Kugel H, Lagerberg TV, Lawrie SM, Linke JO, McIntosh A, Elisa M.T Melloni EMT, Mitchell PB, Pomarol-Clotet E, Repple J, Rosa PGP, Salvador R, Sarró S, Schofield PR, Serpa MH, Sim K, Stein DJ, Sussmann JE, Temmingh HS, Thompson PM, Verdolini N, Vieta E, Wessa M, Whalley HC, Zanetti MV, Leboyer M, Mangin JF, Henry C, Duchesnay E, Houenou J, for the ENIGMA Bipolar Disorder Working Group. Widespread White Matter Microstructural Abnormalities in Bipolar Disorder: Evidence from mega, meta and machine learning analyses across 3033 individuals from the ENIGMA Bipolar Disorder Working Group. In review (Biological Psychiatry 2018)

de Zwarte SMC, Brouwer RM, ... (70+ authors) ... Andreassen OA, **Ching CRK**, van Erp TGM, Turner JA, Jahanshad N, Thompson PM, Kahn RS, van Haren NEM, for the ENIGMA Relatives Group. The association between familial risk and brain abnormalities is disease-specific: an ENIGMA–Relatives study of schizophrenia and bipolar disorder. Submitted (Biological Psychiatry 2018)

UK Haukvik, TP Gurholt, S Nerland, PM Thompson, **CRK Ching**, OA Andreassen, I Agartz, for the ENIGMA Bipolar Disorder Working Group. In vivo hippocampal subfield volumes in bipolar disorder – a multisite ENIGMA mega-approach. Organization for Human Brain Mapping 2019, Rome, Italy.

Haukvik UK, Gurholt TP, Nerland S, ... (60+ authors) ... Thompson PM, **Ching CRK**, Andreassen OA, Agartz I, for the ENIGMA Bipolar Disorder Working Group. In vivo hippocampal subfield volumes in bipolar disorder: A multisite ENIGMA mega-approach. In preparation (Molecular Psychiatry)

4.5 Chapter 4 references

Altshuler et al. An MRI study of temporal lobe structures in men with bipolar disorder or schizophrenia. *Biol Psychiatry*. 2000;48(2):147-62.

Blumberg HP, Krystal JH, Bansal R, Martin A, Dziura J, Durkin K, Martin L, Gerard E, Charney DS, Peterson BS. Age, rapid-cycling, and pharmacotherapy effects on ventral prefrontal cortex in bipolar disorder: a cross-sectional study. *Biol Psychiatry*. 2006;59(7):611-8.

Bschor et al. Are bipolar disorders underdiagnosed in patients with depressive episodes? Results of the multicenter BRIDGE screening study in Germany. *J Affect Disord*. 2012;142(1-3):45-52.

Chang et al. Reduced amygdalar gray matter volume in familial pediatric bipolar disorder. *Journal of the American Academy of Child and Adolescent Psychiatry*. 2005;44(6):565-73.

Conus et al. Public health significance of bipolar disorder: implications for early intervention and prevention. *Bipolar Disord*. 2014;16(5):548-56.

Dickstein DP, Milham MP, Nugent AC, Drevets WC, Charney DS, Pine DS, Leibenluft E. Frontotemporal alterations in pediatric bipolar disorder: results of a voxel-based morphometry study. *Arch Gen Psychiatry*. 2005;62(7):734-41.

Duffy et al. Early course of bipolar disorder in high-risk offspring: prospective study. *Br J Psychiatry*. 2009;195(5):457-8.

Ganzola and Duchesne. Voxel-based morphometry meta-analysis of gray and white matter finds significant areas of differences in bipolar patients from healthy controls. *Bipolar Disord*. 2017;19(2):74-83.

Ghaemi et al. Is bipolar disorder still underdiagnosed? Are antidepressants overutilized? *J Affect Disord*. 1999;52(1-3):135-44.

Gogtay N, Ordonez A, Herman DH, Hayashi KM, Greenstein D, Vaituzis C, Lenane M, Clasen L, Sharp W, Giedd JN, Jung D, Nugent TF, 3rd, Toga AW, Leibenluft E, Thompson PM, Rapoport JL. Dynamic mapping of cortical development before and after the onset of pediatric bipolar illness. *J Child Psychol Psychiatry*. 2007;48(9):852-62.

Grande et al. Bipolar disorder. *Lancet*. 2016;387(10027):1561-72.

Hajek et al. Brain structural signature of familial predisposition for bipolar disorder: replicable evidence for involvement of the right inferior frontal gyrus. *Biol Psychiatry*. 2013;73(2):144-52. PMID: 4830692.

Hajek et al. Smaller hippocampal volumes in patients with bipolar disorder are masked by exposure to lithium: a meta-analysis. *J Psychiatry Neurosci*. 2012;37(5):333-43. PMID: 3447132.

Hajek et al. Amygdala volumes in mood disorders--meta-analysis of magnetic resonance volumetry studies. *J Affect Disord.* 2009;115(3):395-410.

Hibar et al. Subcortical volumetric abnormalities in bipolar disorder. *Mol Psychiatry.* 2016;21(12):1710-6. PMID: 5116479.

LeDoux JE. Emotion: clues from the brain. *Annu Rev Psychol.* 1995;46:209-35.

Mamah et al. Subcortical neuromorphometry in schizophrenia spectrum and bipolar disorders. *Neuroimage Clin.* 2016;11:276-86. PMID: 4781974.

McGuffin et al. Prevalence and correlates of bipolar spectrum disorder in the world mental health survey initiative. *Arch Gen Psychiatry.* 2011;68(3):241-51. PMID: 3486639.

Regier et al. DSM-5 field trials in the United States and Canada, Part II: test-retest reliability of selected categorical diagnoses. *Am J Psychiatry.* 2013;170(1):59-70.

Savitz et al. Clinical application of brain imaging for the diagnosis of mood disorders: the current state of play. *Mol Psychiatry.* 2013;18(5):528-39. PMID: 3633788.

Strakowski et al. The functional neuroanatomy of bipolar disorder: a consensus model. *Bipolar Disord.* 2012;14(4):313-25. PMID: 3874804.

van Erp et al. Hippocampal morphology in lithium and non-lithium-treated bipolar I disorder patients, non-bipolar co-twins, and control twins. *Human brain mapping.* 2012;33(3):501-10. PMID: 4383766.

Wray and Gottesman. Using summary data from the danish national registers to estimate heritabilities for schizophrenia, bipolar disorder, and major depressive disorder. *Front Genet.* 2012;3:118. PMID: 3387670.

CHAPTER 5

Future Work

5.1 Future work overview

Even in the case of large-scale meta-analyses, neuroimaging studies generally compare single clinical groups, often defined by DSM criteria, to matched healthy controls. Rarely are groups compared cross-diagnostically (Busatto, 2013; Wise et al., 2016; Hanford et al, 2016). However, it's well established that psychiatric disorders show significant overlap in symptomatology, response to medication and even in underlying genetic risk. Such examples include known overlap between bipolar disorder and major depression, as well as mood disorders and schizophrenia (Pearlson 2015; Rink et al 2016). Importantly, whether shared features reflect similar underlying brain structure and function is poorly understood.

As the ENIGMA disease working groups begin to complete their initial case/control studies of cortical and subcortical structure, we are entering a new phase of the ENIGMA project. Tens of thousands of subjects have now been processed using ENIGMA-harmonized and quality control protocols. These data represent the largest collections of psychiatric neuroimaging data ever amassed using standardized processing techniques, and include the largest samples of bipolar disorder (BD), major depression (MDD), and schizophrenia (SCZ) data ever analysed. The efforts of these three groups have made possible one of the founding goals of the ENIGMA consortium: direct cross-diagnostic comparisons.

Some cross-disorder work is already underway within the ENIGMA consortium. As co-chair of the ENIGMA bipolar disorder working group, we have an ongoing project to derive a multivariate brain-age metric. The goal of this project is to determine whether psychiatric

populations experience accelerated brain aging and whether deviations from normal aging trajectories are associated with factors such as disease severity and medication effects.

Future work also involves studying how genetic risk for BD influences ENIGMA-harmonized brain measures. Dr. Ole Andreassen, co-chair of the ENIGMA bipolar disorder working group, leads the Psychiatric Genomics Consortium Working Group on Bipolar Disorders (PGC-BD). Our collaborative effort involves deriving polygenic risk scores (PRS) based on the latest PGC GWAS findings and mapping PRS vulnerability across brain structures in the ENIGMA bipolar working group.

In the following sections I will discuss my role with regard to these large-scale studies. On this scale, these projects provide the unprecedented opportunity to address some of the major challenges in our field.

5.2 Large-Scale cross-disorder studies of psychiatric disease: direct comparison of harmonized brain measures

I am currently leading an effort to centralize harmonized brain measures from the ENIGMA bipolar, schizophrenia, and major depression working groups. These three working groups, having each published the largest cortical and subcortical case/control MRI studies of their kind, have paved the way for direct comparisons (Hibar et al., 2016; Schmaal et al., 2016; van Erp et al. 2016; Hibar et al., 2018; Schmaal et al., 2017; van Erp et al., 2018). These data will be used in an unprecedented mega-analysis, incorporating datasets from over 100 international sites (**Table 5.2**).

	Study Sites	Cases	Controls
ENIGMA Bipolar	42	3,071	7,979
ENIGMA Schizophrenia	63	5,517	7,130
ENIGMA Major Depression	35	3,310	9,137
Total	140	11,898	24,246

Table 5.2. Current estimated sample sizes from the ENIGMA bipolar, schizophrenia and depression working groups.

Figure 5.2a shows case/control effect sizes from each of the three working group cortical publications plotted on the same scale.

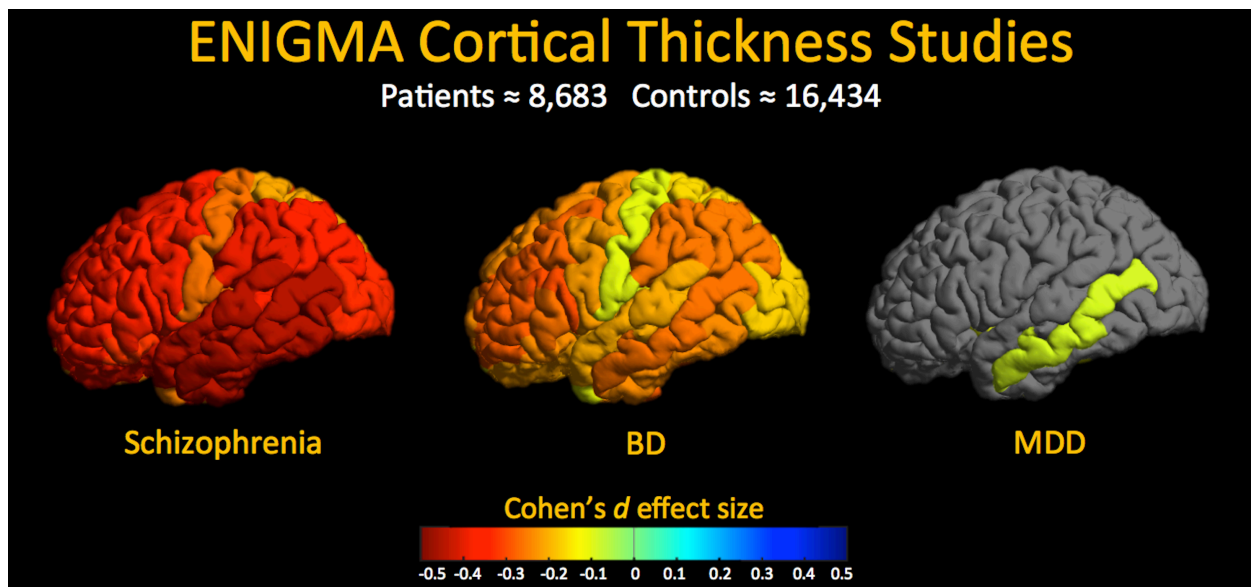


Figure 5.2a. Case/control cortical thickness Cohen's *d* effect sizes from the ENIGMA schizophrenia, bipolar and major depression working group studies.

The initial aims of the cross-disorder project are the following:

1. Deeper Phenotyping

Over the past year I have helped lead an effort to collect in-depth clinical and demographic information from across the ENIGMA disease working groups. For pragmatic reasons, the initial case/control studies for all three working groups tended to include only the essential variables such as age, sex, diagnosis, age of onset, binary (yes/no) medication status at the time of scan, and simple severity measures. Our recent harmonized covariate request, now being collected across over 100 datasets, includes measures such as: education, socioeconomic status, IQ, obesity/body mass index, number of psychiatric hospitalizations, number of episodes (depressive, manic, psychotic), substance use disorder, comorbid psychiatric disorders, current/lifetime medication treatment, medication dose, medication serum level, detailed behavioral/symptom information (common scales/questionnaires). These measures will provide the basis for alternative groupings and allow for more dynamic comparisons not dependent on classic diagnostic categorizations (e.g. BD vs. MDD). Work is currently underway to find overlapping scales and measures and to resolve clinical/behavioral measurement harmonization (McMahon et al., 2018).

2. Estimating possible site effects

As patients (and healthy controls) from the different disease working groups are most often scanned at separate sites, comparisons may be confounded by diagnosis-by-site interactions. This potential confounding effect will be studied by estimating possible bias across healthy control subjects from each site.

One method to test this bias would be a likelihood ratio test where the predictor of interest in the fully specified model is a three-level factor indicating healthy controls from each diagnostic cohort, including age, sex, and intracranial volume as covariates (the exact combination depending on the imaging trait under study). The outcome of interest will be the brain measure of interest (subcortical volume, cortical thickness/surface area). Regions with significant differences between groups may indicate an inherent bias across diagnostic groups.

Importantly, several studies within these three ENIGMA working groups collected data on multiple disorders. Any possible site effects found in the full sample can be examined in the subset of studies that scanned multiple disorders to confirm that the finding is not necessarily driven by site. Though, this test will have considerably less power given that few samples collected multiple diagnostic groups.

The effect of a site-by-diagnosis interaction will also be directly tested in the models described in aim 3. Note that it is possible that the site and diagnosis effects may be highly correlated, in which case the aforementioned bias estimates will be important to any thorough discussion of the final results.

3. Cross-diagnosis models

Linear mixed effect models will be performed with diagnosis (HC, SCZ, BD, MDD), sex, age, diagnosis-by-age, diagnosis-by-sex and sex-by-age as fixed factors. Study site will be used as a random factor. Pooled subcortical volume, cortical thickness and cortical surface

area measures will be the outcome variables of interest. Importantly, this analysis will be repeated including medication status as covariates.

Similar regression models will be fit by replacing diagnosis with the following variables to determine the main effect across disorders:

- Presence of affective (depressive) symptoms,
- Presence of psychotic symptoms (time of scan/history)
- Disease severity
- Age of onset
- Disease duration
- Medication status
- Number of Psychiatric hospitalizations

More complex models will be investigated including interactions between these clinical variables and diagnosis, diagnosis-by-age and diagnosis-by-sex. The influences of substance abuse/dependence, smoking status and IQ will be explored.

4. Machine Learning

We recently published the largest neuroimaging machine learning study of bipolar disorder in which we found modest case/control classification accuracies based on cortical and subcortical measures (Nunes 2018). Supervised machine learning will be applied to examine whether BD, MDD and SZ can be discriminated on the basis of subcortical volumes, cortical thickness and/or surface area. Of great interest will be whether multivariate, machine

learning techniques can discriminate between alternative groupings, such as presence of depressive or psychotic symptoms, disease severity, disease duration, substance use, and other shared characteristics across these three disorders.

5.3 Brain age

There is growing evidence that individual psychiatric disorders may experience accelerated brain atrophy, beyond that expected from normal aging. (Koutsouleris et al., 2014, Nenadic et al. 2017). Accelerated brain aging has been found in schizophrenia but to a lesser extent in bipolar and major depressive disorder. However, these previous studies are based on modest sample sizes and tend to focus on voxel-based metrics. Using ENIGMA-harmonized brain measures, several ongoing and future studies have incorporated much larger samples of healthy control data to derive a more generalizable model of normative brain age and incorporated measures such as cortical thickness and surface area — brain phenotypes known to be under the influence of differential neurodevelopmental genetic factors.

In two forthcoming studies, the ENIGMA major depression working group has collaborated with the ENIGMA bipolar working group to develop a robust, multivariate estimator of brain age (Hahn et al., 2019; Eyler et al., 2019). Measures of subcortical volume, cortical thickness and cortical surface area were used from ~5,000 healthy MDD controls to derive a support vector regression model with a linear kernel to predict chronological age. This model was validated within the MDD sample and then tested for generalizability to the ENIGMA bipolar group's healthy controls to determine whether mean absolute error (i.e. difference between chronological age and predicted brain age) was comparable to that of the MDD healthy control test sample.

Final measures of brain age discrepancy, or Brain-PAD (predicted brain-based age – chronological age), were calculated for the test samples (not included in the training of the brain age model). Importantly, the Brain-PAD models (separate for male and female) will be made available to the wider research community.

Work is underway to evaluate the association between Brain-PAD measures and clinical characteristics within the ENIGMA BD working group. ENIGMA disease working groups are now beginning projects to derive Brain-PAD measures based on this model, resulting in a number of future large-scale psychiatric brain age studies. Future work will include evaluating the extent of accelerated brain aging across a range of disorders and in comparison to polygenic risk.

5.4 Psychiatric genetics

The ENIGMA bipolar disorder working group is uniquely positioned to study how genetic risk loci affect brain structure and function. In close collaboration with the Psychiatric Genomics Consortium Working Group on Bipolar Disorders (PGC-BD), we have begun a project to identify regions of the brain that are associated with the latest bipolar genetic risk loci, as well as genetic risk for other psychiatric disorders. This effort aims to both identify regions at risk in bipolar disorder and also construct overlapping genotype-phenotype risk maps across multiple psychiatric disorders (major depression, schizophrenia) with the goal of yielding more mechanistic models of shared and unique disease processes.

Using recent discoveries from the PGC-BD group (Stahl et al. 2018; Bipolar Disorder and Schizophrenia Working Group of the PGC 2018), we are currently working to calculate polygenic risk scores (PRS) across participating ENIGMA sites (2/3 of BD sites have collected genetic data). The ENIGMA PRS protocol was developed by Dr. Sarah Medland and the ENIGMA Genetics Working Group and is freely available (<http://enigma.ini.usc.edu/protocols/>).

Chapter 5 includes findings and work adapted from the following studies:

Hahn LKM, Hahn T, ... (130+ authors) ... Andreassen OA, **Ching CRK**, Thompson PM, Schmaal L, for the ENIGMA Major Depressive Disorder Working Group. Brain Aging in Major Depressive Disorder: results from the ENIGMA Major Depressive Disorder working group. In submission (Lancet Psychiatry)

Eyler LT, ... (70+ authors) ... Thompson PM, **Ching CRK**, Andreassen OA, for the ENIGMA Bipolar Disorder Working Group. Advanced Brain Age and its Clinical Correlates in Bipolar Disorder: A Global, Multi-Site Analysis Data from the ENIGMA Bipolar Disorder Working Group. In preparation (Molecular Psychiatry)

McMahon MAB, D Garijo, R Espiritu, F Rashid, M Jang, T Patted, V Knight, **CRK Ching**, V Ratnakar, Y Gil, PM Thompson, N Jahanshad. ENIGMA-ODS: A Platform for Global Neuroscience Collaborations in the ENIGMA Consortium, Society of Biological Psychiatry 2018, New York, May 2018.

5.5 Chapter 5 references

- Busatto GF. Structural and functional neuroimaging studies in major depressive disorder with psychotic features: a critical review. *Schizophr Bull.* 2013 Jul;39(4):776-86
- Bipolar Disorder and Schizophrenia Working Group of the Psychiatric Genomics Consortium. Genomic Dissection of Bipolar Disorder and Schizophrenia, Including 28 Subphenotypes. *Cell.* 2018;173(7):1705-15 e16.
- Hanford LC et al. Cortical thickness in bipolar disorder: a systematic review. *Bipolar Disord.* 2016 Feb;18(1):4-18.
- Hibar DP et al. Subcortical volumetric abnormalities in bipolar disorder. *Mol Psychiatry.* 2016 Dec;21(12):1710–1716. PMID: PMC5116479
- Hibar DP et al. Cortical abnormalities in bipolar disorder: an MRI analysis of 6503 individuals from the ENIGMA Bipolar Disorder Working Group. *Mol Psychiatry.* 2018 Apr;23(4):932–942. PMID: PMC5668195
- Koutsouleris N et al. Accelerated brain aging in schizophrenia and beyond: A neuroanatomical marker of psychiatric disorders. *Schizophr Bull* 2014; 40: 1140–53.
- Nenadic I et al. BrainAGE score indicates accelerated brain aging in schizophrenia, but not bipolar disorder. *Psychiatry Research: Neuroimaging* 2017. DOI:10.1016/j.psychresns.2017.05.006.
- Nunes A et al. Using structural MRI to identify bipolar disorders - 13 site machine learning study in 3020 individuals from the ENIGMA Bipolar Disorders Working Group. *Mol Psychiatry.* 2018. doi:10.1038/s41380-018-0228-9.
- Pearlson GD. Etiologic, phenomenologic, and endophenotypic overlap of schizophrenia and bipolar disorder. *Annu Rev Clin Psychol.* 2015;11:251-81.
- Rink L et al. Characteristics and heterogeneity of schizoaffective disorder compared with unipolar depression and schizophrenia - a systematic literature review and meta-analysis. *J Affect Disord.* 2016 Feb;191:8-14.
- Schmaal L et al. Subcortical brain alterations in major depressive disorder: findings from the ENIGMA Major Depressive Disorder working group. *Mol Psychiatry.* 2016 Jun;21(6):806–812. PMID: PMC4879183
- Schmaal L et al. Cortical abnormalities in adults and adolescents with major depression based on brain scans from 20 cohorts worldwide in the ENIGMA Major Depressive Disorder Working Group. *Mol Psychiatry.* 2017;22(6):900-9. PMID: 5444023.

Stalh E et al. Genomewide association study identifies 30 loci associated with bipolar disorder. BioRxiv doi: <https://doi.org/10.1101/173062>.

van Erp TGM et al. Subcortical brain volume abnormalities in 2028 individuals with schizophrenia and 2540 healthy controls via the ENIGMA consortium. *Mol Psychiatry*. 2016 Apr;21(4):585. PMID: PMC5751698

van Erp TGM et al. Cortical Brain Abnormalities in 4474 Individuals With Schizophrenia and 5098 Control Subjects via the Enhancing Neuro Imaging Genetics Through Meta Analysis (ENIGMA) Consortium. *Biol Psychiatry*. 2018 Nov 1;84(9):644–654. PMID: PMC6177304

Wise T et al. Common and distinct patterns of grey-matter volume alteration in major depression and bipolar disorder: evidence from voxel-based meta-analysis. *Mol Psychiatry*. 2017;22(10):1455-63. PMID: 5622121.

CHAPTER 6

Tensor-Based Morphometry and Longitudinal Brain Change

6.1 Tensor-based morphometry: Scan parameter effects on longitudinal brain change

As tensor-based morphometry (TBM) processing lead for the Imaging Genetics Center, I have overseen the longitudinal brain change processing and analysis for the Alzheimer's Disease Neuroimaging Initiative (ADNI). The goal of this work has been to develop neuroimaging metrics to empower clinical trials and to combine imaging with multiscale disease biomarkers to improve degenerative disease detection. An important part of our work is to make these longitudinal brain measures available to the wider research community (<https://ida.loni.usc.edu/login.jsp>).

TBM is a validated method for detecting whole brain, voxel-wise morphometric differences between groups and across time. TBM uses a non-linear inverse consistent elastic intensity-based registration that has been shown to be an unbiased and robust surrogate marker for large, multi-site neuroimaging studies. Subject scans are first linearly registered to a common space. Brain extraction is used to remove inconsistencies in the image background (due to site/scanner differences) that may affect follow-up registration steps. Follow-up time points are non-linearly registered to the baseline scan to create within subject 3D Jacobian maps of structural change over the scan interval. These 3D Jacobian maps are then non-linearly aligned to a study specific mean deformation template where all subjects share a common anatomical coordinate system (Hua et al., 2013). Statistical analyses of Jacobian determinants may be performed on a voxel-wise or ROI level. These Jacobian determinant maps represent brain tissue shrinkage (e.g. temporal atrophy) or expansion (e.g. ventricular dilation) (**Figure 6.1**).

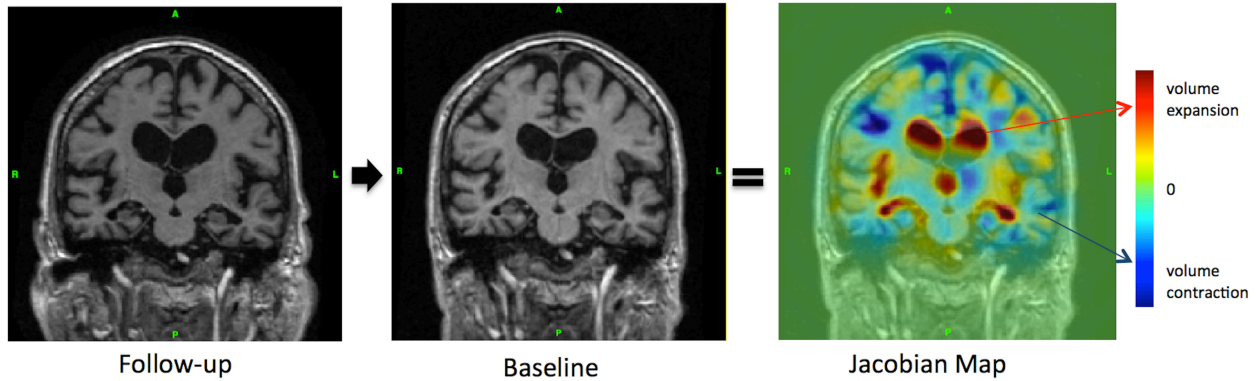


Figure 6.1. Tensor-based morphometry uses non-linear inverse consistent elastic intensity-based registration to derive voxel-wise Jacobian determinant maps that represent unbiased longitudinal brain expansion and contraction across a scan interval for each research subject.

We have tested and applied this pipeline extensively to the ADNI cohort. When developing a potential biomarker for longitudinal brain using a technique like TBM, it is important to determine how protocol changes may affect the power to detect the measure of interest. In order to improve future large-scale trails of neurodegenerative disease, I have investigated the effects of phantom-based scaling and scan acceleration on the power to detect longitudinal brain change in dementia (Hua et al., 2013, Jack et al., 2015, Hua et al., 2016). Thanks in part to work presented here, the third phase of the ADNI project adopted accelerated T1-weighted acquisitions, freeing up valuable scan time for other cutting-edge sequences to track brain change and continue the search for biomarkers of Alzheimer’s disease (Ching et al., 2012; Ching et al., 2015).

6.2 Phantom-based MRI corrections and power to track brain change

CRK Ching, X Hua, C Ward, J Gunter, M Bernstein, CR Jack, M Weiner, PM Thompson. Phantom-based MRI corrections and power to track brain change. ISBI 2012, Barcelona, Spain, May 2-5 2012. © 20XX IEEE. Reprinted, with permission.

PHANTOM-BASED MRI CORRECTIONS AND POWER TO TRACK BRAIN CHANGE

Christopher R. K. Ching¹, Xue Hua¹, Chadwick Ward², Jeff Gunter², Matt A. Bernstein²,
Clifford R. Jack Jr², Michael W. Weiner^{3,4,5}, Paul M. Thompson^{1,6}, The Alzheimer's Disease Neuroimaging Initiative

- ¹ Laboratory of Neuro Imaging, Dept. of Neurology, UCLA School of Medicine, CA, USA
- ² Mayo Clinic and University of Minnesota, Rochester, MN, USA
- ³ Dept. of Radiology, UCSF, CA, USA
- ⁴ Dept. Medicine and Psychiatry, UCSF, CA, USA
- ⁵ Dept. Veterans Affairs Medical Center, San Francisco, CA, USA
- ⁶ Dept. of Neurology and Psychiatry, UCLA School of Medicine, CA, USA

ABSTRACT

The Alzheimer's Disease Neuroimaging Initiative (ADNI) employed phantom-based scaling of T1-weighted MP-RAGE brain images to improve spatial calibration of scans and longitudinal stability across study sites. Early in ADNI, errors in phantom based scaling were identified due to incorrect acquisition protocols or replacement of phantoms. Images initially made available with questionable scaling factors (scaled) were reprocessed (scaled₂) and made available to the scientific community. As many studies were conducted using images with sub-optimal scaling, we aimed to determine if the power to detect brain change differed between scaled and scaled₂ images. Using tensor-based morphometry, we found a high degree of correlation and no significant difference between scaled and scaled₂ images. We detected no significant differences between effect sizes derived from scaled and scaled₂ images. Our findings support the ADNI MRI core assessment that analyses carried out with either scaled or scaled₂ images may not offer a substantial difference in power.

Index Terms— Magnetic Resonance Imaging, Phantoms, Tensor-Based Morphometry, Brain Modeling

1. INTRODUCTION

The Alzheimer's Disease Neuroimaging Initiative (ADNI) is a multi-site longitudinal study with the goal of developing and evaluating reliable imaging biomarkers to track and predict the progression of Alzheimer's disease (AD). ADNI recruited 842 subjects at 58 North American sites using standardized protocols. The ADNI data are freely available online [1]. Due to imperfections in the spatial calibrations of scanners, images collected at different sites, or at the same site over time, may differ slightly in their geometric calibration. To compensate for differences in spatial calibration across time and across ADNI scanning sites, phantom scans were used to correct for linear and nonlinear spatial distortions, as well as variations in signal-to-noise

ratio (SNR) and image contrast across sites. In addition to adjusting scans using phantom-based geometric corrections, phantom scanning can allow investigators to quickly identify sites with incorrect spatial calibration, or temporal drift beyond a range deemed acceptable. Early on in the ADNI project, several well-documented errors (see Methods) in phantom scaling were identified [2]. When those errors were identified, an effort was made to quickly correct the scaling for the erroneous images. Corrected images were re-uploaded and made available to the scientific community [3]. As several analyses had already been published using images with known errors due to phantom based scaling, we set out to estimate the impact of phantom scaling errors on one popular type of longitudinal analysis of brain change - tensor-based morphometry (TBM). We used the most relevant subset of the ADNI data, from all subjects who have images with both sets of scaling factors (scaled vs. scaled₂ images). We examined the correlation between changes computed from scaled and scaled₂ images in a TBM analysis. We also determined whether there was any bias depending on the scaling factor (over- or under-estimate of change), and tested for any difference in effect sizes calculated from scaled and scaled₂ images. In short, we wanted to see if the correction improved the power to detect brain change, or whether it made no significant difference using a popular brain MRI analysis tool.

2. METHODS

ADNI was launched in 2003 by the National Institute on Aging, the National Institute of Biomedical Imaging and Bioengineering, the Food and Drug Administration, private pharmaceutical companies and non-profit organizations, as a \$60 million, 5-year public and private partnership. The principal Investigator of ADNI is Michael Weiner, M.D. of the VA Medical center and the University of California San Francisco. The primary goal of ADNI is to determine the sensitivity of magnetic resonance imaging (MRI), positron emission tomography (PET), other biological markers, and

clinical neuropsychological assessment in measuring the progression of mild cognitive impairment (MCI) and early Alzheimer’s disease (AD). The study has collected brain MRI data from over 842 adults (aged 55-90). Baseline data was collected from 200 patients with AD, 410 with MCI and 232 cognitively normal elderly controls (CN). All subjects were scanned every 6 months to help evaluate the statistical power of methods to detect brain change.

2.1 Phantom Scaling

The ADNI phantom was used to compute a geometric scaling transform to correct for scanner and session-specific calibration errors. Problems in phantom scaling of T1-weighted MRI images were identified in two situations:

1. Some ADNI phantoms had to be replaced due to manufacturing defects or on-site damage; this resulted in unreliable scaling in the A/P direction.
2. Eleven 1.5T MRI scanners initially received an incorrect protocol parameter in which autoslim was disabled, resulting in unreliable scaling in the S/I dimension.

In October 2008, a new set of scans termed “scaled_2 scans” were created to set scaling to the value of 1.0 on the axis for which the accuracy of phantom based scaling was in question. These new scaled_2 scans were made accessible online [1]. The details of phantom based scaling in ADNI are well documented in a prior publication [4].

2.2 Image acquisition

We downloaded 1.5 Tesla T1-weighted MP-RAGE images for subjects that had both a scaled and scaled_2 scan available. Table 1 summarizes the scans available on the date of download (7/14/2011). All subjects underwent clinical and cognitive assessment when the scans were acquired. The ADNI protocol is available online [1].

	6 Month	12 Month	18 Month	24 Month
AD	27	15	0	0
MCI	72	36	13	3
CN	44	23	0	3
Total	143	74	13	6

Table 1: Total sample sizes at each time point separated by diagnosis. AD: Alzheimer’s disease; MCI: Mild cognitive impairment; CN: Cognitively Normal Control

2.3 Image Analysis: Tensor Based Morphometry (TBM)

TBM is an automated technique used to identify regional structural differences between MRI images, as well as brain changes over time. To estimate brain change in each subject, follow-up scans were linearly registered with a 9 parameter

(9P) linear transformation to their corresponding screening scan (SC) and both scans were then aligned to the standard ICBM space using the same 9P registration derived from spatial alignment of the SC to the ICBM [5]. Second, a non-linear inverse-consistent elastic intensity-based registration algorithm was utilized to assess volumetric tissue differences at a voxel-wise level, also known as the determinant of the Jacobian matrix [6]. TBM processing is further detailed in the following reference [7]. To enforce inverse-consistency, we used the algorithm from [6] for both cross-sectional and longitudinal analyses.

2.4 Numerical summaries

Numerical summaries were derived from 3D rate-of-atrophy maps to summarize the amount of cumulative atrophy over 6, 12, 18 and 24 months, in a statistically-defined ROI (stat-ROI, computed from a non-overlapping AD training sample, $p < 0.00001$), and anatomically-defined ROIs (temporal lobe and temporal lobe gray matter). Methods to derive these numerical summaries are described in [7].

2.5 Statistics

Scatter plots were generated to compare scaled and scaled_2 numerical summaries at each time point. Correlation coefficients (R^2) and p -values from paired two-sample t -tests were calculated. Power analysis was conducted at 6 and 12 months, but not at later time points due to the limited number of subjects. As defined by the ADNI Biostatistics Core, the sample size was estimated that would be required to detect a 25% reduction in the mean annual rate of atrophy with 80% power using a two-sided test with a standard significance level ($\alpha = 0.05$) for a hypothetical two-arm study. These sample sizes are referred to as “n80’s”, and are computed as in [8]. Confidence intervals (95%) for each n80 estimate were computed from 10,000 bootstrapped samples [7].

3. RESULTS

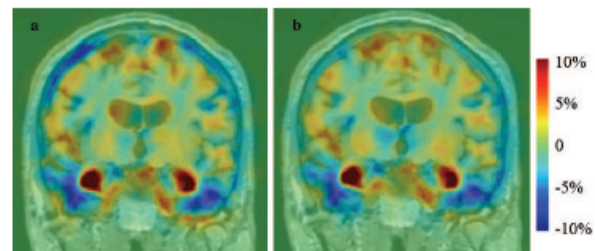


Figure 1: Visual comparison of whole-brain Jacobian maps for a 67 year old male AD subject at a 12-month follow up derived from scaled (a) and scaled_2 (b) scans. In the same coronal slice, the Jacobian maps show visually similar levels of temporal lobe atrophy (blue) and ventricular expansion (red), over this 1-year follow-up interval, although minor

differences are visible in some CSF regions outside the brain (top left).

Figure 2 compares TBM numerical summary measures from scaled and scaled₂ images. Table 2 shows the correlation coefficients for the comparisons (all greater than 0.71). Correlations were greater when the changes were larger (24 months).

	6 Month	12 Month	18 Month	24 Month
Stat-ROI (p<.00001)	0.42	0.49	0.27	0.81
Temporal lobe ROI	0.68	0.72	0.11	0.90
Temporal GM ROI	0.78	0.77	0.15	0.81

Table 2: Squared correlation coefficients (R² values) for linear regressions fitted to compare numerical summaries (% cumulative atrophy) from scaled vs. scaled₂ images, for the entire ADNI cohort (AD+MCI+CN) at each follow up time-point.

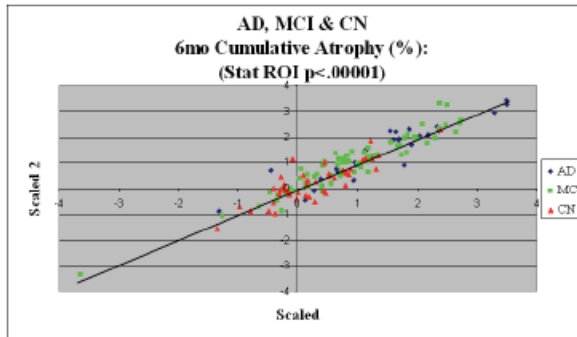


Figure 2: Plot comparing 6 month scaled and scaled₂ numerical summaries taken from the Stat-ROI (with threshold $p < 0.00001$) across all diagnoses. Each point represents the scaled (x axis) and scaled₂ (y axis) numerical summary for a single subject. Individual subjects are color-coded by diagnosis. Measures are highly but not perfectly correlated ($R^2=0.88$); there is no detectable bias in the amount of change detected.

	6 Month	12 Month	18 Month	24 Month
Stat-ROI (p<.00001)	0.88	0.94	0.87	0.98
Temporal lobe ROI	0.73	0.78	0.86	0.91
Temporal GM ROI	0.72	0.78	0.88	0.93

Table 3: P-values from paired two-sample t-tests comparing numerical summaries (% cumulative atrophy) from scaled and scaled₂ images for the combined ADNI group (AD+MCI+CN) at each follow up time-point. Despite the

large sample, no difference was detected between scaled and scaled₂ scans (all $p > 0.05$).

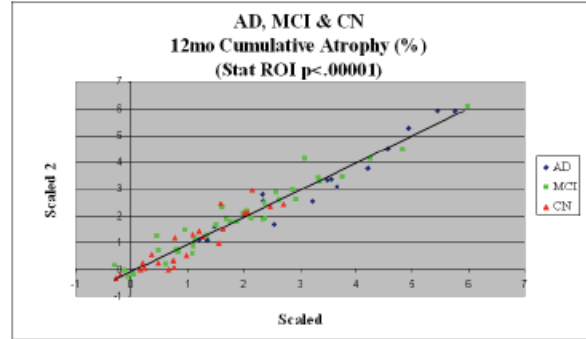


Figure 3: Plot comparing 12-month scaled and scaled₂ numerical summaries taken from the stat-ROI (with threshold $p < 0.00001$) across all diagnoses. Measures are highly but not perfectly correlated ($R^2=0.94$).

Paired two-sample t-tests were calculated to detect any differences between scaled and scaled₂ numerical summaries at each time point. As summarized in Table 3, no differences were detected (all $p > 0.05$).

At 6 months, where enough subjects were available, correlation coefficients and p-values from paired two-sample t-tests for each diagnostic group were calculated for each diagnostic group (AD, MCI and CN). We found no significant difference between scaled and scaled₂ images within diagnostic groups, all $R^2 > 0.69$.

As the available sample size was lower after 12 months, we only computed n80's for 6 and 12 month follow-up intervals. Twelve-month results are shown in Table 4 (last page). Due to space limits, 6-month results are not shown, but show a similar pattern. Effect sizes and n80's were not detectably different for scaled versus scaled₂ images.

4. CONCLUSION

There are two main findings for this study. First, we found a high degree of correlation and no significant difference between scaled and scaled₂ numerical summaries derived from TBM analysis. For groups with adequate sample size (6-month), we found no difference and a high correlation between scaled and scaled₂ images even within diagnostic groups. Second, n80 measures for all three numerical summaries were similar when derived from scaled versus scaled₂ images.

One reason for such close correlation between scaled and scaled₂ images in TBM analysis may be the use of 9 parameter scaling as an image pre-processing step. Nine parameter linear registration allows independent scaling in

x-, y-, and z- dimension and it has been shown to outperform 6P registration to correct for scanner voxel size variations in large studies involving multiple sites, scanners, and acquisition sequences [7,9]. Furthermore, 9P registration has been shown to produce similar levels of scaling correction compared to phantom-based image correction methods in ADNI [3]. In the case of TBM analyses, it may be unnecessary to re-do studies conducted with scaled data that has been 9P registered, as we detected no significant improvement in power (or any consistent difference at all) when scaled_2 images were used. Because we did not test for a difference in scaled and scaled_2 images using 6P registrations we cannot say whether past experiments using 6P scaled data should be repeated. Most modern image processing pipelines now include a 9- or 12-parameter adjustment for brain scale, so phantom-based scaling was in fact abandoned for ADNI2, the follow-on project from ADNI. The present study demonstrates that these unforeseen differences in scaling may be compensated for by image processing techniques such as 9P registration and lends evidence to the argument against using phantom-based scaling in future multi-site MRI studies modeled after ADNI.

Our finding of no significant difference between scaled and scaled_2 images in terms of TBM analysis agrees with suggestions made by the ADNI MRI core [10]. Moving forward, the MRI core has suggested that scaled_2 images be used for subjects that have both scaled and scaled_2 images uploaded to the ADNI database. Based on **Table 4**, our power analysis suggests that, at least in the case of TBM, scaled images may sometimes appear to offer more power to detect change (smaller n80's) depending on the ROI and diagnostic group, although the confidence limits overlap.

5. REFERENCES

- [1] <http://adni.loni.ucla.edu/>
- [2] Gunter J. et al. Validation testing of the MRI calibration phantom for the Alzheimer's Disease Neuroimaging Initiative Study. ISMRM 14th Scientific Meeting and Exhibition (2006).
- [3] Clarkson, M.J. et al. Comparison of phantom and registration scaling corrections using the ADNI cohort. NeuroImage 47, 1506–1513. 2009
- [4] Gunter J. et al. Measurement of MRI scanner performance with the ADNI phantom. Med Phys. 36(6): 2193-205 (2009)
- [5] Mazziotta J. et al. A probabilistic atlas and reference system for the human brain. International Consortium for Brain Mapping (ICBM). Philos. Trans. R. Soc. Lond., B Biol. Sci. 356, 1293-1322 (2001)
- [6] Leow A. et al. Inverse consistent Mapping in 3D Deformable Image Registration: Its Construction and Statistical Properties. Information Processing in Medical Imaging. Springer Berlin, Glenwood Springs, Colorado, USA 493-503 (2005)
- [7] Hua X. et al. Accurate measurement of brain changes in longitudinal MRI scans using tensor-based morphometry. Neuroimage 57, 5-14 (2011)
- [8] Rosner, B. Fundamentals of Biostatistics. PWS-Kent Publishing Company, Boston. (1990)
- [9] Paling, S.M. et al. The application of serial MRI analysis techniques to the study of cerebral atrophy in late-onset dementia. Med Image Anal. 8(1):69-79 (2004)
- [10] <http://adni.loni.ucla.edu/2008/10/scaled-2-uploads/>

AD	Scaled_2 Stat ROI p<.00001	Scaled Stat ROI p<.00001	Scaled_2 Temporal ROI	Scaled Temporal ROI	Scaled_2 Temporal GM ROI	Scaled Temporal GM ROI
% Tissue atrophy	3.2287	3.3401	1.2395	1.3209	1.7603	1.8487
Std	1.3988	1.4591	0.6393	0.5476	0.8101	0.6981
n80	62 [36, 116]	48 [26, 90]	69 [40, 123]	44 [20, 113]	54 [31, 97]	36 [14, 96]
MCI	Scaled_2 Stat ROI p<.00001	Scaled Stat ROI p<.00001	Scaled_2 Temporal ROI	Scaled Temporal ROI	Scaled_2 Temporal GM ROI	Scaled Temporal GM ROI
% Tissue atrophy	1.9499	1.9345	0.9083	0.8958	1.1402	1.1152
Std	1.4354	1.4254	0.7891	0.7871	1.0579	1.0528
n80	136 [83, 241]	136 [85, 244]	189 [99, 327]	194 [105, 458]	216 [109, 601]	224 [120, 523]
CN	Scaled_2 Stat ROI p<.00001	Scaled Stat ROI p<.00001	Scaled_2 Temporal ROI	Scaled Temporal ROI	Scaled_2 Temporal GM ROI	Scaled Temporal GM ROI
% Tissue atrophy	1.0198	1.0699	0.4069	0.4334	0.5444	0.5773
Std	1.0007	0.8417	0.5008	0.4670	0.6742	0.6003
n80	242 [124, 350]	155 [85, 359]	380 [151, 4007]	291 [113, 1483]	385 [144, 3350]	271 [98, 1481]

Table 4: 12 month effect sizes for brain changes, split by diagnostic group. Mean % tissue atrophy over the interval, standard deviation (Std) of the % atrophy, and n80 [confidence interval] are provided for each of the three numerical summaries for both scaled and scaled_2 images by diagnostic group. As expected, the change in the statistical ROI is higher than that in the temporal lobe overall, as it focuses on voxels expected to change the most.

6.3 MRI scan acceleration and power to track brain change

Ching CR, Hua X, Hibar DP, Ward CP, Gunter JL, Bernstein MA, Jack CR, Jr., Weiner MW, Thompson PM. Does MRI scan acceleration affect power to track brain change? *Neurobiology of aging*. 2015;36 Suppl 1:S167-77. PMID: 4374606.



ELSEVIER

Contents lists available at ScienceDirect

Neurobiology of Aging

journal homepage: www.elsevier.com/locate/neuaging

Imaging technology

Does MRI scan acceleration affect power to track brain change?



Christopher R.K. Ching^{a,b}, Xue Hua^b, Derrek P. Hibar^b, Chadwick P. Ward^c,
 Jeffrey L. Gunter^c, Matt A. Bernstein^c, Clifford R. Jack Jr^c, Michael W. Weiner^{d,e,f,g},
 Paul M. Thompson^{a,b,h,i,j,k,l,m,*}, and the Alzheimer's Disease Neuroimaging Initiative¹

^a Department of Neurology, Neuroscience Graduate Program, UCLA School of Medicine, Los Angeles, CA, USA

^b Department of Neurology, Imaging Genetics Center, Institute for Neuroimaging & Informatics, University of Southern California, Los Angeles, CA, USA

^c Department of Neurology, Mayo Clinic and Foundation, Rochester, MN, USA

^d Department of Radiology, UCSF, San Francisco, CA, USA

^e Department of Medicine, UCSF, San Francisco, CA, USA

^f Department of Psychiatry, UCSF, San Francisco, CA, USA

^g Center for Imaging of Neurodegenerative Diseases (CIND), Department Veterans Affairs Medical Center, San Francisco, CA, USA

^h Department of Neurology, USC, Los Angeles, CA, USA

ⁱ Department of Psychiatry, USC, Los Angeles, CA, USA

^j Department of Radiology, USC, Los Angeles, CA, USA

^k Department of Engineering, USC, Los Angeles, CA, USA

^l Department of Pediatrics, USC, Los Angeles, CA, USA

^m Department of Ophthalmology, USC, Los Angeles, CA, USA

ARTICLE INFO

Article history:

Received 2 May 2013

Received in revised form 28 April 2014

Accepted 8 May 2014

Available online 7 October 2014

Keywords:

Alzheimer's disease

MRI

Scan acceleration

Longitudinal

Tensor-based morphometry

Neuroimaging

Biomarker

Drug trial enrichment

ABSTRACT

The Alzheimer's Disease Neuroimaging Initiative recently implemented accelerated T1-weighted structural imaging to reduce scan times. Faster scans may reduce study costs and patient attrition by accommodating people who cannot tolerate long scan sessions. However, little is known about how scan acceleration affects the power to detect longitudinal brain change. Using tensor-based morphometry, no significant difference was detected in numerical summaries of atrophy rates from accelerated and nonaccelerated scans in subgroups of patients with Alzheimer's disease, early or late mild cognitive impairment, or healthy controls over a 6- and 12-month scan interval. Whole-brain voxelwise mapping analyses revealed some apparent regional differences in 6-month atrophy rates when comparing all subjects irrespective of diagnosis ($n = 345$). No such whole-brain difference was detected for the 12-month scan interval ($n = 156$). Effect sizes for structural brain changes were not detectably different in accelerated versus nonaccelerated data. Scan acceleration may influence brain measures but has minimal effects on tensor-based morphometry-derived atrophy measures, at least over the 6- and 12-month intervals examined here.

© 2015 Elsevier Inc. All rights reserved.

1. Introduction

The Alzheimer's Disease Neuroimaging Initiative (ADNI) is a large multisite longitudinal study that aims to develop and

evaluate reliable biomarkers to track and predict the progression of Alzheimer's disease (AD) (Weiner et al., 2010, 2012). As AD pathology develops, the rate of brain tissue loss, also known as brain atrophy, accelerates. Structural-magnetic resonance imaging (MRI) is widely used to estimate brain atrophy rates and is used in some clinical treatment trials to track therapeutic effects in AD and MCI (Jack et al., 2003). Advances in MRI scan acquisition, such as parallel imaging (Deshmane et al., 2012), can speed up scanning protocols (Bammer et al., 2005; Krueger et al., 2012). However, the effects of accelerated scans on MRI derived estimates of brain change have not been well studied. These accelerated sequences reduce scan time, which may lower study costs and allow researchers and clinicians to collect imaging data from individuals unable to tolerate longer scanning sessions. For example, greater effect sizes might be achievable if faster scans are less affected by

* Corresponding author at: Department of Neurology, Imaging Genetics Center and Institute for Neuroimaging and Informatics, Keck School of Medicine of USC, University of Southern California, 2001 N. Soto Street, SSB1-102, Los Angeles, CA 90032, USA. Tel.: +1 323 442 7246; fax: +1 323 442 0137.

E-mail address: pthomp@usc.edu (P.M. Thompson).

¹ Data used in preparing this article were obtained from the Alzheimer's Disease Neuroimaging Initiative (ADNI) database (www.loni.usc.edu/ADNI). As such, investigators within the ADNI contributed to the design and implementation of ADNI and/or provided data but many of them did not participate in the analysis or writing of this report. ADNI investigators include those listed at the following URL: http://adni.loni.usc.edu/wp-content/uploads/how_to_apply/ADNI_Acknowledgement_List.pdf.

patient motion. On the other hand, shorter scans may have a reduced signal-to-noise ratio (SNR), which might inflate the error in estimating brain change. Conversely, head motion may be greater in longer scans, so it cannot be assumed that a longer scan necessarily has greater SNR.

For subjects recruited as part of the ADNI-2 study (an ongoing project following the first phase of ADNI), both accelerated and nonaccelerated structural images were acquired back-to-back in the same session (<http://adni.loni.usc.edu/methods/documents/mri-protocols/>). With the significant benefits expected from faster scans, it is crucial to determine whether or not longitudinal brain change measures are adversely affected by accelerated acquisition. Here, we examined the correlation between brain changes computed from accelerated and nonaccelerated T1-weighted images, using tensor-based morphometry (TBM). We evaluated differences in measured atrophy rates and effect sizes for brain changes over 6- and 12-month intervals computed from accelerated versus nonaccelerated data. Any difference in power to detect brain change between sequences may inform future large-scale imaging studies on which MRI sequence parameters can best track change. We tested a 2-tailed hypothesis that effect sizes for brain change might differ in the accelerated scans, as we did not want to assume which scan type would give the better effect size. To produce images with visually acceptable noise levels using the standard 8- or 12-channel head coils used in ADNI-2, the loss of SNR was partially compensated in the protocol design by a small increase in pixel area (see Table 2). This, in turn, slightly reduces spatial resolution.

At the outset, we were aware that our conclusions would apply specifically to TBM and the types of scans and coils chosen for ADNI. But given the interest in this question, especially by interventional trials now being planned, and the lack of published data, we present this preliminary but thorough study.

2. Methods

Data used in preparing this article were obtained from the ADNI database. In 2011, ADNI-2 began to recruit an additional group of subjects with AD, early mild cognitive impairment (EMCI), late mild cognitive impairment (LMCI), and healthy controls (CN). These subjects, and others carried forward from ADNI-1, were scanned with an updated neuroimaging protocol. ADNI-2 has been acquiring both accelerated and nonaccelerated 3 Tesla structural MRI data, whereas ADNI-1 only acquired nonaccelerated scans. Both scans were acquired in ADNI-2, as there was a need to evaluate any advantages or disadvantages that might be associated with each scan protocol before either of them was advocated or abandoned. For up-to-date information on ADNI protocols, see www.adni-info.org.

2.1. Image acquisition

Data from all ADNI-2 subjects with both an accelerated and nonaccelerated 3T sagittal T1-weighted scan acquired in the same scan session were downloaded on January 19, 2013 from the Laboratory of Neuro Imaging Image Data Archive (<http://adni.loni.usc.edu>). All data available on the Laboratory of Neuro Imaging Image Data Archive is evaluated by quality control group at the Mayo Clinic. Only scans that meet quality control standards are available for download. Only subjects with baseline and follow-up scans at 6 and 12 months were included (6 months: $n = 345$, age: 73.4 ± 7.3 years, 192 males and 153 females; 12 months: $n = 156$, age: 74.2 ± 7.4 years, 87 males and 69 females). All longitudinal data not acquired on a consistent scanner model and/or manufacturer

Table 1

Number of scans at 6 and 12 months (equal for accelerated and nonaccelerated) broken down by vendor sequence (nonaccelerated/accelerated) and by diagnosis

Scanner vendor (accelerated/nonaccelerated sequence)	Diagnosis				
	AD	EMCI	LMCI	CN	Total
6 mo					
GE (IR_FSPGR/ASSET)	7	15	12	27	61
Philips (MPRAGE/SENSE)	6	15	23	29	73
Siemens (MPRAGE/GRAPPA)	16	64	57	74	211
Total	29	94	92	130	345
12 mo					
GE (IR_FSPGR/ASSET)	2	6	4	8	20
Philips (MPRAGE/SENSE)	3	8	11	15	37
Siemens (MPRAGE/GRAPPA)	8	33	23	35	99
Total	13	47	38	58	156

Key: AD, Alzheimer's disease; CN, healthy controls; EMCI, early mild cognitive impairment; LMCI, late mild cognitive impairment.

was excluded, to avoid confounding effects of scanner change on longitudinal analysis.

Each subject received an accelerated T1-weighted scan immediately after a nonaccelerated scan and without leaving the scanner. By vendor, General Electric scanners use IR_FSPGR sequences and Philips and Siemens use MP-RAGE sequences. For details on scan vendor and sequence for the study sample see Tables 1 and 2. Accelerated scan times are shorter than nonaccelerated scans by approximately 4 minutes or roughly 43% (nonaccelerated scan times range from roughly 9:06 to 9:26 minutes and accelerated scans from 5:12 to 5:34 minutes). Detailed MRI scanner protocols for accelerated and nonaccelerated T1-weighted sequences by vendor type are online (<http://adni.loni.usc.edu/methods/documents/mri-protocols/>). All subjects in the ADNI study are assessed clinically and cognitively at the time of scan acquisition. Written informed consent was obtained from all participants before experimental procedures were performed with detailed subject exclusion and inclusion criteria to be found online (<http://adni.loni.usc.edu/>). The full dataset included 345 subjects at 6 months and 156 subjects at 12 months with diagnostic and demographic information outlined in Table 3.

2.2. TBM image analysis

Follow-up scans were linearly registered to baseline (screening) scans with a 9-parameter transformation driven by a mutual information based cost function (Collins et al., 1994) to correct for linear differences in head position and size. To account for global differences in brain scale across the study population, both scans were then aligned to ICBM space (Mazziotta et al., 2001) using the same 9-parameter registration, taking care to apply interpolation only once and handle each scan identically. Brain masks excluding skull were generated for screening and follow-up scans independently using a parameter free robust brain extraction tool (Iglesias et al., 2011), and a joint mask was created to skull strip both scans (i.e., remove all non-brain regions). A minimal deformation target (MDT) image was created from 40 randomly selected healthy elderly controls from the ADNI database. The MDT served as an unbiased average template and has been described previously (Davison and Hinkley, 1997; Efron and Tibshirani, 1993; Hua et al., 2008).

TBM automatically identifies regional structural differences in sets of MR images as well as brain change over time in individuals or groups of subjects scanned longitudinally. A nonlinear, inverse-consistent, elastic, intensity-based registration algorithm was used to estimate volumetric tissue differences (relative volume change over time) at a voxelwise level, based on the determinant of the

Table 2
Details for all scan protocols, which vary slightly by vendor including TE, TR and TI

Scanner vendor	TE (ms)	TR: short and/or long (ms)	TI (ms)	Flip angle (degrees)	Acquired pixel size: nonaccelerated/accelerated (mm)	Slice thickness (mm)
GE	2.8–3.0	6.9–7.3/min	400	11	1.016 × 1.016/1.055 × 1.055	1.20
Philips	3.0–3.1	6.7/2500	900	9	1.000 × 1.000/1.055 × 1.055	1.20
Siemens	2.9	7.0–7.1/2300	900	9	1.000 × 1.000/1.055 × 1.055	1.20

Key: TE, echo time; TR, repetition time; TI, inversion time.

Jacobian matrix of the deformation field, mapping the initial scan to the later one (Leow et al., 2005, 2007). Individual Jacobian maps showing tissue loss and ventricular and/or CSF expansion were then spatially normalized across all subjects by nonlinear alignment to the MDT allowing for statistical comparison. TBM processing is detailed in the following reference Hua et al. (2013). Voxelwise group average Jacobian maps showing the degree of atrophy over 6 and 12 months were created for all diagnostic groups (AD, EMCI, LMCI, and CN) as well as together irrespective of diagnosis (All Dx).

2.3. Numerical summaries

Numerical summaries describing the degree of brain atrophy and/or expansion in each subject were calculated from 3D “Jacobian” maps. Cumulative atrophy over 6 and 12 months was estimated in both a statistically defined region-of-interest (ROI) as well as in an anatomically defined ROI. In the statistically defined ROI (stat-ROI), numerical summaries were computed based on voxels with significant rates of atrophy ($p < 0.00001$) within the temporal lobe as determined from a nonoverlapping training sample of subjects with AD over a 12-month period (20 AD subjects; age at baseline: 74.8 ± 6.3 years; 7 men, 13 women). In the anatomically defined ROI (temporal-ROI), numerical summaries were derived from a temporal lobe mask based on an atlas. Methods to derive these numerical summaries have been described previously (Davison and Hinkley, 1997; Efron and Tibshirani, 1993; Hua et al., 2013).

2.4. Whole-brain analysis

To test for regional differences across the whole brain, we performed a paired 2-sample Student t test at every voxel in the brain, comparing volumetric tissue change in the group of subjects with both accelerated and nonaccelerated scans at 6 and 12 months. To avoid basing inferences on differences that would arise by chance when assessing a large number of voxels, a standard false discovery rate (FDR) correction was applied at the conventionally accepted level of 5% ($q = 0.05$) (Benjamini and Hochberg, 1995). For voxels that were significantly different between scan types, voxelwise average Jacobian values were calculated for each of the groups separately. Mean difference maps were computed by subtracting the nonaccelerated mean map from the accelerated mean maps. The mean difference map was projected on to clusters of voxels that passed FDR correction allowing for visual identification of which group had higher or lower mean Jacobian values (i.e., apparently faster or slower atrophy) for a given significant cluster.

Table 3
Average age (in years at time of scan) and sex of subjects with 6- and 12-month follow-up scans, broken down by diagnosis (Dx)

	AD	EMCI	LMCI	CN	All Dx
6 mo					
Average age (y)	77.2 (± 8.6)	71.5 (± 7.5)	72.8 (± 7.6)	74.3 (± 6.1)	73.4 (± 7.3)
Male/female	20/9	51/43	53/39	68/62	192/153
12 mo					
Average age (y)	76.2 (± 10.6)	71.2 (± 7)	74 (± 8.2)	76.2 (± 5.3)	74.2 (± 7.4)
Male/female	11/2	25/22	20/18	31/27	87/69

Key: AD, Alzheimer's disease; CN, healthy controls; EMCI, early mild cognitive impairment; LMCI, late mild cognitive impairment. Numbers in parentheses are the standard deviations.

2.5. Statistics and sample size analysis

Correlation coefficients and p -values from paired 2-sample t tests were calculated for numerical summaries. Power analysis was conducted at 6 and 12 months for each of the 4 diagnostic groups (AD, EMCI, LMCI, and CN). The sample size was estimated that would be required to detect a 25% reduction in the mean annual rate of atrophy with 80% power using a 2-sided test with a standard significance level ($\alpha = 0.05$) for a hypothetical 2-arm study, as defined by the ADNI Biostatistics Core. These sample sizes are referred to as “n80's” and are computed from the formula in the following, where n is the minimum sample size for each arm, σ_D is the standard deviation, and β is the mean estimated change (Rosner, 1990).

$$n = \frac{2\hat{\sigma}_D^2 (z_{1-\alpha/2} + z_{\text{power}})^2}{(0.25\hat{\beta})^2}$$

Confidence intervals (95%) for each n80 estimate were computed from 10,000 bootstrapped samples (Davison and Hinkley, 1997; Efron and Tibshirani, 1993). The n80's are a useful heuristic to understand effect sizes for change measures but have several well-known limitations (see Discussion in Hua et al., 2013). Although it may not make sense to compare the n80's for different brain measures, where a 25% slowing may have different functional consequences for the patient (or none at all), it does make sense to compare them for accelerated versus non accelerated scans. Sample size estimates adjusted for normal aging were calculated to detect a 25% reduction in the mean annual rate of atrophy after subtracting the mean atrophy rate of controls from the mean atrophy rate of the diagnostic group of interest at 6 and 12 months. Pairwise comparisons of accelerated and nonaccelerated n80's (both standard and age adjusted) were computed from 10,000 bootstrapped samples with replacement.

3. Results

There were no obvious visual differences between raw accelerated and nonaccelerated T1-weighted scans, consistent with prior qualitative visual inspections of accelerated and nonaccelerated data (Krueger et al., 2012). Maps of average cumulative brain atrophy, derived from accelerated and nonaccelerated T1-weighted scans over a 6- and 12-month interval, were visually very similar in each diagnostic group and in the combined group. Fig. 1 shows this visual similarity at 6 months. The mild ventricular expansion and mild lobar atrophy,

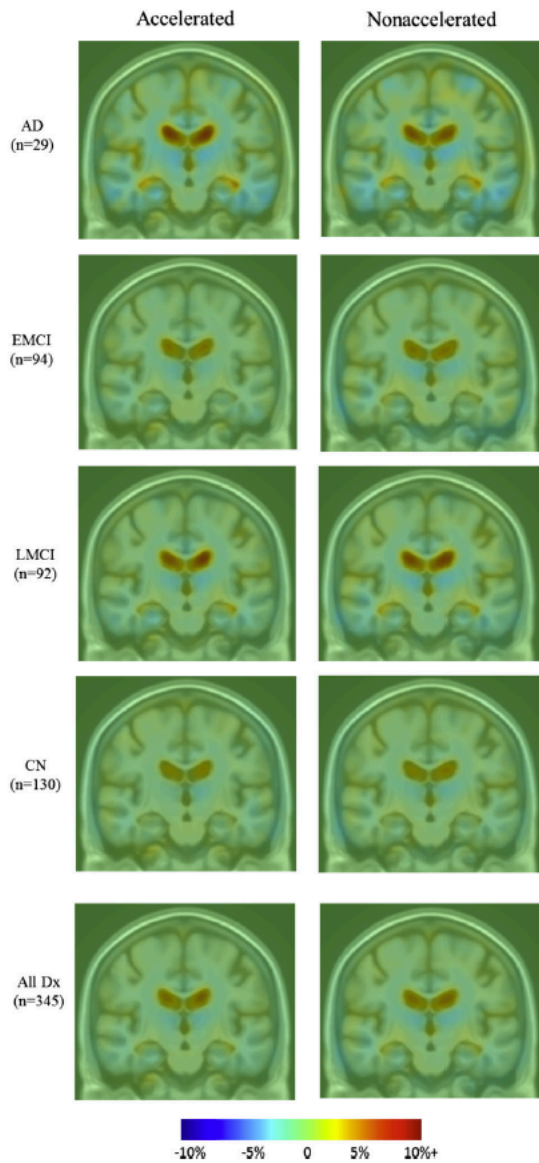


Fig. 1. Average maps of cumulative brain atrophy over 6 months derived from all diagnostic groups separately (AD, EMCI, LMCI, and CN) and together (all Dx) with both accelerated and nonaccelerated follow-up scans. Average patterns of brain atrophy computed from accelerated and nonaccelerated scans are highly similar. Color bar represents percentage of tissue change at 6 months relative to baseline. Red indicates expansion (ventricles) and blue indicates contraction (temporal lobes). Abbreviations: AD, Alzheimer's disease; CN, healthy controls; Dx, diagnosis; EMCI, early mild cognitive impairment; LMCI, late mild cognitive impairment. (For interpretation of the references to color in this figure, the reader is referred to the web version of this article.)

especially in temporal lobes, is consistent with prior reports and matches the now well-known profile of atrophy in AD and MCI (Leow et al., 2009).

Paired 2-sample *t* tests split by diagnosis and in the full sample detected no significant difference between numerical summaries derived with TBM from accelerated versus nonaccelerated scans (Table 4) at 6- and 12-month intervals, after correcting for multiple testing (Bonferroni corrected alpha: $0.05/10 = 0.005$).

Table 4
Effects of MRI scan acceleration on changes detected at 6- and 12-month follow-up scan intervals

	<i>t</i> test <i>p</i> -value at 6 mo/12 mo	Correlation <i>r</i> at 6 mo/12 mo
All Dx cumulative atrophy		
Stat ROI	0.2/0.02	0.71/0.81
Temporal ROI	0.78/0.11	0.65/0.71
AD cumulative atrophy		
Stat ROI	0.32/0.57	0.72/0.89
Temporal ROI	0.54/0.5	0.46/0.69
EMCI cumulative atrophy		
Stat ROI	0.49/0.08	0.68/0.84
Temporal ROI	0.38/0.43	0.68/0.78
LMCI cumulative atrophy		
Stat ROI	0.75/0.32	0.71/0.81
Temporal ROI	0.81/0.77	0.63/0.76
CN cumulative atrophy		
Stat ROI	0.19/0.08	0.63/0.62
Temporal ROI	0.7/0.08	0.69/0.58

p-values from paired 2-sample *t* tests and correlation coefficients (*r*) comparing numerical summaries (% cumulative atrophy) from accelerated and nonaccelerated scans at each follow-up time point. No difference was detected between scan types (all $p > 0.005$), and, as expected, correlations (reported in the final column) were relatively high.

Key: AD, Alzheimer's disease; CN, healthy controls; Dx, diagnosis; EMCI, early mild cognitive impairment; LMCI, late mild cognitive impairment; MRI, magnetic resonance imaging; ROI, region of interest.

Estimates of the mean tissue atrophy (as a percentage), its standard deviation, and *n*80 estimates for the 2 types of numerical summaries (stat-ROI and temporal-ROI) over 6 and 12 months are given in Tables 5 and 6. At the 6-month time interval, accelerated scans provided smaller *n*80's for all numerical summaries except for the EMCI stat-ROI and the CN stat- and temporal-ROI. At 12 months, nonaccelerated scans provide smaller *n*80's for all numerical summaries except for LMCI temporal-ROI. Even so, the percent tissue atrophy and *n*80 estimates did not differ significantly for accelerated versus nonaccelerated scans, as shown by the overlapping confidence intervals and direct comparison (see Table 8). As noted in prior work, the confidence interval on *n*80 tends to be wide, especially when the expected changes are small (e.g., over short-scan interval or with normal diagnosis), even in a large sample.

Sample size estimates adjusted for normal aging were computed that would be sufficient to detect a 25% reduction in the mean annual rate of atrophy after subtracting the mean atrophy rate in controls from the mean atrophy rate of the diagnostic group of interest. The subtraction of the control rate of atrophy leads to conservative (possibly overly conservative) sample size estimates, as it assumes that a treatment would have no effect on the rate of brain atrophy in controls. Depending on the treatment, this may or may not be a realistic assumption. Age-adjusted *n*80 sample size estimates are provided in Table 7. Age-adjusted *n*80's are larger than the standard estimates, as expected. Accelerated scans provided smaller age-adjusted *n*80 estimates for all numerical summaries except at the 6-month EMCI statistical ROI and 12-month AD temporal ROI's. However, the percent tissue atrophy and age-adjusted *n*80 estimates did not differ significantly for accelerated versus nonaccelerated scans, as shown by the overlapping confidence intervals (see Table 7) and the direct comparison (see Table 8).

Pairwise comparisons of accelerated and/or nonaccelerated *n*80 sample size estimates (standard and age adjusted) detected no significant differences between accelerated and nonaccelerated *n*80 sample size estimates after correcting for multiple testing (Bonferroni corrected alpha: $0.05/8 = 0.006$) as shown in Table 8.

To better assess atrophy rates between the different scan types at 6 and 12 months, Fig. 2 contains plots where for each subject the average of accelerated and nonaccelerated numerical summaries (representing average absolute tissue change in percentage) is

Table 5
Six-month effect sizes for brain change

	Accelerated stat ROI <i>p</i> < 0.00001	Nonaccelerated stat ROI <i>p</i> < 0.00001	Accelerated temporal ROI	Nonaccelerated temporal ROI
AD				
Tissue atrophy (%)	1.22	1.34	0.49	0.60
SD	0.79	0.94	0.58	0.85
n80 (CI)	104 (62–214)	123 (78–209)	355 (167–1905)	501 (219–1994)
LMCI				
Tissue atrophy (%)	0.86	0.84	0.32	0.30
SD	0.91	0.93	0.60	0.65
n80 (CI)	284 (178–508)	313 (192–507)	869 (472–2294)	1152 (546–4159)
EMCI				
Tissue atrophy (%)	0.39	0.43	0.20	0.11
SD	0.81	0.79	0.70	0.66
n80 (CI)	1123 (496–6178)	844 (466–2188)	3133 (1028–51,467)	8717 (1700–136,4600)
CN				
Tissue atrophy (%)	0.40	0.47	0.14	0.17
SD	0.76	0.78	0.61	0.68
n80 (CI)	915 (484–2431)	681 (379–1549)	4846 (1593–76,991)	4138 (1440–57,015)

Mean percentage tissue atrophy over the interval, standard deviation (SD) of the atrophy (also in %), and n80 (with 95% confidence interval) for each of the 2 numerical summaries and for both accelerated and nonaccelerated images across all 4 diagnostic groups (AD, EMCI, LMCI, and CN). As expected, the change in the statistical ROI is higher than that detected in the overall temporal lobe ROI, as it focuses on voxels expected to change the most.

Key: AD, Alzheimer's disease; CI, confidence interval; CN, healthy controls; EMCI, early mild cognitive impairment; LMCI, late mild cognitive impairment; MRI, magnetic resonance imaging; ROI, region of interest; SD, standard deviation.

plotted versus the absolute difference between accelerated and nonaccelerated numerical summaries (in percentage). All plots, except for the 6-month temporal-ROI, show a trend toward lower absolute difference between accelerated and nonaccelerated numerical summaries as absolute tissue change increases, although none was significant at $p = 0.05$.

Bland-Altman plots (Altman and Bland, 1987) show agreement between numerical summaries derived from accelerated and nonaccelerated scans (Figs. 3 and 4), and how they depend on the magnitude of the detected changes. There were a number of data points at 6 and 12 months with differences between accelerated and nonaccelerated numerical summaries lying outside ± 1.96 standard deviations of the mean. On further analysis of these data with multiple linear regression, there were no significant factors (scanner vendor, head coil, study site, sex, age, or diagnosis) that predicted the difference in accelerated and nonaccelerated numerical summaries.

To search for any differences across the entire brain, we performed a paired 2-sample *t* test at every voxel, comparing

estimated rates of atrophy for the accelerated and nonaccelerated scans, using the 6- and 12-month TBM maps. There were no significant differences in regional brain atrophy measured between accelerated and nonaccelerated sequences at 6 months after applying an FDR correction at 5% ($q = 0.05$) for any of the within-diagnosis comparisons. However, when combining all the diagnostic groups, some small differences were detected on a whole-brain level that survived FDR correction. These differences are displayed in Fig. 5. Some of the differences between accelerated and nonaccelerated scans were found in clusters of significant voxels in the thalamus as well as anterior portions of the internal and external capsule. These were driven by apparently greater tissue atrophy in the accelerated scans. Conversely, clusters of significant voxels including small portions of the putamen, lateral ventricles, cerebral peduncles, and parietal lobe were driven by apparently greater tissue atrophy in the nonaccelerated scans.

There were no significant differences in regional brain atrophy measured between accelerated and nonaccelerated sequences at

Table 6
Twelve-month effect sizes for brain change

	Accelerated stat ROI <i>p</i> < 0.00001	Nonaccelerated stat ROI <i>p</i> < 0.00001	Accelerated temporal ROI	Nonaccelerated temporal ROI
AD				
Tissue atrophy (%)	1.72	1.63	0.46	0.57
SD	1.20	0.99	0.78	0.65
n80 (CI)	123 (49–445)	92 (46–216)	710 (157–40,340)	323 (107–3117)
LMCI				
Tissue atrophy (%)	1.29	1.41	0.45	0.43
SD	1.20	1.21	0.77	0.83
n80 (CI)	220 (119–471)	186 (104–391)	720 (305–2896)	951 (335–11,061)
EMCI				
Tissue atrophy (%)	0.73	0.88	0.23	0.29
SD	0.94	1.06	0.72	0.81
n80 (CI)	420 (251–892)	366 (222–715)	2399 (630–269,830)	1896 (543–88,109)
CN				
Tissue atrophy (%)	0.59	0.74	0.09	0.22
SD	0.80	0.68	0.61	0.58
n80 (CI)	468 (223–1542)	217 (126–576)	11,358 (1400–6,887,100)	1768 (614–20,580)

Mean tissue atrophy (%) over the interval, standard deviation (SD) of the atrophy (also in %), and n80 (with 95% confidence interval) for each of the 2 numerical summaries and for both accelerated and nonaccelerated images across all 4 diagnostic groups (AD, EMCI, LMCI, and CN). As expected, the change in the statistical ROI is higher than that detected in the overall temporal lobe ROI, as it focuses on voxels expected to change the most.

Key: AD, Alzheimer's disease; CI, confidence interval; CN, healthy controls; EMCI, early mild cognitive impairment; LMCI, late mild cognitive impairment; ROI, region of interest; SD, standard deviation.

Table 7

Six- and 12-month accelerated and nonaccelerated n80 estimates (95% confidence interval) adjusted for normal aging (average CN atrophy) for statistical and temporal ROI numerical summaries across all 3 diagnostic groups (AD, EMCI, and LMCI)

	Accelerated stat ROI $p < 0.00001$	Nonaccelerated stat ROI $p < 0.00001$	Accelerated temporal ROI	Nonaccelerated temporal ROI
AD				
6 mo n80 (CI)	229 (160–568)	293 (143–366)	692 (219–2284)	963 (398–3881)
12 mo n80 (CI)	282 (89–697)	306 (208–489)	1098 (263–32,169)	846 (229–3369)
LMCI				
6 mo n80 (CI)	983 (839–2041)	1669 (1147–2026)	2632 (1122–8189)	5912 (4866–6006)
12 mo n80 (CI)	745 (307–1672)	815 (356–7263)	1124 (473–2958)	3997 (836–513,617)
EMCI				
6 mo n80 (CI)	1,076,662 (76,500–1,554,330)	81,761 (3500–1,268,210)	33,042 (2775–2,378,708)	33,163 (11,200–2,928,600)
12 mo n80 (CI)	11,439 (2458–63,066)	14,417 (1450–1,992,043)	6433 (2338–42,350)	29,645 (910–367,920)

Key: AD, Alzheimer's disease; CI, confidence interval; CN, healthy controls; EMCI, early mild cognitive impairment; LMCI, late mild cognitive impairment; ROI, region of interest.

12 months after applying an FDR correction at 5% ($q = 0.05$) for any of the within diagnosis comparisons. Additionally, after combining all the diagnostic groups there were no significant differences detected between accelerated and nonaccelerated scans on a whole-brain level at 12 months.

In addition to the whole-brain test, and given the interest in temporal lobe change in AD, we wished to rule out any differences between accelerated and nonaccelerated TBM estimates of temporal lobe atrophy by conducting a comparison within a manually derived bilateral temporal lobe ROI. After applying a standard FDR correction at 5% ($q = 0.05$), there were no significant differences between 6- or 12-month accelerated and nonaccelerated TBM estimates of brain change in the entire temporal lobe for any of the within diagnosis or combined diagnostic groups.

4. Discussion

Our study has 3 main findings. First, we detected no significant difference between numerical summaries of atrophy rates from accelerated and nonaccelerated scans within diagnosis at 6 and 12 months, using the TBM analysis method. Second, n80 measures (which arguably relate to sample size requirements for treatment trials) for all 6- and 12-month numerical summaries (standard and age-adjusted) were similar when derived from either accelerated or nonaccelerated images as shown by overlapping confidence intervals and direct pairwise comparison. Third, voxel-based comparisons

found no differences between accelerated and nonaccelerated 6- or 12-month TBM estimates of brain change in the temporal lobes for any of the within diagnosis (AD, EMCI, LMCI, or CN) or combined diagnosis groups. On a whole-brain level, no significant differences were found within any diagnostic group for 6- or 12-month comparisons. The only difference on a whole-brain level was found at 6 months when collapsing all the diagnostic groups into 1 cohort for comparison. The most plausible reason why the 6-month difference was not detected at 12 months is that the available sample size of scans at 12-month follow-up was smaller, making smaller differences hard to detect. Alternatively, there may be no consistently detectable differences, even in samples of over a hundred scans.

In the 6-month whole-brain comparison, there were a number of cortical and subcortical regions with atrophy rates that were apparently different. Clusters of significant voxels in the thalamus, and the anterior limb of the internal and external capsule, were driven by apparently greater tissue atrophy in the accelerated scans. Conversely, clusters of significant voxels including small portions of the putamen, lateral ventricles, cerebral peduncles, and parietal lobe were driven by apparently greater tissue atrophy in the non-accelerated scans. There was no clearly evident systematic pattern indicative of bias in tracking brain change for either accelerated or nonaccelerated images. There was no uniform order in terms of significant clusters being associated with tissue atrophy in accelerated or nonaccelerated scans. The differences found at 6 months may be due to a combination of factors including the poorer signal to noise for accelerated scans and reduced TBM-derived signal (brain atrophy/expansion estimates) to noise over very short-scan intervals. As no whole-brain differences were detected at 12 months, we conclude that there may not be consistent differences between scan types for detecting longitudinal brain change in this particular elderly population, at longer scan intervals, and using this method.

Overlapping confidence intervals as well as direct comparisons between accelerated and nonaccelerated n80's (standard and age-adjusted) detected no significant difference between TBM-derived accelerated and nonaccelerated sample size estimates. Correlation coefficients between accelerated and nonaccelerated numerical summaries ranged from 0.46 to 0.89. Unfortunately, because of the lack of test-retest data in this sample (i.e., people scanned twice at the same time points), we were not able to determine what an acceptable correlation might be for TBM-derived numerical summaries in back-to-back sequences of the same kind. Fig. 2 demonstrates that in general, the 6-month temporal-ROI withstanding, there was a trend toward lower absolute difference between accelerated and nonaccelerated numerical summaries as absolute tissue change increased. Bland-Altman plots for accelerated and nonaccelerated numerical summaries at 6 and 12 months and across all 4 diagnostic groups studied revealed a minority of subjects with differences between accelerated and nonaccelerated numerical summaries lying

Table 8

p -values testing for differences between accelerated and nonaccelerated n80 sample size requirements for both standard- and age-adjusted estimates at 6 and 12 months for Stat ROI $p < 0.00001$ and Temporal ROI

AD	Stat ROI $p < 0.00001$	Temporal ROI
6 mo n80 standard/age-adjusted	0.48/0.41	0.59/0.68
12 mo n80 standard/age-adjusted	0.46/0.78	0.1/0.7
LMCI		
6 mo n80 standard/age-adjusted	0.71/0.19	0.43/0.23
12 mo n80 standard/age-adjusted	0.5/0.87	0.64/0.12
EMCI		
6 mo n80 standard/age-adjusted	0.6/0.91	0.17/0.97
12 mo n80 standard/age-adjusted	0.61/0.89	0.72/0.5
CN		
6 mo n80 standard/age-adjusted	0.35/NA	0.78/NA
12 mo n80 standard/age-adjusted	0.01/NA	0.09/NA

No difference was detected between scan types (all $p > 0.006$).

Key: AD, Alzheimer's disease; CI, confidence interval; CN, healthy controls; EMCI, early mild cognitive impairment; LMCI, late mild cognitive impairment; NA, not applicable; ROI, region of interest.

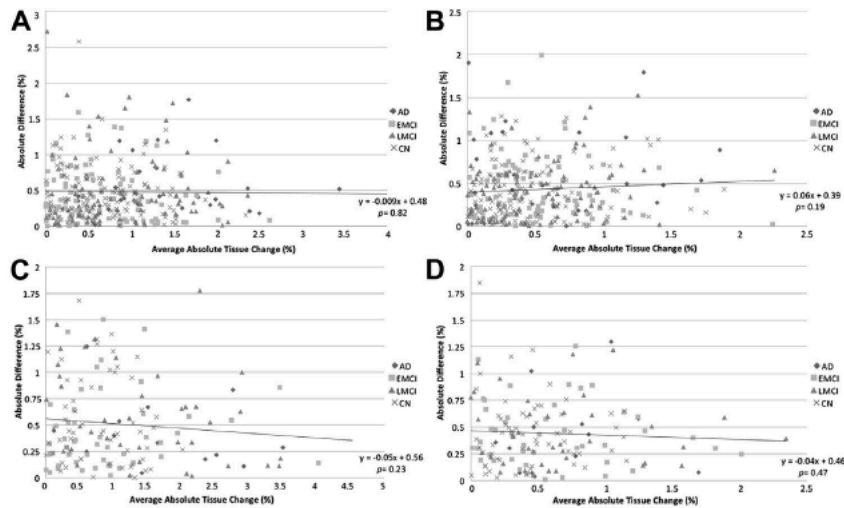


Fig. 2. Plots of average absolute tissue change (%) versus absolute difference (%) for accelerated and nonaccelerated numerical summaries. Each point represents a single subject where the average of the accelerated and nonaccelerated numerical summary (absolute tissue change in %) is plotted along the x-axis, and the absolute difference between accelerated and nonaccelerated numerical summary (%) is plotted along the y-axis. The data are organized by diagnosis including linear trend lines with *p*-values for the entire sample. A: 6-month stat-ROI; B: 6-month temporal-ROI; C: 12-month stat-ROI; and D: 12-month temporal-ROI. Abbreviation: ROI, region of interest.

outside ± 1.96 standard deviations of the mean. There were no significant factors (scanner vendor, head coil, study site, sex, age, or diagnosis) that predicted this difference in accelerated and nonaccelerated numerical summaries.

Although we found no large difference in statistical power to detect brain change from accelerated and nonaccelerated scans at 6 and 12 months, we consider this to be a preliminary finding. Unfortunately, many studies lack the advantage of the larger sample sizes found in ADNI, so differences between accelerated and nonaccelerated derived brain change may not be found in smaller samples. To this point, our comparison of accelerated and nonaccelerated scans at the 12-month interval, while better powered to detect a structural change (as more brain change is expected over longer intervals), has less power to detect a protocol effect as fewer scans were available (6-month $N = 345$ compared with 12-month $N = 156$). The possibility remains that at a larger sample and/or a longer follow-up interval, we may be able to pick up a difference between scan types.

One limitation of the current analysis is that we were not able to further investigate how the type of head coil or the number and distribution of coils might affect the quality of the acceleration data. This may be important to consider within scanner vendor type and with different vendors implementing different versions of acceleration. The ADNI database does not specifically record what type of head coil is used in all the scans. Even so, coils are given a code, which we used as a covariate in our multiple linear regressions, and it did not account for a significant proportion of the variation in the data.

Our study used only 1 MRI analysis technique, so these results may not generalize to other MRI analysis methods, which may be more sensitive to true or artifactual differences in scans, or may rely on different aspects of the signal in the scan. Validation with other MRI analysis tools, such as methods used for cortical and subcortical segmentation, should be considered.

Further study is needed before long-term changes are made to future MRI acquisition protocols, as some analysis techniques may be more sensitive to differences between accelerated and nonaccelerated sequences. Analyses are planned that use a larger reference dataset and multiple types of analyses at multiple sites. As such analyses take longer to complete, we are reporting this data

now while cautioning that more comprehensive studies are needed. Of course, even a study using more methods would never fully address whether acceleration affected analyses not included or data from other kinds of scanners or coil types. When more scans become available in the ADNI database, similar analyses at even longer time intervals (beyond 1 year) will be useful in determining whether or not scan acceleration leads to apparent differences when the true change between scans is greater.

A preliminary (unpublished) report, presented at a past ADNI MRI Core Steering Committee Meeting (Jack et al., ADNI Steering Committee Meeting New Orleans, April 2012), found a difference between accelerated and nonaccelerated 3T MRI scans in a small sample of EMCI subjects from the ADNI cohort. A significant difference was found between cross-sectional accelerated and nonaccelerated groups in whole-brain volume with around 1% lower brain volume measurements at baseline in accelerated scans. Using another popular imaging analysis technique called the brain boundary shift integral (Freeborough and Fox, 1997), a group of researchers found a “near significant” difference in longitudinal measures of whole-brain atrophy in a small sample of subjects over a 12-month period with nonaccelerated scans generating more change (% of baseline) than accelerated scans (Jack et al., 2012).

A recent report described the use of a newer 32-channel head coil, which has higher SNR and obviates the need to sacrifice any spatial resolution to produce visually acceptable accelerated image sets (Krueger et al., 2012). Although differing in regard to the methods, specifically the use of 12- and 32-channel head coils as opposed to the 8- and 12-channel coils used in ADNI-2, as well as the use of composite width and boundary shift integral as the primary quantitative measurement as opposed to our TBM method, Krueger et al. (2012) and our own findings support the claim that accelerated imaging provides high-quality data to track structural brain change. Although our study is largely but not exclusively negative, it would be remiss not to report it, as there is so little information available on effects of scan acceleration for those designing MRI protocols. Interventional trials that are currently in later planning stages are in great need of large scale empirical information on scan acceleration, as we provide in this study. Decisions about scan acceleration are a serious concern for drug trial and epidemiologic

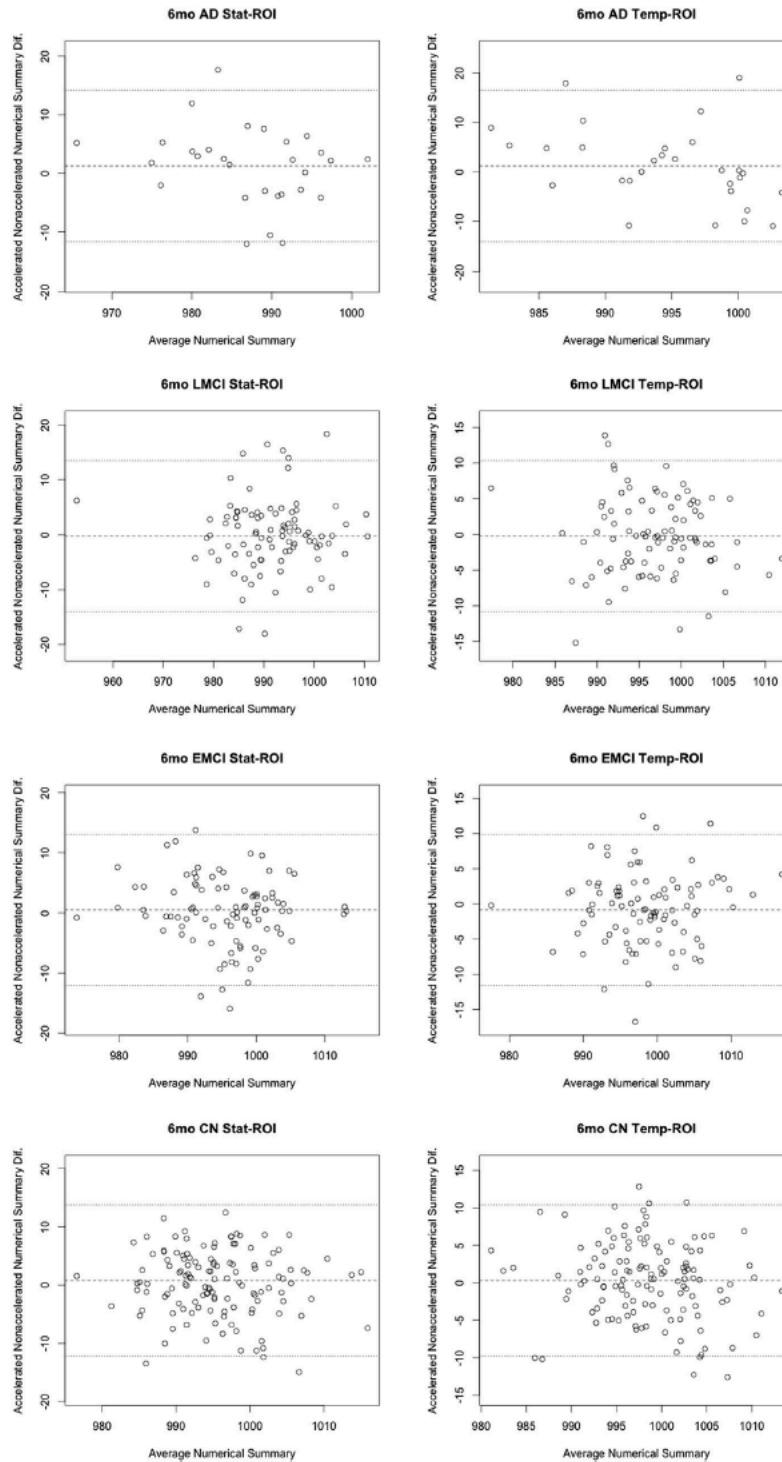


Fig. 3. Six-month Bland-Altman plots for both statistical and temporal-ROI numerical summary measures for each of the 4 diagnostic groups (AD, EMCI, LMCI, and CN). Each point represents the mean of raw accelerated and nonaccelerated TBM-derived numerical summary value (x-axis) plotted against difference between those values. Mean of the accelerated-nonaccelerated numerical summary difference and ± 1.96 standard deviation lines are provided. The scale is based on TBM-derived Jacobian values. These use arbitrary units where 1000 denotes no change and 990 denotes 1% loss of volume over the scan interval. Abbreviations: AD, Alzheimer's disease; CN, healthy controls; EMCI, early mild cognitive impairment; LMCI, late mild cognitive impairment; TBM, tensor-based morphometry.

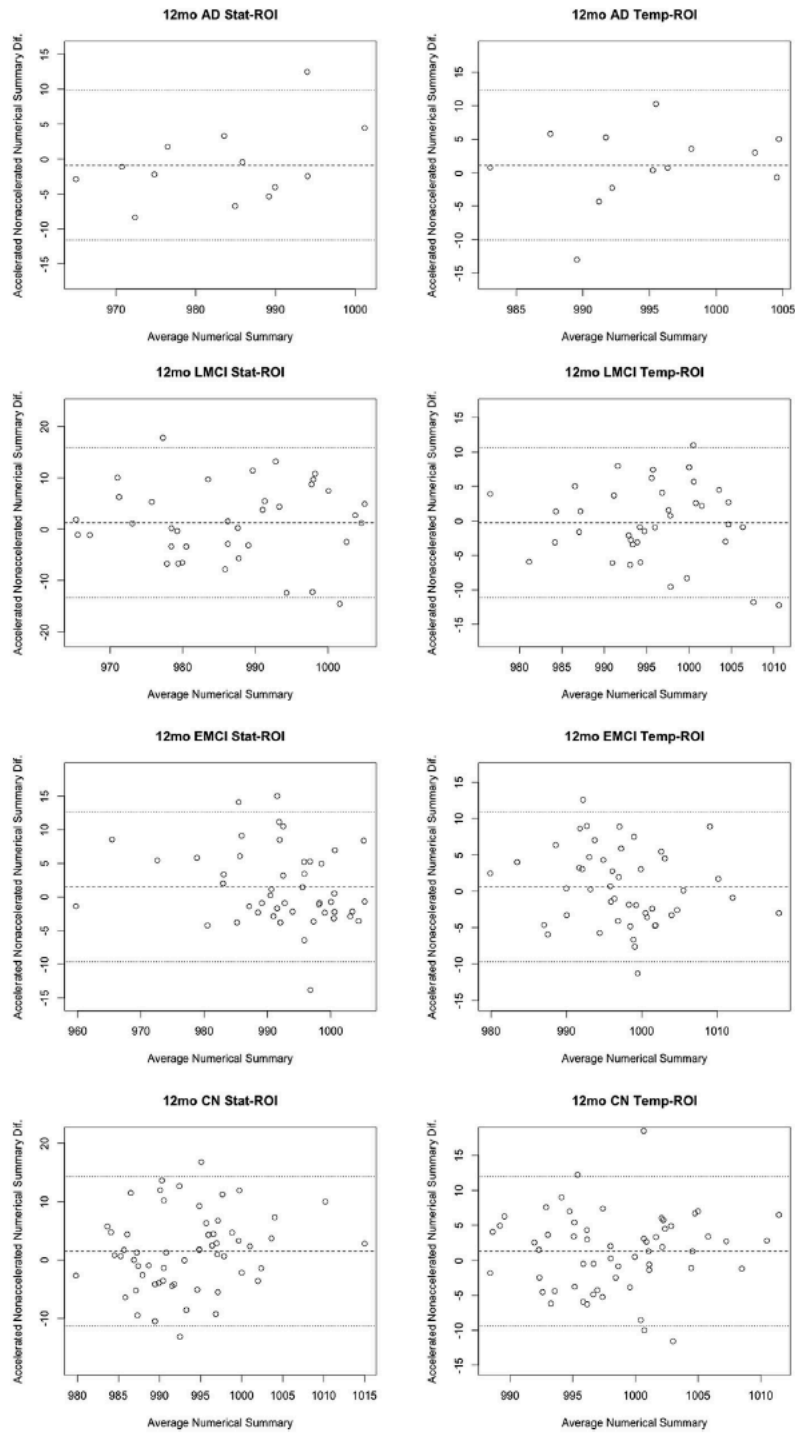


Fig. 4. Twelve-month Bland-Altman plots for both statistical and temporal ROI numerical summary measures for each of the 4 diagnostic groups (AD, EMCI, LMCI, and CN). Each point represents the mean of raw accelerated and nonaccelerated TBM-derived numerical summary value (x-axis) plotted against difference between those values. Mean of the accelerated-nonaccelerated numerical summary difference and ± 1.96 standard deviation lines are provided. The scale is based on TBM-derived Jacobian values, which provide arbitrary units where 1000 denotes no change and 990 denotes 1% loss of volume over the scan interval. Abbreviations: AD, Alzheimer’s disease; CN, healthy controls; EMCI, early mild cognitive impairment; LMCI, late mild cognitive impairment; ROI, region of interest; TBM, tensor-based morphometry.

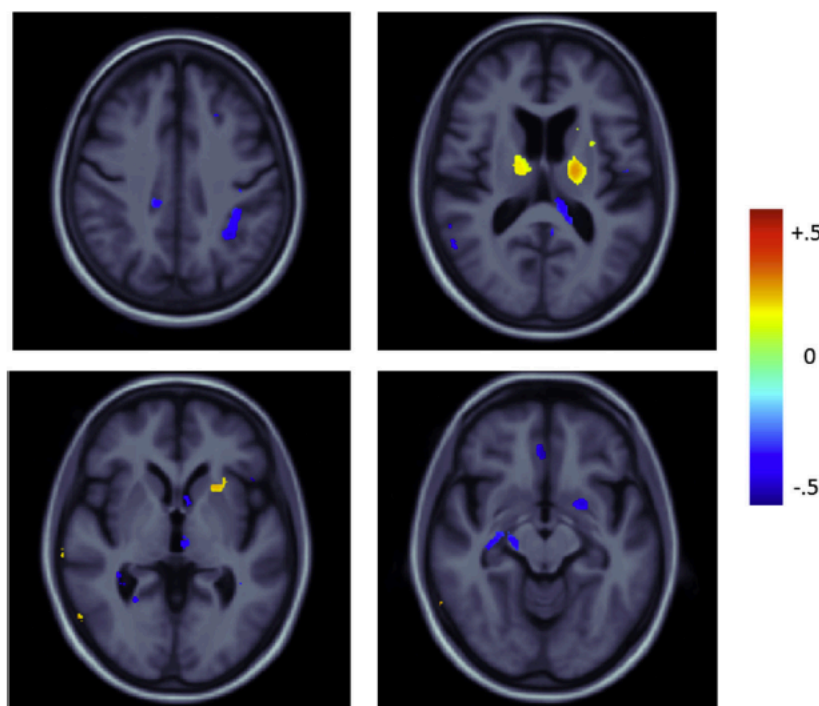


Fig. 5. Mean difference maps displaying the percent difference in the mean atrophy rate of accelerated minus nonaccelerated scans for significant voxels (after FDR correction at 5%) in the full-group comparison over 6-month period relative to baseline. Negative values (blue) represent areas where the mean atrophy rate was higher in nonaccelerated scans. Positive values (red) represent areas where the mean atrophy rate was higher in accelerated scans. Abbreviation: FDR, false discovery rate. (For interpretation of the references to color in this Figure, the reader is referred to the web version of this article.)

studies, as total scan time may affect subject attrition and determines the time available for other scans assessing functional connectivity, blood flow, and more.

Disclosure statement

One of the authors, Dr Michael Weiner, has received private funding unrelated to the content of this article.

All other authors have no potential financial or personal conflicts of interest including relationships with other people or organization within 3 years of beginning the work submitted that could inappropriately influence their work.

Acknowledgements

Algorithm development and image analysis for this study was funded, in part, by grants to Paul Thompson from the NIBIB (R01 EB008281, R01 EB008432 and R21 EB01651) and by the NIA (P50 AG016570-019002, R01 AG040060, U01 AG024904-01), NIBIB, NIMH, the U.S. National Library of Medicine (R01 LM05639), and the National Center for Research Resources (AG016570, AG040060, EB01651, MH097268, LM05639, and RR019771 to Paul Thompson). Data collection and sharing for this project was funded by ADNI (NIH grant U01 AG024904). ADNI is funded by the National Institute on Aging, the National Institute of Biomedical Imaging and Bioengineering, and through contributions from the following: Abbott; Alzheimer's Association; Alzheimer Drug Discovery Foundation; Amofix Life Sciences Ltd; AstraZeneca; Bayer Healthcare; BioClinica, Inc; Biogen Idec Inc; Bristol-Myers Squibb Company; Eisai; Elan Pharmaceuticals Inc; Eli Lilly and Company; F. Hoffmann-La Roche Ltd; and its affiliated company Genentech,

Inc; GE Healthcare; Innogenetics, N.V.; IXICO Ltd; Janssen Alzheimer Immunotherapy Research & Development, LLC; Johnson & Johnson Pharmaceutical Research & Development LLC; Medpace, Inc; Merck & Co, Inc; Meso Scale Diagnostics, LLC; Novartis Pharmaceuticals Corporation; Pfizer; Servier; Synarc Inc; and Takeda Pharmaceutical North America. The Canadian Institutes of Health Research is providing funds to support ADNI clinical sites in Canada. Private sector contributions are facilitated by the Foundation for the National Institutes of Health. The grantee organization is the Northern California Institute for Research and Education, and the study is coordinated by the Alzheimer's Disease Cooperative Study at the University of California, San Diego. ADNI data are disseminated by the Laboratory for Neuro Imaging at the University of Southern California. This research was also supported by NIH grants P30 AG010129 and K01 AG030514 from the National Institute of General Medical Sciences. Investigators within ADNI contributed to the design and implementation of ADNI and/or provided data, but many of them did not participate in analysis or writing of this report. For a complete listing of ADNI investigators, please see http://adni.loni.usc.edu/wp-content/uploads/how_to_apply/ADNI_Acknowledgement_List.pdf. Christopher R. K. Ching was partially funded by the UCLA Neuroimaging Training Program Fellowship, National Institutes of Health, grant numbers R90 DA022768 and T90 DA023422 (UCLA, 2012).

References

- Altman, D.G., Bland, J.M., 1987. Measurement in medicine: the analysis of method comparison studies. *Statistician* 32, 307–317.
- Bammer, R., Skare, S., Newbould, R., Liu, C., Thijs, V., Ropele, S., Clayton, D.B., Krueger, G., Moseley, M.E., Glover, G.H., 2005. Foundations of advanced magnetic resonance imaging. *NeuroRx* 2, 167–196.

- Benjamini, Y., Hochberg, Y., 1995. Controlling the false discovery rate: a practical and powerful approach to multiple testing. *J. R. Stat. Soc.* 57, 289–300.
- Collins, D.L., Neelin, P., Peters, T.M., Evans, A.C., 1994. Automatic 3D intersubject registration of MR volumetric data in standardized Talairach space. *J. Comput. Assist. Tomogr.* 18, 192–205.
- Davison, A.C., Hinkley, D.V., 1997. *Bootstrap methods and their application*. Cambridge University Press, New York.
- Deshmane, A., Gulani, V., Griswold, M.A., Seiberlich, N., 2012. Parallel MR imaging. *J. Magn. Reson. Imaging* 36, 55–72.
- Efron, B., Tibshirani, R.J., 1993. *An introduction to the bootstrap*. Chapman & Hall, New York.
- Freeborough, P.A., Fox, N.C., 1997. The boundary shift integral: an accurate and robust measure of cerebral volume changes from registered repeat MRI. *IEEE Trans. Med. Imaging* 16, 623–629.
- <http://adni.loni.usc.edu/>. **The Alzheimer's Disease Neuroimaging Initiative**. <http://adni.loni.usc.edu/methods/documents/mri-protocols/>. **ADNI MRI Imaging Protocols**.
- <http://https://ida.loni.usc.edu>. **Laboratory of neuro imaging Image Data Archive**.
- Hua, X., Hibar, D.P., Ching, C.R., Boyle, C.P., Rajagopalan, P., Gutman, B.A., Leow, A.D., Toga, A.W., Jack Jr., C.R., Harvey, D., Weiner, M.W., Thompson, P.M., 2013. Unbiased tensor-based morphometry: improved robustness and sample size estimates for Alzheimer's disease clinical trials. *Neuroimage* 66, 648–661.
- Hua, X., Leow, A.D., Lee, S., Klunder, A.D., Toga, A.W., Lepore, N., Chou, Y.Y., Brun, C., Chiang, M.C., Barysheva, M., Jack Jr., C.R., Bernstein, M.A., Britson, P.J., Ward, C.P., Whitwell, J.L., Borowski, B., Fleisher, A.S., Fox, N.C., Boyes, R.G., Barnes, J., Harvey, D., Kornak, J., Schuff, N., Boreta, L., Alexander, G.E., Weiner, M.W., Thompson, P.M., Alzheimer's Disease Neuroimaging Initiative, 2008. 3D characterization of brain atrophy in Alzheimer's disease and mild cognitive impairment using tensor-based morphometry. *Neuroimage* 41, 19–34.
- Iglesias, J.E., Liu, C.Y., Thompson, P.M., Tu, Z., 2011. Robust brain extraction across datasets and comparison with publicly available methods. *IEEE Trans. Med. Imaging* 30, 1617–1634.
- Jack, C., Borowski, B., Bernstein, M., Gunter, J., Jones, D., Kantarci, K., Reyes, D., Senjem, M., Vemuri, P., Ward, C., DeCarli, C., Fox, N., Schuff, N., Thompson, P., 2012. ADNI MRI core steering committee meeting. New Orleans. <http://www.adni-info.org/scientists/Meetings/ADNISteeringCommitteeMeetings.aspx>.
- Jack, C.R., Slomkowski, M., Gracon, S., Hoover, T.M., Felmlee, J.P., Stewart, K., Xu, Y., Shung, M., O'Brien, P.C., Cha, R., Knopman, D., Petersen, R.C., 2003. MRI as a biomarker of disease progression in a therapeutic trial of milameline for AD. *Neurology* 60, 253–260.
- Krueger, G., Granziera, C., Jack Jr., C.R., Gunter, J.L., Littmann, A., Mortamet, B., Kannengiesser, S., Sorensen, A.G., Ward, C.P., Reyes, D.A., Britson, P.J., Fischer, H., Bernstein, M.A., 2012. Effects of MRI scan acceleration on brain volume measurement consistency. *J. Magn. Reson. Imaging* 36, 1234–1240.
- Leow, A., Huang, S.C., Geng, A., Becker, J., Davis, S., Toga, A., Thompson, P., 2005. Inverse consistent mapping in 3D deformable image registration: its construction and statistical properties. *Inf. Process. Med. Imaging* 19, 493–503.
- Leow, A.D., Yanovsky, I., Chiang, M.C., Lee, A.D., Klunder, A.D., Lu, A., Becker, J.T., Davis, S.W., Toga, A.W., Thompson, P.M., 2007. Statistical properties of Jacobian maps and the realization of unbiased large-deformation nonlinear image registration. *IEEE Trans. Med. Imaging* 26, 822–832.
- Leow, A.D., Yanovsky, I., Parikshak, N., Hua, X., Lee, S., Toga, A.W., Jack Jr., C.R., Bernstein, M.A., Britson, P.J., Gunter, J.L., Ward, C.P., Borowski, B., Shaw, L.M., Trojanowski, J.Q., Fleisher, A.S., Harvey, D., Kornak, J., Schuff, N., Alexander, G.E., Weiner, M.W., Thompson, P.M., 2009. Alzheimer's disease neuroimaging initiative: a one-year follow up study using tensor-based morphometry correlating degenerative rates, biomarkers and cognition. *Neuroimage* 45, 645–655.
- Mazziotta, J., Toga, A., Evans, A., Fox, P., Lancaster, J., Zilles, K., Woods, R., Paus, T., Simpson, G., Pike, B., Holmes, C., Collins, L., Thompson, P., MacDonald, D., Iacononi, M., Schormann, T., Amunts, K., Palomero-Gallagher, N., Geyer, S., Parsons, L., Narr, K., Kabani, N., Le Goualher, G., Boomsma, D., Cannon, T., Kawashima, R., Mazoyer, B., 2001. A probabilistic atlas and reference system for the human brain: International Consortium for Brain Mapping (ICBM). *Philos. Trans. R. Soc. Lond. B Biol. Sci.* 356, 1293–1322.
- Rosner, B., 1990. *Fundamentals of Biostatistics*, third ed. PWS-Kent Pub. Co., Boston, Mass.
- Weiner, M.W., Aisen, P.S., Jack Jr., C.R., Jagust, W.J., Trojanowski, J.Q., Shaw, L., Saykin, A.J., Morris, J.C., Cairns, N., Beckett, L.A., Toga, A., Green, R., Walter, S., Soares, H., Snyder, P., Siemers, E., Potter, W., Cole, P.E., Schmidt, M., 2010. The Alzheimer's disease neuroimaging initiative: progress report and future plans. *Alzheimers Dement.* 6, 202–211 e7.
- Weiner, M.W., Veitch, D.P., Aisen, P.S., Beckett, L.A., Cairns, N.J., Green, R.C., Harvey, D., Jack, C.R., Jagust, W., Liu, E., Morris, J.C., Petersen, R.C., Saykin, A.J., Schmidt, M.E., Shaw, L., Siuciak, J.A., Soares, H., Toga, A.W., Trojanowski, J.Q., 2012. The Alzheimer's disease neuroimaging initiative: a review of papers published since its inception. *Alzheimers Dement.* 8 (1 Suppl), S1–S68.

6.4 Chapter 6 selected works

Chapter 6 includes findings adapted from the following selected studies:

CRK Ching, X Hua, C Ward, J Gunter, M Bernstein, CR Jack, M Weiner, PM Thompson. Phantom-based MRI corrections and power to track brain change. ISBI 2012, Barcelona, Spain, May 2-5 2012. © 20XX IEEE. Reprinted, with permission.

CRK Ching, X Hua, DP Hibar, CP Ward, JL Gunter, MA Bernstein, CR Jack Jr, M W Weiner, PM Thompson and the Alzheimer's Disease Neuroimaging Initiative (2012). MRI scan acceleration and power to track brain change, MICCAI NIBAD, Nice, France, Oct. 5, 2012.

Hua X, Hibar DP, **Ching CR**, Boyle CP, Rajagopalan P, Gutman BA, Leow AD, Toga AW, Jack CR, Jr., Harvey D, Weiner MW, Thompson PM. Unbiased tensor-based morphometry: improved robustness and sample size estimates for Alzheimer's disease clinical trials. *NeuroImage*. 2013;66:648-61. PMID: 3785376.

Ching CR, Hua X, Hibar DP, Ward CP, Gunter JL, Bernstein MA, Jack CR, Jr., Weiner MW, Thompson PM. Does MRI scan acceleration affect power to track brain change? *Neurobiology of aging*. 2015;36 Suppl 1:S167-77. PMID: 4374606.

Hua X, **Ching CRK**, Mezher A, Gutman BA, Hibar DP, Bhatt P, Leow AD, Jack CR, Jr., Bernstein MA, Weiner MW, Thompson PM. MRI-based brain atrophy rates in ADNI phase 2: acceleration and enrichment considerations for clinical trials. *Neurobiology of aging*. 2016;37:26-37. PMID: 4827255.

Jack CR, Jr., Barnes J, Bernstein MA, Borowski BJ, Brewer J, Clegg S, Dale AM, Carmichael O, **Ching C**, DeCarli C, Desikan RS, Fennema-Notestine C, Fjell AM, Fletcher E, Fox NC, Gunter J, Gutman BA, Holland D, Hua X, Insel P, Kantarci K, Killiany RJ, Krueger G, Leung KK, Mackin S, Maillard P, Malone IB, Mattsson N, McEvoy L, Modat M, Mueller S, Nosheny R, Ourselin S, Schuff N, Senjem ML, Simonson A, Thompson PM, Rettmann D, Vemuri P, Walhovd K, Zhao Y, Zuk S, Weiner M. Magnetic resonance imaging in Alzheimer's Disease Neuroimaging Initiative 2. *Alzheimers Dement*. 2015;11(7):740-56. PMID: 4523217.

CHAPTER 7

Related Works Completed During Graduate Studies

7.1 Related works

The studies included in this chapter were conducted during my graduate work. While not central to this dissertation thesis, these studies further convey the overall breadth of my research activities to date. Of special note is the following study: *A Model For Teaching Advanced Neuroscience Methods: A Student-Run Seminar to Increase Practical Understanding and Confidence*. This was an effort completed with a fellow graduate student, Tessa Harrison, in which we developed a student-taught course on advanced neuroscience research methods. This is the first student-taught course to be part of the required first year curriculum for the UCLA Interdepartmental Neuroscience PhD program.

7.2 Chapter 7 selected works

Adams HH, Hibar DP, Chouraki V, Stein JL, Nyquist PA, Renteria ME, Trompet S, Arias-Vasquez A, Seshadri S, Desrivieres S, Beecham AH, Jahanshad N, Wittfeld K, Van der Lee SJ, Abramovic L, Alhusaini S, Amin N, Andersson M, Arfanakis K, Aribisala BS, Armstrong NJ, Athanasiu L, Axelsson T, Beiser A, Bernard M, Bis JC, Blanken LM, Blanton SH, Bohlken MM, Boks MP, Bralten J, Brickman AM, Carmichael O, Chakravarty MM, Chauhan G, Chen Q, **Ching CR**, ... (304 authors)... Franke B, Debette S, Medland SE, Ikram MA, Thompson PM. Novel genetic loci underlying human intracranial volume identified through genome-wide association. *Nature Neuroscience*. 2016;19(12):1569-82. PMID: 5227112.

Harrison TM, **Ching CR**, Andrews AM. A Model For Teaching Advanced Neuroscience Methods: A Student-Run Seminar to Increase Practical Understanding and Confidence. *J Undergrad Neurosci Educ*. 2016;15(1):A5-A10. PMID: 5105964

Looi JC, Rajagopalan P, Walterfang M, Madsen SK, Thompson PM, Macfarlane MD, **Ching C**, Chua P, Velakoulis D. Differential putaminal morphology in Huntington's disease, frontotemporal dementia and Alzheimer's disease. *Aust N Z J Psychiatry*. 2012;46(12):1145-58. PMID: 4113021

Nir TM, Jahanshad N, **Ching CRK**, Cohen RA, Harezlak J, Schifitto G, Lam HY, Hua X, Zhong J, Zhu T, Taylor MJ, Campbell TB, Daar ES, Singer EJ, Alger JR, Thompson PM, Navia BA, On behalf of the HIV Neuroimaging Consortium. Progressive Brain Atrophy in Chronically Infected and Treated HIV+ Individuals. Accepted Journal of NeuroVirology January 2019

Salminen LE, Wilcox R, Zhu AH, Riedel BC, **Ching CRK**, Boyle CP, Knight V, Saremi A, Rashid F, Thomopoulos SI, Harrison MB, Ragothaman A, Medland SE, Thompson PM, Jahanshad N. Altered cortical brain structure and increased risk for disease seen decades after perinatal exposure to maternal smoking: A study of 9,000 adults in the UK Biobank. Submitted (Cerebral Cortex 2018) BioRxiv doi: <https://doi.org/10.1101/471839>

Tao C, Nichols TE, Hua X, **Ching CRK**, Rolls ET, Thompson PM, Feng J. Generalized reduced rank latent factor regression for high dimensional tensor fields, and neuroimaging-genetic applications. *NeuroImage*. 2017;144(Pt A):35-57. PMID: 5798650.